2013

Shear behaviour of rock joints under cyclic loading and constant normal stiffness conditions

Ali Mirzaghorbanali
University of Wollongong

SHEAR BEHAVIOUR OF ROCK JOINTS UNDER CYCLIC LOADING AND CONSTANT NORMAL STIFFNESS CONDITIONS

A thesis submitted in fulfilment of the requirements

for the award of the degree of

DOCTOR OF PHILOSOPHY

from

UNIVERSITY OF WOLLONGONG

by

Ali Mirzaghorbanali

B.Eng (IUT), M.Eng (Curtin), M.Sc (PUT)

Faculty of Engineering and Information Sciences

2013

CERTIFICATION

I, Ali Mirzaghorbanali, declare that this thesis, submitted in fulfilment of the requirements for the award of Doctor of Philosophy, in the School of Civil, Mining, and Environmental Engineering, University of Wollongong, is wholly my own work except where specific references or acknowledgements are made. The document has not been submitted for qualifications at any other academic institution.

Ali Mirzaghorbanali

08/2013

LIST OF PUBLICATIONS

Journal articles:

MIRZAGHORBANALI, **A**. NEMCIK, J. and AZIZ, N. (2013). Effects of shear rate on cyclic loading shear behaviour of rock joints under constant normal stiffness conditions. *Rock Mechanics and Rock Engineering* (**accepted** for publication). DOI: 10.1007/s00603-013-0453-0

MIRZAGHORBANALI, **A**. NEMCIK, J. and AZIZ, N. (2013). Effects of cyclic loading on the shear behaviour of infilled rock joints under constant normal stiffness conditions. *Rock Mechanics and Rock Engineering* (**accepted** for publication). DOI: 10.1007/s00603-013-0452-1

NEMCIK, J. **MIRZAGHORBANALI**, **A**. and AZIZ, N. (2013). An elasto-plastic constitutive model for rock joints under cyclic loading and constant normal stiffness conditions. *Geotechnical and Geological Engineering* (**accepted** for publication). DOI: 10.1007/s10706-013-9716-5

Conference articles:

MIRZAGHORBANALI, **A**. and NEMCIK, J. (2013). Numerical modelling of cyclic shear behaviour of rock joints under constant normal stiffness condition. *Coal Operators' Conference*, Wollongong, Australia, pp. 406-413.

MIRZAGHORBANALI, **A**. NEMCIK, J. and AZIZ, N. (2014). A study on the shear behaviour of infilled rock joints under cyclic loading and constant normal stiffness conditions. *Coal Operators' Conference*, Wollongong, Australia (**accepted** for publication).

ACKNOWLEDGMENTS

I would like to express my deepest appreciation to my thesis supervisors Dr. Jan Nemcik and Prof. Naj Aziz, Faculty of Engineering, University of Wollongong, who provided me the opportunity to conduct my thesis. This thesis would not have been possible without their technical support, generous help, tolerance and encouragement during the period of research work. Beside academic issues, the good advice and friendly attitude of my supervisors on personal level have been invaluable for which I am extremely grateful. My sincere thanks also goes to Prof. Chris Cook (Executive Dean of the Faculty of Engineering and Information Sciences) and Ms. Lynne Wright for their significant support during this study.

My parents have provided me unconditional love and support throughout, as always, for which my mere expression of thanks likewise does not suffice. Special thanks I give to my brother Mohsen, for his continuous inspiration and support in all aspects of my life. His great personality has deeply influenced my attitudes and ideology.

I would like to offer my special thanks to my colleagues and friends Mohammad Ramezanianpour, Mahdi Zoorabadi, Zhenyu Zhang and Setayesh Gholami in promoting a welcoming academic and social environment. I am also grateful to Dr. Heather Jamieson and Bob Kininmonth for their kindness and support in writing this thesis.

Thanks are extended to technical staff of the Faculty of Engineering Mr. Alan Grant, Mr. Ritchie Mc Lean, Mr. Ian Laird, Mr. Frank Crabtree and Mr. Cameron Neilson for their generous assistance and availability at various stages of research work.

I would like to acknowledge the financial support of the University of Wollongong provided for this research through the International Postgraduate Tuition Award (IPTA) and University Postgraduate Award (UPA).

Finally, I would like to dedicate my thesis to my mother. Her spiritual support enabled me to overcome all difficulties I encountered during my PhD period.

ABSTRACT

Shear behaviour of rock joints subjected to cyclic loading was previously studied mostly under Constant Normal Load (CNL) conditions which does not accurately simulate the actual deformation behaviour of field rock joints. Natural joints are often filled with materials such as sand, clay or silt. The shear behaviour of rock joints is affected considerably by the presence of the infill within joints. This poses significant concern for excavations which are constructed in close proximity of jointed rock mass. None of the previous research investigated the shear behaviour of infilled rock joints under cyclic loading. This thesis studies the shear behaviour of rock joints under cyclic loading and Constant Normal Stiffness (CNS) conditions.

Triangular joints asperities with initial angles of 9.5° (Type I), 18.5° (Type II) and 26.5° (Type III) to the shear movement, and replicas of a field rock joint surface cast using high strength Plaster of Paris were tested. Experiments were performed using the CNS cyclic direct shear apparatus updated for this study. The samples were sheared under initial normal stress levels ranging from 0.16 MPa to 2.5 MPa, representing the *in-situ* stress conditions as experienced in the field. Laboratory test results indicate that, the shear strength and the dilation component decrease with increase in the loading cycles. The asperity damage appeared to be a function of the external energy exerted on asperities during shearing. Thus, the asperity damage was higher for greater initial asperity angles and normal stresses. Furthermore, the effects of shear rate on shear behaviour of rock joints under cyclic loading were investigated. The strength decreased with increase in the shear rate.

The shear behaviour of rock joints infilled with mixture of Clay and Sand at initial moisture content of 12.5% was studied under cyclic loading and various normal stresses ranging from 0.56 MPa to 2.4 MPa while a constant shear rate of 0.5 mm/min and a constant normal stiffness of 8 kN/mm were applied. Types I and II asperity surfaces were selected to prepare infilled joints with infill thickness to asperity height ratio of 0.3, 0.6 and 1. The shear strength of infilled joints was observed to decrease with increase in the number of shear cycles due to asperity damage and deformation of infill material. The variation of normal displacement with shear displacement was dominated by dilation and contraction, depending on the infill thickness to asperity height ratio and initial normal stress.

An analytical model based on the energy balance theory was developed to predict the shear behaviour of clean (non-filled) rock joints under cyclic loading and CNS conditions. An empirical relationship was also proposed to account for the effect of shear rate on cyclic loading shear strength. The concept of Normalised Cyclic Strength Reduction of infilled joints ($NCSR^i$) was introduced and incorporated in a mathematical model to replicate the reduction in the shear strength of infilled rock joints with increase in the number of shear cycles. Model coefficients were calibrated using laboratory results. In general, the modelled results were in good agreement with the experimental data.

The capabilities of the two built-in constitutive models, simulating the shear behaviour of rock joints under cyclic loading and CNS conditions that are available in Universal Distinct Element Code (UDEC), were investigated. The Coulomb slip model replicates different shear behaviour in forward and backward shearing when the asperity damage

is not significant. For the asperity breakage mechanism, the continuously yielding model describes the effects of asperity damage on shear strength and dilation angle.

CONTENTS

LIST OF FIGURES

LIST OF TABLES

LIST OF SYMBOLS AND ABBREVIATIONS

Symbols

σ_c	Uniaxial compressive strength
E	Young's modulus
φ_b	Basic friction angle of asperity surface
τ	Shear strength
σ_n	Normal stress
i	Dilation angle
σ_{n0}	Initial normal stress
dv	Increment of normal displacement
du	Increment of shear displacement
φ_{fill}	Friction angle of infill material
C_{fill}	Cohesion of infill material
Cc	Compression index
Cs	Swelling index
i_0	Initial asperity angle
t	Infill thickness

a	Asperity height
e	Elastic state
p	Plastic state
E^e	Elastic stiffness
$d\tau$	Increment of shear stress
$d\sigma$	Increment of normal stress
s	Shear direction
n	Normal direction
Q	Plastic potential function
λ	Proportional scalar factor
F	Yield function
E^{ep}	Elasto-plastic stiffness
E_i	Energy term
S	Shear force
N	Normal force
μ	Friction coefficient
E_d	Energy dissipated due to asperity damage
φ_m	Mobilised friction angle

i_{sec}	Secant dilation angle
v^*	Normal displacement at half of the asperity length
T	Asperity length
c_s	Sliding damage coefficient
k	Boundary normal stiffness
τ^c_h	Cyclic loading shear strength of high shear rate
τ^c_l	Cyclic loading shear strength of low shear rate (0.5 mm/min)
c^s_1	Model coefficient
c^s_2	Model coefficient
N_c	Number of loading cycles
τ^{ci}_p	Peak shear strength of infilled rock joints under cyclic loading
τ^{mi}_p	Peak shear strength of infilled rock joints under monotonic loading
$\Delta\tau^i$	Reduction in shear strength with increase in the number of loading cycles
α	Model coefficient
β	Model coefficient
c_1	Model coefficient
c_2	Model coefficient

c_3	Model coefficient

Abbreviations

CNL	Constant Normal Load
CNS	Constant Normal Stiffness
JRC	Joint Roughness Coefficient
JCS	Joint Compressive Strength
JRC_m	Mobilised Joint Roughness Coefficient
OCR	Over Consolidation Ratio
LVDT	Linear Variable Differential Transformer
AD	Asperity Damage
$NCSR^i$	Normalised Cyclic Strength Reduction of infilled joints
UDEC	Universal Distinct Element Code

Chapter I

1. INTRODUCTION

1.1. General introduction

Rock mechanics deals with the mechanical properties of rocks and techniques required for the design of rock structures. In numerous rock engineering projects involving slopes and underground excavations, it is important to consider the effects of discontinuities on the rock mass behaviour. This is of particular relevance where stability of infrastructure is influenced by the shear behaviour of a single joint or multiple discontinuities in the surrounding rocks.

1.2. Importance of the study

According to Gens *et al.,* (1990), an adequate representation of discontinuities and interfaces is essential to properly model rock masses, interacting with a structure. Oliveira (2010) in his research on shear behaviour of rock joints mentioned two major catastrophic rock failures caused by sliding and failure of discontinuities. Due to this significant impact on overall stability of the rock structure, a considerable volume of study has been carried out in the past by different researchers to understand the mechanical behaviour of rock joints under monotonic loading. Following these studies, a number of different model types have been proposed in the literature to deal with the monotonic loading shear behaviour of rock joints (Patton 1966; Ladanyi and Archambault 1969; Barton 1973; 1976; Seidel and Haberfield 1995*a*; Indrarata and Haque 2000).

Hutson and Dowding (1990) and Yang and Chiang (2000) stated the need to evaluate dynamic stability of rock structures due to an increased concern for earthquakes and explosion safety of critical military and civilian facilities such as nuclear power plants and waste repositories.

When a seismic event for example earthquake or explosion occurs, energy is transferred to the surrounding rocks. Initially, the pressure of the seismic wave is higher than the compressive strength of the rocks adjacent to the source of shaking and the rocks are crushed. As the wave travels away from the source, its energy is being attenuated and becomes less than the limit required to destroy the rocks. After this stage, the wave travels through the rocks without breaking them.

The waves generated during a seismic event exert cyclic loading to the rock structures in the proximity of active seismic zones. Although underground excavations may be more resilient to seismic movements when compared with the ground surface structures, they are still subject to damage and potential failure (Ma and Brady 1999). When a joint set is loaded or unloaded during a seismic event, it may undergo a sequence of cyclic loading shearing. During strong earthquakes, the sequence of cyclic loading is accompanied by relatively large shear displacements that degrade asperities along the joint surface (Jafari *et al.*, 2004). Due to the asperity damage, the mechanical parameters of rock joints including the effective normal stress, friction angle and dilation angle, are affected resulting in different shear behaviour to that observed under monotonic loading. This emphasises the need for a better understanding of shear behaviour of rock joints under cyclic loading to design safe rock structures close to the active seismic zones.

1.3. Background to the study

In the study of shear behaviour of rock joints, loading conditions are divided into two main categories: monotonic and cyclic. Models developed for monotonic loading conditions can be used only to conduct static stability analysis of geo-structures, since they do not take into account the effects of cyclic shear displacement on the asperity surface. When dynamic stability analysis is desired, models describing shear behaviour under cyclic loading must be used. These models consider the reduction in shear strength and decay of the asperity surface during shear displacement.

By representing joint shearing as an interaction between two media, Plesha (1987) introduced a softening cyclic loading model by assuming sliding mechanism along an inclined asperity angle degraded exponentially due to a portion of the plastic shear work. The analytical model of Plesha (1987) was further verified by Hutson and Dowding (1990) under constant normal load (CNL) conditions in which the normal load remains constant during shearing. The original model of Plesha (1987) was later revised to represent sinusoidal asperities and to include the second order asperity effects (Qiu and Plesha 1991; Lee *et al.,* 2001). In another study, Jafari *et al.,* (2003) performed a series of cyclic loading shear tests on undulated joints under CNL conditions for different applied normal stresses and suggested an empirical relationship for the variation of peak shear strength against the number of loading cycles. Other studies on shear behaviour of rock joints under cyclic loading and CNL conditions were carried out by Aubry *et al.,* (1990), Huang *et al.,* (1993), Souley *et al.,* (1995), Dong and Pan (1996), Fox *et al.,* (1998), Stupkiewicz and Mróz (2001) and Puntel *et al.,* (2006). All these studies were performed under the conventional CNL conditions and not under

Constant Normal Stiffness (CNS) conditions to imitate the stiffness of the surrounding media.

The importance of CNS conditions to simulate the actual shear behaviour in the field under monotonic loading has been described by Johnston and Lam (1989), Skinas *et al.,* (1990) and Indraratna *et al.,* (1998). For a joint with a rough surface, dilation is observed during shearing as one asperity rides over another. If the stiffness of the surrounding rock mass restricts the dilation, the normal stress acting on the joint surface will inevitably increase. This affects the external energy exerted on asperities and as a result increases the asperity damage which is an important factor in the cyclic loading shearing of rock joints. Therefore, the CNS conditions should be incorporated in circumstances where the normal stress in the field changes considerably during shearing such as in the case of underground excavations.

Following investigation in the literature, it was revealed that only limited systematic studies are available for the effects of normal stiffness on the shear behaviour of rock joints under cyclic loading. For instance, Belem *et al.,* (2007, 2009) proposed empirical degradation equations for undulated joints under CNS conditions. Therefore, the shear behaviour of rock joints under cyclic loading and CNS conditions has not been well understood.

Crawford and Curran (1981) carried out a series of experiments on artificial rock joints with various shear rates and normal stresses under CNL conditions. Based on the measured data, they concluded that the shear rate may influence shear strength of hard and soft rock joints differently. In another study on shear rate, Jafari *et al.,* (2004) verified the results of Crawford and Curran (1981) for shear rates between 0.05 mm/min and 0.4 mm/min under monotonic loading. In active seismic zones, the rate of joint

shearing might vary depending on the source of load and type of rocks around the excavation that influences the shear strength of rock joints under cyclic loading. Therefore, the effects of shear rate should be taken into account for stability analysis of underground structures subjected to seismic events.

The monotonic loading shear behaviour of infilled rock joints under both CNL and CNS conditions have been discussed by Ladanyi and Archambault (1977), Papaliangas *et al.,* (1990,1993), Phien-wej *et al.,* (1991), de Toledo and de Freitas (1993), Indraratna *et al.,* (1999), Oliveira (2009) and Oliveira and Indraratna (2010). According to Oliveira (2009), a very thin infill material may reduce the monotonic loading shear strength up to 50% compared to the strength of an equivalent clean (non-filled) joint. If the discontinuity walls are separated by infill material, the rock to rock contact will decrease and, therefore, the shear strength will decrease depending on the type and thickness of the infill. During shearing of infilled rock joints, the rock to rock contact may occur after squeezing the infill material. The degradation of asperities in the first cycle increases the ratio of infill thickness to asperity height for further shearing. Therefore, different shear behaviour under cyclic loading is expected for infilled rock joints rather than that under monotonic loading.

Despite the frequent occurrence of infilled rock joints, studies conducted on shear behaviour of rock joints under cyclic loading only focused on clean interfaces. As far as can be determined, no experimental data has been published in the literature on the influence of infill material on the shear strength of rock joints under cyclic loading and CNS conditions.

Accordingly, the research study reported in this thesis is intended to investigate the complex problem of shear behaviour of rock joints under cyclic loading. In particular,

an appropriate incremental constitutive model to predict the shear behaviour of clean rock joints under cyclic loading and CNS conditions along with an experimental relationship to account for the effects of shear rate are proposed. In addition, a mathematical model to represent the reduction in the shear strength of infilled rock joints with increase in the number of loading cycles is developed. The model captures measureable parameters such as the initial asperity angle, basic friction angle of the joint surface, friction angle of the infill material, ratio of infill thickness to asperity height and the number of loading cycles.

1.4. Key objectives

The main objective of this thesis is to explore the effects of cyclic loading on shear behaviour of rock joints under CNS conditions. This study also explains the effects of shear rate and infill material on shear behaviour of rock joints under cyclic loading. The key objectives of this thesis include:

- Critical literature reviews of the past research work on the area of shear behaviour of rock joints under CNL and CNS conditions. It includes the shear behaviour of rock joints under both monotonic and cyclic loading.
- Laboratory investigation of the shear behaviour of clean rock joints under cyclic loading and CNS conditions. Both triangular asperities and replicas of a field rock surface were tested.
- Limited laboratory study of the shear rate effects on shear behaviour of triangular joints under cyclic loading and CNS conditions.
- Laboratory investigation of shear behaviour of mixture of clay and sand infilled triangular joints under cyclic loading and CNS conditions.

- Development of an incremental constitutive model to predict the shear behaviour of clean rock joints under cyclic loading and CNS conditions. An experimental relationship is also proposed to consider the effects of shear rate on shear strength of clean rock joints under cyclic loading.
- Development of a mathematical model to predict the shear strength of infilled rock joints under cyclic loading and CNS conditions.
- Numerical modelling of shear behaviour of rock joints under cyclic loading and CNS conditions using Universal Distinct Element Code (UDEC). Moreover, stability analysis of an underground structure for clean and infilled joints subjected to seismic loading is conducted in UDEC.

1.5. Outline of the thesis

The thesis consists of eight chapters followed by a list of reference and appendices. The thesis is organized as follows:

This chapter presents a general introduction to the present research, background to the study and key objectives of the research. Chapter II contains a comprehensive literature review on the shear behaviour of clean rock joints under CNL and CNS conditions. It includes the past experimental work and models developed for the shear behaviour of clean rock joints under monotonic and cyclic loading.

Chapter III reviews the past research work on shear behaviour of infilled rock joints under CNL and CNS conditions. It contains the results of laboratory work and models available for describing the shear behaviour of infilled rock joints under monotonic loading.

Chapter IV presents the results of laboratory testing conducted on shear behaviour of clean rock joints under cyclic loading and CNS conditions. It discusses the details of large scale cyclic direct shear apparatus, sample preparation and experimental plan for studying the effects of cyclic loading on shear behaviour of clean rock joints. The shear behaviour of artificial triangular joints asperities inclined at 9.5° (Type I), 18.5° (Type II) and 26.5° (Type III) to the direction of shearing as well as replicas of a field asperity surface cast using high strength Plaster of Paris are investigated under cyclic loading and CNS conditions with initial normal stress levels ranging from 0.16 MPa to 2.5 MPa. In addition, the experimental results of cyclic loading direct shear tests for 100 consecutive loading cycles carried out on Type I asperity surface with shear rates of 5 mm/s and 20 mm/s are discussed. This investigates the effects of shear rate on shear behaviour of clean rock joints under cyclic loading and CNS conditions.

Chapter V is devoted to examining experimentally the shear behaviour of infilled rock joints under cyclic loading and CNS conditions. It contains the details of infill material, procedure of sample preparation and experimental plan applied in the study. The interpretation of experimental results including shear stress - shear displacement, normal stress – shear displacement and normal displacement - shear displacement are provided.

Chapter VI proposes an incremental elasto-plastic constitutive model for shear behaviour of clean rock joints under cyclic loading and CNS conditions. The model is developed by capturing the contribution of asperity damage in the shear strength of the first forward shear cycle where degradation is maximum followed by a sliding mechanism for further shearing. Moreover, an empirical relationship is proposed to account for the effects of shear rate on shear behaviour of clean rock joints under cyclic

loading. The concept of Normalised Cyclic Strength Reduction of infilled joints ($NCSR^i$) is introduced to simulate the reduction in the shear strength of infilled rock joints with increase in the number of loading cycles.

Chapter VII presents the numerical simulation of shear behaviour of clean rock joints under cyclic loading and CNS conditions using current constitutive models available in UDEC. In addition, stability analysis of an underground structure subjected to seismic events is carried out for clean and infilled rock joints.

Chapter VIII provides a summary of the findings and conclusions of this research as well as recommendations for further studies.

Chapter II

2. LITERATURE REVIEW OF THE SHEAR BEHAVIOUR OF CLEAN ROCK JOINTS

2.1. Introduction

Rock masses are heterogeneous and often consist of joints and discontinuities, separating them into different blocks. When a rock mass is excavated, sliding along the joints may be experienced. The magnitude and direction of these movements is controlled by the shear behaviour of joints present within the rock mass.

Depending on the origin of joints and mineralogy of the rock, joints may have planar or rough surfaces. For planar (smooth) joints, the shear strength is equal to the frictional resistance only as there are no asperities. In the case of rough joints, an additional shear resistance is generated by the roughness of the joint surface. Moreover, in circumstances where the dilation is confined by the surrounding rocks, the increase in the normal stress due to overriding of asperities increases the joint shear strength.

2.2. Basic studies

One of the early researches on the monotonic loading shear behaviour of rough rock joints was carried out by Newland and Alley (1957) in which the joint shear strength (τ) is related to the normal stress (σ_n) as:

$$\tau = \sigma_n \tan(\varphi_b + i_0) \tag{2.1}$$

where, φ_b is the basic friction angle determined by tilt test on planar interface and i_0 is the mean slope of the asperities.

During earthquakes and blasting, cyclic loading shearing degrades the joint roughness. The asperity degradation also decreases the dilation magnitude and eventually reduces the normal stress acting on the joint surface. Thus, applying the monotonic loading models for shear strength of joints such as the one proposed by Newland and Alley (1957) in the stability analysis of underground structures (e.g. mining or civil excavations) subjected to seismic events, will overestimate the stability.

In order to consider degradation of asperities during shearing in cyclic loading, Plesha (1987) introduced a degradation equation as a function of the sliding plastic shear work as:

$$i = i_0 \exp(-C_d W_p) \tag{2.2a}$$

$$W_p = \int_o^{u_p} \tau du_p \tag{2.2b}$$

where, i is the dilation angle, C_d is the damage coefficient determined by fitting the exponential equation to the plot of normalised secant dilation angle (normalised to the initial asperity angle) versus sliding plastic shear work and u_p is the plastic shear displacement.

This chapter covers the important factors that control the shear behaviour of rock joints and models developed for describing shear behaviour of clean joints (non-filled joints) under monotonic and cyclic loading and Constant Normal Load (CNL) and Constant Normal Stiffness (CNS) conditions.

2.3. Factors controlling the shear behaviour of rock joints

Determining the shear strength of discontinuities is a crucial task of rock mechanics as only a small variation in the angle of friction of a discontinuity may considerably affect the stability of a rock structure.

According to the previous studies, some important factors that can influence the shear behaviour of joints can be classified as:

- Joint roughness
- Scale effects
- Boundary conditions
- Shear rate
- Pore water pressure
- Pre-loading (over closure)

2.3.1. Joint roughness

The friction angle (φ) and the shear strength (τ) depend on the surface roughness. To clarify this issue, a triangular joint that is inclined at an angle i_o from the direction of shearing subjected to shear (S) and normal (N) forces is considered as shown in Figure 2-1. If the joint degradation during shearing is neglected, the orientation of the resultant force (R) on the joint surface is inclined at an angle (90 - φ_b) from the shearing direction. Since the asperities are inclined at an angle i_o, the joint friction angle is (φ_b + i_o).

The real joints encountered in the field possess arbitrarily distributed roughness in three directions. Therefore, attempts have been made by researchers to properly quantify the joint roughness.

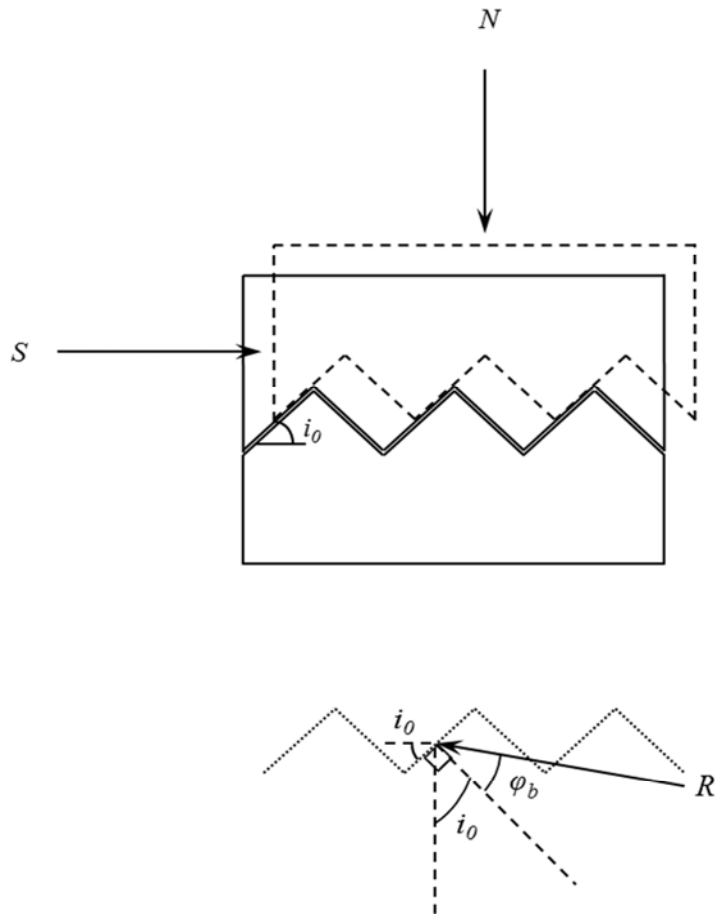

Figure 2-1 Triangular joint under shear and normal forces

2.3.1.1. Joint roughness coefficient

Barton (1973) proposed the concept of Joint Roughness Coefficient (*JRC*), the value of which is estimated by comparing visually the appearance of a discontinuity surface with the standard profiles, ranging from 0 to 20. Typical roughness profiles and corresponding *JRC* was presented by Barton and Choubey (1977) and is shown in Figure 2-2. An alternative method for estimating *JRC* by measuring the surface

roughness amplitude from a straight edge was later proposed by Barton and Bandis (1982), and is shown in Figure 2-3.

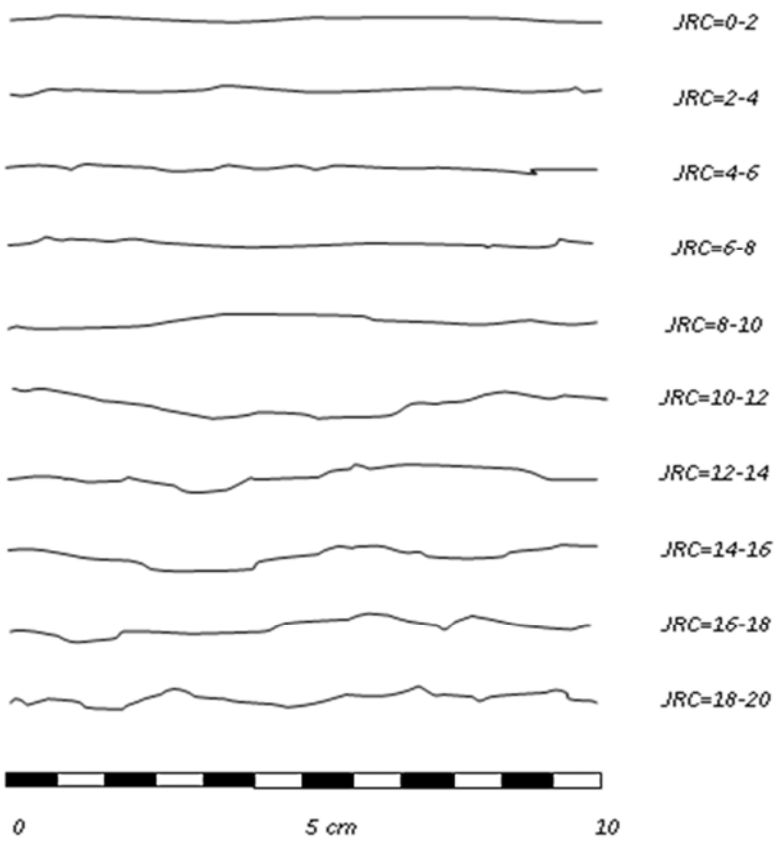

Figure 2-2 Roughness profiles and corresponding *JRC* values (after Barton and Choubey 1977)

The value of *JRC* can also be obtained by back calculation using the experimental data from the tilt tests on rough joints and saw cut rough surfaces, and the Schmidt Hammer Index test as:

$$JRC_n = \frac{\alpha^0 - \varphi_r}{\log_{10}\left(\frac{JCS_n}{\sigma_n}\right)} \tag{2.3a}$$

$$\varphi_r = (\varphi_b - 20) + 20\left(\frac{r}{R}\right) \tag{2.3b}$$

where, JRC_n is the *JRC* number, α^0 is the tilt angle, φ_r is the residual friction angle, JCS_n is the joint compressive strength (MPa) from Schmidt Hammer scaled for joint lengths > 10 cm, σ_n is in MPa, r is the Schmidt Hammer rebound on a wet joint surface and R is Schmidt Hammer rebound on a dry non-weathered sawn surface.

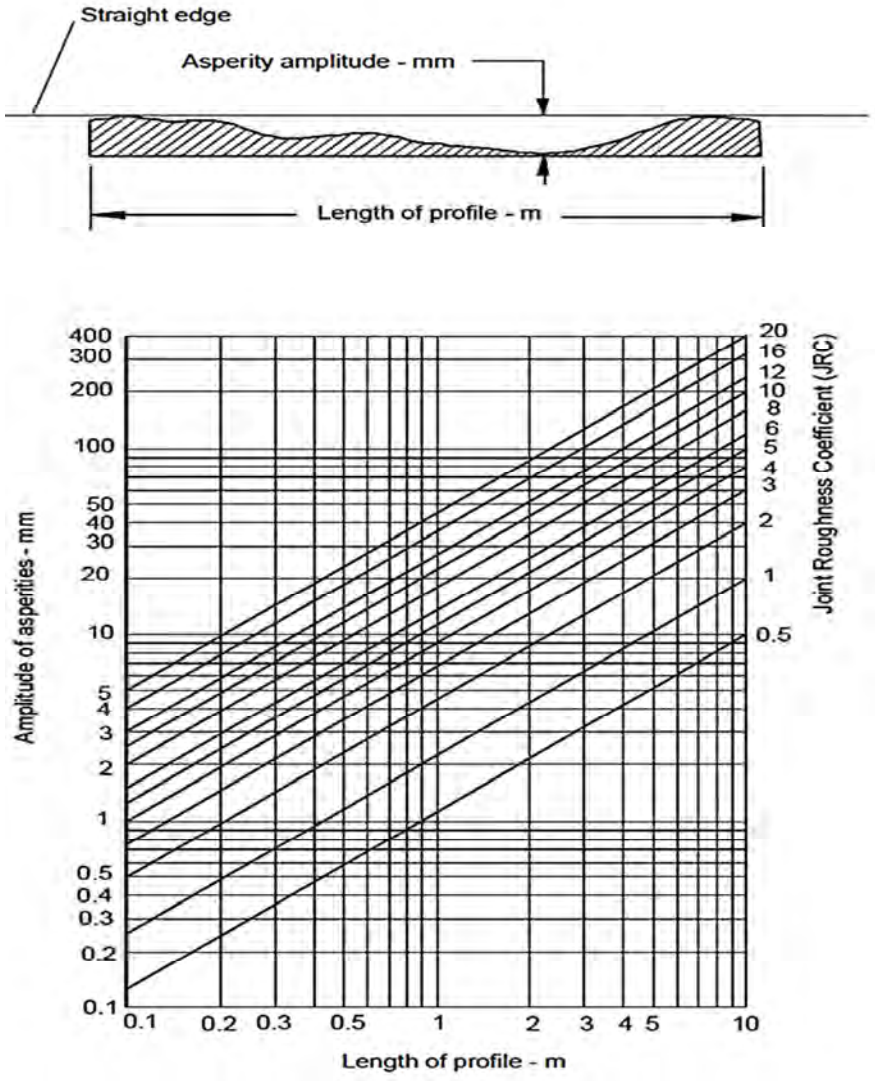

Figure 2-3 Estimating *JRC* from measurement of surface roughness amplitude from straight line (after Barton and Bandis 1982)

Tse and Cruden (1979) performed statistical studies and stated that the most correlated variables for description of surface roughness are the root mean square (*RMS*) of the first derivative of the profile Z_2 and the structure function *SF* given by:

$$Z_2=RMS\left(\frac{\Delta Z}{\Delta X}\right)=\frac{1}{L}\sqrt{\int_{X=0}^{X=L}\left(\frac{dZ}{dX}\right)^2}=\sqrt{\frac{1}{m(\Delta X)^2}\sum_{i=1}^{m}(Z_{i+1}-Z_i)^2} \tag{2.4a}$$

$$SF=\int_0^1 (f(x)-f(x+\Delta x))^2\,dx \tag{2.4b}$$

where, m is the number of measured points, Z is roughness amplitude about the centre line, Δx is the interval between amplitude reading, $f(x)$ is the roughness amplitude at a distance x along a profile of length L.

They proposed two equations for *JRC* according to Z_2 and *SF* as:

$$JRC = 32.69 + 32.98\log_{10}^{Z_2} \tag{2.5a}$$

$$JRC = 37.28 + 16.58\log_{10}^{SF} \tag{2.5b}$$

A simplified method to relate the *JRC* to the corresponding value of triangular asperity angle was proposed by Macksimovic (1996). Based on this method, the *JRC* value is equal to half of the initial asperity angle ($i_0/2$).

Graselli and Egger (2003) based on the extensive number of direct shear tests carried out on joint samples suggested the following relationship for estimating the value of *JRC* as:

$$JRC = \frac{\tan^{-1}\left\{\tan\left[\varphi_b + (\theta^*_{\max}/C)^{1.18\cos\alpha}\right]\left[1+e^{-(\theta^*_{\max}/9A_0C)(\sigma_n/\sigma_t)}\right]\right\}-\varphi_b}{\log_{10}^{(\sigma_c/\sigma_n)}} \tag{2.6}$$

where, θ^*_{max} is the maximum apparent dip angle of the surface with respect to the shear direction, C is the roughness parameter, α is the angle between schistosity plane and the

normal to the joint, A_0 is the maximum potential contact area for the specified shear direction, σ_t is the tensile strength and σ_c is the uniaxial compressive strength.

2.3.1.2. Fractal method

Seidel and Haberfield (1995*b*) applied the fractal method to characterize the joint surface. According to this theory, the mean angle statistic ($\bar{\theta}$) is related to the standard deviation of angle (S_Θ) by the relationship ($S_\theta = \sqrt{\frac{\pi}{2}}\left|\bar{\theta}\right|$), if the asperity angle follows a Gaussian distribution. The fractal dimension, standard deviation of angle and height of a joint profile of unit direct length can be defined as (Figure 2-4):

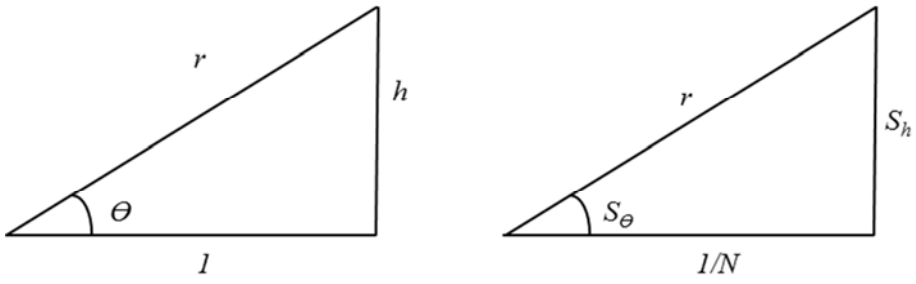

Figure 2-4 [left] Single chord geometry, [right] Definition of standard deviation of chord length (after Seidel and Haberfield 1995*b*)

$$S_\theta = \cos^{-1}(N^{(1-D)/D}) \tag{2.7a}$$

$$S_h \approx \sqrt{N^{-2/D} - N^{-2}} \tag{2.7b}$$

$$D \approx -\frac{\log(N)}{\log(S_h^2 + \frac{1}{N^2})^{1/2}} \tag{2.7c}$$

where, S_Θ is the standard deviation to angle, S_h is the standard deviation to height, D is the fractal dimension and N is the number of segments.

Seidel and Haberfield (1995*b*) proposed the standard deviation of height for k_{th} bisections applying the mid-point displacement method as ($N=2^k$):

$$S_{h,k} \approx L_d \sqrt{N^{-2(\frac{1+KD}{D})} - 2^{2k}} \tag{2.8}$$

The standard deviation of angle is obtained as:

$$S_{\theta,k} = \sqrt{K} S_{\theta,1} \approx \sqrt{k} \cos^{-1}(2^{\frac{1-D}{D}}) \tag{2.9}$$

Xie and Pariseau (1992) also applied the fractal method to define *JRC* value for saw tooth profiles as:

$$JRC = 85.27(D-1)^{0.57} \tag{2.10a}$$

$$D = \frac{\log(4)}{\log[2(1+\cos\tan^{-1}(\frac{2h}{L}))]} \tag{2.10b}$$

where, h is the average height of asperity and L is the average base length of asperities.

2.3.1.3. Spectral method

Durham and Bonner (1995) introduced a spectral method to characterize surface roughness of rock joints. According to this method, initially, the rock surface is digitized using profilometer by measuring coordinates (x,y,z) at any given points. Subsequently, an averaged value is taken for the Power Spectral Density (PSD) of each x,z profile digitized, to represent the entire joint surface by a single estimate. The PSD for each profile is calculated as:

$$G_i(f) = \frac{h^2}{L} |Z_i(f)|^2 \tag{2.11}$$

where, h is the sampling interval, L is length of the profile and $Z_i(f)$ is the fast Fourier transformation (FFT) of the discretely sampled profile.

2.3.1.4. Fourier transform method

The Fourier series is a mathematical technique, incorporated to solve a large variety of engineering problems, mainly adopting the principle of superposition for rigid body deformations. Applying the principle of superposition, a linear combination of sinusoidal solutions can be obtained, enabling Fourier functions to represent the roughness of a joint surface as:

$$h = \frac{a_0}{2} + \sum_{n=1}^{\infty}\left[a_n \cos(\frac{2\pi nX}{T}) + b_n \sin(\frac{2\pi nX}{T}) \right] \quad (2.12a)$$

$$a_n = \frac{2}{T}\int_a^b h \cos(\frac{2\pi nX}{T}) \quad (2.12b)$$

$$b_n = \frac{2}{T}\int_a^b h \sin(\frac{2\pi nX}{T}) \quad (2.12c)$$

where, h is the measured asperity height corresponding to X coordinate for (x,z) profile, a_n and b_n are Fourier coefficients, T is the asperity length, n is the number of harmonics and a and b are boundary limits.

The applications of Fourier series in characterizing joint roughness and describing the dilation of rock joints in relation to shear displacement have been discussed by Qiu and Plesha (1991) and Indraratna and Haque (2000).

2.3.1.5. Digital coordinate measuring machine

The digital Coordinate Measurement Machine (CMM) can be used to assess the roughness of joint profiles. The CMM consists of a set of probes and a microprocessor with the resolution of one micron.

The granite table is considered as the datum plane and the sample is placed on top of it. The surface profile of the joint is examined with respect to the datum plane. A digital coordinate measuring machine (CMM) and granite datum surface are shown in Figure 2-5.

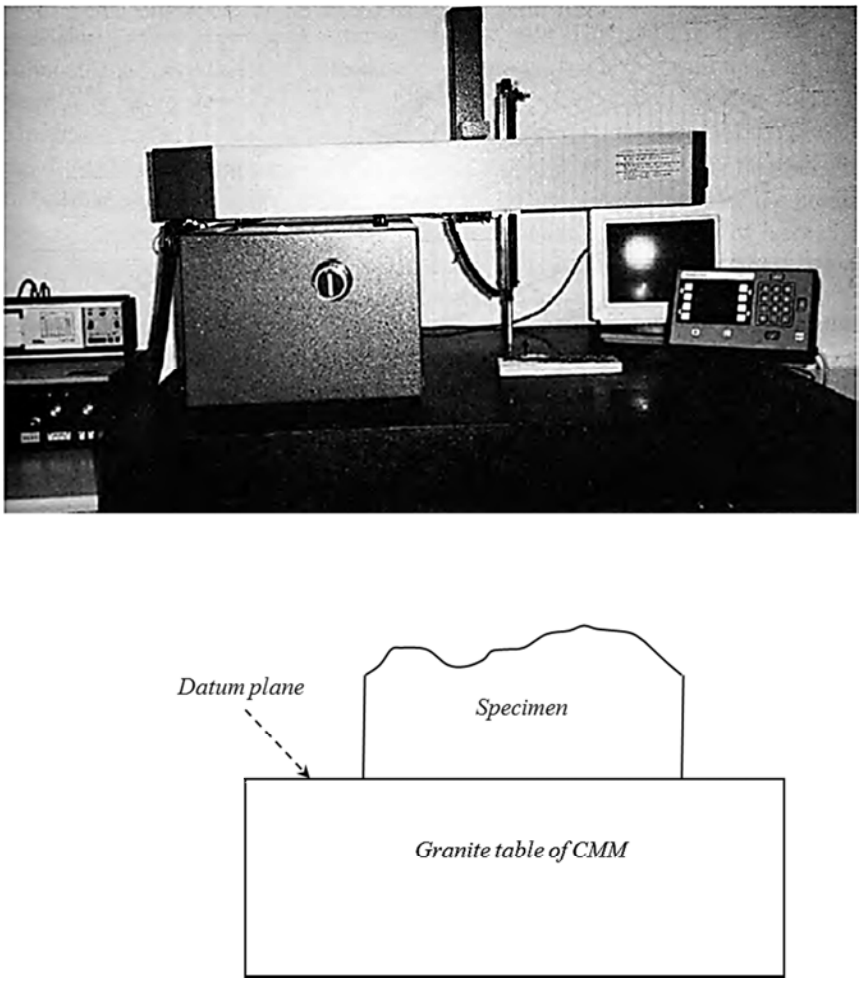

Figure 2-5 [up] Digital Coordinate Measuring Machine (CMM), [down] Datum surface of CMM (after Islam 1990)

2.3.2. Scale effects

The shear behaviour of dilatant joints is influenced noticeably with the change in scale of the sample. Barton *et al.*, (1985) studied the scale effects on the joint shear behaviour by performing direct shear tests, on replicas of different size, cast from various natural joint surfaces. They divided the larger samples into smaller sections to investigate the scale effect. It was observed:

- A gradual increase in the peak shear displacement with increase in the block size or joints length.
- Scale effects are more prominent in rough and undulating joints types.
- *JRC* and *JCS* reduce with increasing sample scale.

According to the experimental data, the following relationships were proposed to account for the scale effects on *JRC* and *JCS*:

$$JRC_n = JRC_0 \left[\frac{L_n}{L_0} \right]^{-0.02 JRC_0} \tag{2.13a}$$

$$JCS_n = JCS_0 \left[\frac{L_n}{L_0} \right]^{-0.03 JRC_0} \tag{2.13b}$$

where, JRC_n is the scaled *JRC*, JRC_0 is the *JRC* at laboratory scale, L_n is the length of the sample, L_0 is the laboratory sample length, JCS_n is the scaled joint compressive strength and JCS_0 is the *JCS* at laboratory scale.

In another study on the scale effects, Ohnishi and Yoshinaka (1992) reported that the scale effect is strongly related to regularity and irregularity of the joint surface. They concluded that joints consisting of different numbers of repeated pattern of size B mm

(Figure 2-6), are expected to show the same shear behaviour. However, if the specimen of size B is divided into smaller parts and tested, the scale effect will be observed.

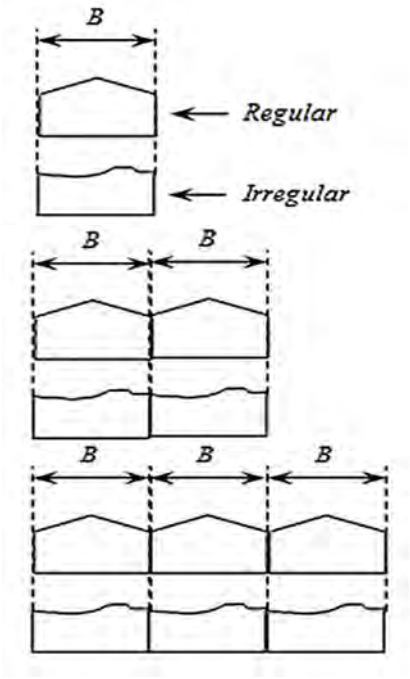

Figure 2-6 Repeated joint pattern of size B mm (after Ohnishi and Yoshinaka 1992)

Other studies on the scale effects have been carried out by Swan and Zongqi (1985) and Yoshinaka *et al.*, (1991).

2.3.3. Boundary conditions

If the joint surface is smooth enough and provides negligible dilation, then, the shear test under CNL conditions where the normal load acting on the joint surface is constant, is adequate to represent the shear behaviour. However, for rough discontinuities, the dilation is observed as asperities ride over each other. In this situation, if the surrounding rock mass cannot deform sufficiently, the normal load applied on the joint surface increases during shearing and the CNL can no longer simulate properly the boundary conditions. The mode of shear test in which the normal load changes due to

stiffness of the surrounding media is defined as the shearing under CNS conditions. The comparison between the asperity shearing under CNL and CNS conditions is shown schematically in Figure 2-7.

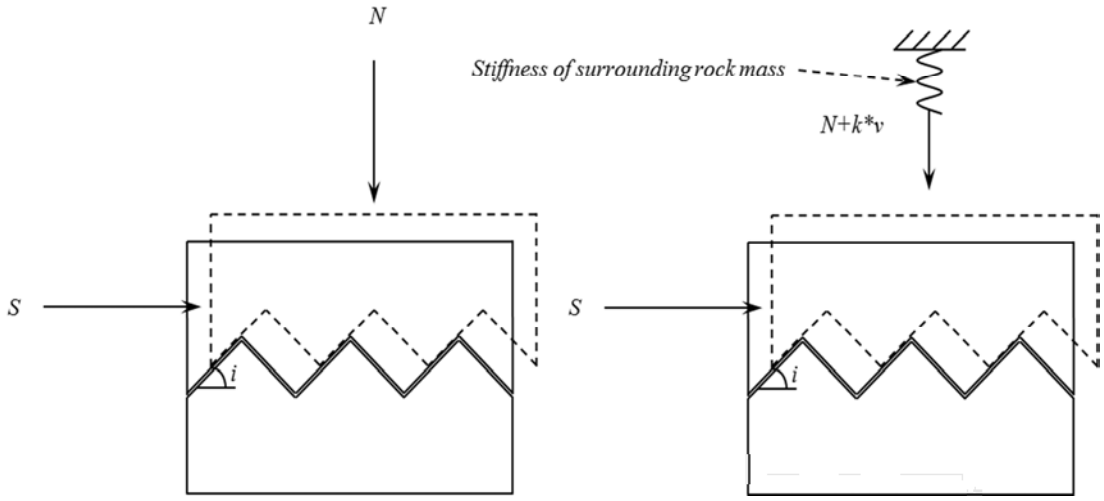

Figure 2-7 Comparison between asperity shearing under CNL and CNS conditions: [left] CNL conditions, [right] CNS conditions

In the above Figure, *k* and *v* are the boundary normal stiffness and normal displacement respectively.

Several authors have published experimental results of direct shear tests of joints under CNS conditions (Obert *et al.*, 1976; Goodman 1976; Leichnitz 1985; Benmokrane and Ballivy 1989; Van Sint Jan 1990; Ohnishi and Dharmaratne 1990; Benjelloun *et al.*, 1990). In particular, Johnston and Lam (1989), Skinas *et al.*, (1990) and Indraratna and Haque (2000) have described the importance of CNS conditions to replicate the actual shear behaviour in the field.

Skinas *et al.*, (1990) showed that an increase in the normal stiffness leads to an increase in the normal stress and a reduction in dilation. In addition, the peak shear strength was increased with increase in the normal stiffness.

Indraratna and Haque (2000) carried out experimental studies on idealised soft rock joints cast using low strength Plaster of Paris and tension joints. Samples were sheared under both CNL and CNS conditions with the constant normal stiffness value of 8.5 kN/mm. The comparison between the shear and dilation behaviours of soft triangular rock joints with 9.5º of asperity angle and tension joints under CNL and CNS conditions is shown in Figure 2-8.

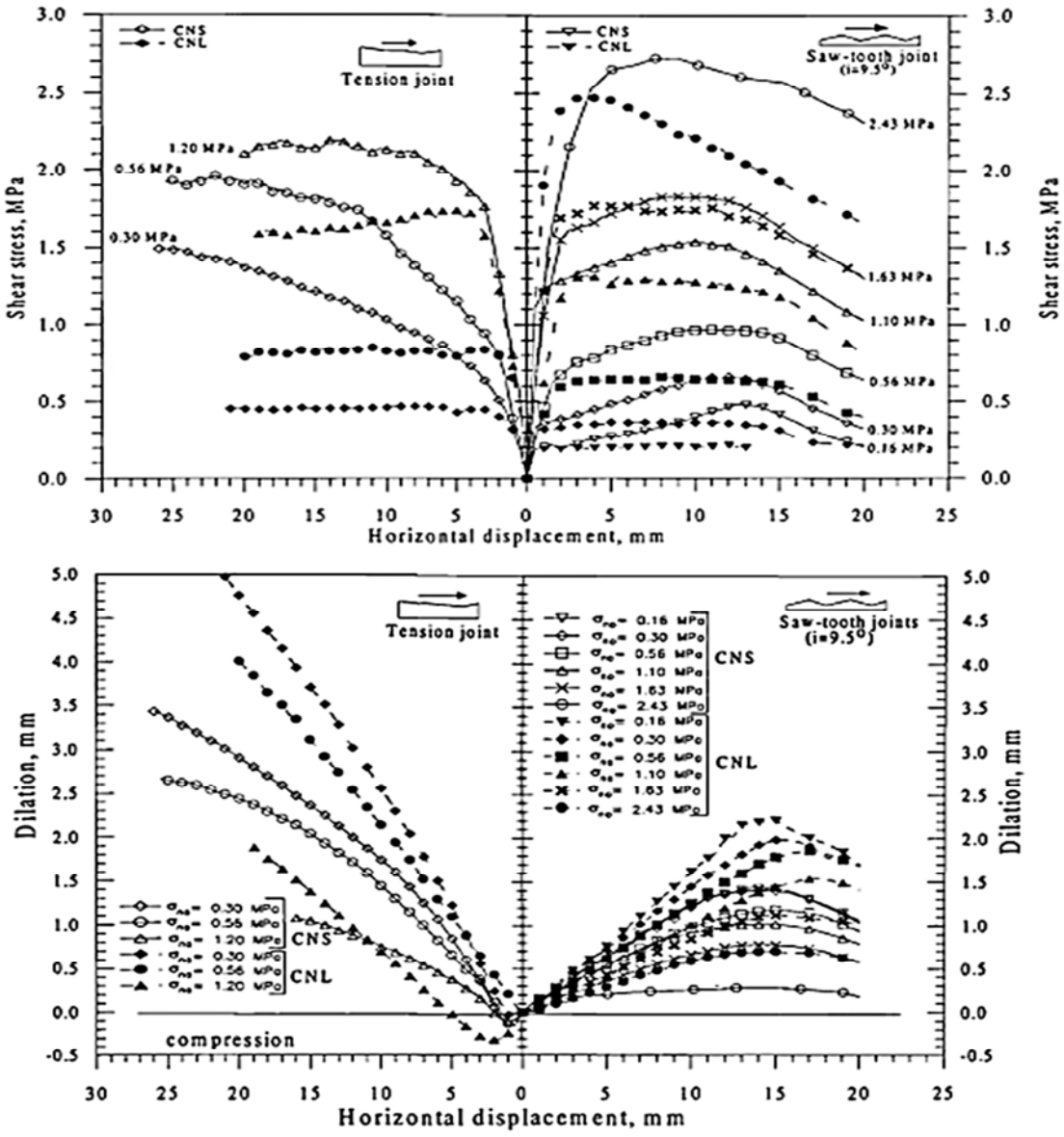

Figure 2-8 Shear behaviour of saw tooth and tension joints under CNL and CNS conditions (after Indraratna and Haque 2000)

According to the experimental studies, it was concluded:

- The CNL conditions underestimates the shear strength of the joints compared to those under CNS conditions.
- The values of dilation are higher under CNL conditions than those under CNS conditions.
- The shear displacement at peak shear strength is larger under CNS conditions than under CNL conditions.
- The peak friction angle obtained under CNS conditions is always lower than under CNL conditions.
- The CNS peak shear strength envelope appears linear unlike the shear strength envelope under CNL conditions which can be described by a bi-linear relationship. For higher roughness, the CNS strength envelope appears to deviate from the linearity.

Similar conclusions discussed here have been reported by Goodman (1976), Leichnitz (1985), Ohnishi and Dharmaratne (1990) and Van Sint Jan (1990).

2.3.4. Shear rate

Crawford and Curran (1981) investigated the effect of shear rate on shear behaviour of soft and hard rock joints by performing direct shear tests with shear rates of 0.05-50 mm/s under CNL conditions. They conducted the tests on the samples with normal stress ranging from 0.62 MPa to 2.78 MPa. The results indicated that the shear rate may influence the shear strength of hard and soft rock joints differently. In general, the shear strength of hard rock joints decreased with increase in the shear rate. In contrast, the frictional resistance increases up to a critical shear displacement for softer rock joints

with increase in the shear rate, but remains unaffected thereafter. In another study on shear rate, Jafari *et al.,* (2004) verified the results of Crawford and Curran (1981) for shear rates between 0.05 mm/min and 0.4 mm/min for harder joints.

Indraratna and Haque (2000) studied the shear behaviour of triangular soft rock joints with various shear rates ranging from 0.35 mm/min to 1.67 mm/min under CNS conditions. Tests were performed with 0.56 MPa of initial normal stress and 18.5º of asperity angle. The value of normal stiffness was set to 8.5 kN/mm. It was observed that the peak shear strength increases with increase in the shear rate.

2.3.5. Pore water pressure

The water pressure in a joint directly counteracts the effective normal stress acting on the joint. During shearing and in an undrained conditions, water pressure may either increase or decrease depending on the joint deformation. The water pressure in a joint will drop if the joint aperture increases due to asperity overriding. In contrast, if aperture decreases due to contraction behaviour of joint undergone shearing, the water pressure will increase.

According to Goodman and Ohnishi (1973), the safety of rock structures in jointed rock mass such as various dams, powerhouse excavations and underground reservoirs is influenced by the change in the pore water pressure of the joints. Goodman and Ohnishi (1973) studied the effect of pore water pressure on the mechanical behaviour of joints and stated:

- The shear strength of joint decreases as pore pressure increases in accordance with the effective stress principle.

- At a low confining pressure, the induced pressure becomes negative at peak load for rough joints, but remains positive at high confining pressure.
- For rough joints, the water pressure drops after slip initiation as aperture increases.

Archambault *et al.,* (1998, 1999) investigated experimentally the pore pressure in an undrained triaxial shearing of intact and jointed rock samples. They reported that during the friction mobilisation phase, the application of deviator stress increases the pore water pressure. Subsequently, the pore water pressure starts to decrease progressively as roughness is mobilised. Moreover, the increase or decrease in excess pore water pressure depends on the roughness morphology.

2.3.6. Pre-loading (over-closure)

Barton (1973) accidentally preloaded a joint sample to the maximum load capacity of a testing machine and observed that the sample could not even be sheared at a reduced normal load. In jointed rocks when the rock matrix is mostly deformed elastically, the non-planar discontinuities may become over-closed. When field rock joints are taken to be tested in shear, there might be a sample disturbance that destroys the over-closure effect. In order to recover the over-closure, the sample should be preloaded to the maximum normal load experienced in the field, before shear testing.

Barton (1973) investigated the effect of over-closure on shear behaviour of rock joints with over-closure ratios (preloaded normal stress to loaded normal stress) of 1, 4 and 8. It was observed that the friction angle was increased by approximately 5º and 10º when the over-closure ratio increased from 1 to 4 and from 1 to 8, respectively. Larger

dilation angles for peak shear strength were also measured for higher over-closure ratios.

Babanouri *et al.,* (2011) performed direct shear tests on replicas of real rock joints cast using Plaster of Paris for different over-closure ratios. They observed that the shear strength within a large range of roughness, joint wall strength and normal stress values, significantly increases with increasing over-closure ratios. An experimental relationship was also proposed to consider the over-closure effect on *JRC* as:

$$\frac{JRC_{OC}}{JRC_0} = 1 + \frac{\log(JOC)}{\log(\frac{JCS}{\sigma_n})} \tag{2.14}$$

where, JRC_{oc} and *JOC* are modified joint roughness coefficient and joint over-closure ratio respectively.

2.4. Models developed for shear behaviour of rock joints

A number of different model types have been proposed in the literature to deal with the shear behaviour of rock joints under monotonic loading and CNL and CNS conditions which are described below.

2.4.1. Mechanistically based models

Patton (1966) was among the first to study the shear behaviour of rock joints by conducting a series of experiments on regular tooth shape asperities under CNL conditions and proposed a bilinear shear strength criterion:

For asperity sliding:

$$\tau_p = \sigma_n \tan(\varphi_b + i_0) \tag{2.15a}$$

For asperity breakage:

$$\tau_p = \sigma_n \tan(\varphi_b) + c_0 \tag{2.15b}$$

where, τ_p is the peak shear strength and c_0 is the cohesion.

Jaeger (1971) replaced the bilinear relationship of Patton (1966) with a non-linear equation and introduced a new failure criterion as:

$$\tau_p = \sigma_n \tan(\varphi_b) + (1 - e^{-\frac{\sigma_n}{\sigma_*}})c_0 \tag{2.16}$$

where, σ_* is a transition stress that illustrates two mechanisms captured by Patton (19666) 's model.

Barton (1973) incorporated the concept of *JRC* and introduced a non-linear failure criterion based on the extensive direct shear tests conducted on real rock joints under CNL conditions as:

$$\tau_p = \sigma_n \tan\left[JRC \log\left(\frac{JCS}{\sigma_n} \right) + \varphi_r \right] \tag{2.17}$$

For non-weathered joints, the *JCS* value is equal to the uniaxial compressive strength of rock. The relevant value of *JCS* for weathered rocks can be measured by Schmidt's hammer applied directly to the exposed joint walls. The *JRC* value also represents roughness of the joint surface ranging from 0 to 20 determined as discussed in section

2.2.2.1. The comparison between the above mentioned three criteria is shown in Figure 2-9.

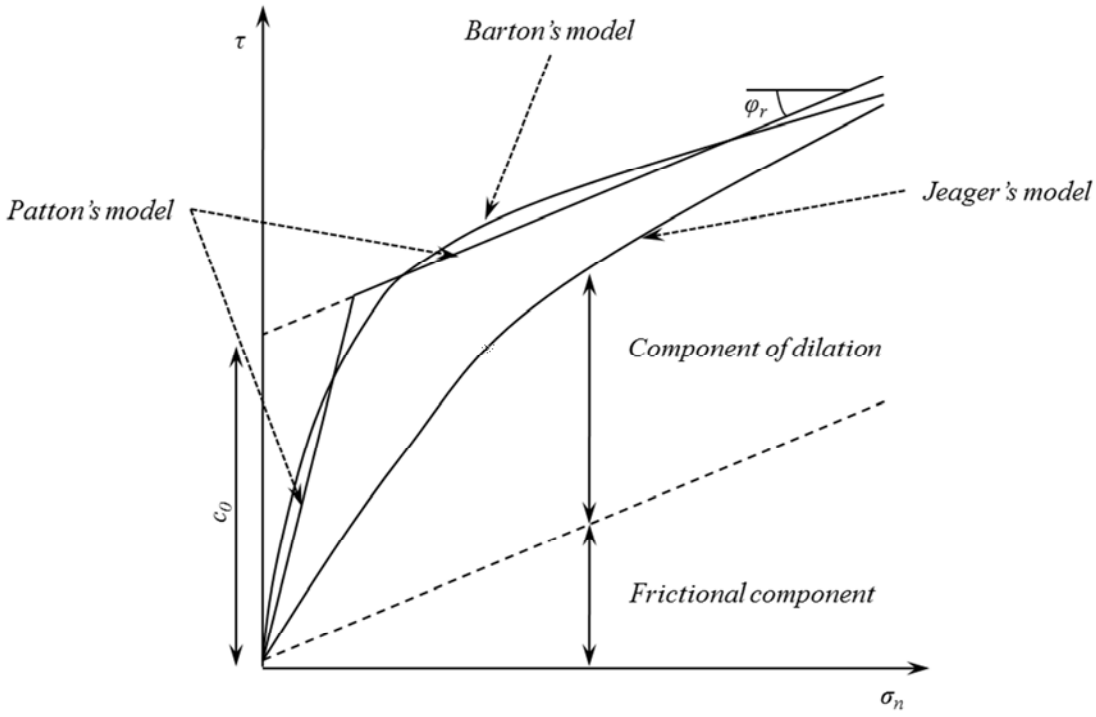

Figure 2-9 Comparison between shear strength criteria of rock joints

Barton (1976) presented a comprehensive model for the shear behaviour of rock joints under CNL conditions using the concept of Mobilised Joint Roughness Coefficient (JRC_m) to capture the effect of asperity degradation as a function of the normalised shear displacement. According to this model, the friction angle increases from the basic friction angle till peak value at peak shear strength and then diminishes along the post peak due to the asperity damage. Barton suggested that JRC_m should be equal to zero when the shear displacement is higher than 100 times of the peak shear displacement. The concept of JRC_m is shown schematically in Figure 2-10.

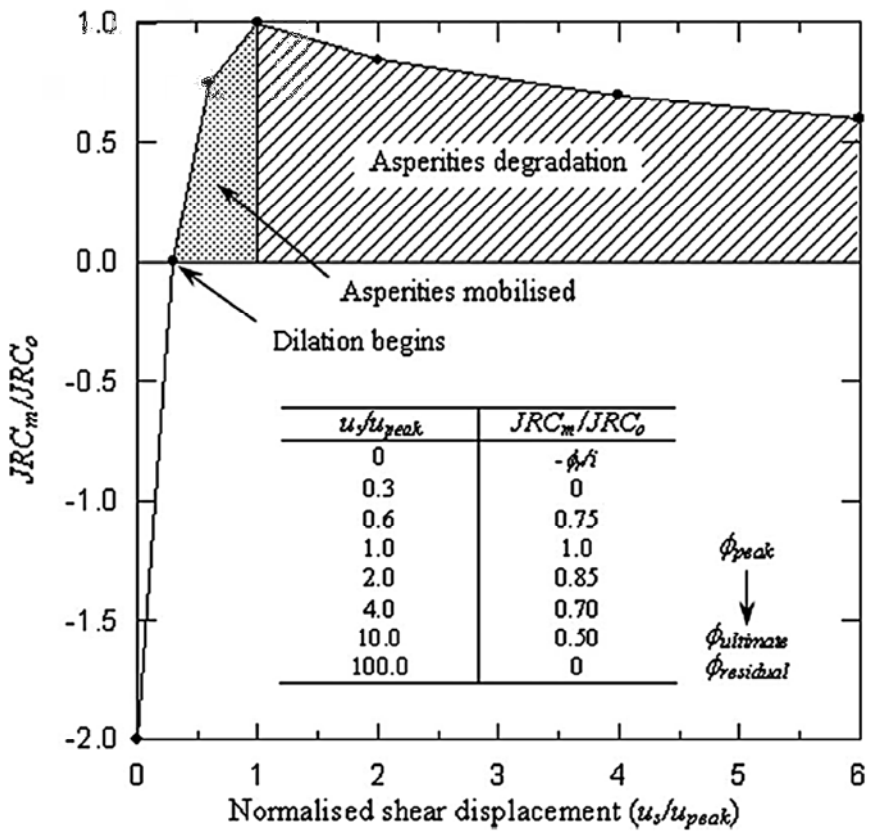

Figure 2-10 Dimensionless model for shear stress-shear displacement modelling (after Barton 1976)

In the Figure 2-10, u_s is the shear displacement and u_{peak} is the shear displacement at peak shear strength.

The magnitude of JRC_m also can be calculated from a measured shear stress - shear displacement curve as:

$$JRC_m = \frac{\tan^{-1}(\tau(u_s)/\sigma_n) - \varphi_r}{\log(JCS/\sigma_n)} \tag{2.18}$$

By reviewing a large number of shear tests data available in the literature Barton (1976) suggested the following relationship for the peak shear displacement as a function of the asperity length (L):

$$u_{peak} - = 0.004L^{0.6} \tag{2.19}$$

Bandis *et al.,* (1981) related the peak shear displacement to the *JRC* based on the analysis of the measured data as:

$$\frac{u_{peak}}{L} = \frac{1}{500}\left(\frac{JRC}{L}\right)^{0.33} \tag{2.20}$$

where, L is in metre.

The peak secant dilation angle ($d_{s,peak}$) and the peak dilation angle ($d_{t,peak}$) are defined as:

$$d_{s,peak} = \tan^{-1}\left(\frac{v_{peak}}{u_{peak}}\right) \tag{2.21a}$$

$$d_{t,peak} = \tan^{-1}\left(\frac{dv}{du}\right) \quad at \quad u = u_{peak} \tag{2.21b}$$

where, v_{peak} is the normal displacement at peak shear strength.

Barton and Choubey (1977) suggested the following relationships to estimate the peak tangent and secant dilation angles as:

$$d_{t,peak} = (1/M)JRC\log\left(\frac{JCS}{\sigma_n}\right) \tag{2.22a}$$

$$d_{s,peak} = (1/3)JRC\log\left(\frac{JCS}{\sigma_n}\right) \tag{2.22b}$$

where, M is the damage coefficient that takes value of 1 or 2 for shearing under low or high normal stresses respectively, or can be obtained from the following relationship:

$$M = \frac{JRC}{12\log(JCS/\sigma_n)} + 0.7 \tag{2.23}$$

In addition, the dilation starts at the onset of plastic deformation and dilation angle as a function of JRC_m can be calculated by:

$$d_{n,mob} = (1/M)\,JRC_m \log(\frac{JCS}{\sigma_n}) \tag{2.24}$$

Asadollahi and Tonon (2010) investigated Barton (1976)'s model and reported the following limitations in estimating the peak shear displacement, post-peak shear strength, dilation and surface degradation as:

- The peak shear displacement is independent of normal stress which is not consistent with experimental observations.
- The *JRC* value is suggested to be zero when shear displacement is greater than 100 times the peak shear displacement. This is only an approximation for the end of the shear stress - shear displacement curve.
- There is an inconsistency in term of roughness mobilisation for planar joints.
- The negative dilation up to one third of peak shear displacement is disregarded while many experimental studies showed that there is a contraction at small shear displacements.

Skinas *et al.*, (1990) incorporated the mobilised dilation concept of the *JRC-JCS* model of Barton (1976) and presented a joint model based on CNS conditions. The change in dilation with the change in shear displacement is defined by:

$$\Delta v = \Delta u \tan d_{n,mob} \tag{2.25}$$

where, $d_{n,mob}$ is described by Equation (2.24).

The dilation and corresponding normal stress of any point (e.g. point *Q* in Figure 2-11) with increment of shear displacement can be obtained as:

$$v_{i+1} = v_i^{/} + (u_{i+1} - u_i)\tan(d_{ni+1}) \tag{2.26a}$$

$$\sigma_{ni+1} = \sigma_{ni} + K(v_{i+1} - v_i) \tag{2.26b}$$

where, u_i is shear displacement.

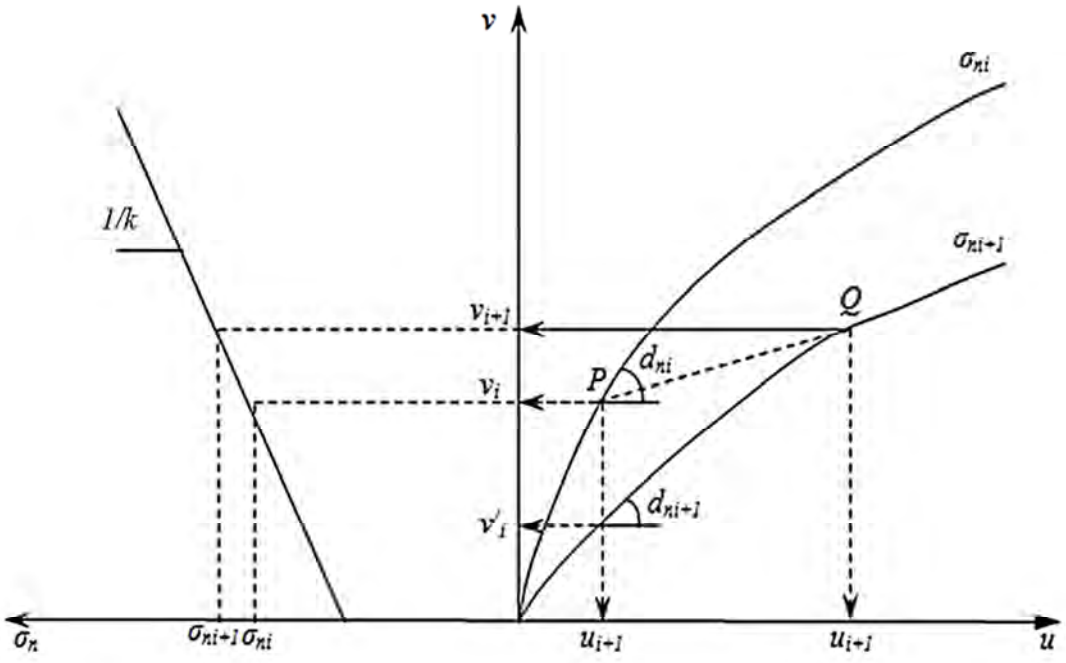

Figure 2-11 Calculation procedure for modelling dilation behaviour under CNS condition (after Skinas *et al*., 1990)

Applying the mobilised dilation concept, the above dilation equation can be rearranged as:

$$v_{i+1} = v_i^{/} + (u_{i+1} - u_i)\tan\left[\frac{1}{M} JRC_m^{u_i} \log(\frac{JCS}{\sigma_{ni+1}}) + \varphi_r\right] \tag{2.27}$$

By having the σ_{ni+1} and $JRC^{ui}{}_{m}$, the shear stress against shear displacement under CNS conditions is obtained as:

$$\tau = \sigma_{ni+1} \tan\left[JRC_m^{u_{i+1}} \log\left(\frac{JCS}{\sigma_{ni+1}}\right) + \varphi_r \right] \tag{2.28}$$

2.4.2. Mathematical models

Goodman (1976) proposed a model for the shear stress - shear displacement of rock joints under CNL conditions. In this model, the shear stiffness (k_s) and the slope of the post peak region were assumed to be independent of the normal stress applied on the joint surface. The relationships for shear strength are defined as:

$$\tau = k_s u \quad with \quad k_s = \frac{\tau_p}{u_p} \quad for \quad u < u_p \tag{2.29a}$$

$$\tau = \left(\frac{\tau_p - \tau_r}{u_p - u_r}\right) u + \left(\frac{\tau_r u_p - \tau_p u_r}{u_p - u_r}\right) \quad for \quad u_p < u < u_r \tag{2.29b}$$

$$\tau = \tau_r \quad for \quad u > u_r \tag{2.29c}$$

where, u_p is the peak shear displacement, τ_r is the residual shear strength and u_r is the residual shear displacement.

Heuze and Barbour (1982) proposed a three parameters model to describe the effect of joint dilation on the shear behaviour of rock joints. The model was introduced to predict the strength envelope below the uniaxial compressive strength beyond which no dilation was observed. In this model, the following relationships applied:

$$\tau_p = A\sigma_n + B\sigma_n^2 + C\sigma_n^3 \tag{2.30a}$$

$$A = \tan\varphi_p \tag{2.30b}$$

$$B = \frac{3C_p}{\sigma_c^2}\frac{2(\tan\varphi_p - \tan\varphi_r)}{\sigma_c} \tag{2.30c}$$

$$C = \frac{-2C_p}{\sigma_c^3}\frac{\tan\varphi_p - \tan\varphi_r}{\sigma_c^2} \tag{2.30d}$$

where, φ_p is the peak friction angle, φ_r is the residual friction angle, C_p is the cohesion at peak shear strength.

The instantaneous dilation angle is determined as:

$$\frac{d\tau}{d\sigma_n} = \tan(\varphi_r + \delta) \tag{2.31a}$$

$$\delta = \tan^{-1}(A + 2B\sigma_n + 3C\sigma_n^2) - \varphi_r \tag{2.31b}$$

When $\sigma_n > \sigma_c$ then the peak shear strength is obtained by:

$$\tau_p = \sigma_n \tan(\varphi_r) + C_p \tag{2.32a}$$

The residual shear strength also is given by:

$$\tau_r = \sigma_n \tan(\varphi_r) \tag{2.32b}$$

As the normal stress incorporated in the above equations needs to be indicated before evaluating the shear strength of dilatant joints, a conceptual incremental equation described in Figure 2-12 was presented as:

$$\Delta\sigma_n = \tan(\delta)\frac{KN.KNEFF}{KN + KNEFF}\Delta u \tag{2.33}$$

where, *KN* is the normal stiffness of the joint itself and *KNEFF* is the stiffness of the adjacent structure.

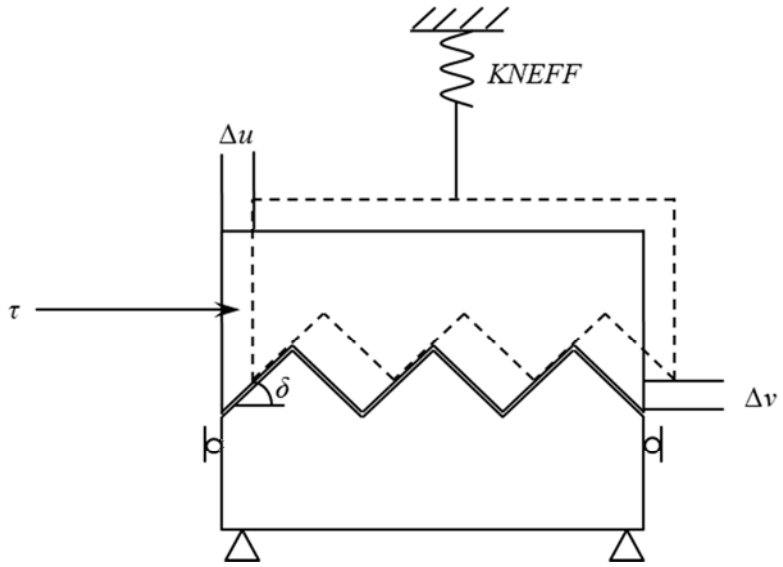

Figure 2-12 Conceptual model of a dilatant joint undergoing shear (after Heuze and Barbour 1982)

Gens *et al.*, (1990) developed a three dimensional elasto plastic constitutive model for rock joints under CNL conditions by considering a hyperbolic yield function as:

$$F = \tau_1^2 + \tau_2^2 - \tan^2 \varphi(\sigma_n^2 + 2a\sigma_n) \tag{2.34}$$

where, *F* is the yield function, *tan (φ)* and *a* are hardening parameters and subscripts *1* and *2* denote direction of shearing.

The variation of hardening parameters produces the corresponding family of yield surfaces. The hardening and softening of the model is controlled by a single internal variable (ζ) given by:

$$\zeta = \sqrt{\left(dv_1^p\right)^2 + \left(dv_2^p\right)^2} \tag{2.35}$$

where, dv_1^p and dv_2^p are the plastic tangential relative displacements.

A second degree parabola in the pre-peak range and a third degree polynomial after the peak were adopted to model the variations of hardening parameters with ξ as shown in Figure 2-13.

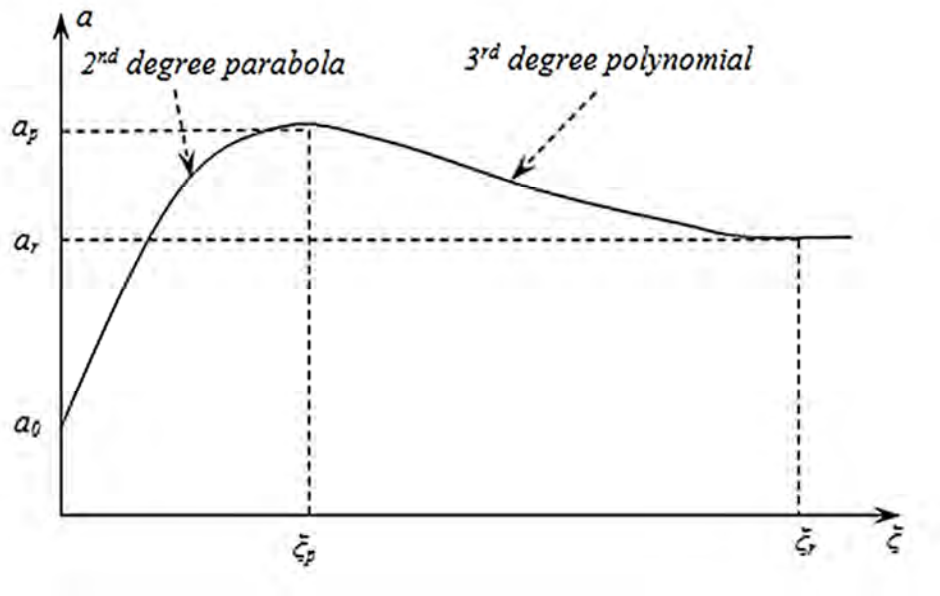

Figure 2-13 Hardening and softening law for parameter a (after Gens *et al.*, 1990)

In Figure 2-13, subscripts *p* and *r* denote peak and residual conditions respectively and superscript *0* shows the onset of plastic deformation.

The dilation angle was assumed to follow the same trend as the hardening parameter with ξ whereby the tangent of peak dilation angle (i_p) as a function of the normal stress is given by:

$$\tan(i_p) = \tan(i_p^0)(1-\frac{\sigma_n}{q_u})^4 \qquad (2.36)$$

where, i_p^0 is the peak dilatancy angle for zero applied compression and q_u is the unconfined compression strength of the rock.

Indraratna *et al.,* (1998) proposed a mathematical model to predict the shear strength of soft rock joints under CNS conditions as:

$$\frac{\tau_p}{\sigma_{n(CNS)}} = \tan\left[\varphi_b + i_0\left(1-\frac{\sigma_{n(CNS)}}{\sigma_c}\right)^{c_1}\right] \tag{2.37a}$$

$$\sigma_{n(CNS)} = \sigma_{n0} + kd_v / A \tag{2.37b}$$

$$d_v = c_2 a \exp(-c_3\sigma_{n0}) \tag{2.37c}$$

where, σ_{n0} is the initial normal stress, d_v is the dilation at peak shear strength, a is the initial asperity height and c_1, c_2, and c_3 are model coefficients determined experimentally.

Grasselli and Egger (2003) formulated a model to simulate the shear strength provided by the joint under CNL conditions at each state of displacement as:

$$\frac{\tau}{\sigma_n} = 0 \quad 0 \le u \le u_m \tag{2.38a}$$

$$\frac{\tau}{\sigma_n} = \frac{1}{\Delta u_p}\frac{\tau_p}{\sigma_n}(u-u_m) \quad u_m \le u \le u_p \tag{2.38b}$$

$$\frac{\tau}{\sigma_n} = \frac{\tau_r}{\sigma_n} + \frac{\tau_p-\tau_r}{\sigma_n}\frac{u_p}{u} \quad u > u_p \tag{2.38c}$$

where, u_m is the shear displacement necessary to mate the joint.

A visco-plastic multi laminate model for the shear behaviour of rock joints under CNL conditions was introduced by Roosta *et al.,* (2006). This model is based on the Mohr-Coulomb failure criterion with changing friction angle, cohesion and dilation angle as a

function of the plastic shear displacement or joint degradation. Yield functions in shear and tension at joint are defined as:

$$F = \tau - \sigma_n \tan(\varphi_m) - c_m \quad in \quad shear \tag{2.39a}$$

$$F = \sigma_n - \sigma^t \quad in \quad tension \tag{2.39b}$$

where, φ_m is the mobilised friction angle, c_m is the mobilised cohesion and σ^t is the tensile strength of rock joints.

Increasing or decreasing the mobilised cohesion or mobilised friction angle with plastic shear displacement leads to the hardening and softening phenomena. In order to model hardening behaviour the following relationship was proposed for the mobilised friction angle:

$$\varphi_m = \frac{2\sqrt{u^p \times u_p^p}}{u^p + u_p^p}(\sin(\varphi_p) - \sin(\varphi_0)) + \sin(\varphi_0) \quad u \le u_p \tag{2.40a}$$

where, u^p is the plastic shear displacement, $u_p{}^p$ is the plastic shear displacement at peak shear strength, φ_p is the friction angle at peak shear strength and φ_0 is the friction angle at onset of plastic deformation.

In softening part, a linear relationship was proposed to define the mobilised friction angle from the peak friction angle to the residual value.

Mobilised cohesion and tangent of mobilised dilation angle (ψ_m) as a function of the plastic shear displacement are given by:

$$c_m = c_0 \exp(-\lambda u^p) \tag{2.41a}$$

$$\tan(\psi_m) = \alpha u^{p} + \beta \qquad (2.41b)$$

where, c_0 is the value of cohesion at onset of plastic deformation, λ presents the rate of reduction in cohesion and α and β are parameters depending on the normal stress and joint roughness.

2.4.3. Graphical model

Saeb and Amadi (1990, 1992) emphasised that constant or variable boundary conditions are more likely to exist rather than CNL conditions and presented a graphical model to predict the shear behaviour of rock joints under any boundary conditions. This model relates the normal load - deformation response of a joint to its shear load - deformation and associated dilation behaviour. It is based on the response curves shown in Figure 2-14. The following remarks can be made about Figure 2-14:

- The curve $u = u_0$ which represents the joint under mated condition is identical to the joint closure against normal stress curve (Figure 2-14 *a*).
- Each curve $u = u_i$ represents the behaviour of the joint under normal loading after being mismatched by a shear displacement u_i.
- There is no further dilation for values of u larger than u_4 (Figure 2-14 *c*). Therefore, the joint response is admissible if it is contained in the domain limited by the curves $u = u_0$ and $u = u_4$.
- Since joint dilation decreases as normal stress increases, all curves $u = u_i$ (i = 1, 4) become closer to the curve $u = u_0$.

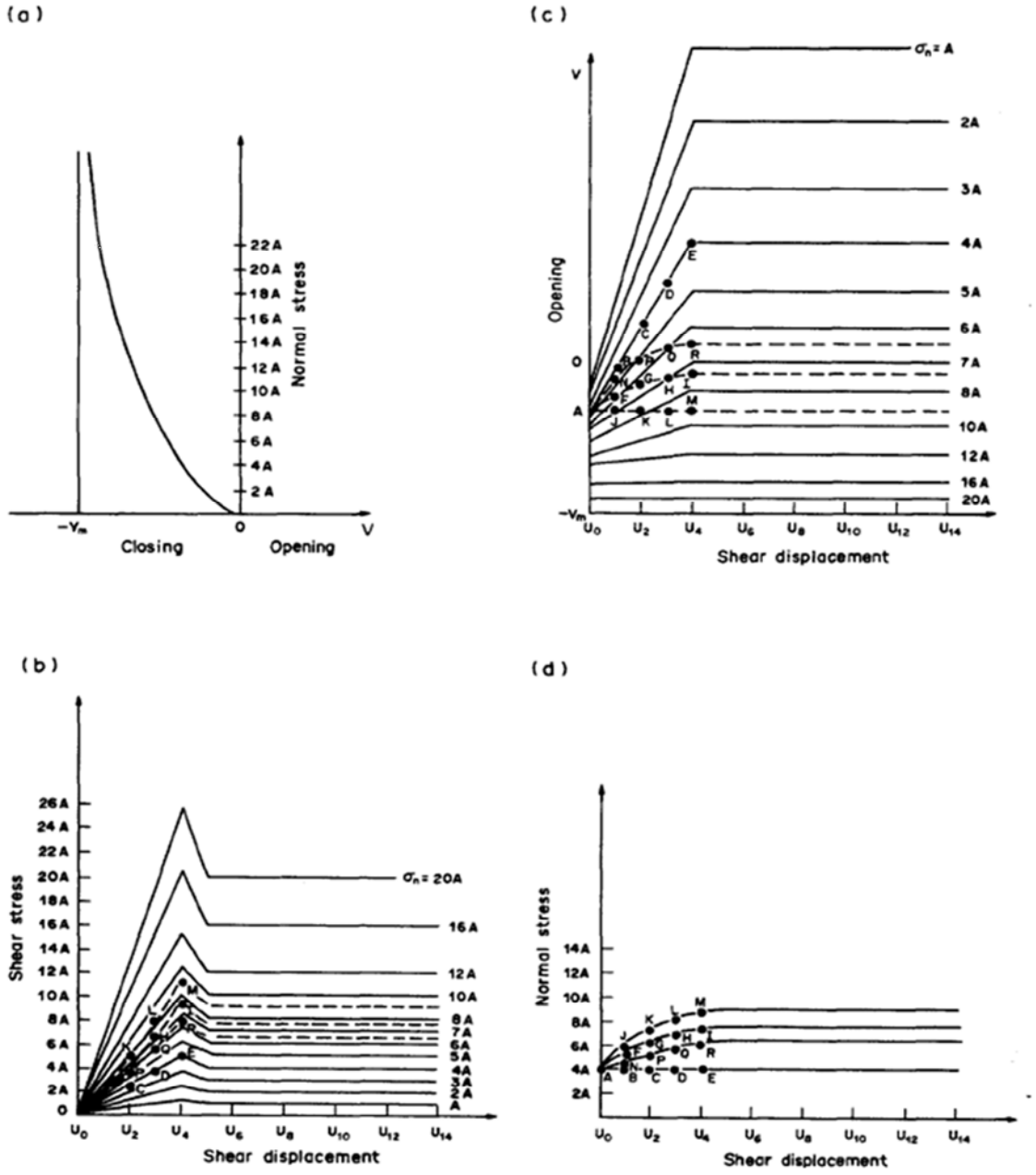

Figure 2-14 Joint response curve for normal stress ranging between 0 to 20A (after Saeb and Amadi 1990)

Figures 2-14 and 2-15 can be used to estimate the shear strength of rock joints for any load path. For instance, four distinct load paths are shown in Figure 2-14. These paths initiate from point *A* assuming that a normal stress of 4*A* was first applied without any shearing. Depending on the boundary conditions, the joint follows path *AFGHI* for a constant applied normal stiffness *k* and ABCDE for CNL conditions. It follows path

AJKLM when no change in joint normal displacement is allowed. Finally, path ANPQR corresponds to a joint in a rock mass with an increasing applied normal stiffness. By recording in Figure 2-15 the values of normal stress and *u* at the point of intersection of each path with curves u_i and using Figures 2-14 *b-c*, the shear stress against shear displacement for normal stress equal to 4*A* can be obtained. These curves are plotted as dashed lines in Figures 2-14 *b, c* and as solid lines in Figure 2-14 *d*, respectively.

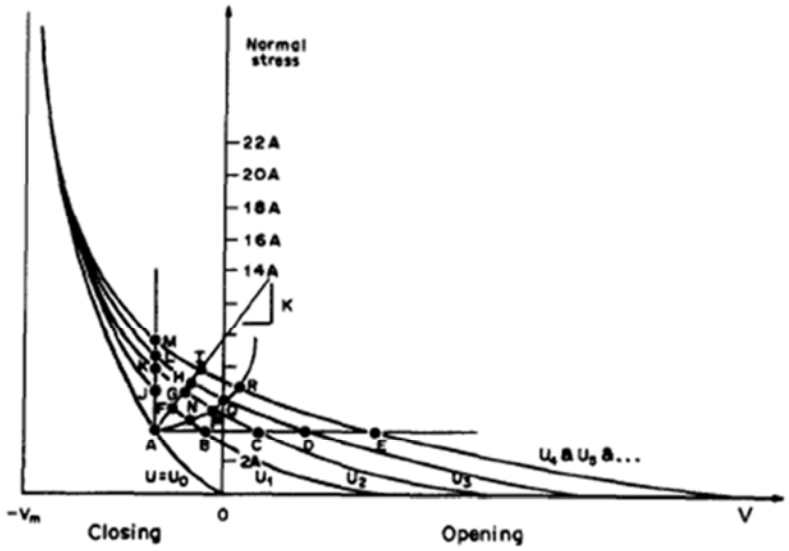

Figure 2-15 Normal stress against normal displacement curves at different shear displacement levels (after Saeb and Amadi 1990)

This model can be used to evaluate the shear strength of rock joints under CNS conditions by knowing its shear strength under CNL conditions.

2.4.4. Energy based models

Ladanyi and Archambault (1969) applied the energy balance theory to develop a general failure model for rock joints. According to these authors, in shearing of an indented surface if there is only sliding along asperities, the total shearing force (*S*) can be considered as a sum of three components:

$$S = S_1 + S_2 + S_3 \tag{2.42}$$

where, S_1 is the component due to external work done in dilating against the external force N, S_2 is the component due to additional internal work in friction due to dilation, and S_3 is the component due to work done in internal friction if sample did not change volume in shear.

The values of the three components from work equation and statical consideration can be defined as:

$$S_1 = Ni \tag{2.43a}$$

$$S_2 = S\tan(i)\tan(\varphi_b) \tag{2.43b}$$

$$S_3 = N\tan\varphi_b \tag{2.43c}$$

Another component (S_4) may be obtained as in the bilinear model of Patton (1966), if all the teeth are sheared off at the base as (i.e. asperity breakage):

$$S_4 = N\tan\varphi_{rock} + Ac_0 \tag{2.44}$$

where, φ_{rock} is the intact rock friction angle.

In shearing along irregular joint surfaces, both sliding and breakage mechanisms occur simultaneously, each covering its own portion of the total area, thus:

$$S = (S_1 + S_2 + S_3)(1 - a_s) + S_4(a_s) \tag{2.45a}$$

$$a_s = \frac{A_s}{A} \tag{2.45b}$$

where, A_s is the area of joint subjected to shearing.

Substituting in Equation (2.45*a*) for S_1 to S_4 according to Equation (2.44) and dividing all the forces to A, the shear strength criterion is obtained as:

$$\tau = \frac{\sigma_n(1-a_s)(\tan\varphi_b + \tan i) + a_s(\sigma_n \tan\varphi_{rock} + C_0)}{1-(1-a_s)\tan(i)\tan(\varphi_b)} \tag{2.46}$$

Johnston and Lam (1989) formulated an analytical method for the shear resistance of concrete/rock interface under CNS conditions. They considered the mobilised cohesion (C_m) for the penetration of the micro-asperities of concrete into the rock surface when the contact normal stress exceeds the uniaxial compressive strength as:

$$C_m = \frac{C_{sl}}{\pi}\cos^{-1}\left(1-\frac{2\sigma_n}{q_u}\right) \tag{2.47}$$

where, C_{si} is the cohesion of rock asperity sliding and q_u is the uniaxial compressive strength.

Applying the energy balance theory in a way similar to Ladanyi and Archambault (1969) and by modifying the additional work done in friction due to dilation to incorporate the mobilised cohesion, the following relationship was proposed to predict the average shear stress for sliding:

$$\tau_{sl}^{p} = (\sigma_{n0} + \Delta\sigma_n)\tan(i+\varphi_{sl}^{p}) + \frac{\pi C_{sl}}{2\pi\cos^2(i)(1-\tan(i)\tan(\varphi_{sl}^{p}))}\cos^{-1}\left(1-\frac{4\tau_{sl}^{p}\sin(i)\cos(i)}{\eta q_u}\right) \tag{2.48}$$

where, φ^{p}_{sl} is the peak friction angle in sliding and η is the interlocking factor.

The average shear stress at shearing to initiate a plane of weakness through asperities is obtained by:

$$\tau_{sh}^{p} = (\sigma_{n0} + \Delta\sigma)\tan(\theta_1 + \varphi_{sh}^{p}) + \frac{C_{sh}\eta\tan i}{\cos^2\theta_1(\tan i + \tan\theta_1)(1 - \tan(\theta_1)\tan(\varphi_{sh}^{p})} \quad (2.49)$$

where, θ_1 is the inclination of shear plane, φ^p_{sh} is the peak friction angle in shear, C_{sh} is the cohesion for shearing.

Once the shear plane is extended and displacement continues along the shear plane, the cohesion in the above equation is assigned to zero. The average shear strength relationship for subsequent extension of shear plane at different inclinations was also developed by Johnston and Lam (1989).

Haberfield and Johnston (1994) adopted the shear strength model described by Johnston and Lam (1989) and proposed a model for shear strength of irregular profiles. They defined the following roughness parameters obtained statistically as:

- i_m = mean chord inclination from the horizon.
- i_{sd} = standard deviation of chord inclination.
- h_m = mean chord height above a horizontal datum.
- h_{sd} = standard deviation of chord heights.

The distribution of normal force on the individual asperities is given by the following equation as:

$$N_j = n_j^r \cos i_j - s_j \sin i_j \quad (2.50)$$

where, N_j is the estimated normal force on asperity j, n^r_j is the rebound normal force for asperity j, s_j is the shear resistance on asperity j and i_j is the asperity angle of asperity j.

The value of s_j is obtained using the following equation as:

$$s_j = \frac{c_j L_j}{\cos i_j} + n_j^r \tan \varphi_j \tag{2.51}$$

where, c_j and φ_j are the cohesion and friction angle for sliding on asperity j.

The normal force N_j carried out by the j^{th} asperity is calculated considering the relative magnitude of deformation from one asperity to another one, using the following averaging process as:

$$\overline{N}_j = \frac{N_j}{\sum N_j} N \tag{2.52}$$

where, N is the actual total applied normal force on the joint.

If any asperity is sheared, then the normal force carried out by the asperity will be different from the above and is determined as:

$$\overline{N}_j^s = \frac{L_j}{\sum L_j} N \tag{2.53}$$

where, $\overline{N}_j^s$ is the normal force carried out by the j^{th} sheared asperities.

For the intact asperities, the normal force distribution is calculated as:

$$\overline{N}_j = \frac{N_j}{\sum N_j} (N - \sum \overline{N}_j^s) \tag{2.54}$$

where, $\sum \overline{N}_j^s$ is the total force carried out by the sheared asperities.

In this model, the displacements for irregular rock interfaces are estimated based on the method suggested by Milovic *et al.,* (1970) for the determination of vertical and horizontal displacements of a rigid infinite strip on a finite layer.

Seidel and Haberfield (1995*a*) showed that the Ladanyi and Archambault (1969) model would only hold true for elastic asperities, but for plastic shearing it underestimated the joint shear strength. By assuming the energy dissipated due to asperity damage to be equal with the inelastic work done due to dilation against the normal force (Figure 2-16), the energy balance theory as described by Ladanyi and Archambault (1969) was extended as:

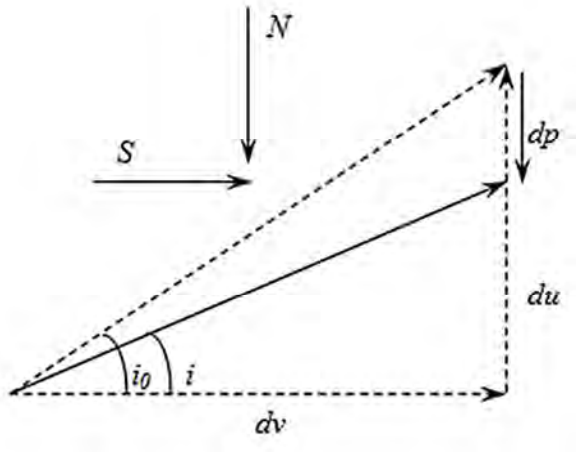

Figure 2-16 Deformation due to inelasticity (after Seidel and Haberfield 1995*a*)

$$S_1 = N\frac{(dv - dp)}{du} + N\frac{dp}{du} = N\tan i_0 \qquad (2.55a)$$

$$S_2 = S\tan(i)\tan(\varphi_b) \qquad (2.55b)$$

$$S_3 = N\tan\varphi_b \qquad (2.55c)$$

where, *Ndp* is the additional work required to increase the internal strain energy of the asperities.

Combining all these three components of work done, the following equation was introduced to relate the shear stress to normal stress as:

$$\tau = \frac{\sigma_n(\tan\varphi_b + \tan i_0)}{1-\tan(i)\tan(\varphi_b)} \tag{2.56}$$

Indraratna and Haque (2000) incorporated the Fourier series concept to describe the relationship between normal and shear displacement of undulated joints under CNS conditions, extending the energy based model proposed by Seidel and Haberfield (1995*a*) as:

$$\tau = (\sigma_{n0} + kv/A)\left[\frac{\tan\varphi_b + \tan i_0}{1-\tan\varphi_b + \tan i}\right] \tag{2.57a}$$

$$v = \frac{a_0}{2} + \sum_{n=1}^{\infty}\left[a_n\cos(\frac{2\pi nu}{T}) + b_n\sin(\frac{2\pi nu}{T})\right] \tag{2.57b}$$

$$i = \tan^{-1}(\frac{dv}{du}) \tag{2.57c}$$

where, a_n and b_n are coefficients found by performing conventional harmonic analysis of the Fourier series.

Oliveira and Indraratna (2010) revised the above model and presented a semi-empirical relationship for the shear strength of rock joints to describe better post peak behaviour as:

$$\tau = \sigma_n\left[\frac{\tan(\varphi_b) + \tan(i_d)}{1-\tan(\varphi_b)\tan(i)}\right] \tag{2.58a}$$

$$i_d = (i_0 - i)\exp\left[-\frac{(u_s - u_{peak})^2 JRC}{100ca^2}\right] + i \qquad (2.58b)$$

where, u_s is the accumulated shear displacement, u_{peak} is the peak shear displacement and c is the empirical constant determined by curve fitting.

2.5. Shear behaviour of rock joints under cyclic loading

Asperities are damaged and therefore degraded during shearing. In cyclic loading, asperities are further crushed and this may reduce the dilation angle and would likely decrease the shear strength.

The variation of shear displacement in a complete shear loading cycle against time of loading is depicted in Figure 2-17.

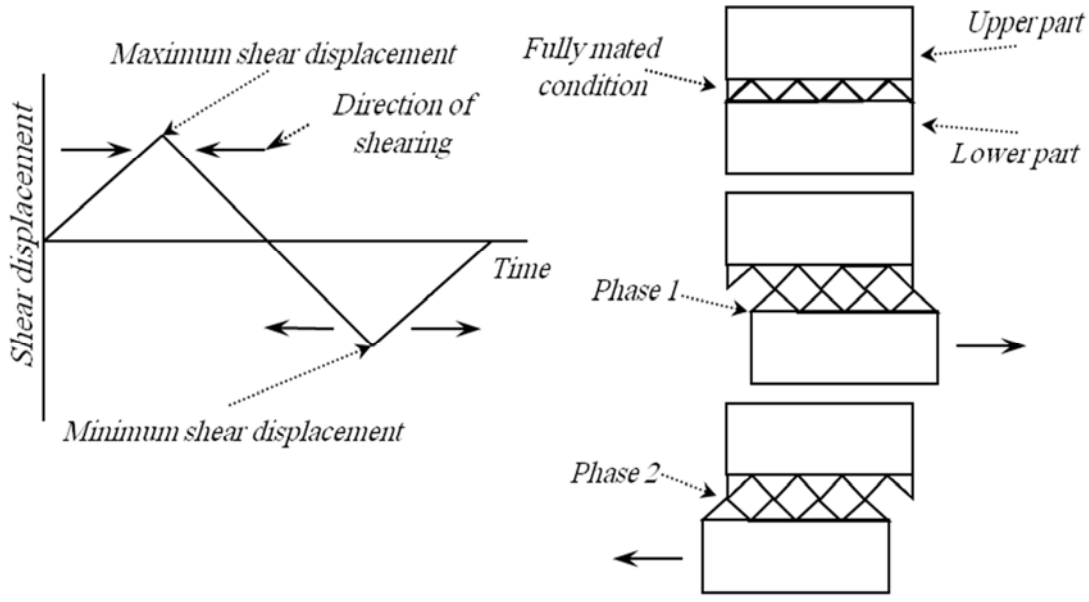

Figure 2-17 Variation of shear displacement in a complete loading cycle

As shown in Figure 2-17, in a cyclic test the lower specimen moves from its initial fully mated position to a positive maximum shear displacement (Phase 1), followed by a

shearing direction reversal in which the specimen reaches a negative maximum shear displacement in the opposite direction (Phase 2). The lower specimen returns to the fully mated condition in a complete cycle. The values of maximum and minimum shear displacements are the same in phases 1 and 2. In forward shearing, asperities override each other while in loading reversal asperities move toward the fully mated condition.

2.5.1. Experimental studies

Hutson and Dowding (1990) performed direct shear tests on sinusoidal joints under cyclic loading and CNL conditions. They reported when sliding occurs toward the asperity tips, the apparent coefficient of friction decreased visibly with each cycle due to asperity damage. In the downward sliding, however, the opposite was true. Higher asperity damage and eventually more suppression in the dilation component were observed for greater (σ_n/σ_c) ratios.

Huang *et al.*, (1993) carried out shear tests on artificial saw tooth shaped asperities moulded of hydro-stone and natural joints for various initial normal stresses under cyclic loading and CNL conditions. It was concluded that:

- For low values of initial normal stress, the normal displacement versus shear displacement responses indicated no apparent surface damage. In this condition, the shear strength gradually increased from a minimum value during the first cycle of shear displacement to a higher and more uniform value as cycling continued.
- For moderate compressive stress, the normal displacement versus shear displacement responses showed a substantial amount of surface damage in which the asperity slope significantly decreased. The shear stress against shear

displacement responses showed softening behaviour because of the reduced asperity orientation.

- At slightly higher compressive stress, after a limited number of loading cycles, the asperity surfaces were almost completely destroyed and the shear stress versus shear displacement responses were rather close to that of two apparently smooth surfaces.
- As expected, at high compressive stress, the surface damage was more aggressive and rapid.
- The asperity debris appeared to migrate from one side of an asperity through to the other depending on the shear direction.
- The shear behaviour of natural rock joints under cyclic loading was found to be similar to that of saw tooth shaped joints. However, the peak shear strength for natural rock joints in the first cycle was larger than those during the remainder of the shearing process and the stress softening behaviour was more pronounced. The shear strength during dilatant deformation increased from cycle to cycle rather than showing a reduction trend.

Jafari *et al.*, (2003) investigated experimentally the effects of small and large shear displacements on artificial saw toothed shape asperities and replicas of a rock surface under cyclic loading and CNL conditions. They related small and large shear displacements to small and strong earthquakes and expressed the following main conclusions:

- During cyclic loading, degradation of both first and second order asperities occurs, depending on the applied normal stress. In small earthquake and low amplitude cyclic loading, second order asperities are mainly affected,

but in strong earthquakes and high amplitude dynamic loading, both first and second order asperities may be damaged.

- The number of loading cycles and stress amplitudes are two main factors, controlling the shear behaviour of rock joints under cyclic loading.
- During large cyclic shear displacement, the shear strength of rock joints is affected by dilation angle, degradation of asperities and wearing.
- The shear strength of rock joints during sliding is in direct relationship with normal stress and may change from sliding to breakage during cyclic displacement.

Wibowo *et al.,* (1992) conducted a series of 5-cycle direct shear tests on replicas of a real asperity surface at size 15.24 cm ×7.62 cm ×7.62 cm cast gypsum cement (σ_c = 27.58 *MPa*) under CNL and CNS conditions. The initial normal stress of 2.26 MPa was applied during the test under CNL conditions. In CNS test, the stiffness of 25.86 kN/mm was considered to restrict the dilation. The comparison between shear behaviour of rock joints under CNL and CNS conditions is shown in Figure 2-18. The dilation was suppressed and shear strength increased as a result of the application of normal stiffness. The increase in shear strength was related to the increase in normal stress acting on the joint surface during the dilation stage. In reverse shearing, the shear behaviour under CNS conditions was close to that under CNL conditions as dilation was small, especially for later cycles.

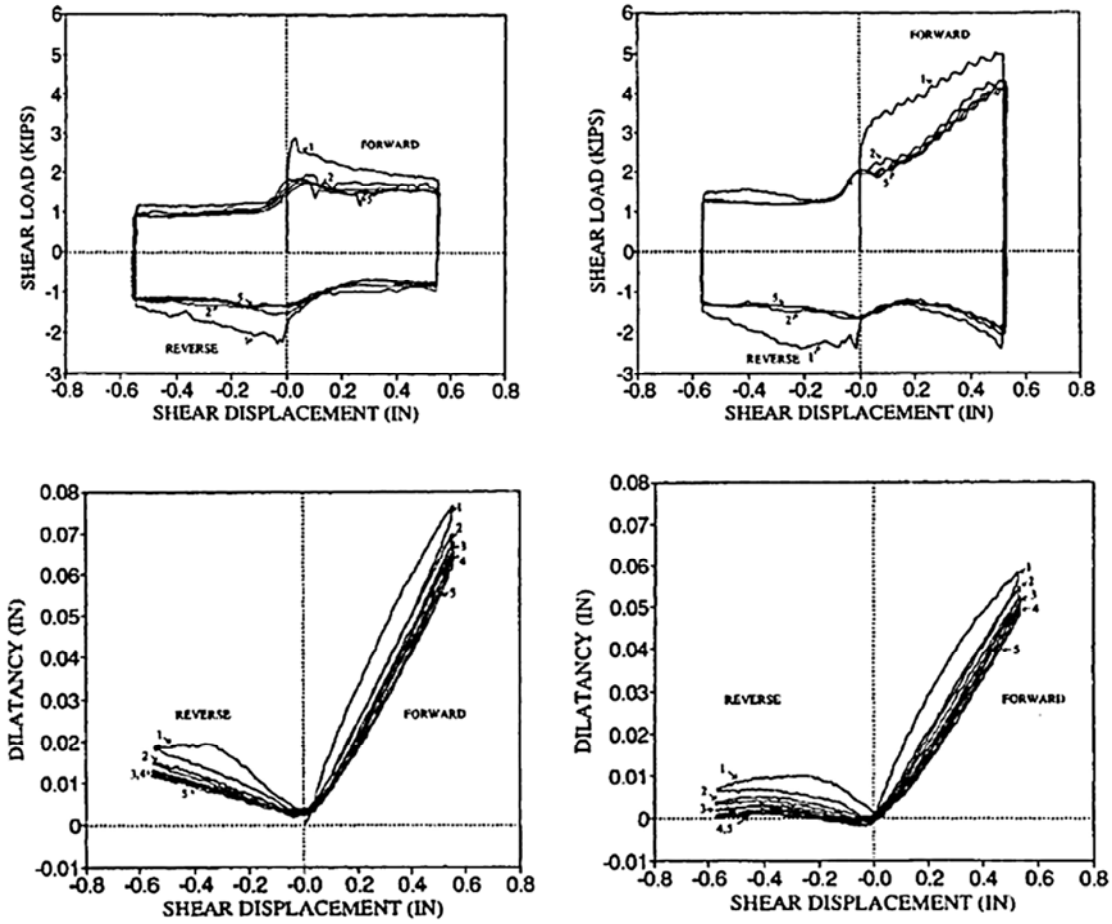

Figure 2-18 Comparison between shear behaviour of rock joints under CNL and CNS conditions: [left] Under CNL conditions, [right] Under CNS conditions (after Wibowo *et al*., 1992)

Different shear behaviour to those given by Hutson and Dowding (1990), Huang *et al.*, (1993) and Jafari *et al.*, (2003) was observed by Homand-Etienne *et al.*, (1999) for undulated artificial joints under cyclic loading and CNL and CNS conditions. The shear stress - shear displacement curves showed an increase of shear stress as a function of loading cycles while dilation decreased. The increase in the contact area due to asperity damage was suggested as the reason for the increase in shear strength with increase in loading cycles.

2.5.2. Models developed for shear behaviour of rock joints under cyclic loading

Models available in literature for the cyclic loading shear behaviour of rock joints can be categorised in two main groups: mechanistically based and mathematical models.

2.5.2.1. Mechanistically based models

An effective mechanical model for cyclic loading shear behaviour of rock joints was introduced by Plesha (1987). In this model, firstly, an interface with no undulating asperity (i.e. perfectly smooth) was considered. It was furthermore assumed that this smooth interface has Coulomb friction with no hardening or softening behaviour. In such an interface, the shear stress must satisfy the inequality:

$$|\tau| \leq -\tan(\varphi_b)\sigma_n \tag{2.59}$$

Corresponding to the above equation is the yield function:

$$F = |\tau| + \tan(\varphi_b)\sigma_n \tag{2.60}$$

The potential function, whose gradient gives the direction of the slip, is given by:

$$G = \tau \tag{2.61}$$

If the Coulomb function on the asperity surface is assumed, then Equations (2.60) and (2.61) for the yield function and plastic potential are applicable with τ and σ_n replaced by σ_1 and σ_2, respectively, where subscripts *1* and *2* denote the shear and normal directions to the active asperity surface as:

$$\sigma_1 = \frac{A}{A'}[\tau\cos i + \sigma_n \sin i] \tag{2.62a}$$

$$\sigma_2 = \frac{A}{A'}\left[-\tau \sin i + \sigma_n \cos i\right] \tag{2.62b}$$

where, A/A' is the ratio of the macroscopic contact area to the microscopic contact area which is shown in Figure 2-19.

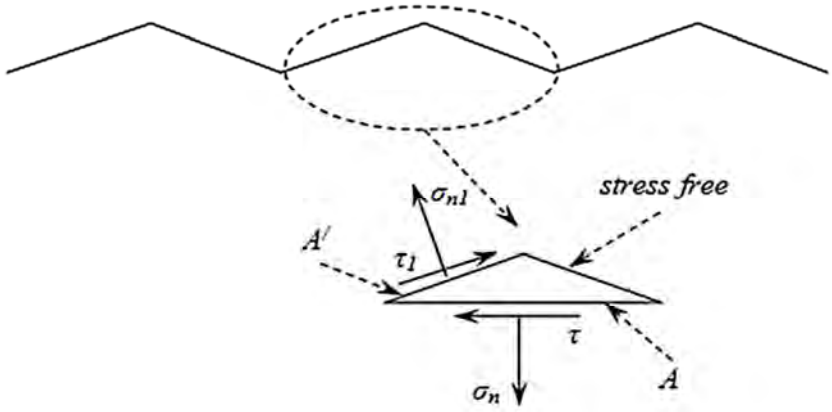

Figure 2-19 Stress diagram used for transformation between stresses (after Plesha 1987)

Combining Equations (2.62*a*) and (2.62*b*) with Equations (2.60) and (2.61) and dividing by the positive factor A/A':

$$F = \left|\sigma_n \sin i + \tau \cos i\right| + \tan(\varphi_b)\left[\sigma_n \cos i - \tau \sin i\right] \tag{2.63a}$$

$$G = \left|\sigma_n \sin i + \tau \cos i\right| \tag{2.63b}$$

A simple tribological model for asperity degradation was also proposed by assuming that degradation is a function of the sliding plastic tangential work (W_p) as:

$$i = i_0 \exp(-C_d \int_o^{u_p} \pi du_p) \tag{2.64}$$

In the above equation, the asperity behaviour is characterized as:

- Under high compressive stresses, high tangential stresses are required to produce slip and rapid asperity degradation.
- Under low compressive stresses, low tangential stresses will produce slip, yet if the amount of slip is large, then asperity degradation can occur from surface damage.

Therefore, if a particular degree of degradation is attained by a high amount of stress and low displacement, the same degree of degradation can be obtained at a lower stress level and a sufficiently large displacement.

Hutson and Dowding (1990) later performed shear tests on artificial sinusoidal joints under cyclic loading and CNL conditions and reported an empirical relationship for the damage coefficient introduced by Plesha (1987) as:

$$C_d = -0.141 i_0 \frac{\sigma_n}{\sigma_c} \tag{2.65}$$

Qiu and Plesha (1991) revised Plesha (1987)'s degradation model by representing surface roughness by sinusoidal asperities. The model considers the volume of damaged material produced during sliding and includes the possibilities of debris reattachment to the contact surface. The degradation equation based on the Fourier series was proposed as:

$$a_{l1} = \overline{a_{l1}} \exp(-C_{dl} W_p) \tag{2.66a}$$

$$a_{l0} = \overline{a_{10}} + \lambda \overline{a_{l1}} \left[1 - \exp(-C_{dl} W_p)\right] \tag{2.66b}$$

where, a_{l1} is the second order Fourier coefficient, a_{0l} is the first order Fourier coefficient, $\overline{a_{l1}}$ is the initial value of the second order Fourier coefficient, $\overline{a_{10}}$ is the

initial value of first order Fourier coefficient, λ is a parameter depends on the histories of σ_n and shear displacement and subscript *l* denotes lower block.

In the above equations, it was assumed that the asperity surface is characterized only by the first and second orders Fourier coefficients. Moreover, similar equations to those for lower block were proposed for the wear of upper block.

Jing *et al.*, (1993) investigated shear behaviour of rock joints under cyclic loading and CNL conditions and proposed a conceptual model based on Plesha (1987)'s damage law and empirical hardening and softening relationships. In another study, Jing *et al.*, (1994) extended the roughness degradation model of Plesha to a 3D form as:

$$\alpha_1 = \alpha_1^0 \exp\left[-D\left(\frac{\sigma_n}{\sigma_c}\right) W_p \left|\cos(\theta - \varphi)\right| \right] \tag{2.67a}$$

$$\alpha_2 = \alpha_2^0 \exp\left[-D\left(\frac{\sigma_n}{\sigma_c}\right) W_p \left|\cos(\theta - \varphi)\right| \right] \tag{2.67b}$$

where, α_1 and α_2 are the principal values of the asperity angle which also forms the major and minor semi-axes of the asperity ellipse, α^0_1 and α^0_2 are the initial values of α_1 and α_2, *D* is a material parameter, θ is the current shear direction, φ is the angle between the major axis and the local coordinate direction along the strike of the joints.

Dong and Pan (1996) presented a model that considers the contact structure within the rock joint as a multi-level hierarchical system as shown in Figure 2-20.

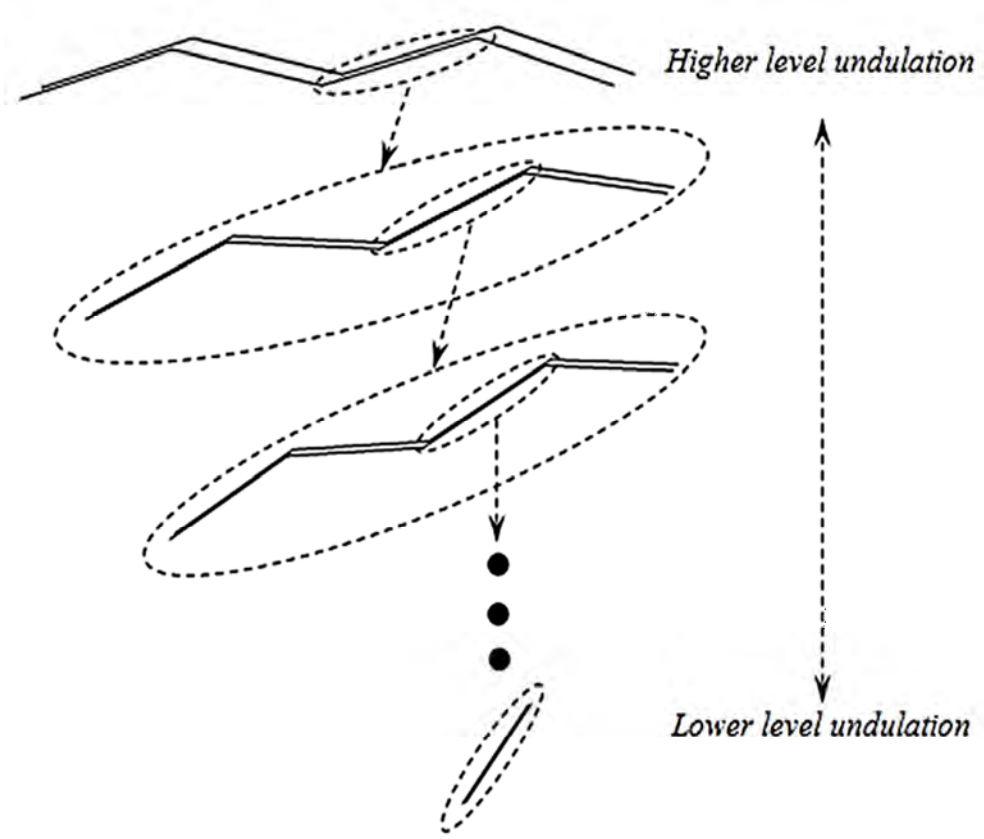

Figure 2-20 Hierarchical structure of joint profile (after Dong and Pan 1996)

The asperity of a rock joint was represented as multi-level asperities in a saw tooth shape. Asperity saw teeth may have random orientations in any level. In addition, Plesha (1987)'s degradation law was further extended to account for the residual asperity angle as:

$$i = (i_0 - i_r)\exp(-\int_0^{u_p} c_d \, dw_p) + i_r \tag{2.68}$$

where, i_r is the residual contact inclined angle after the degradation process is complete.

Lee *et al.,* (2001) introduced the concept of equivalent asperity angle as the representative of numerous asperities shown in Figure 2-21.

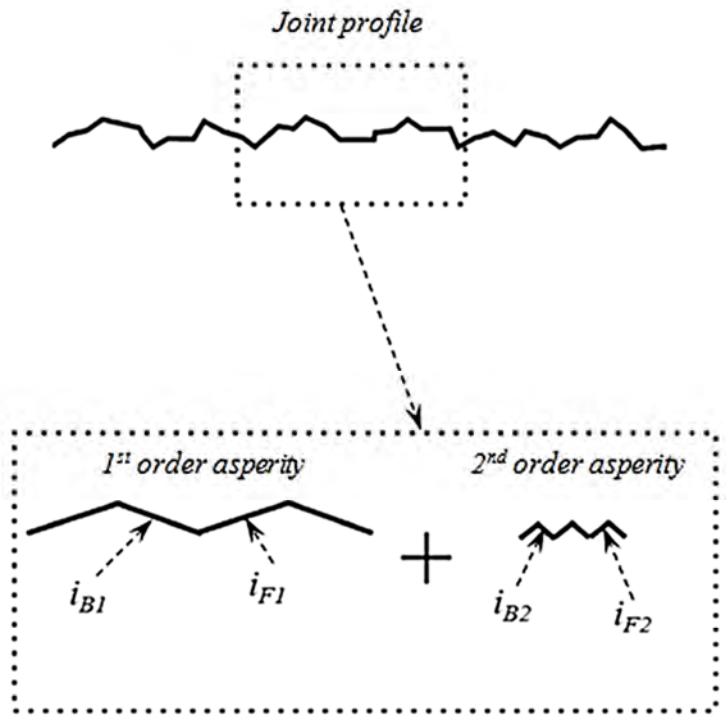

Figure 2-21 Concept of equivalent asperity angle (after Lee *et al*., 2001)

In Figure 2-21, subscripts *F* and *B* denote forward and backward shearing. Also, *1* and *2* represent the first and second order asperity angles, respectively.

Applying the concept of equivalent asperity angle and dividing asperity shearing into forward and backward directions, the following equations for asperity degradation was proposed as:

$$i_F = i_{F1}\exp(-C_{d1}W_p) + i_{F2}\exp(-C_{d2}W_P) \tag{2.69a}$$

$$i_B = i_{B1}\exp(-C_{d1}W_p) + i_{B2}\exp(-C_{d2}W_P) \tag{2.69b}$$

Another type of sliding model for cyclic loading was suggested by Stupkiewicz and Mróz (2001) in which the dilation angle follows a hyperbolic equation. In order to model the asperity damage, the initial asperity height was assumed to degrade due to a portion of the sliding plastic shear work as:

$$v = a\left[\exp(-C_d W_p)\right]\tanh\left[\frac{\sqrt{(u_r \tan i_0)^2 + g^2 + g_0^2} - g_0}{h_0}\right] \quad (2.70a)$$

$$g = g_f\left[1 - \exp(-C_d W_P)\right] \quad (2.70b)$$

where, u_r is the relative shear displacement and g_0 and g_f are model parameters related to the wear effects.

The difference between the previous model and Plesha (1987)'s damage law is the consideration of relative shear displacement in dilation behaviour.

Following the formulations of Stupkiewicz and Mróz (2001), a Gaussian asperity curve relationship also was presented by Puntel *et al.,* (2006).

2.5.2.2. Mathematical models

Lotfi *et al.,* (1994) proposed a three parameters hyperbolic criterion for interfaces under cyclic loading that provides a smooth transition between the Mohr-Coulomb and tension cut off as:

$$F = \tau^2 - \mu_s^2(\sigma_n - \sigma_c)^2 + 2r(\sigma_n - \sigma_t) = 0 \quad (2.71a)$$

$$r = (C^2 - \mu_s^2\sigma_t^2)/2\sigma_c \quad (2.71b)$$

where, μ_s is the slope of the asymptotes of the hyperbola.

In this model, it is assumed that plastic loading in the tension-shear region decreases the tensile strength, while the shear strength generated by μ_s and r, which is termed frictional strength here, remains constant. Moreover, plastic loading in the compression-shear region decreases both the tensile and frictional strength. For frictional-strength

degradation, only the portion of the plastic work associated with the shear stress is taken into account.

Fox *et al.*, (1998) presented the interlock-friction model for shear behaviour of joints under dynamic loading and CNL conditions as:

$$\tau = \sigma_n \left[\mu_m sign(u) + \tan(\gamma) \tanh(\eta_s u) \right] \tag{2.72}$$

where, μ_m is the mean shear stress of forward and reverse motion to initial normal stress, $\tan(\gamma)$ is the average offset shear stress magnitude per initial normal stress and η_s is related to the slope of the offset function near zero displacement.

The normal displacement was considered symmetric and is given by:

$$v = u \tan(i_0) \tag{2.73}$$

In the later model, the effect of asperity damage in shear stress and dilation is neglected. Therefore, the shear strength and dilation of the first cycle are similar to subsequent cycles.

A general roughness degradation (D_W) model for undulated joint surfaces was proposed by Homand-Etienne *et al.*, (1999) based on the experimental data as:

$$D_W = 1 - (1 - \frac{\sigma_{ni}}{\sigma_c}) \exp(-\frac{k_a^{3/2}}{\tan\theta_s} \frac{T}{L_s} \frac{W_t}{L_{cy}} \left(\frac{\sigma_{ni}}{\sigma_c} + \frac{K_n \tan\theta_s L_{cy}}{4\sigma_c} \right) \tag{2.74}$$

where, θ_s is the surface mean angle, k_a is the apparent anisotropy coefficient, T is the undulation period, L_s is the sample length along the shear direction, L_{cy} is the total displacement for one shear cycle, W_t is the accumulated total displacement, σ_{ni} is the initial normal stress and K_n is the normal stiffness.

In another study, Homand *et al.*, (2001) presented a roughness degradation model for CNL conditions based on roughness parameters as:

$$D_W = 1-(1-\frac{\sigma_n}{\sigma_c})\exp(-\frac{k_a^2}{2DR_r^0}\frac{\sigma_n}{\sigma_c}) \tag{2.75}$$

where, k_a is the apparent anisotropy coefficient and DR^0_r is the degree of joint relative roughness prior to shearing.

Belem *et al.*, (2007) reported two empirical joint surface asperity degradation models (models 1 and 2) for CNL and CNS, monotonic shearing and cyclic shearing conditions. Model 1 was formulated based on the evolution of surface secondary roughness and Model 2 was developed based on the concept of average asperity probable contact as:

Model 1:

$$D_W = 1-(1-\frac{\sigma_{n0}}{\sigma_c})\exp(-\beta_d\frac{\sigma_{n0}+k_n u_{s0}\tan(\delta_{ave})}{\sigma_c}) \tag{2.76a}$$

Model 2:

$$D_W = k_w\left[1-\exp(-\chi\frac{\sigma_{n0}+k_n u_{s0}\tan(\delta_{ave})}{\sigma_c})\right] \tag{2.76b}$$

where,

$$\beta_d = \frac{3k_a^3}{8DR_r\tan(\theta_s)}\log(\frac{u_{s-total}}{a_0 k_a}) \tag{2.76c}$$

$$\delta_{ave} = \theta_s\left(\frac{u_{s0}}{5a_0}\right)\exp(-\log(\frac{u_{s-total}}{a_0})\frac{k_n a_0}{\sigma_c}\sqrt{\frac{\sigma_{n0}}{\sigma_c}}) \tag{2.76d}$$

$$k_w \approx (\alpha_0 - k_a)\sqrt{\tan\theta_s} \approx 1.13506 + 0.13403\cos(1.55173k_a + 1.78383) \quad (2.76e)$$

$$\chi = \frac{7k_a^3}{15\tan\theta_s DR_r}\log\left(\frac{u_{s-tot}}{a_0 k_a}\right) \quad (2.76f)$$

where, θ_s is the surface asperity average angle, α_0 is a constant, k_a is the apparent anisotropy coefficient, DR_r is the degree of joint surface relative roughness, a_0 is the roughness amplitude (equivalent to parameter R_t, the peak-to-valley height, k_n is the normal stiffness, u_{s0} is the relative shear displacement and $u_{s\text{-}tot}$ is the total accumulated shear displacement.

2.6. Summary

A brief description of the studies on clean rock joints under monotonic and cyclic loading has been given. Environments such as underground excavations, namely, mining and tunnelling are closely represented by CNS conditions. The importance of considering stiffness on joint shear behaviour was well emphasised under the monotonic loading in these studies (Johnston and Lam 1989; Skinas *et al.*, 1990; Indraratna and Haque 2000).

It was revealed from the literature review that a majority of the experimental studies carried out on shear behaviour of rock joints was under monotonic loading. Furthermore, a limited number of experimental studies were reported in the literature investigating the effects of cyclic loading on shear behaviour of rock joints under CNS conditions.

It was concluded from the literature reviewed above that the models based on energy balance principals (Ladanyi and Archambault 1969; Johnston and Lam 1989; Seidel and

Haberfield 1995*a*) and methods based on shearing modes realistically quantify shear behaviour of rock joints under monotonic loading. In addition, the analytical methods available in the literature for describing shear behaviour of rock joints under cyclic loading are mostly based on the sliding mechanism.

It is noted that Jafari *et al.*, (2003) studied experimentally the shear behaviour of artificial clean rock joints cast using cement based mortar under cyclic loading and CNL conditions where the normal load remains constant during shearing. In contrast, this thesis investigates the shear behaviour of clean and infilled rock joints cast using high strength Plaster of Paris for various initial normal stresses, asperity types and infill thickness to asperity height ratios under cyclic loading and CNS conditions where the normal load changes due to stiffness of surrounding rock mass. These rock joint conditions were designed to simulate the actual joint deformation encountered in the field. Furthermore, the experimental studies are accompanied by mathematical and numerical models to describe the effects of cyclic loading on shear strength of clean and infilled rock joints.

The following chapter reviews the research work on infilled joints and models developed to predict their strength.

Chapter III

3. LITERATURE REVIEW OF THE SHEAR BEHAVIOUR OF INFILLED ROCK JOINTS

3.1. Introduction

As discussed in chapter II, the shear and deformability behaviour of a rock mass are influenced significantly by the existence of joints. Jointed rocks are often infilled with material between the joint planes which considerably affect their strength. As these infilled joints are likely to have less shear strength than other elements of a rock mass, it is essential to apply appropriate shear strength parameters in the design of underground excavations and when considering slope stability.

It is obvious that joint infill reduces the rock to rock contact, which decreases the shear strength of the joints. However, some infilled joints will be cemented by the infill material and in these situations; the joints shear strength may approach the strength of the intact rock.

3.2. Infill material

Brekke and Howard (1972) reported the following seven groups of joints based on infill materials according to their strength and behaviour:

- Healed or “welded” discontinuities.
- Clean discontinuities, i.e., closed but without filling or coatings.
- Calcite fillings.

- Coatings or fillings of chlorite, talc and graphite.
- Inactive clay material.
- Swelling clay.
- Material that has been altered to a more cohesionless (sand-like) material.

In spite of the high complexity seen in the natural joints and their fillings, Ladanyi and Archambault (1977) divided infill material types found in joints into four groups:

- Clean, i.e. non-filled or without coating.
- Coated.
- Clay-like infilling.
- Sand-like infilling.

According to Lama (1978), the filling material that exists within interfaces can be categorised into the following groups, based on the material origin and the method of transport:

- Loose material brought from the surface such as sand, clay.
- Deposition by ground water flow containing products of leaching of calcareous or ferruginous rocks.
- Loose material from tectonically crushed rock.
- Products of decomposition and weathering of joints.

Barton (1974) explained the role of infill in shear behaviour of rock joints by considering four groups of thickness:

- For low infill thickness, the rock to rock contact occurs almost immediately when the normal stress that is applied on the contact points is high enough to

scatter the clay in these critical regions. The dilation component of the peak strength reduces slightly which may be more than compensated for by "adhesive" action of the clay infill in these critical regions. There is not a significant difference in the shear strength from non-filled joints because the rock to rock contact area at peak strength is always small. If there is a fast shearing rate, negative pore pressure is developed within the filling due to dilation (i.e. rock to rock contact).

- In order to develop the same amount of rock to rock contact for slightly higher thicknesses, larger shear displacement will be required. The dilation component at peak strength is greatly reduced since the new position of the asperities at peak stress is similar to the asperity arrangement of an non-filled joint at its residual strength. Due to the reduced dilation, no negative pore pressure is developed.
- When the adjacent rock asperities come close together, no rock to rock contact is expected, but stress will increase within the filling. There will be an increased pore pressure in the highly stressed zones with a high shear rate which will cause lower shear strength, but if the shear rate is lower, consolidation will take place and the pore pressure will dissipate to low stress pockets on both sides of the consolidated zones. The net results will be a marked increase in shear strength, similar to the fast shear rate.
- The influence of the rock walls will disappear, when the infill thickness is several times the asperity amplitude. Provided that the filling is uniformly graded and predominately clay or silt, the shear strength is dominated by straightforward soil mechanics principles.

Past studies have evaluated the laboratory shear strength parameters of both natural and artificial infilled rock joints under monotonic loading and proposed models to quantify them (e.g. Goodman 1970; Kanji 1974; Ladanyi and Archambault 1977; Lama 1978; Barla *et al.,* 1985; Bertacchi *et al.,* 1986; Pereira 1990; Phien-wej *et al.,* 1991; de Toledo and de Freitas 1993; Indraratna *et al.,* 1999 and 2005; Oliveira and Indraratna, 2010). This chapter summarises the previous work on shear behaviour of infilled rock joints and the models available for evaluating the shear strength under monotonic loading.

3.3. Factors controlling shear strength of infilled rock joints

There are many parameters identified influencing the shear behaviour of infilled rock joints. These important parameters include:

- Joint surface roughness
- Type and thickness of the infill
- Development of pore water pressure and drainage conditions
- Degree of over consolidation ratio
- Boundary conditions

3.3.1. Joint surface roughness

The conditions of the infill interface, as defined by the roughness of the rock wall, may affect the shear strength of infilled joints. The effect of the soil-rock interface was investigated by Kanji (1974). Flat saw-cut and polished surfaces of limestone and basalt were filled with different soils and tested in a shear box. Table 3.1 shows the results of the joint shear strength to the soil strength that makes the infill. Kanji (1974) found that; in some cases an infilled joint can be weaker than the infill material alone and the

reduction in shear strength is a function of surface roughness and the clay mineral present. The shear strength of soil-rock contact surface decreases sharply and at lower shear displacement than the soil alone. For smooth surfaces, a lower shear displacement is required to reach the residual shear strength of the contact surface. This may be explained by the presence of the flat surfaces influencing the orientation of clay particles along the failure plane.

Table 3-1 Influence of boundary conditions on the strength of infilled joints (after Kanji 1974)

Rock	Surface	soil	τ_{joint}/τ_{soil}
Limestone	Saw-cut	Sandy kaolin clay	0.95
Limestone	Saw-cut	Pure kaolin	0.96
Limestone	Polished	Sandy kaolin clay	0.92
Limestone	Polished	Pure kaolin	0.88
Limestone	Polished	Illite	0.91
Limestone	Polished	Montmorillonite clay	0.76
Basalt	Polished	Montmorillonite clay	0.61

NB: τ_{joint} and τ_{soil} are joint shear strength and soil shear strength respectively.

Kutter and Rautenberg (1979) performed shear tests on clay filled planar to rough sandstone joints under CNL conditions and found that the strength is higher for rougher joints.

de Toledo and de Freitas (1993), based on the sand filling between two flat granite blocks, pointed out that the strength of a joint is affected by boundaries in two ways. In clay fills, sliding occurs along the contact area, due to the particle alignment, while the rolling of grains seems to be the major factor to reduce the strength in sands. For an interface filled with sand, the influence of rock boundary may be observed when its surface is smoother than the roughness of the sand surface (defined by particle size distribution) and when the dilation is reduced. Figure 3-1 illustrates two joints with different roughness that are filled with the identical sand. The rougher joint (Figure 3-1 up) impedes the movement of the sand-rock contact, and for failure to take place; the sand friction needs to be overcome. Conversely, the joint shown in Figure 3-1 [down] is smooth and grain rotation can occur on the boundary surface and only rolling friction may be observed.

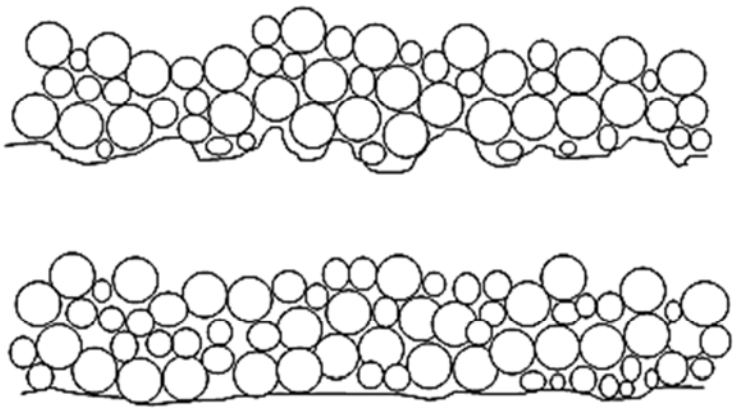

Figure 3-1 Rock joint-sand fill contact: [up] Rough surface with no influence on the joint strength, [down] Smooth surface with grain rotation occurring on the boundary, weakening the joint (after de Toledo and de Freitas 1993)

Jayanathan (2007) later verified Kanji (1974)'s results by performing a few triaxial tests with various infill thicknesses on planar joints. It was shown that the infill thickness of planar joints does not affect its shear strength and pore-pressure development.

3.3.2. Type and thickness of infill

Type and thickness of the infill in rock joints are the most important factors, influencing the strength parameters of a joint. Several studies on shear strength of infilled joints clearly indicated that the thicker the infill layer in the joint the lower the joint strength (Goodman 1970; Kanji 1974; Lama 1978; Phien-wej *et al.*, 1990; Papaliangas *et al.*, 1993; de Toledo and de Freitas 1993; Indraratna and Haque 2000).

Goodman's (1970) research work on saw-tooth shaped joints, filled with crushed mica, revealed that, the shear strength of the joint was greater than the infill for a thickness to asperity height (t/a) ratio of 1.25 (Figure 3-2). Similar results were reported by Ladanyi and Archambault (1977), from direct shear tests using kaolin clay infill (Figure 3-3). They also stated that the value of the shear strength increased with decreasing t/a ratio, and with increasing asperity angle.

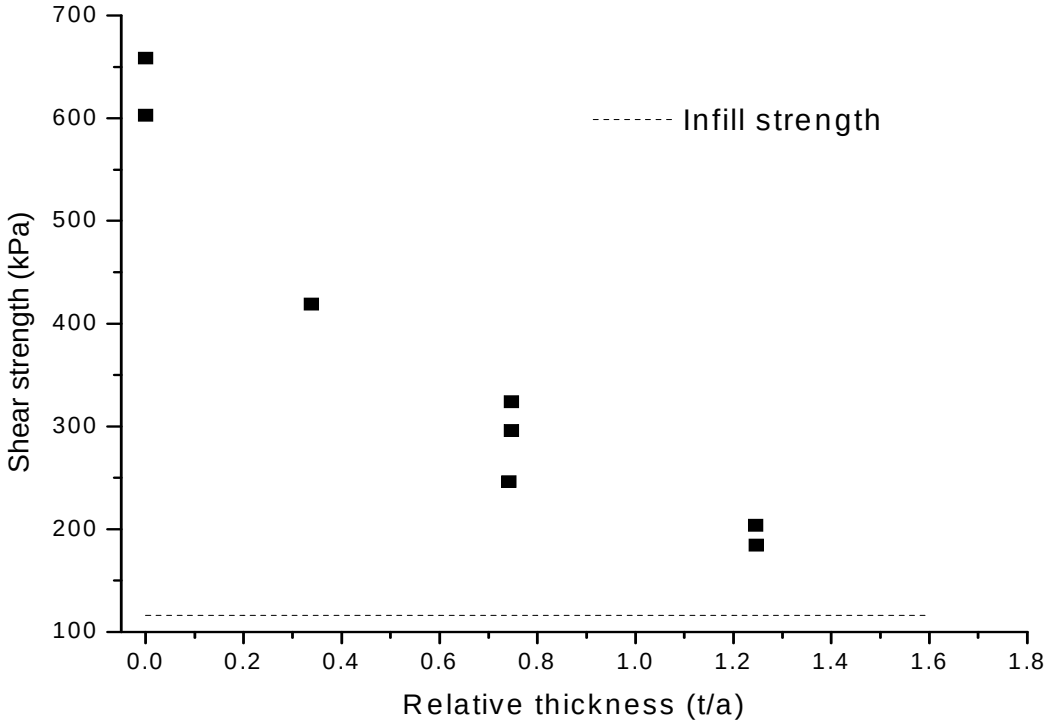

Figure 3-2 Shear strength of mica infilled joints (after Goodman 1970)

Tulinov and Molokov (1971) in their research on sand and clay infilled joints in limestone, sandstone and marl found that, a thin layer of sand did not have a significant influence on the frictional behaviour of hard rocks. The opposite results were shown for tests on soft rocks. Lama (1978) presented a series of laboratory tests performed on replicas of tension joints filled with kaolin, in which high strength gypsum was used to cast the rock. He concluded that the strength of infilled joints approached the strength of infill material when the *t/a* ratio exceeded the critical value of unity.

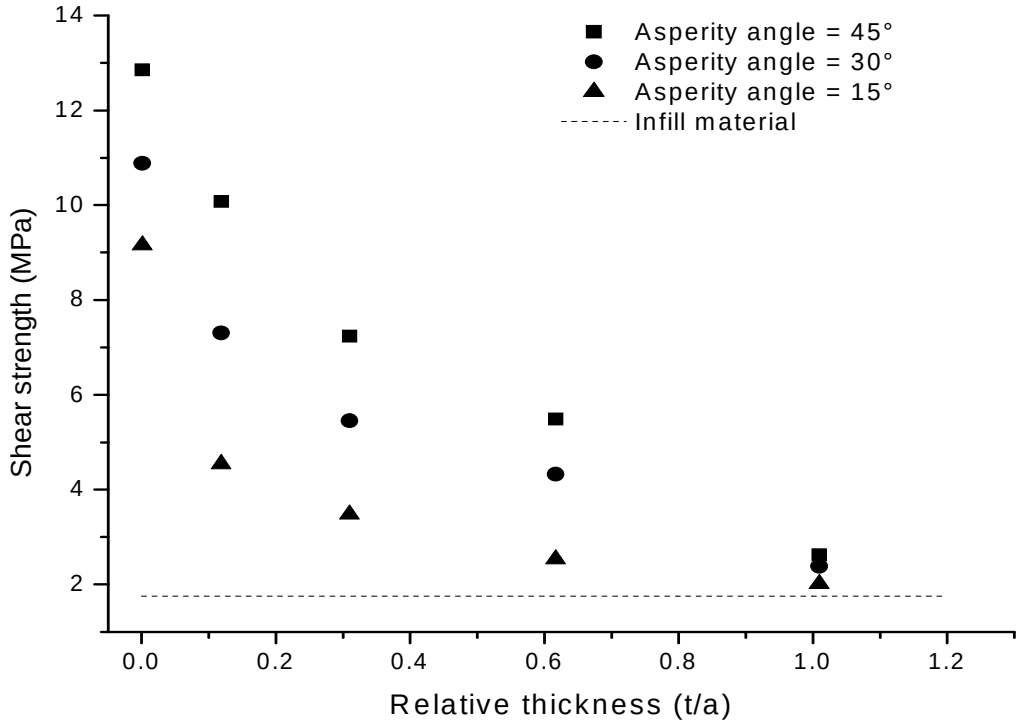

Figure 3-3 Shear strength of kaolin infilled joints (after Ladanyi and Archambault 1977)

Kutter and Rautenberg (1979) found that the shear strength of clay infilled joints increased slightly with increasing surface roughness, whereas for sand filled joints, a considerable increase in shear strength was observed. Generally, the shear strength of the joints decreased with the increase in infill thickness. Wanhe *et al.*, (1981) reported that the shear displacement at peak shear strength increased as the infill thickness increased to a critical value. Under this condition, the shear strength was dominated by the infill when infill thickness was further increased.

Phien-wej *et al.,* (1991) conducted direct shear tests on saw tooth shaped gypsum samples filled with oven dried bentonite and concluded that, the strength of joints becomes equal to that of infill material when the *t/a* ratio approached two (Figure 3-4).

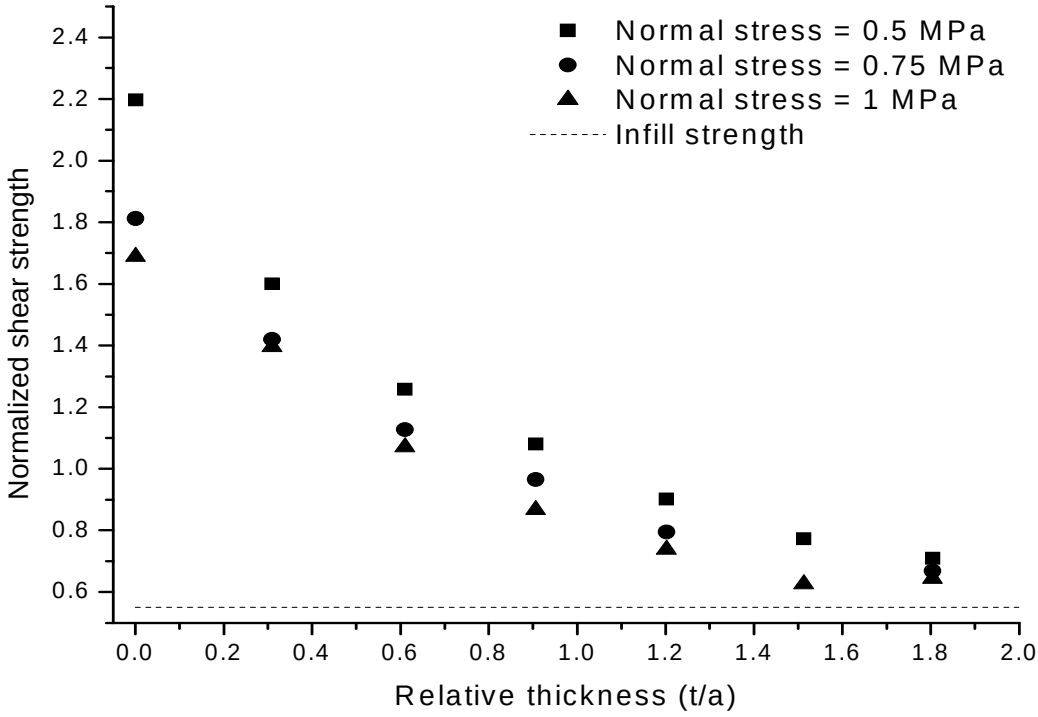

Figure 3-4 Variation of shear strength with asperity angle of 30° against t/a ratio (after Phien-wej *et al*., 1991)

Papalingas *et al.,* (1993) carried out detailed shear tests on plaster-cement joints filled with three different infill materials, kaolin, marble dust and pulverised fuel ash. The results indicate that the shear strength of the joints containing kaolin becomes constant at a *t/a* ratio of approximately 0.6, while the shear strength of joints with either marble dust or fuel becomes constant at *t/a* ratios between 1.25 and 1.5. A reducing trend in shear strength was observed with the addition of a thin layer of infill material. It is inferred from Figure 3-5 that any further increase in *t/a* values of more than 1.5, would not result in any tangible peak shear strength change which is evident by the asymptote of peak shear strength to the *t/a* axis.

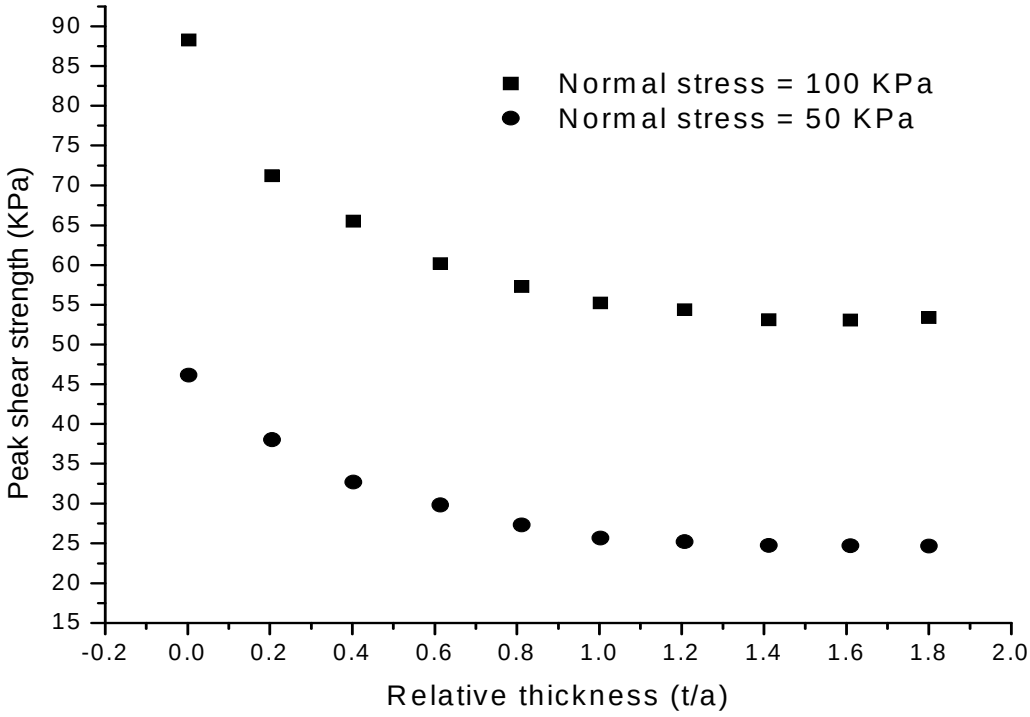

Figure 3-5 Effect of *t/a* ratio on shear strength of infilled joints (after Papalingas *et al*., 1993)

de Toledo and de Freitas (1993) performed ring shear tests on toothed Penrith sandstone and Gault clay. The test results indicate two peaks, namely the soil peak and the rock peak (Figure 3-6). It was found:

- The soil peak shear strength decreased toward a *t/a* ratio of unity and became constant beyond.
- The rock peak shear strength or the ultimate strength of the joint remains unchanged regardless of the consolidation stress of the infill. At the *t/a* ratio of unity, it was higher than the strength of the soil infill.
- It was difficult to distinguish between the two peaks when the strength difference between the infill and the rock was small.
- If the *t/a* ratio is greater than unity, the joint strength may sometimes be considered equal to that of the soil infill but not greater.

- When the shear displacement is high enough for rock to rock contact to take place during the test, the strength of the joint will be dominated by the rock asperities.

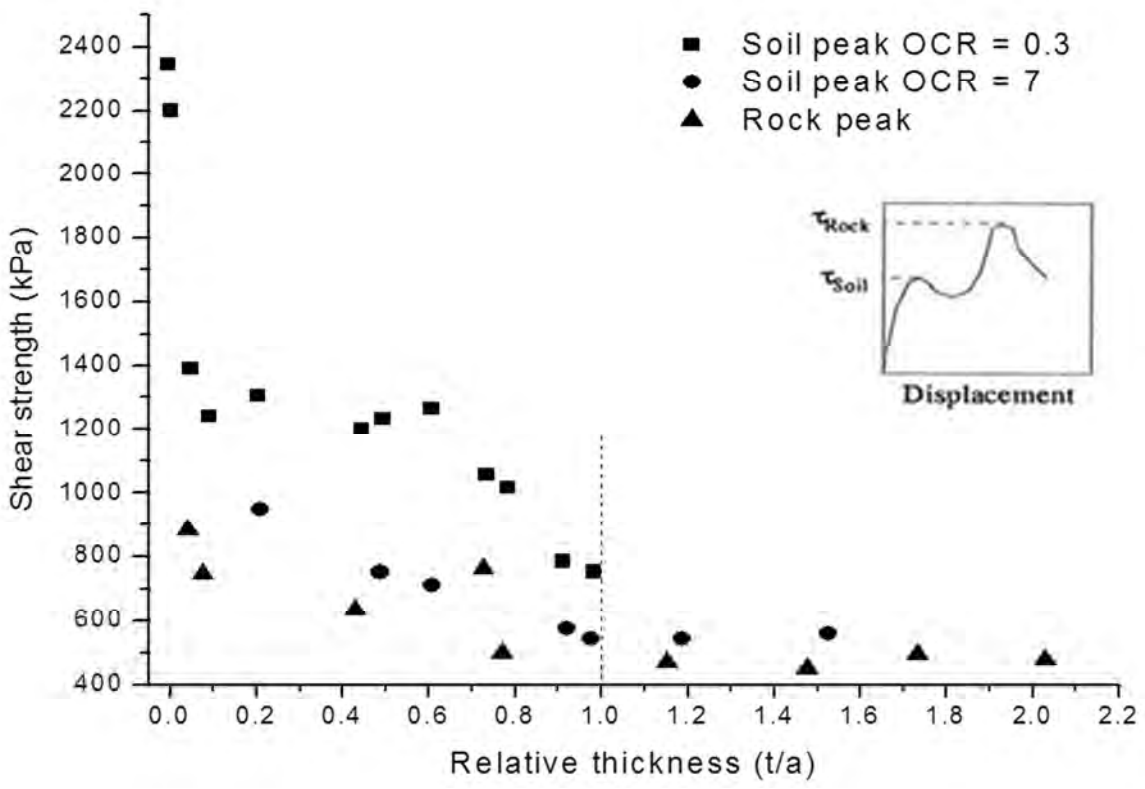

Figure 3-6 Strength of clay infilled sandstone joint tested under CNL in a ring shear device for σ_n = 1 MPa (after de Toledo and de Freitas 1993)

Indraratna *et al.,* (1999) carried out CNS direct shear tests on tooth shaped joints with 9.5° and 18.5° of asperity angle, infilled with soft clay. The samples were sheared with different values of initial normal stress ranging from 0.3 MPa to 1.1 MPa and under a constant normal stiffness of 8.5 kN/mm. It was found that both the shear strength and friction angle were reduced significantly by the presence of infill (Figure 3-7). It was also observed that joint roughness plays an important role on the shear strength up to the *t/a* ratio of 1.4. Beyond the stated critical ratio, the shear behaviour is controlled only by the infill material.

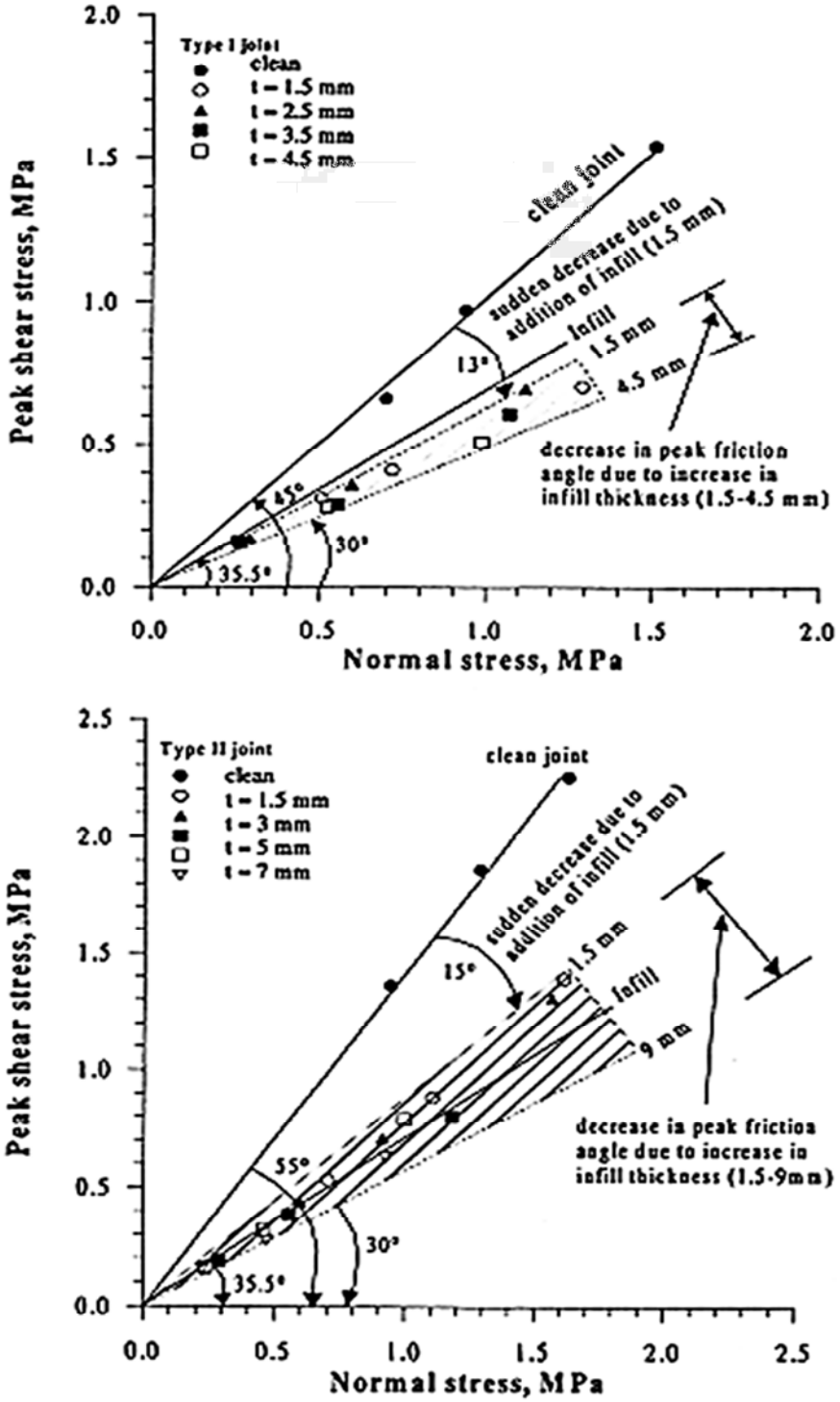

Figure 3-7 Effect of infill on strength envelope: [up] i_0 = 9.5°, [down] i_0 = 18.5° (after Indraratna *et al*., 1999)

Jayanathan (2007) examined the effect of infill thickness on the shear strength envelope. It was found that the angle of friction resistance decreased considerably with addition of

a thin layer of infill in comparison with a clean joint. As expected, the shear strength envelope of joints with thicker infill approached that of infill material.

3.3.3. Development of pore water pressure and drainage conditions

Development of pore water pressure and drainage conditions is another important parameter that affects the shear behaviour of infilled rock joints. The undrained shear strength is always lower than the drained shear strength. The rate of shear displacement determines the drained or undrained status of the tested samples. de Toledo and de Freitas (1993) carried out shear tests on infilled joints at different shear rates. They stated that the shear strength decreases with increase in the shear rate. In addition, it was concluded that even reasonably low shear rate cannot guarantee the full drainage of the infill material.

Jayanathan (2007) conducted undrained triaxial tests on artificial saw tooth shaped joints with normally consolidated silty clay as the infill material. He found that:

- Pore pressure increased during loading. As the joint dilated, pore water pressure decreased to a negative range (suction).
- It was often difficult to interpret the resulting pore water pressure of the mixed infill (mixed with the asperity debris).
- The negative pore pressure was more prominent for axial strain exceeding 1% and when the infill thickness was relatively thin (e.g. $t/a = 0.5$).
- At $t/a > 1$, the pore water pressure increased continuously to a peak value and then remained almost constant when the deviatoric stress attained a plateau at axial strains exceeding approximately 1.5-2%.

- At t/a < 1, the asperity contact was observed (rock to rock contact), particularly after an axial strain of 1-2%.
- For the pronounced asperity interface, the axial strain decreased significantly with increasing confining pressure.
- For a particular t/a ratio at a reduced axial strain, there was a considerable increase in the peak deviatoric stress for higher confining pressures.
- When confining pressure increases, the suction generated in the joint with relatively thin infill (e.g. t/a = 0.5) decreases significantly, which can be attributed to the confined dilation or shearing of asperities.
- At t/a =1, the shearing of asperities is less pronounced and the confining pressure does not affect the development of suction significantly.
- For t/a >1, under high confining pressure, the excess pore water pressure increases with increase in the peak deviatoric stress and the axial strain required to reach a constant pore water pressure decreases.

3.3.4. Degree of over consolidation ratio

According to fundamental soil mechanics, a discontinuity infill is considered normally consolidated if the existing effective *in situ* normal stress (σ_{n0}) equals or exceeds the maximum effective pre-consolidation pressure (P_c). The infill is over consolidated, if σ_{n0} is less than the effective pre-consolidation pressure (P_c).

Barton (1974) reported that almost all discontinuities are probably over consolidated. The only infilled joints likely to be normally consolidated are those from surface weathering. Barton (1974) also stated that in general, clays show a significant difference between peak and residual strength as clay particles are re-oriented within narrow bands close to the shear surfaces.

de Toledo and de Freitas (1993) carried out limited ring shear tests on clay infilled toothed joints for varying *t/a* ratios and two levels of consolidation under drained conditions. They concluded that the value of the soil peak strength increased with increased level of consolidation while the rock peak strength was unaffected. For thick infilled joints (no rock to rock contact) the peak shear strength increased with rising levels of consolidation.

Jayanathan (2007) investigated the effect of over consolidation on the development of shear strength and pore pressure based on a series of triaxial tests of infilled (clay) rock joints. The tests were conducted on filled planar, sand stone and saw toothed joints. The peak value of the deviatoric stress was increased for planar joints, when the Over Consolidation Ratio (OCR) [OCR is the ratio of the pre-consolidation pressure to testing confining pressure] increased from 1 to 4 but it remained relatively constant for higher values of OCR. At lower values of axial strain, a shift in the peak deviatoric stress was observed. The pore pressure showed a gradual reduction trend with increasing OCR and a reverse shift of its peak value in comparison to the deviatoric stress. For over consolidated clays, the deviatoric stress and pore pressure did not decrease after reaching peak stress.

The test results on infilled sand stone joints revealed that with the low thickness of infill material, the effect of OCR is observed mainly in the soil peak shear strength (similar to de Toledo and de Freitas 1993). As OCR increased, the development of positive pore water pressure decreased until it becomes a negative range (suction) in smaller strains. For high infill thickness and with OCR of 4 and 8, there was a drop in pore water pressure after attaining the peak shear strength due to dilation within the infill. Similar

reaction was reported for artificial saw toothed joints with the same clay infill as shown in Figure 3-8.

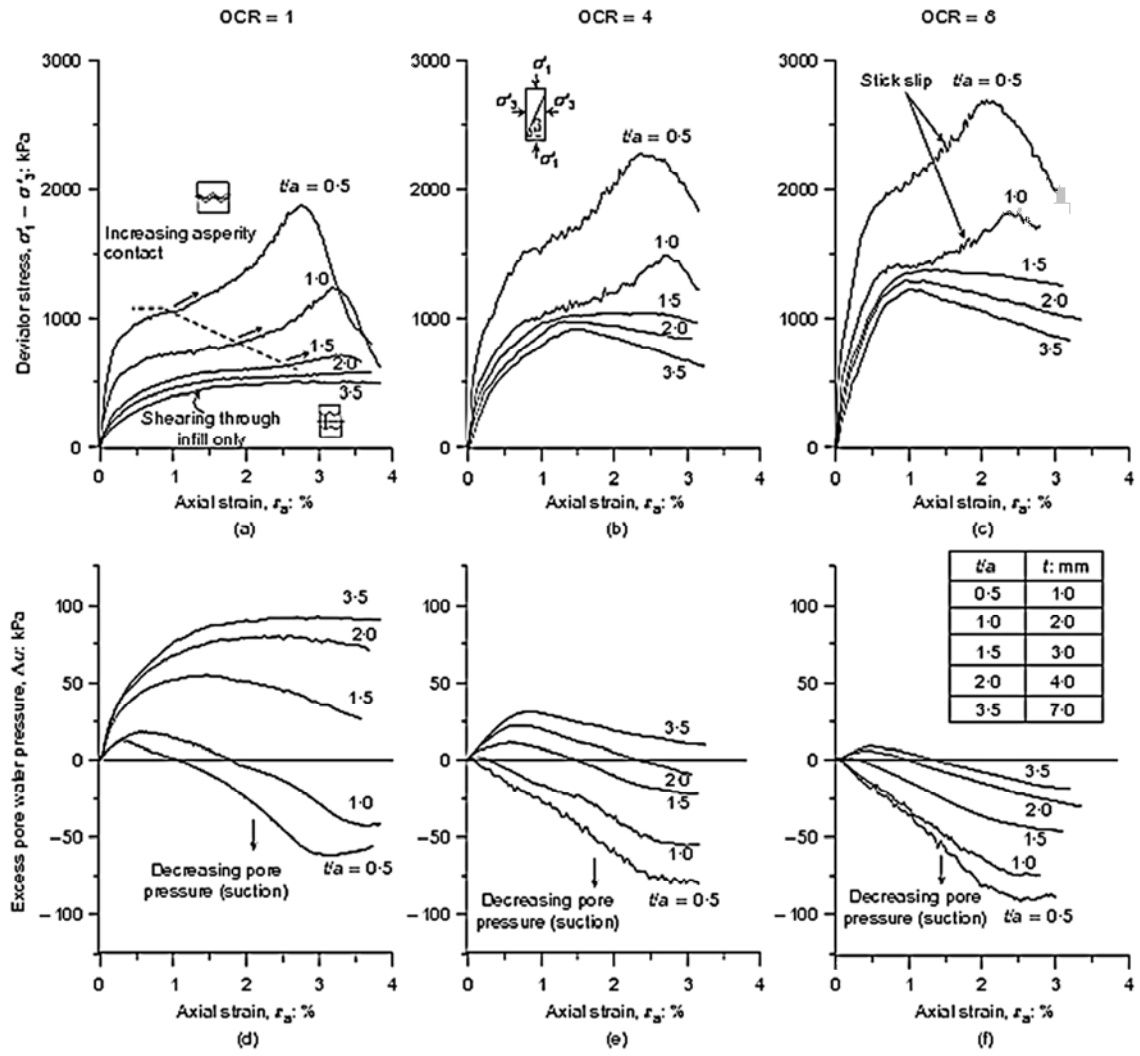

Figure 3-8 Shear behaviour of infilled idealised joints with different OCR values under undrained condition at σ'_3 = 500 kPa (after Jayanathan 2007)

3.3.5. Boundary conditions

Most of the test results on infilled joints reported previously was performed under CNL conditions where no stiffness was applied (Lama 1978; Phien-wej *et al.*, 1991; Papaliangas *et al.*, 1993; de Toledo and de Freitas 1993). Based on these studies, it was concluded that the shear strength increases with increase in the normal stress. In

contrast, dilation diminishes due to asperity damage or compaction as normal stress increases.

Normal stiffness restricts dilation and causes an increase in normal stress over the shear plane. Therefore, the shear strength substantially increases. Considering the relevance and importance of normal stiffness in simulating the actual conditions in an underground environment, some researchers performed shear tests on infilled joints with different levels of initial normal stress under CNS conditions (Cheng *et al.,* 1996; Indraratna *et al.,* 1999, 2005). They reported that the effect of stiffness decreases with increase in the infill thickness due to reduction in the rock to rock contact.

3.4. Shear strength models developed for infilled rock joints

Most of the models proposed for the prediction of shear behaviour of infilled joints are empirical or semi-analytical. These models consider different sets of parameters in their formulations, which pose some limitations. As there is a wide range of parameters influencing the shear behaviour of infilled joints, the models cannot cover all the problems encountered in the field.

Ladanyi and Archambault (1977) incorporated two approaches to extend a mathematical model for estimating the shear strength of infilled cohesive joints (clay filled joints). One model represents the domain in which irregularities remain intact during shearing and the other describes the breakage of irregularities.

For no breakage of irregularities, the shear strength (τ) in relation to normal stress (σ_n) is obtained by:

$$\tau = \frac{C_u}{(1 - \tan i \tan \varphi_b)} + \sigma_n \tan(\varphi_b + i) \tag{3.1}$$

where, C_u is the undrained shear strength parameter of the clay infill, φ_b is the basic friction angle of the joint surface, $tan(i) = m \times tan(i_0)$ and the reduction factor m is given by:

$$m = \left(1 - \frac{2}{3}\left(\frac{t}{a}\right)\right)^2 \tag{3.2}$$

where, m varies between 0 and 1, i_0 is the initial asperity angle, t is the infill thickness and a is the asperity height.

For breakage of irregularities during shearing, the relationship is given by:

$$S = m(R - C) + C \tag{3.3}$$

where, the shear strength of clean joint, $R = \sigma_n \tan(\varphi_b + i)$;

$$\tan(i) = \left[1 - \left(\frac{\sigma_n}{C_0}\right)^{\frac{1}{4}}\right] \tan(i_0) \tag{3.4}$$

where, C_0 is the uniaxial compressive strength.

The shear strength of infill (C) is obtained by:

$$C = C_u + \sigma_n \tan\varphi_u \tag{3.5}$$

where, φ_u is the undrained friction angle of the clay infill.

They also found that the second part was valid only for the following limits:

$$30° \le i_0 \le 45° \quad and \quad 0.1 < \frac{\sigma_n}{C_0} < 0.5 \tag{3.6}$$

When there is no breakage of asperities, the factor *m* is used to reduce the peak dilation angle of the joint due to the presence of infill. For the second domain, it was used to reduce the subtraction of the clean joint shear strength and the infill material.

Lama (1978) introduced a logarithmic relationship to predict the shear strength of a clay infilled joint from regression analysis of the experimental data. The model is given by the following equation:

$$\tau_p = 7.45 + 0.46\sigma_n - 0.3\ln(t)\sigma_n^{0.745} \tag{3.7}$$

where, τ_p is the peak shear strength (kPa), σ_n is the normal stress (kPa) and t is the thickness of the infill (mm).

The application of the above equation is only limited to the specific roughness of the joint tested.

Phien-wej *et al.,* (1991) presented an empirical relation for the prediction of shear strength of infilled joints. The model is based on laboratory data from saw tooth shaped joints and dry bentonite as the infill. They reported that the shear strength envelope changes from a linear to a bilinear relationship as the asperity angle increases. The joint shear strength is controlled by the infill alone when *t/a* reached 2. The proposed exponential function is given by:

$$\frac{\tau_p}{\sigma_n} = \frac{\tau_0}{\sigma_n} - \frac{k_1}{\sigma_n}(t/a)\exp[k_2(t/a)] \tag{3.8}$$

where, τ_p is the peak shear strength (kPa), τ_0 is the peak shear strength of the clean joint at the same normal stress (kPa), σ_n is the normal stress (kPa) and k_1 and k_2 are empirical constants that vary with the surface roughness and applied normal stress.

Papaliangas *et al.*, (1993) incorporated a similar approach to that proposed by Ladanyi and Archambault (1977) and introduced a model to estimate the shear strength of infilled rock joints. They stated that the shear strength of an infilled joint falls between two limits, τ_{max} the maximum shear strength of the non-filled joint and τ_{min}, the potential minimum shear strength of the system for a critical thickness of infill. The potential minimum shear strength is a function of the thickness and type of infill, the roughness of the rock wall and the normal stress. For rough joints, it is postulated that τ_{min} equals the shear strength of the infill. In the case of planar or smooth slightly undulated joints τ_{min} would be equal to the strength along the interface, which can be lower than the shear strength of the infill. The peak shear strength as a percentage of stress ratios is expressed by:

$$\mu = \mu_{\min} + (\mu_{\max} - \mu_{\min})^n \tag{3.9}$$

where,

$$\mu = \left(\frac{\tau}{\sigma_n}\right) \times 100 \tag{3.10a}$$

$$\mu_{\max} = (\tau_{\max} / \sigma) \times 100 \tag{3.10b}$$

$$\mu_{\min} = (\tau_{\min} / \sigma) \times 100 \tag{3.10c}$$

$$n = \left[1 - \frac{1}{c}\left(\frac{t}{a}\right)\right]^m \tag{3.10d}$$

For

$$0 \le \frac{t}{a} \le c \tag{3.11}$$

where, t is the mean thickness of filling material and a is the mean roughness amplitude of the discontinuity.

The constant c is defined as the t/a ratio at which the minimum shear strength is attained and this depends on properties of the filling, the normal stress and the roughness of the discontinuity surface. The constants c and m are experimentally evaluated and for the series of tests conducted by the Papaliangas *et al.,* (1993) were considered as 1.5 and 1 for peak shear strength, respectively. Similar values were also reported by Ladanyi and Archambault (1997). For $t/a = 0$ and μ equals to μ_{max}, the shear strength is equal to the clean joint. For $t/a > c$, μ should be assigned to μ_{min} which gives the minimum shear strength between the filling material and interface. The proposed concept is shown in Figure 3-9.

This model requires an evaluation of the constant for various t/a ratios in advance. In addition, the effect of basic friction angle, the soil friction angle and dilation angle are not explicitly clarified.

A general model for the prediction of shear strength of infilled joints for various infill thicknesses based on the experimental observations was proposed by de Toledo and de Freitas (1993) and is shown in Figure 3-10. They described the infill rock joints interaction as interlocking, interfering and non-interfering. Interlocking refers to the conditions in which the rock surfaces come in contact. Interfering takes place when there is no rock contact but the strength of the joint is greater than the infill alone. The non-interfering represents the joint behaviour controlled by the infill alone. The critical thickness (t_{crit}) is defined by the limit between the interfering and non-interfering regions beyond which the joint shear behaviour is generally controlled by the infill material.

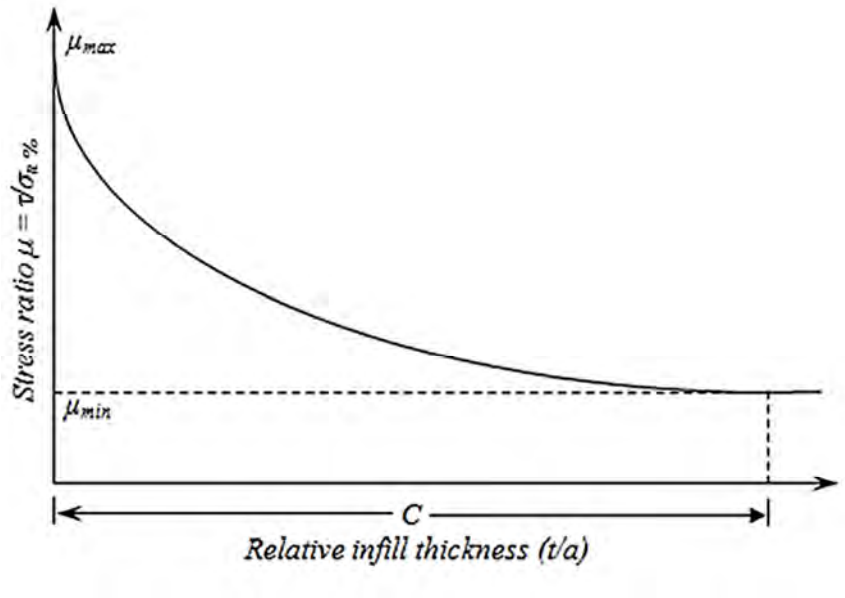

Figure 3-9 Empirical model for the peak shear strength of infilled joints (after Papaliangas *et al.*, 1993)

This critical thickness is a function of the infill material grain size, asperity angle and height. Therefore, materials showing granular behaviour, for instance sandy soil, present a critical *t/a* ratio greater than unity. On the other hand, clays have a critical *t/a* ratio of unity or less.

The key aspects of this model can be highlighted as:

- It is similar to that proposed by Papaliangas *et al.*, (1993), and describes the shear behaviour of infilled rock joints as a combination of a fraction of the strength of the rock (clean joint) and the infill material.
- Unlike the previous models, it was argued that the intercept between the rock peak strength envelope of an infilled joint for a thickness approaching zero is lower than the strength of the clean joint for a given normal stress.
- The intercept of the soil peak shear strength in this model is affected by the initial asperity angle.

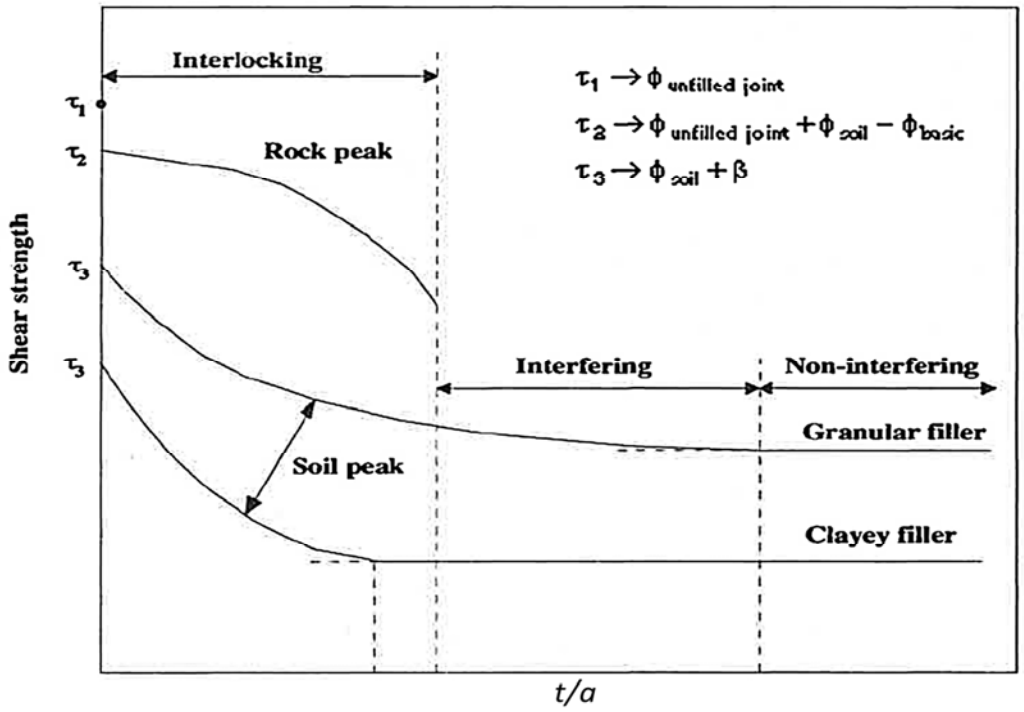

Figure 3-10 Strength model for infilled joints (after de Toledo and de Freitas 1993)

A similar approach to Phien-wej *et al.,* (1991) based on a series of direct shear tests on infilled joints was presented by Indraratna *et al.,* (1999) for the evaluation of the shear strength of infilled joints under CNS conditions. This model is based on the concept of Normalised Shear Drop (*NSD*). *NSD* is defined as the reduction in the peak shear stress due to the presence of infill material divided by the initial normal stress. The authors also stated that the variation of *NSD* with *t/a* ratio can be described using a hyperbolic relationship. The peak shear strength is then given by:

$$(\tau_p)_{\inf ill} = (\tau_p)_{unfilled} - \sigma_{n0} \frac{t/a}{\alpha(t/a) + \beta} \tag{3.12}$$

where, σ_{n0} is the initial normal stress and α and β are model coefficients.

The $(\tau_p)_{non\text{-}filled}$ can be expressed by Equation (2.57), thus:

$$(\tau_p)_{\inf ill} = \left[\sigma_{n0} + \frac{k}{A}\left(\frac{a_0}{2} + a_1 \cos\frac{2\pi h_{\tau p}}{T}\right)\right]\left[\frac{\tan\varphi_b + \tan i_0}{1 - \tan\varphi_b + \tan i_{\tau p}}\right] - \sigma_{n0}\frac{t/a}{\alpha(t/a) + \beta} \qquad (3.13)$$

where, k is the boundary normal stiffness, A is the joint surface area, a_0 and a_1 are the Fourier coefficients, $h_{\tau p}$ is the horizontal displacement corresponding to peak shear strength, T is the asperity length, $i_{\tau p}$ is the dilation angle corresponding to peak shear strength.

Indraratna *et al.,* (1999) also suggested a reduction factor for *NSD* that varies from 0.8 to 0.9. Beyond this cut off, the infill controls the shear behaviour.

The advantage of this model is that it considers the shear strength of clean joints in terms of measured physical parameters, using the peak dilation angle described by Fourier series.

In an attempt to calibrate the later model for the other infill materials, Indraratna *et al.,* (2005) carried out another experimental study on the same type of joints, but with graphite and sandy clay as the infill. They stated that the constants of the previous model were often found to be sensitive to the type of infill material and not always accurate, for instance, in the case of granite infill.

For predicting the shear strength of a variety of infilled joints, Indraratna *et al.,* (2005) introduced a model based on two algebraic functions *A* and *B,* adopting a similar approach to Papaliangas *et al.,* (1993). In this model, the shear strength of infilled joints is described in terms of fractions of the shear strength of the rock interface and the soil infill. As shown in Figure 3-11, function *A* is introduced to replicate the decrease in the influence of the $\tan(\varphi_b + i)$ term, with increasing *t/a* ratio. Function *B* also is considered

to model the increasing effect of the term $tan(\varphi_{fill})$ in the region of $t/a<(t/a)_{cr}$. Function *A* becomes zero and function *B* equals to $tan(\varphi_{fill})$ at $(t/a)_{cr}$.

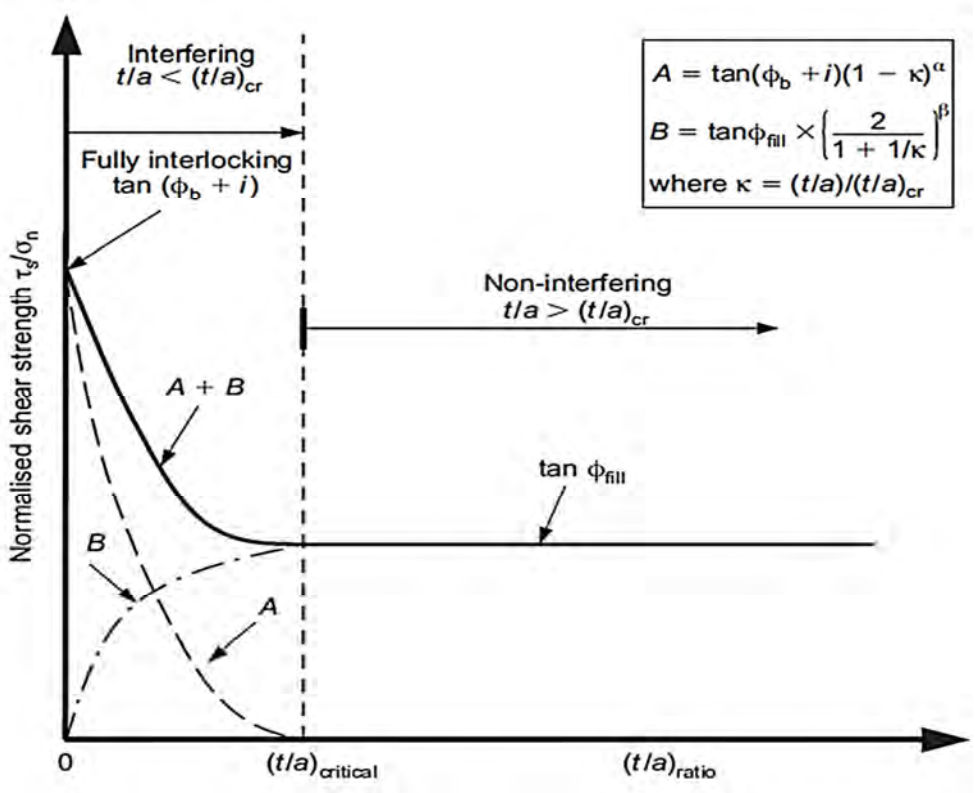

Figure 3-11 Shear strength model for infilled joints showing the role of φ_b and φ_{fill} (after Indraratna *et al*., 2005)

Hence, in the region of asperity interference, for $t/a<(t/a)_{cr}$:

$$\frac{\tau_s}{\sigma_n} = A + B = \tan(\varphi_b + i)(1-\kappa)^{\alpha} + \tan(\varphi_{fill})\left(\frac{2}{1+1/\kappa}\right)^{\beta} \tag{3.14}$$

where, τ_s is the peak shear strength of infilled joints, α and β are empirical constants defining the geometric locus of the functions *A* and *B*, and κ is given by:

$$\kappa = \frac{(t/a)}{(t/a)_{cr}} \tag{3.15}$$

In the case of non-interference, $t/a\geq(t/a)_{cr}$, the normalised shear strength becomes:

$$\frac{\tau_s}{\sigma_n} = \tan(\varphi_{fill}) \tag{3.16}$$

In this model, any cohesion of the joint has been ignored. The cohesion of a natural joint may have to be considered, for instance, if there is joint cementation or there is a clay infill, particularly if this is wet. Under such circumstances, the term C_{infill}/σ_n must be considered in both Equations (3.14) and (3.16).

This later model has been successfully verified for joints with different infill material such as graphite, bentonite and mixture of clay and sand.

The previous model was extended by Indraratna *et al.*, (2008) to describe the effect of over consolidation in the shear strength of infilled rock joints. According to the experimental study on idealised saw tooth shaped infilled joints, the critical *t/a* ratio decreases with increase in the OCR of the infill (Figure 3-12). It was initially assumed that the critical *t/a* ratio for an over consolidated infill can be described in terms of the OCR and the critical *t/a* ratio of the same joint with normally consolidated infill.

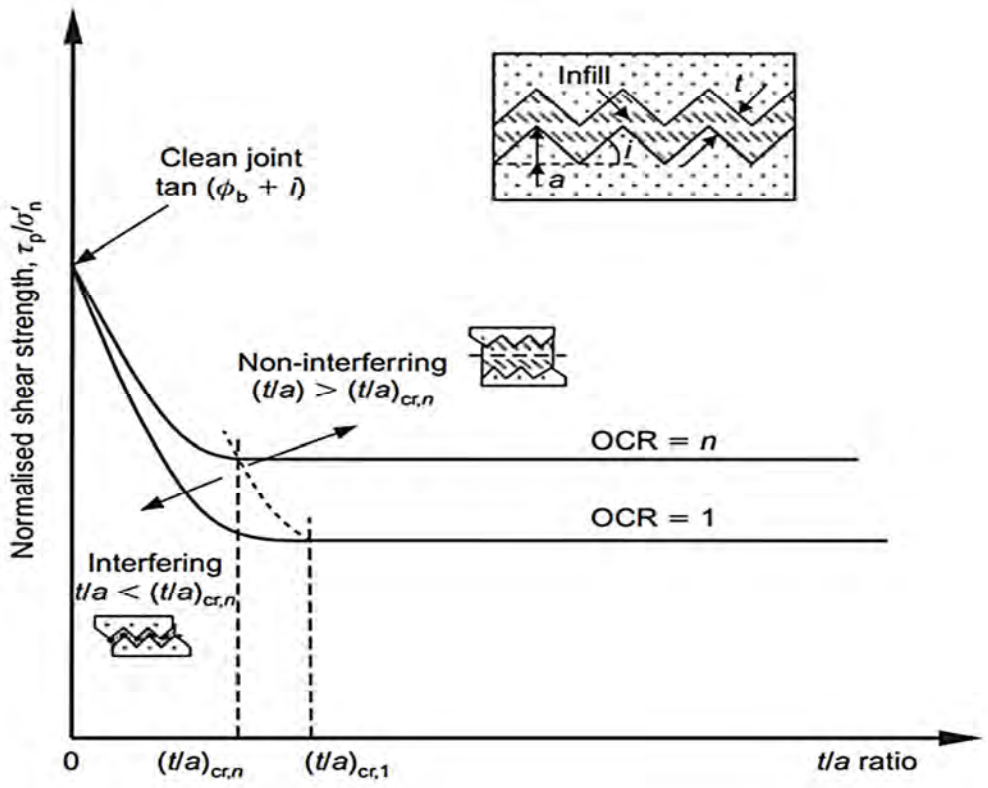

Figure 3-12 Conceptual normalised shear strength variation with *t/a* ratio (after Indraratna *et al*., 2008)

To make the graphical expression of Figure (3-12) convenient for modelling, a ratio $\kappa_{oc,n}$ was introduced as:

$$\kappa_{oc,n} = \frac{(t/a)_{oc,n}}{(t/a)_{cr,n}} \tag{3.17}$$

where, $(t/a)_{cr,n}$ is the critical *t/a* ratio of an infilled joint with an OCR of *n* and $(t/a)_{oc,n}$ is the *t/a* ratio of a given infilled joint with an OCR of *n*.

Using the above ratio, the interfering zone is the same independently of OCR as shown in Figure 3-13.

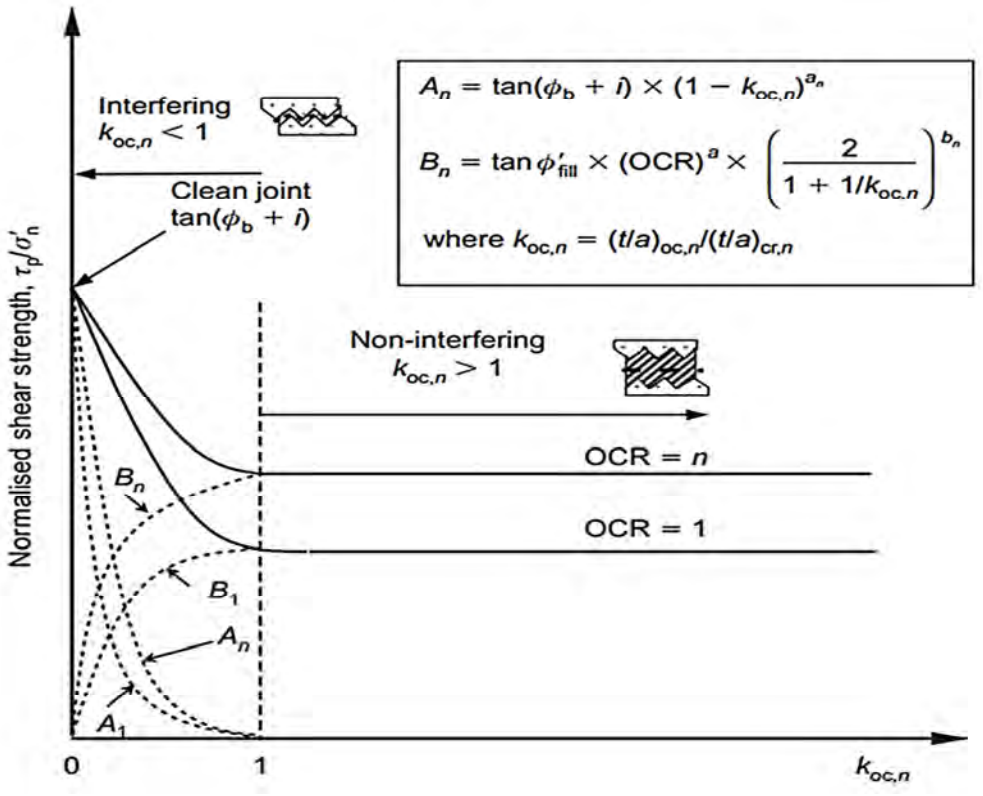

Figure 3-13 Shear strength model for over consolidated infilled idealised joints (after Indraratna *et al*., 2008)

In order to consider the effects of over consolidation on the normalised shear strength model, Indraratna *et al.,* (2008) proposed that the soil infill term can be normalised using the SHANSHEP method (Ladd and Foott 1974) as:

$$\log(\tau_s / \sigma_n)_{oc,n} = \log(\tau_s / \sigma_n)_{oc,1} + \alpha \log(OCR) \tag{3.18a}$$

$$(\tau_s / \sigma_n)_{oc,n} = (\tau_s / \sigma_n)_{oc,1} \times OCR^{\alpha} \tag{3.18b}$$

Resulting in:

$$(\tau_p / \sigma_n) = \tan(\varphi_{fill}) \times OCR^{\alpha} \tag{3.19}$$

The modified model gives the following relationship for the non-interfering zone ($t/a<t/a_{cr}$ or $\kappa_{oc,n}<1$):

$$\left(\frac{\tau_s}{\sigma_n}\right) = A_n + B_n = \tan(\varphi_b + i)\times(1 - \kappa_{oc,n})^{a_n} + \tan(\varphi'_{\text{fill}})\times OCR^{\alpha}\times\left(\frac{2}{1+1/\kappa_{oc,n}}\right)^{b_n} \quad (3.20)$$

where, a_n and b_n are empirical constants defining the geometric loci of the functions A_n and B_n and φ'_{fill} is the effective friction angle of normally consolidated infill.

For non-interfering zone ($\kappa_{oc,n} > 1$), the normalised shear strength is only controlled by function B_n.

Oliveira *et al.,* (2009) stated that the shear strength model proposed by Indraratna *et al.,* (2005) overestimates the shear strength of clean joints. Therefore, they proposed a revised function (A) to keep the energy balance as described by Seidel and Haberfield (1995*a*):

$$A = \left\{\frac{[\tan(\varphi_b) + \tan(i_0)]}{[1 - \tan(\varphi_b)\tan(i_p)_{clean}]}\right\}\left(1 - \frac{t/a}{(t/a)_{cr}}\right)^{\alpha} \quad (3.21)$$

The dilation angle at peak shear stress for clean joints $(i_p)_{clean}$ with a particular profile can be found using the relationship proposed by Indraratna *et al.,* (1998) as:

$$\frac{(i_p)_{clean}}{i_0} = \left(1 \quad \frac{\sigma_n}{\sigma_c}\right)^{c} \quad (3.22)$$

where, c is an empirical constant.

Indraratna *et al.,* (2010) proposed a semi-empirical shear-displacement criterion that includes the effect of infill. This model is based on a homogenised Coulomb type slip model in which the effect of infill squeezing during shearing is considered as shown in Figure 3-14.

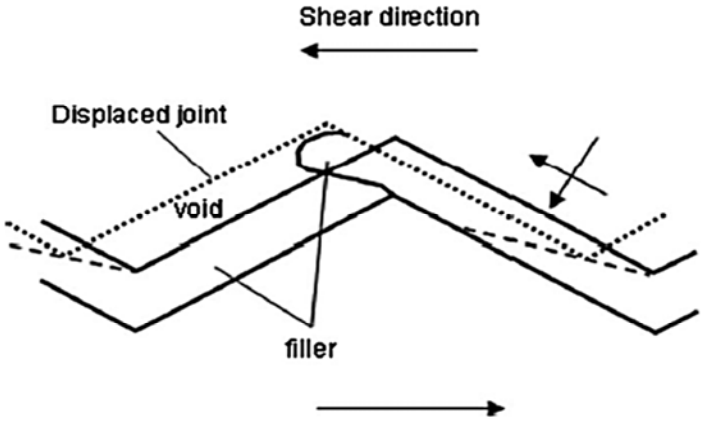

Figure 3-14 Mechanism of infill failure for small thickness (after Indraratna *et al*., 2010)

In model development, the initial assumption was that the shear strength of an infilled rock joints is the sum of the two basic terms:

$$\tau = \sigma_n (A + B) \tag{3.23}$$

where, *A* and *B* are functions related to the joint surface component and infill material respectively.

The mathematical functions that describe both strength terms (*A* and *B*) are dependent on the shearing mechanism. If the sliding is considered, where the infill material has to be squeezed out between the advancing asperities, then the following relationship can be established based on the work done in sliding:

$$A = \tan(\varphi_b + i_r)\eta \tag{3.24a}$$

$$B = \tan(\varphi_{fill} + i_{fill})(1-\eta) \tag{3.24b}$$

where, i_r is the asperity angle at the tip, i_{fill} is the slope angle of the sliding surface within the infill and η is the parameter which describes the ratio of the sliding surface in contact with the rock asperity to the total length of the sliding surface, i.e. $L_r/(L_r+L_{fill})$ at

a given displacement. The parameter η also represents squeezing of infill material during shearing, and, thereby, the change in thickness.

Figure 3-15 shows the assumed bi-linear sliding surface, where, L_r is the length of the sliding surface in contact with the asperity and L_{fill} is the length of the sliding surface within the infill material.

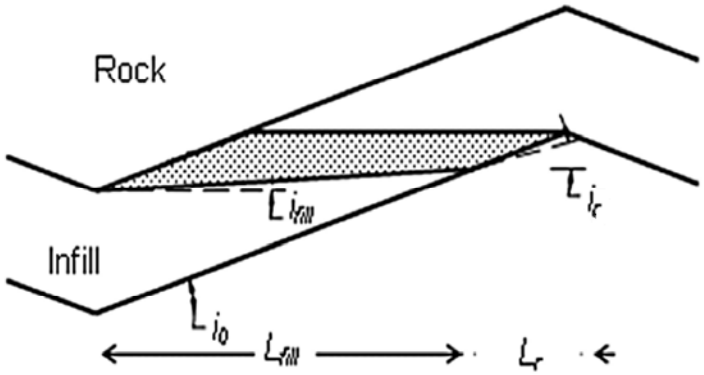

Figure 3-15 Volume of infill to be squeezed out during shearing at a given shear displacement (after Indraratna *et al*., 2010)

This relationship was extended to describe the entire shear displacement behaviour, allowing the squeezing factor to vary with displacement as:

$$\eta = \begin{cases} 0 & if \quad t > t_{cr} \\ \dfrac{u_s - u_0}{c_1 u_s + c_2} & if \quad 0 < t < t_{cr} \\ 1 & otherwise \end{cases} \tag{3.25}$$

where, u_s is the shear displacement, u_0, is the shear displacement beyond which asperity interference is noted and c_1 and c_2 are empirical constants that define the geometric loci of the function. The displacement u_0 establishes the limits of the first peak shear stress plateau and is found experimentally. If no pronounced infill peak shear strength is verified, u_0 vanishes.

In order to capture the energy balance as described by Seidel and Haberfield (1995*a*), the term representing the rock interface strength was expanded and the dilation angle in the numerator modified as follows:

$$A = \left[\frac{\tan(\varphi_b) + \tan(i_0)}{1 - \tan(\varphi_b)\tan(i)}\right]\eta \tag{3.26}$$

The later failure criterion can now be rewritten as:

$$\tau = \sigma_n\left\{\left[\frac{\tan(\varphi_b) + \tan(i_0)}{1 - \tan(\varphi_b)\tan(i)}\right]\eta + \tan(\varphi_{fill} + i)(1-\eta)\right\} \tag{3.27}$$

In the later model, the squeezing mechanism described by the factor η depends on the initial *t/a* ratio. With decreasing the *t/a* ratio, the factor η approaches unity and the model will convert to the clean joint model as proposed by Indraratna *et al.,* (1999). In addition, for $t/a \geq (t/a)_{cr}$ the model is simplified to a typical Coulomb slip model.

In order to better represent the post-peak behaviour, Indraratna *et al.*, (2010) proposed a modification to the soil-infilled joint model, incorporating the semi-empirical model of Equation (2.58). The modified failure criterion was proposed as:

$$\tau = \sigma_n\left(\left[\frac{\tan(\varphi_b) + \tan(i_d)}{1 - \tan(\varphi_b)\tan(i)}\right]\times(1-\eta) + \tan(\varphi_r)\times\eta\right) \tag{3.28a}$$

$$\eta = \exp\left(-\frac{u_s \times JRc}{100 \times c_1 \times (t/a)}\right) \tag{3.28b}$$

where, c_1 is an empirical constant which controls the rate of infill squeezing and i_d is given by Equation (2.58*b*).

3.5. Summary

Stability of rock mass is influenced significantly by infilled rock joints. The shear behaviour of infilled rock joints is controlled by several parameters such as joint surface roughness, type and thickness of infill, development of pore water pressure and drainage conditions, degree of over consolidation and boundary conditions.

In the past, experimental studies were carried out on model and natural joints with a variety of infill materials under monotonic loading (Goodman 1970; Kanji 1974; Ladanyi and Archambault 1977; Lama 1978; Phien-wej *et al.*, 1991; Papaliangas *et al.*, 1990, 1993; Indraratna *et al.*, 1999, 2005, 2007, 2010). The test results showed that the roughness affects the shear behaviour of infilled joints up to a critical infill thickness to asperity height $(t/a)_{cr}$. Beyond this critical value, the shear strength is controlled by the infill alone. The models used for predicting the strength of infilled joints are mostly empirical and are valid for monotonic loading. No study has been reported in the literature on shear behaviour of infilled rock joints under cyclic loading. Accordingly, in this research study, the effects of cyclic loading on the shear behaviour of infilled rock joints under CNS conditions is investigated (Chapter V). A mathematical model also will be proposed in Chapter VI to describe the shear strength in cyclic loading conditions.

Chapter IV

4. SHEAR BEHAVIOUR OF CLEAN ROCK JOINTS UNDER CYCLIC LOADING

4.1. Introduction

Laboratory studies are essential to design safe underground structures. The main objective of this research study is to investigate the shear behaviour of rock joints under cyclic loading and CNS conditions. Thus, a laboratory investigation was conducted based on a comprehensive experimental program using saw tooth shaped asperities and replicas of real rock surface cast in high strength Plaster of Paris for variety of initial normal stresses. The modified CNS cyclic testing machine was applied for this purpose.

4.2. Laboratory investigation

Selection of model material, sample preparation, CNS cyclic direct shear apparatus and plans for the study of cyclic loading effects on the shear behaviour of clean rock joints and shear rate effects on cyclic loading shear behaviour of rock joints under CNS conditions are described.

4.2.1. Selection of model material

High strength Plaster of Paris ($CaSo_4.H_2O$ hemihydrates) with a mixing ratio of 3.5:1 by weight of plaster to water was used to prepare the samples. Plaster of Paris which is a non-toxic material can be moulded into any shape when mixed with water and its long-term strength is independent of time once the chemical hydration is complete and dried

properly. The initial setting time for the gypsum used in this study was around 20 minutes. The mechanical properties of plaster after curing in an oven for 14 days at a constant temperature of 40° C were determined by performing several tests on cylindrical samples with a diameter of 50 mm and height of 110 mm. The tested average uniaxial compressive strength (σ_c) and Young's modulus (E) of the cured samples were approximately 60 MPa and 16 GPa respectively.

4.2.2. Sample preparation

Two types of joint surface were prepared for shear tests: saw tooth and replicas of a real rock surface (*JRC = 6*) collected from Kangaroo Valley NSW, Australia. Three different initial asperity angles 9.5° (Type I), 18.5 ° (Type II) and 26.5° (Type III) as representative of low, intermediate and high levels of roughness were selected to prepare triangular asperity moulds. The equivalent *JRC* values of 4.2, 9 and 13.8 have been calculated for Types I, II and III asperity surfaces using the method suggested by Xie and Pariseau (1992). The real rock joint surface was also physically imprinted on special resin to prepare the mould of the real rock surface. A close view of the mould of Type II asperity surface and joint sample collected from the field is shown in Figure 4-1. For each mould, a number of fully mated joints of high strength Plaster of Paris (*CaSo4.H2O* hemihydrates) were cast using a mixing ratio of 3.5:1 by weight of plaster to water. The bottom block was prepared inside the bottom mould containing the required surface profile and left for two hours to cure. The matching specimen was then cast on the top of the bottom specimen to ensure the fully mated conditions and the whole assembly was left for two additional hours to satisfy the initial setting time.

Figure 4-1 [left] Mould of Type II asperity surface, [right] Field sample

During sample preparation, mild vibration was applied to the mould externally to eliminate any entrapped air within the samples. The samples were then allowed to cure in an oven for 14 days at a constant temperature of 40°C. Prior to the cyclic shearing, the prepared samples were then acclimatised room temperature. A close view of typical prepared samples of the Type I (upper sample) and Type III (lower sample) asperity surfaces are shown in Figure 4-2. The joint surface area of each sample was 187.5 cm^2 (250 × 75 mm) with a total of eight asperities in the direction of shearing for triangular joints.

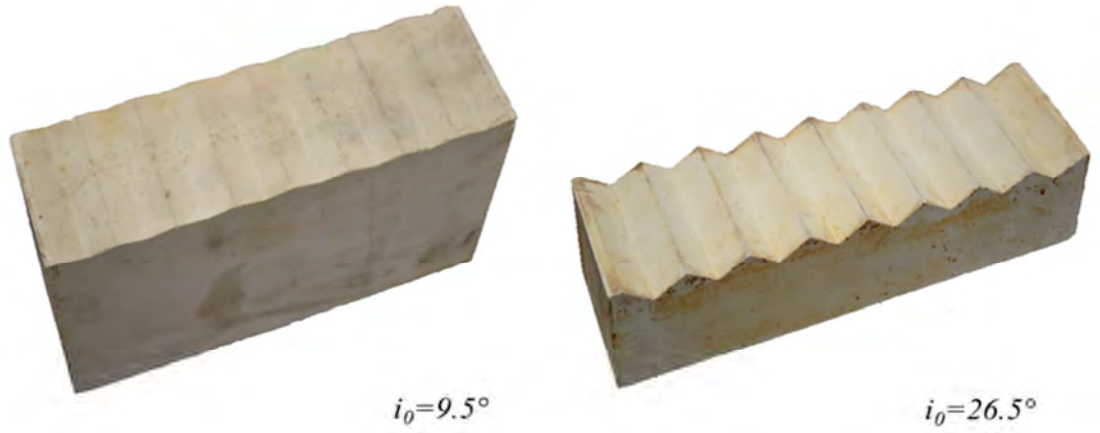

Figure 4-2 [left] Type I asperity surface (upper sample), [right] Type III asperity surface (lower sample)

Tilt test performed on planar interfaces of high strength Plaster of Paris indicated an average basic friction angle (φ_b) of 35°.

4.2.3. CNS cyclic direct shear apparatus

Experiments were carried out at the Rock Mechanics Laboratory, University of Wollongong, NSW, Australia, using the large scale cyclic direct shear apparatus updated for this study. The instrument consisted of two main parts, controller unit and mechanical section as shown in Figure 4-3.

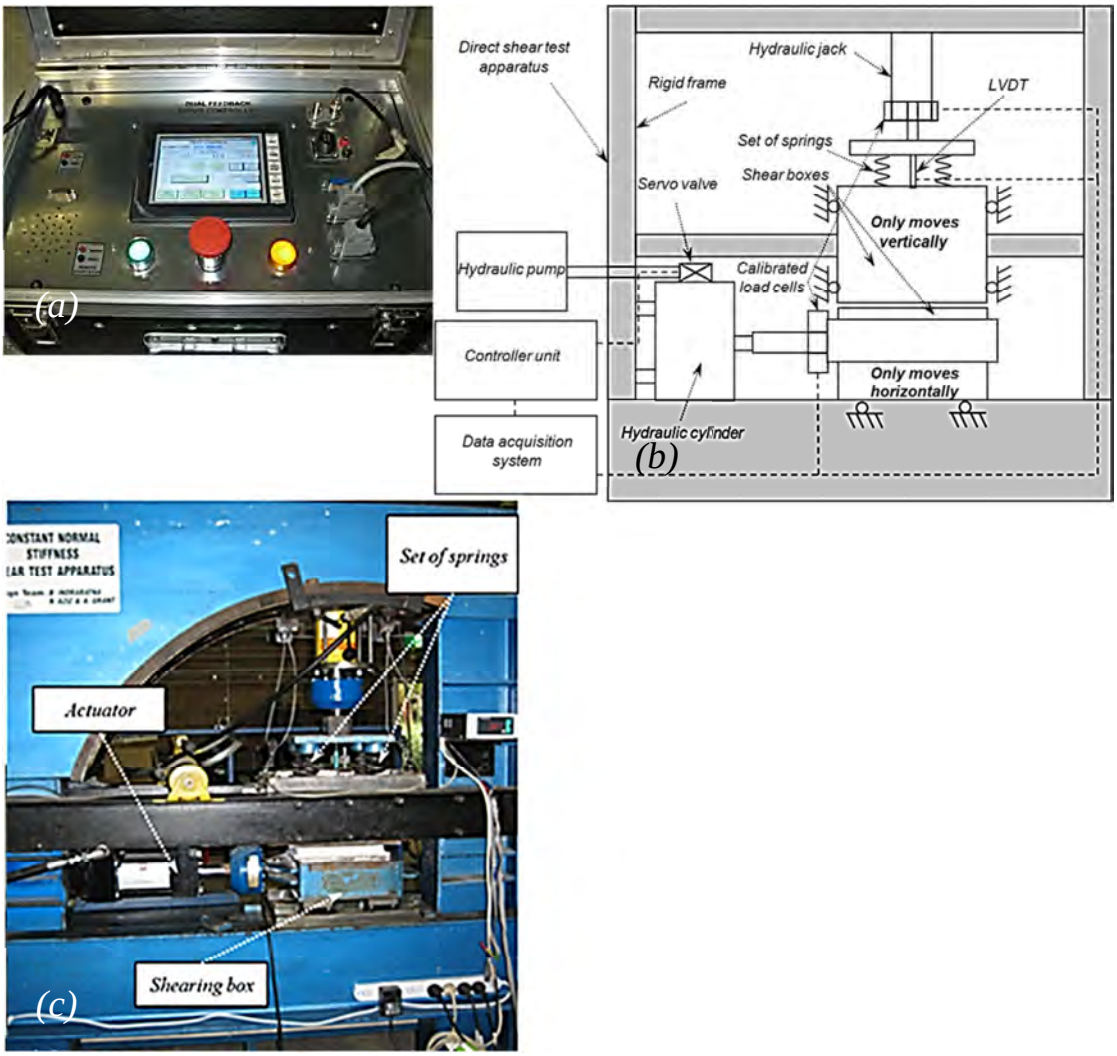

Figure 4-3*(a)* Controller unit, *(b)* Schematic diagram of the cyclic CNS direct shear apparatus, *(c)* General view of the cyclic CNS direct shear apparatus

The digital controller was able to assign the cyclic displacement of the sample. The mechanical part had two steel shearing boxes, 250 mm in length, 75 mm in width, and 150 mm and 100 mm in height of the top and bottom boxes respectively. A hydraulic jack located on top of the instrument was used to apply the initial normal load. A set of springs with stiffness of 8 kN/mm was incorporated to confine the joint dilation simulating the effect of surrounding rock mass. The lower box was only displaced laterally via a hydraulic actuator driven by the digital controller unit. The upper box moves only in a vertical direction on ball bearings such that any relative rotation of the joint surfaces is avoided. The shear and normal loads were measured by strain meters mounted on the load cells and the normal displacement was recorded using Linear Variable Differential Transformer (LVDT).

4.2.4. Experimental plan

The shear behaviour of rock joints under cyclic loading and CNS conditions was investigated in the laboratory by performing a test program on prepared saw tooth shape and replicas of rock surface samples. The experiments were conducted in two steps. Firstly, more than 15 cyclic direct shear tests (given in Table 4.1) were carried out on the joint specimens. Some of the tests were performed twice to ensure repeatability of the measured data. The applied initial normal stresses of the artificial triangular asperity joints were in the range of 0.16 MPa to 2.4 MPa, representing typical variations of normal stresses encountered in both civil and mining excavations. The replicas of the real rock surface were subjected to three different initial normal stresses 0.5 MPa, 1.5 MPa and 2.5 MPa. All samples were sheared for four consecutive cycles (each cycle sheared 60 mm) with shear rate of 0.5 mm/min.

Table 4-1 Experimental program for the study of cyclic loading effects on shear behaviour of rock joints

Test number	*Asperity Type*	*Applied normal stress (MPa)*
1, 2, 3, 4	Type I	0.16, 0.56, 1.64, 2.4
5, 6, 7, 8	Type II	0.16, 0.56, 1.64, 2.4
9, 10, 11, 12	Type III	0.16, 0.56, 1.64, 2.4
13, 14, 15	Replicas	0.5, 1.5, 2.5

The purpose of the first series of tests was to study the effects of cyclic loading on shear behaviour of rock joints under CNS conditions. Subsequently, another series of cyclic shear tests with two different shear rates were carried out on specimens made based on Type I asperity surface as listed in Table 4.2.

Table 4-2 Experimental program for the study of shear rate effects on cyclic loading shear behaviour of rock joints under CNS conditions

Test number	*Shear rate (mm/s)*	*Applied normal stress (MPa)*
16,17,18	5	0.56, 1.64, 2.4
19,20,21	20	0.56, 1.64, 2.4

More than six cyclic direct shear tests with shear rates of 5 mm/s and 20 mm/s and initial normal stresses of 0.56 MPa, 1.64 MPa and 2.4 MPa were conducted on the samples. The tests were continued for 100 consecutive loading cycles. The maximum tangential displacement was half of the asperity length (15 mm). The second series of

tests was intended to investigate the effects of shear rate on cyclic loading shear behaviour of rock joints under CNS conditions. A constant normal stiffness of 8 kN/mm was applied via an assembly of four springs for all the cyclic loading tests. The values of shear load, normal load and normal displacement against shear displacements were constantly monitored during each cyclic shear test. The prescribed shear displacement in cyclic loading conditions was described in section 2.4.

4.3. Experimental results of the first tests series

Figures 4-4 to 4-11 show the results of cyclic loading shear tests performed on the samples for different conditions of initial roughness and normal stress.

4.3.1. Shear strength

For σ_{n0} = 0.16 MPa and 0.56 MPa, the shear strength is higher in the forward shearing represented by the upper right quadrant of shear stress - shear displacement curve rather than the reverse loading (Figures. 4-4, 4-6 and 4-8). In forward shearing, the shear strength decreases with each cycle as the dilation component diminishes due to asperities damage. However, for reverse shearing, the friction angle increases as asperities degrade. This behaviour can be explained using Patton (1966)'s basic formula for the shear resistance [$\tau = \sigma_n \tan(\varphi_b + i)$], where, τ is the shear stress, σ_n is the normal stress, φ_b is the basic friction angle and i is the dilation angle. In forward shearing, the [i] component is positive, and therefore the friction angle will be [$\varphi_b + i$]. For reverse shearing, the dilation component is negative which gives [$\varphi_b - i$] as the friction angle.

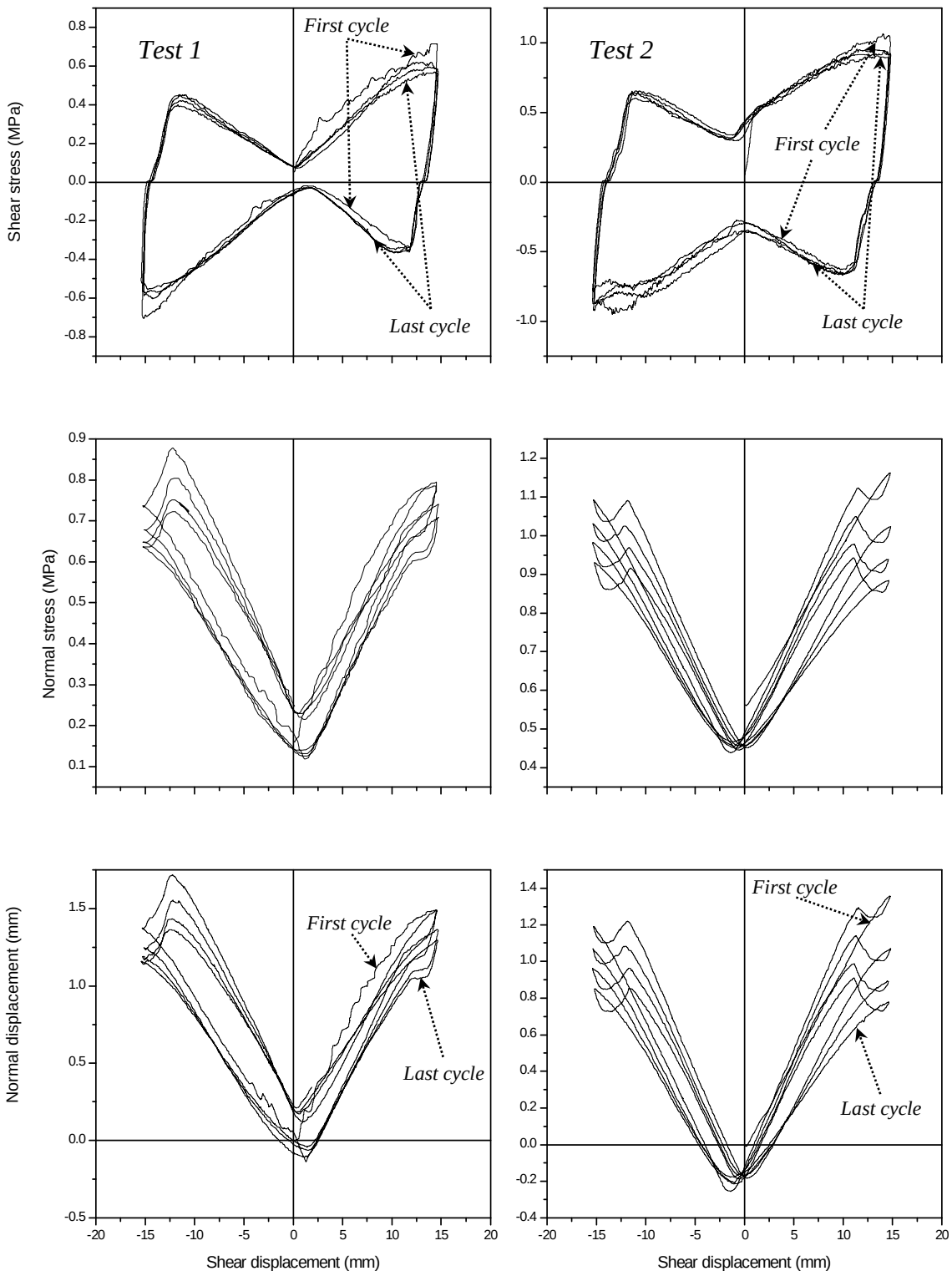

Figure 4-4 Cyclic loading shear behaviour of rock joints with Type I asperity surface: [left] σ_{n0} = 0.16 MPa, [right] σ_{n0} = 0.56 MPa

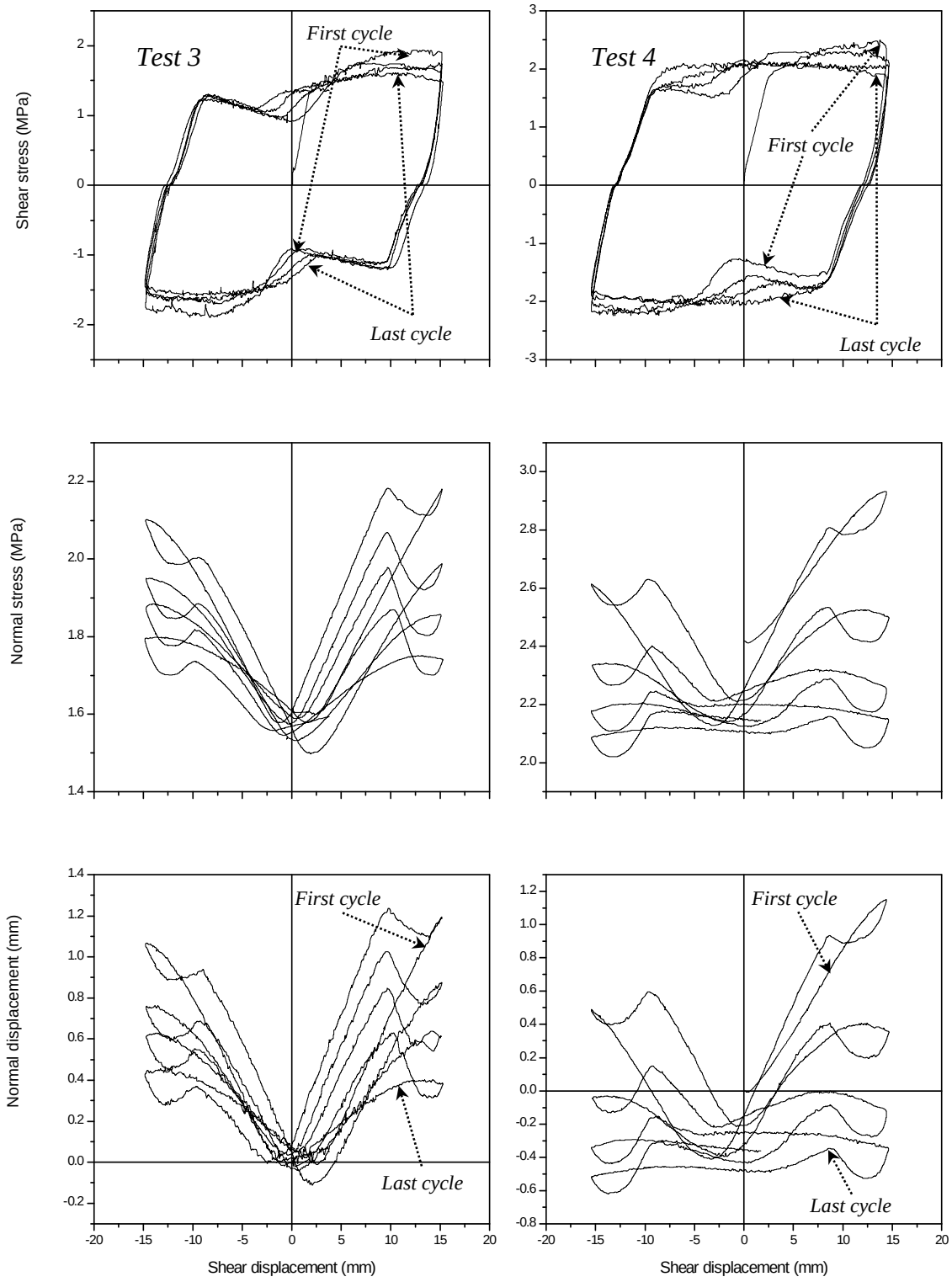

Figure 4-5 Cyclic loading shear behaviour of rock joints with Type I asperity surface: [left] σ_{n0} = 1.64 MPa, [right] σ_{n0} = 2.4 MPa

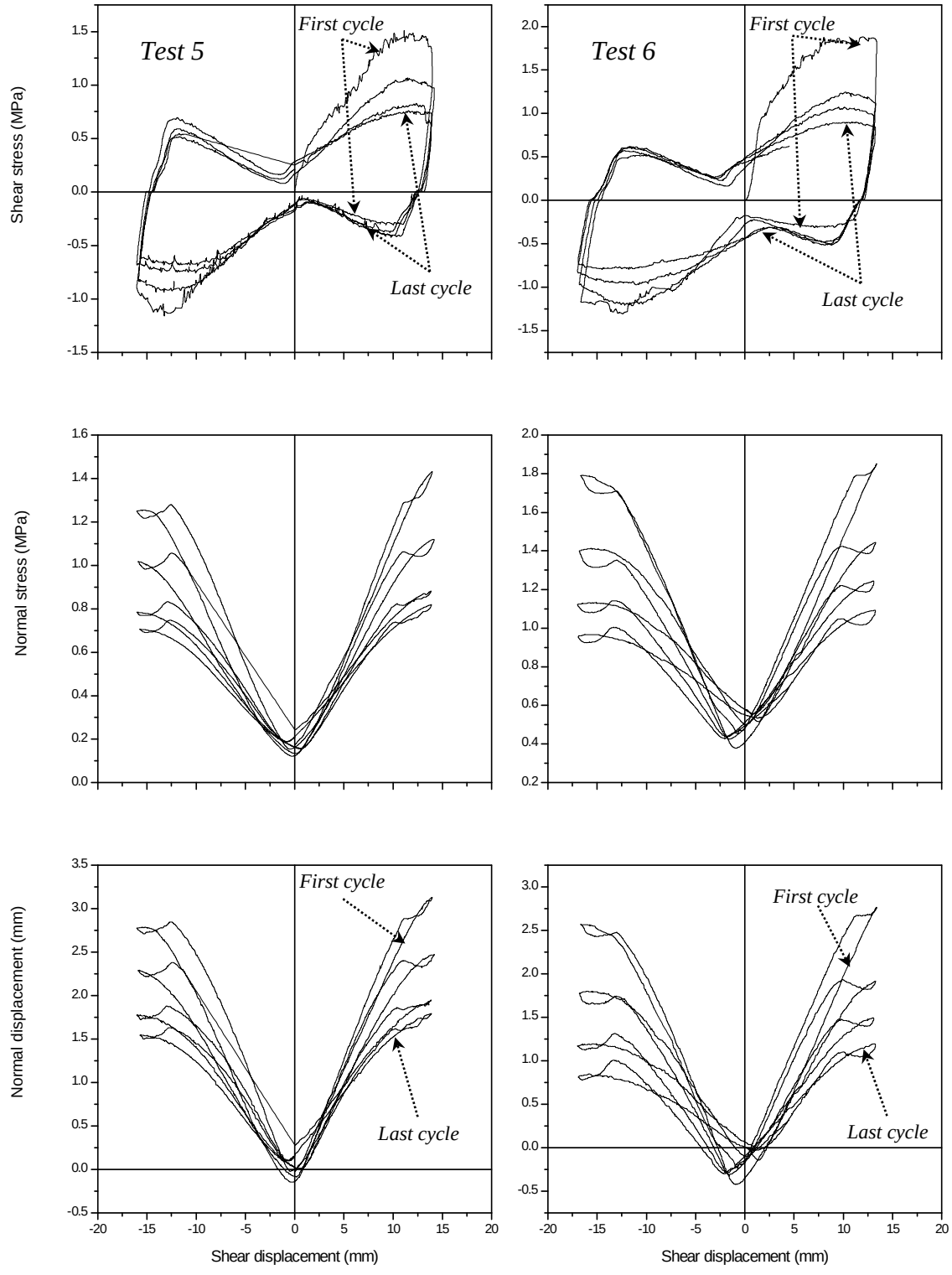

Figure 4-6 Cyclic loading shear behaviour of rock joints with Type II asperity surface: [left] σ_{n0} = 0.16 MPa, [right] σ_{n0} = 0.56 MPa

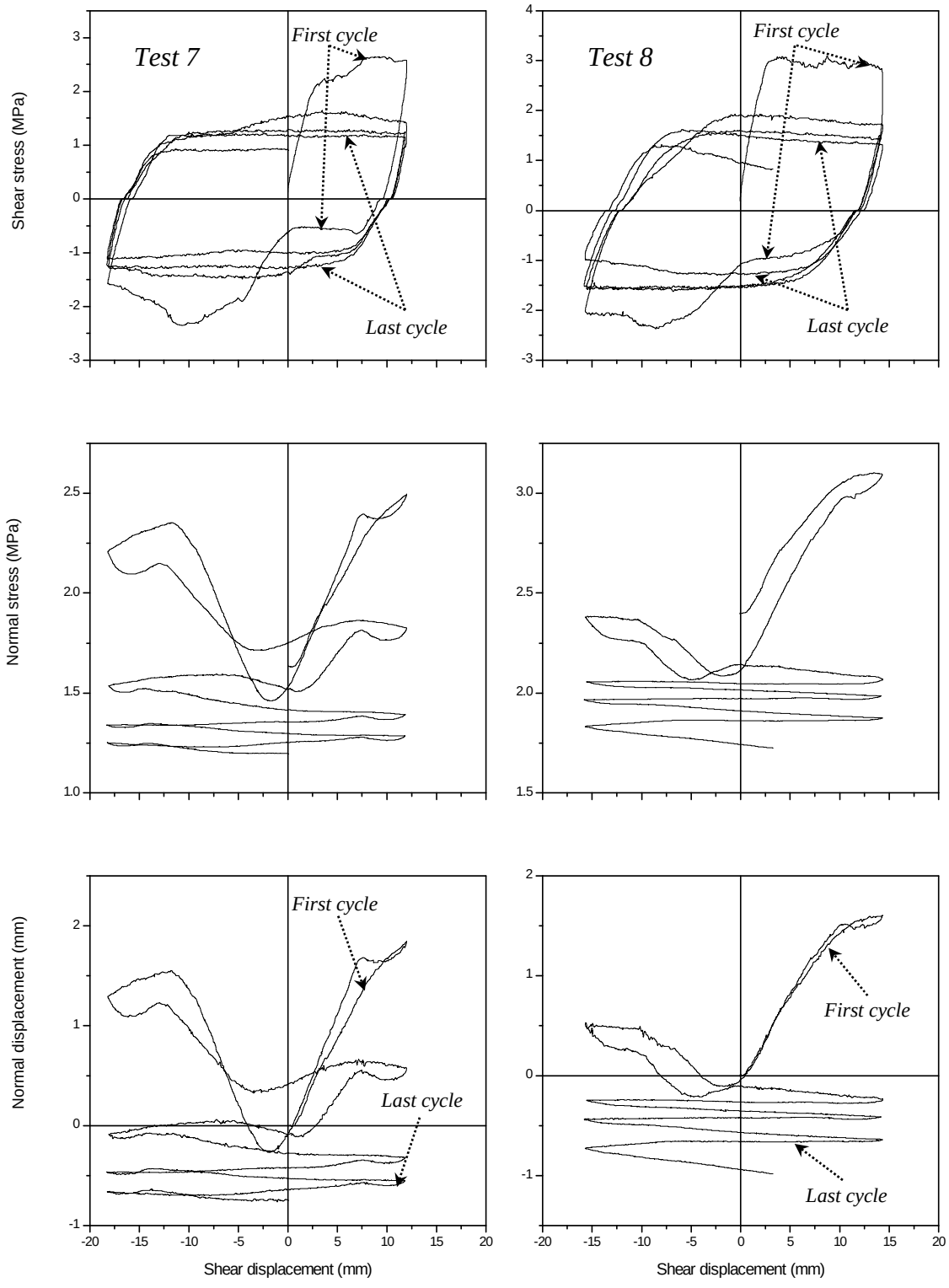

Figure 4-7 Cyclic loading shear behaviour of rock joints with Type II asperity surface: [left] σ_{n0} = 1.64 MPa, [right] σ_{n0} = 2.4 MPa

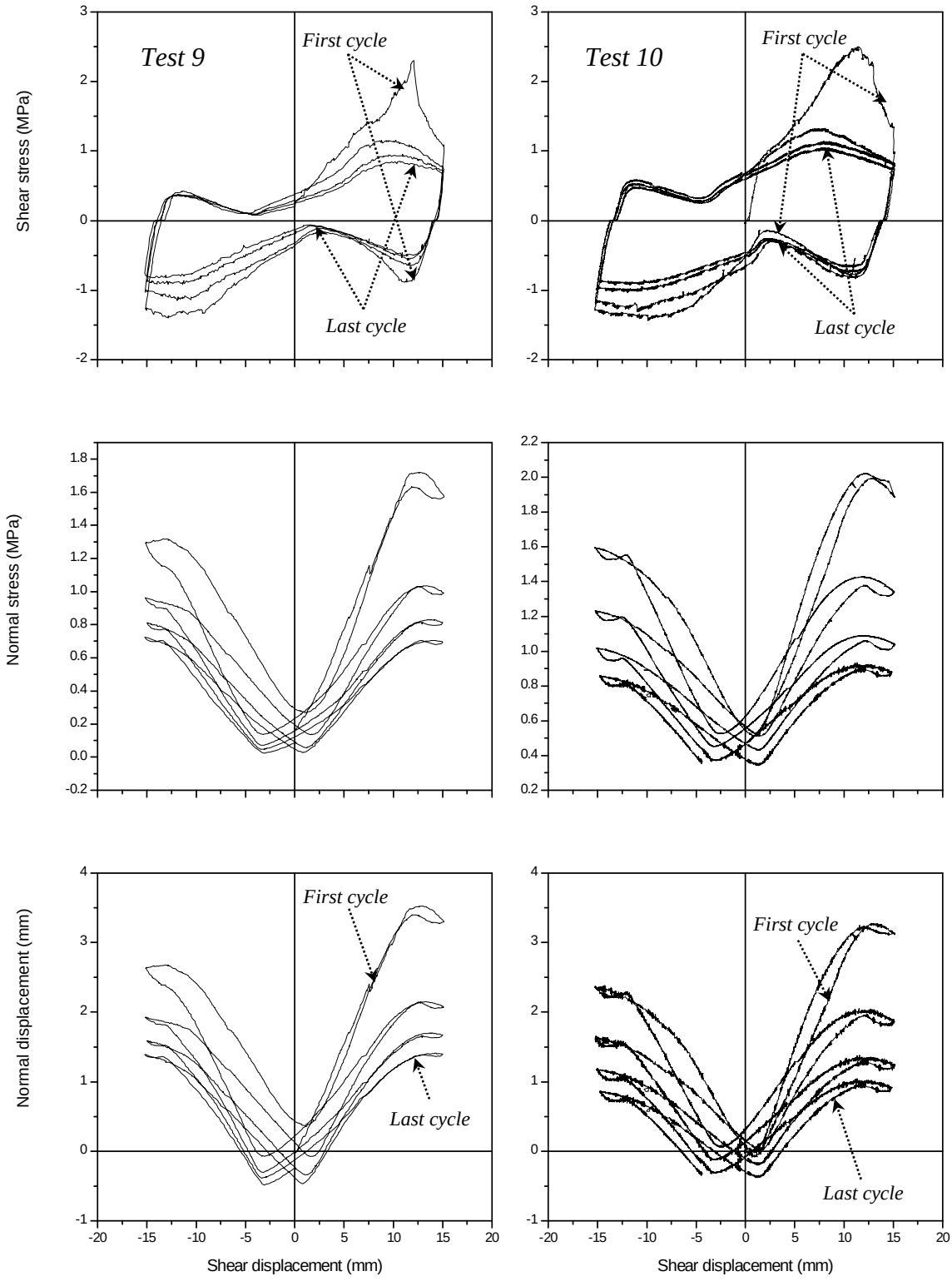

Figure 4-8 Cyclic loading shear behaviour of rock joints with Type III asperity surface: [left] σ_{n0} = 0.16 MPa, [right] σ_{n0} = 0.56 MPa

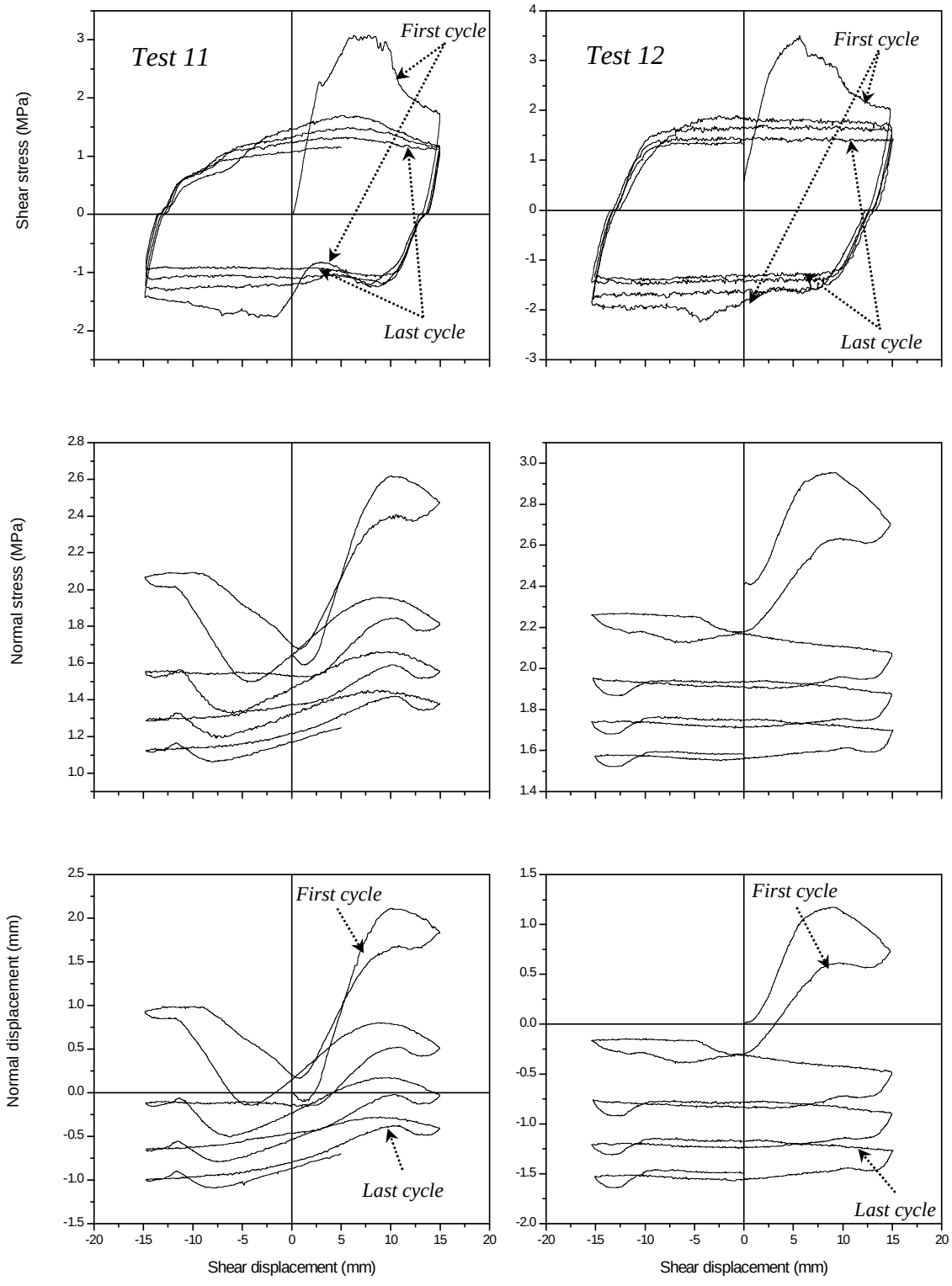

Figure 4-9 Cyclic loading shear behaviour of rock joints with Type III asperity surface: [left] σ_{n0} = 1.64 MPa, [right] σ_{n0} = 2.4 MPa

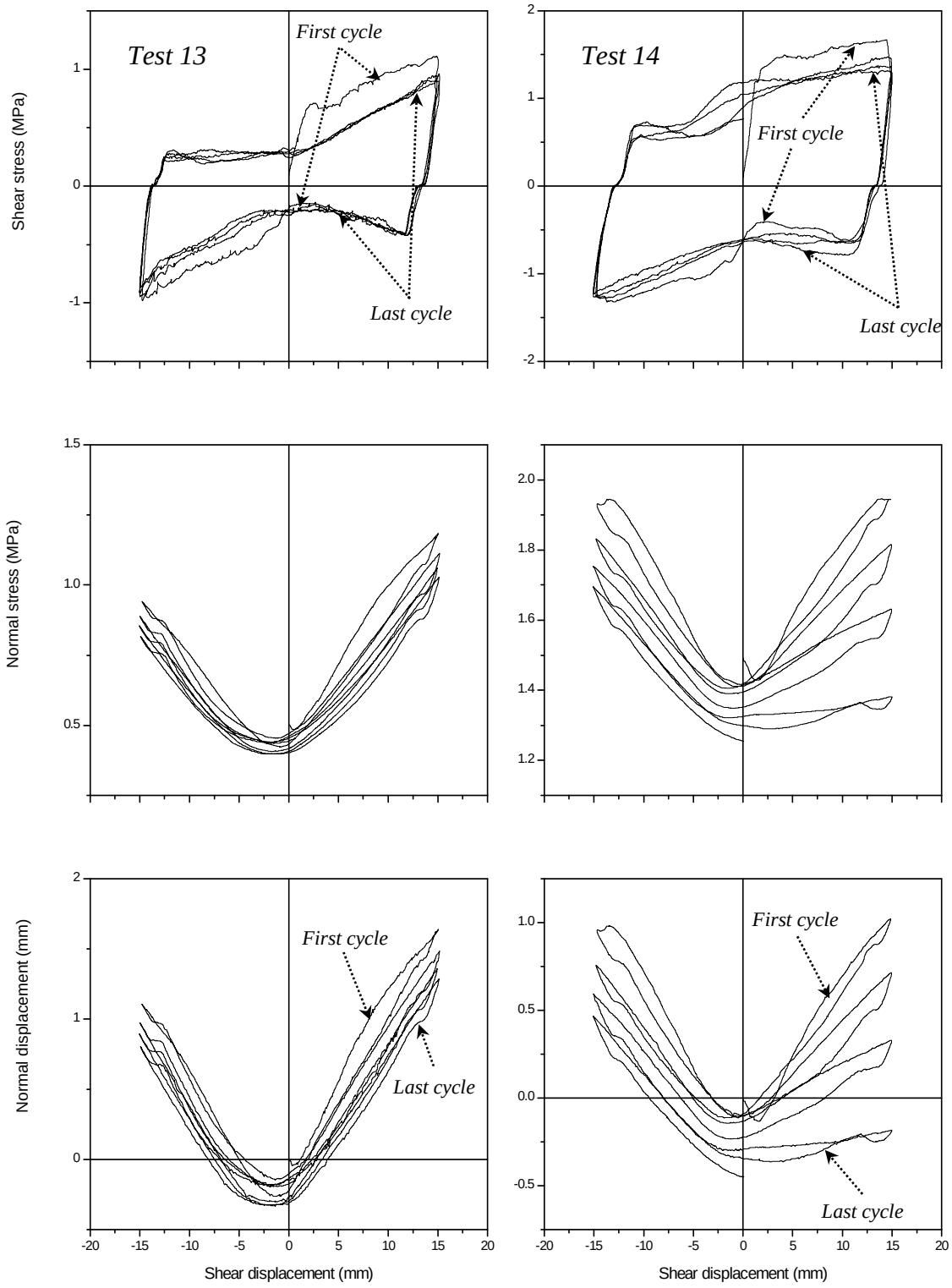

Figure 4-10 Cyclic loading shear behaviour of replicas of real asperity surface: [left] σ_{n0} = 0.5 MPa, [right] σ_{n0} = 1.5 MPa

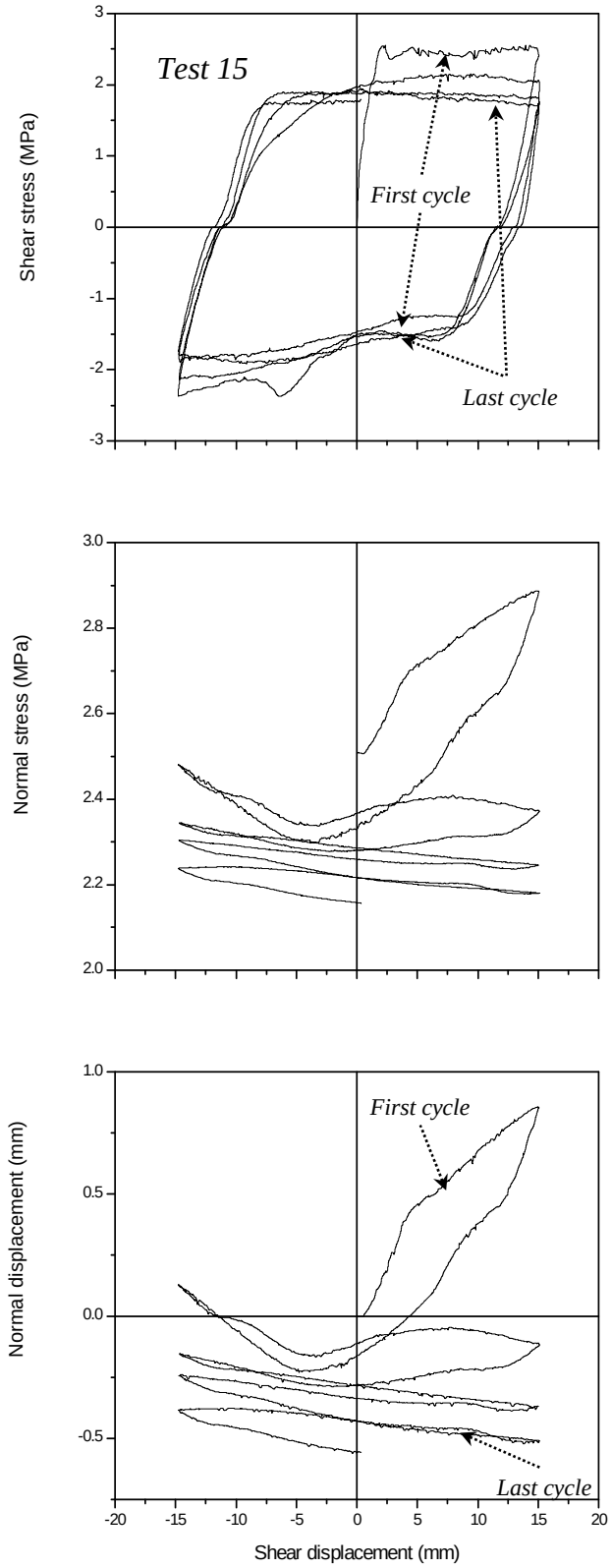

Figure 4-11 Cyclic loading shear behaviour of replicas of real asperity surface with σ_{n0} = 2.5 MPa

As cyclic loading is exerted on the asperities, the [i] component decreases which results in the less friction angle for the forward shearing of later cycles than initial cycles. In reverse loading, the opposite is true and [$\varphi_b - i$] becomes larger as [i] decreases. The difference between the shear stress profiles shown in Figure 4-4 was insignificant for cyclic loading shearing of Type I asperity surface. This difference gradually increased with increasing initial asperity angles for Types II and III asperity surfaces (Figures 4-6 and 4-8). In the case of Type I asperity surface, the relative movement between the asperities surfaces caused an intangible damage of joints surfaces. Thus, keeping the friction angle roughly unchanged. For each additional cycle of shearing, the shear strength was marginally decreased. As the initial asperity angle was increased (Types II and III joints surfaces), the shearing of the asperities surfaces also increased, and the difference in shear stress profiles for various cycles of loading became significant. In the tests where the initial normal stress was increased to 1.64 MPa and 2.4 MPa (Figures 4-5, 4-7 and 4-9), the difference between forward and backward shearing after the first shear cycle became less pronounced, indicating the asperity breakage mechanism. The data reveals that as the asperity angle increases from Type I to Type III, the asperity breakage mechanism is more pronounced due to higher interlocking between asperities. For instance in Type III joint profile shown in Figure 4-9 [right], no further substantial decrease in the shear stress profile was noted after the first forward loading cycle. Beyond this stage, any negligible reduction in shear strength under cyclic loading is related to the change in the effective normal stress.

4.3.2. Normal displacement and asperity damage

The initial negative dilation may be ascribed to the sample compaction, closure of holes and the initial settlement of fine irregularities along the joint surface. Generally, the

dilation during overriding of asperities is recovered in loading reversal. Due to the damage of asperities, dilation and the dilation angle reduced with increase in the shear cycles. The asperity damage and reduction in dilation is higher in the forward shearing rather than the reverse one. In the same way, asperities undergo less degradation with increase in the loading cycles. This can be described by the external energy exerted on asperities during shearing as higher energy generates more damage. The total external energy subjected to asperities during shearing to the asperity area is defined as: $[\int \sigma_n dv + \tau du]$, where, *dv* and *du* are the increments of normal and shear displacement. Thus, any increase in the normal stress or initial asperity angle, increases the external energy subjected to asperities, resulting in higher asperity degradation. The values of Asperity Damage (*AD*), defined as the reduction in the asperity height to the initial asperity height for different asperity types, initial normal stresses and number of loading cycles are given in Table 4.3. It is evident that the asperity damage is greater for higher initial normal stresses, asperity angles and loading cycles where higher shear and normal energies are generated. In addition, the values of asperity damage for all cases after four consecutive cycles of shearing under CNS conditions are higher than 50% and increases to 100% for greater initial normal stresses and asperity angles. As the normal stress increased to 2.4 MPa, the asperities were sheared off close to the asperity tips giving dome shaped dilation curves (Figures 4-7 and 4-9). Following the initial rapid degradation during the first shear cycle due to the high level of initial normal stress (σ_{n0} = 2.4 MPa), contraction rather than dilation may be observed in subsequent shearing (Figures 4-5, 4-7 and 4-9). This might be related to the loss of the gouge at the sample edge of the shear box during cyclic shearing when asperities are broken up from the base. This behaviour may not happen along the field joints where the gouge is confined by the surrounding media.

Table 4-3 Asperity damage (*AD*) for various initial normal stresses and asperity angle

Asperity Type	*Applied normal stress (MPa)*	*AD 1th cycle*	*AD 2nd cycle*	*AD 3rd cycle*	*AD 4th cycle*
Type I	0.16	45%	50%	53%	54%
	0.56	53%	57%	61%	66%
	1.64	58%	70%	76%	83%
	2.4	81%	100%	100%	100%
Type II	0.16	45%	54%	65%	69%
	0.56	49%	64%	77%	84%
	1.64	74%	100%	100%	100%
	2.4	90%	100%	100%	100%
Type III	0.16	64%	74%	78%	81%
	0.56	68%	78%	84%	88%
	1.64	87%	100%	100%	100%
	2.4	100%	100%	100%	100%

4.3.3. Normal stress

The main difference between the CNS and CNL conditions is the change in normal stress with shear displacement. In the similar way to normal displacement, the normal stress increases during asperity overriding and decreases toward its initial value in loading reversal. This will result in higher asperity damage particularly in the first cycle and around the asperity tips rather than the subsequent cycles and around the asperity

valleys. In the case of contraction in the normal displacement after the initial rapid degradation of asperities (Figures 4-5, 4-7 and 4-9), the normal stress may fall below the value of initial normal stress. As discussed in section 4.3.2, this phenomenon is limited only to the laboratory conditions where the gouge might escape the shearing box under cyclic loading. The normal stress variation with shear deformation contributes to the shear strength whereby higher shear strength is observed during the dilation stage. The change in the profile of normal stress decreases with increasing asperity damage which is a function of the initial normal stress and number of loading cycles for a particular asperity angle and normal stiffness. The maximum values of normal stress for Type I asperity surface recorded in the first shear cycle were 0.79 MPa and 2.94 MPa corresponding to the initial normal stress levels of 0.16 MPa and 2.4 MPa respectively. The values for Type III asperity surface were 1.72 MPa and 2.95 MPa.

4.3.4. Replicas of a real rock surface

Figures 4-10 and 4-11 show the results of cyclic shear tests conducted on replicas of a real rock surface with 0.5 MPa, 1.5 MPa and 2.5 MPa of applied initial normal stresses. The main differences between the shear behaviour of real rock surface replicas and triangular asperities are attributed to the influence of the second order asperities and spatial distribution of roughness. The effect of second order asperities is depicted in Figure 4-10 for cyclic loading shearing with 0.5 MPa of initial normal stress where higher shear strength is attained in the first cycle in comparison to the subsequent cycles. Nevertheless, the second order asperities are mostly damaged in the first cycle and afterward the shear behaviour is dominated by the first order asperities. In the case of shearing with initial normal stress of 2.5 MPa (Figure 4-11), the behaviour of real rock joint imprint is similar to triangular asperities as both the first and second order

asperities are sheared off in the first cycle and the friction angle approaches the value of the residual friction angle during further shearing. In addition, due to spatial distribution of roughness, different shear behaviour including shear stress against shear displacement and associated dilation are observed for the left and right sides of cyclic shearing. The damage trend of real joint replicas is identical to triangular joints which is proportional to the external applied shear and normal energies.

4.3.5. Strength envelope

The strength envelopes representing the relationship between the peak shear stress and normal stress for different conditions of initial normal stress, asperity types and number of cycles are plotted in Figure 4-12. For Type I asperity surface, it is evident that the strength envelopes do not change considerably with increase in the number of shear cycles. In this condition, the strength envelopes are close to that of planar asperities indicated by the dashed line in Figure 4-12(*a*). As the initial asperity angle increases (Type II and III asperity surfaces), the gap between cyclic loading strength envelopes also increases, getting close to the minimum boundary after four loading cycles (i.e. planar joints). This is related to the asperity damage with increase in the number of shear cycles that diminishes the joint roughness. Moreover, it can be noted that in the case of the Type III asperity surface, there is a sharp difference between the strength envelopes of the first and second loading cycles due to high initial asperity interlocking (Figure 4-12*c*). In general, the current test results reveal that the variation of the strength envelopes under cyclic loading with increase in the number of shear cycles is proportional to the asperity damage. When considerable asperity damage takes place, the strength envelopes show significant differences and approach that of planar joints as

cyclic loading continues. Conversely, strength envelopes will not be significantly affected in the case of low asperity damage during cyclic loading.

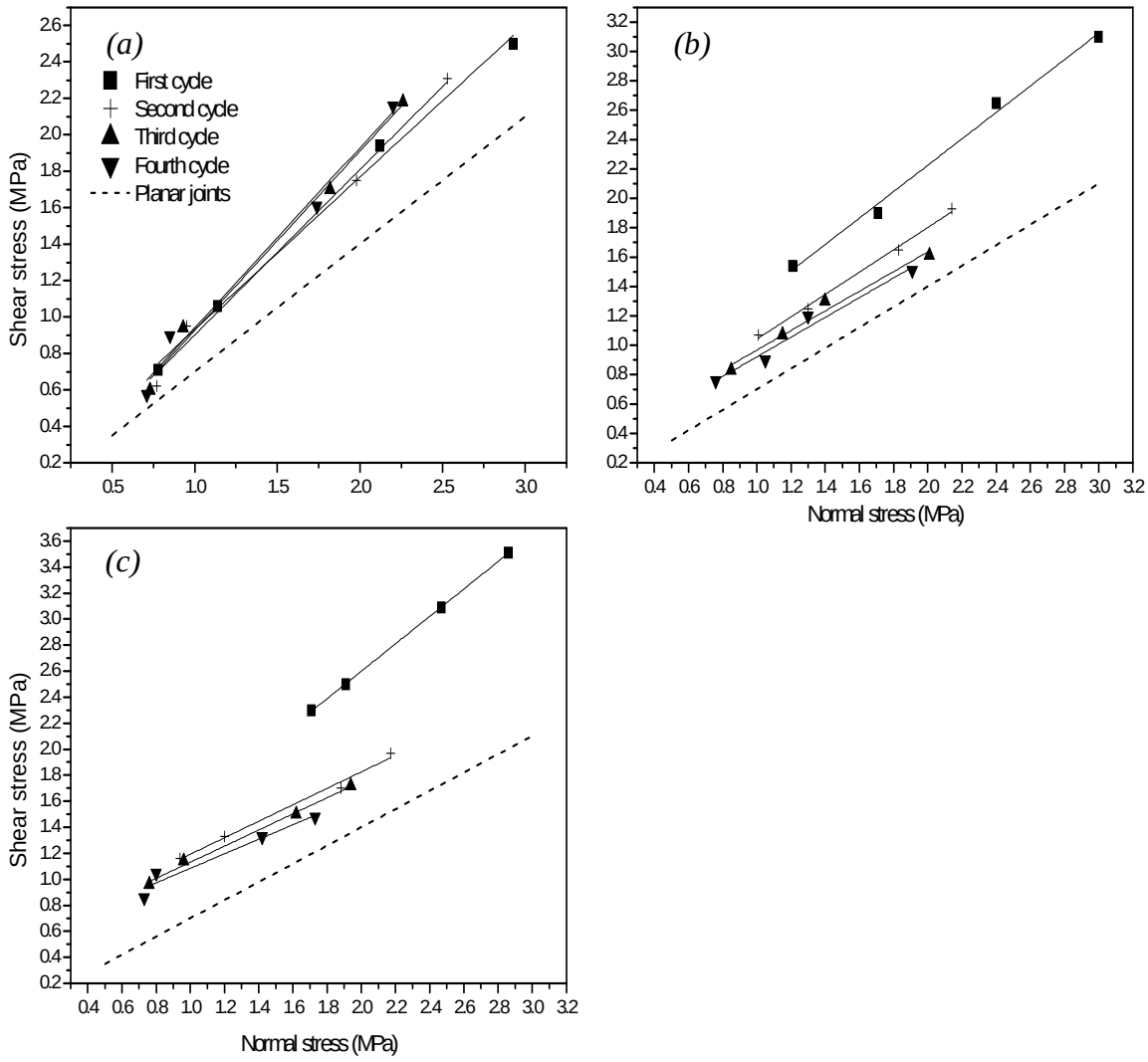

Figure 4-12 Strength envelope for cyclic loading shear strength of rock joints: *(a)* Type I asperity surface, *(b)* Type II asperity surface, *(c)* Type III asperity surface

4.3.6. Profile of damaged joints

At the end of the test, the shear boxes were dismantled and the final joint profile was mapped where possible. In Figure 4-13 [up], Type I asperity surface after application of cyclic shear loading with 0.56 MPa of initial normal stress has been shown. It appears

that asperities were damaged mostly around the tips where the true joint area that resists against the shearing, is less than the partially and fully mated conditions. The asperities shapes have deformed from the triangular shape at the beginning of shearing to the sinusoidal shape after completion of four consecutive shear cycles. It is inferred from Figure 4-13 [down] (Type I and σ_{n0} = 1.64 MPa) that the asperity valleys have been somehow filled up with firmly compacted damaged materials (gouge) during shearing.

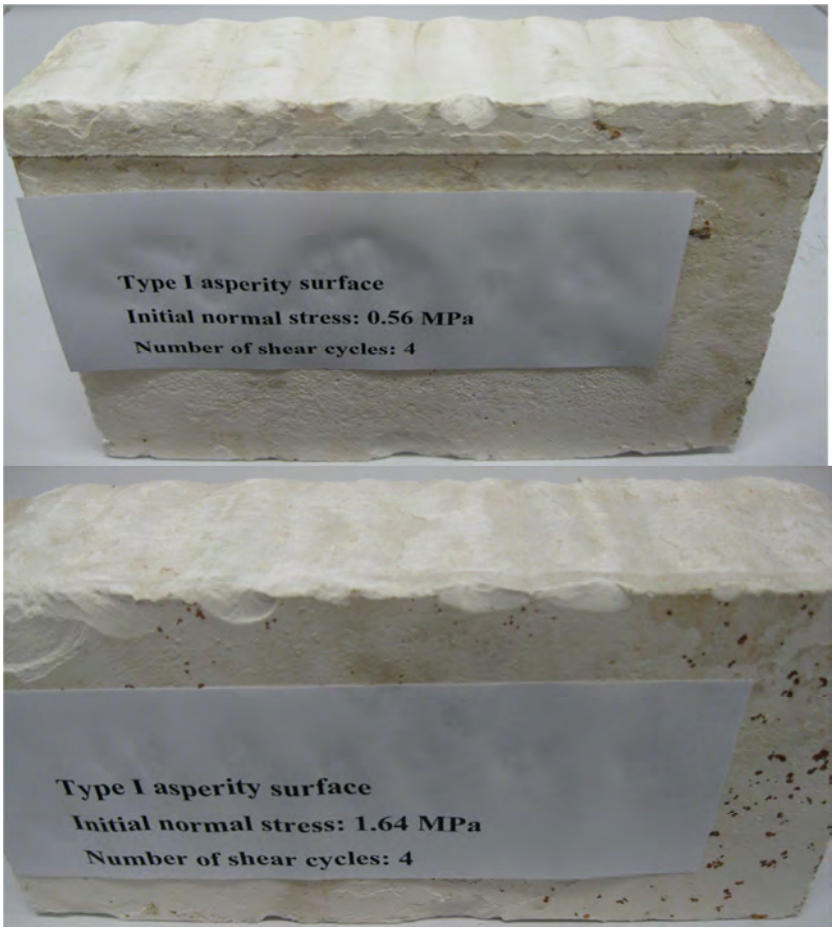

Figure 4-13 Type I asperity surface after completion of cyclic loading: [up] σ_{n0} = 0.56 MPa, [down] σ_{n0} = 1.64 MPa

The reattached gouge may again be chipped off and moves depending on the direction of shearing that might affect the shear behaviour under cyclic loading. As expected for Type III asperity surface and 2.4 MPa of initial normal stress (Figure 4-14), asperities have been sheared off from the base. The close view of the asperity profile shows a non-

uniform breakage trend through the joint surface. Some of the asperities have been almost destroyed while the others exhibit residual roughness. The reattachment of the gouge is also observed in this specimen particularly around the asperities subjected to higher damage.

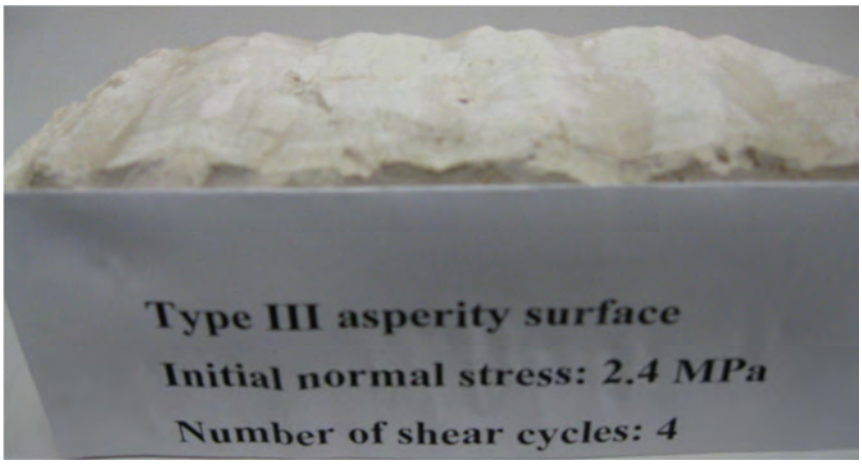

Figure 4-14 Type III asperity surface after application of cyclic loading with σ_{n0} = 2.4 MPa

4.4. Experimental results of the second tests series

The results of cyclic shear tests for various initial normal stresses conducted on Type I asperity surface with 5 mm/s and 20 mm/s of shear rates are plotted in Figures 4-15 to 4-17. For the comprehensive investigation of the shear rate effects on cyclic loading shear behaviour of rock joints under CNS conditions, the previous data sets collected with shear rate of 0.5 mm/min for Type I asperity surface are also recalled (Figures 4-4 and 4-5). The results indicate that the shear rate significantly affects the shear strength of hard rock joints under cyclic loading and CNS conditions. In general, the cyclic loading shear strength under CNS conditions is observed to decrease as the shear rate is increased. The peak shear strength recorded for the first and fourth cycles of shearing with shear rate of 0.5 mm/min and 20 mm/s and under initial normal stress of 0.56 MPa were 1.06 MPa, 0.9 MPa, 0.64 MPa and 0.62 MPa respectively.

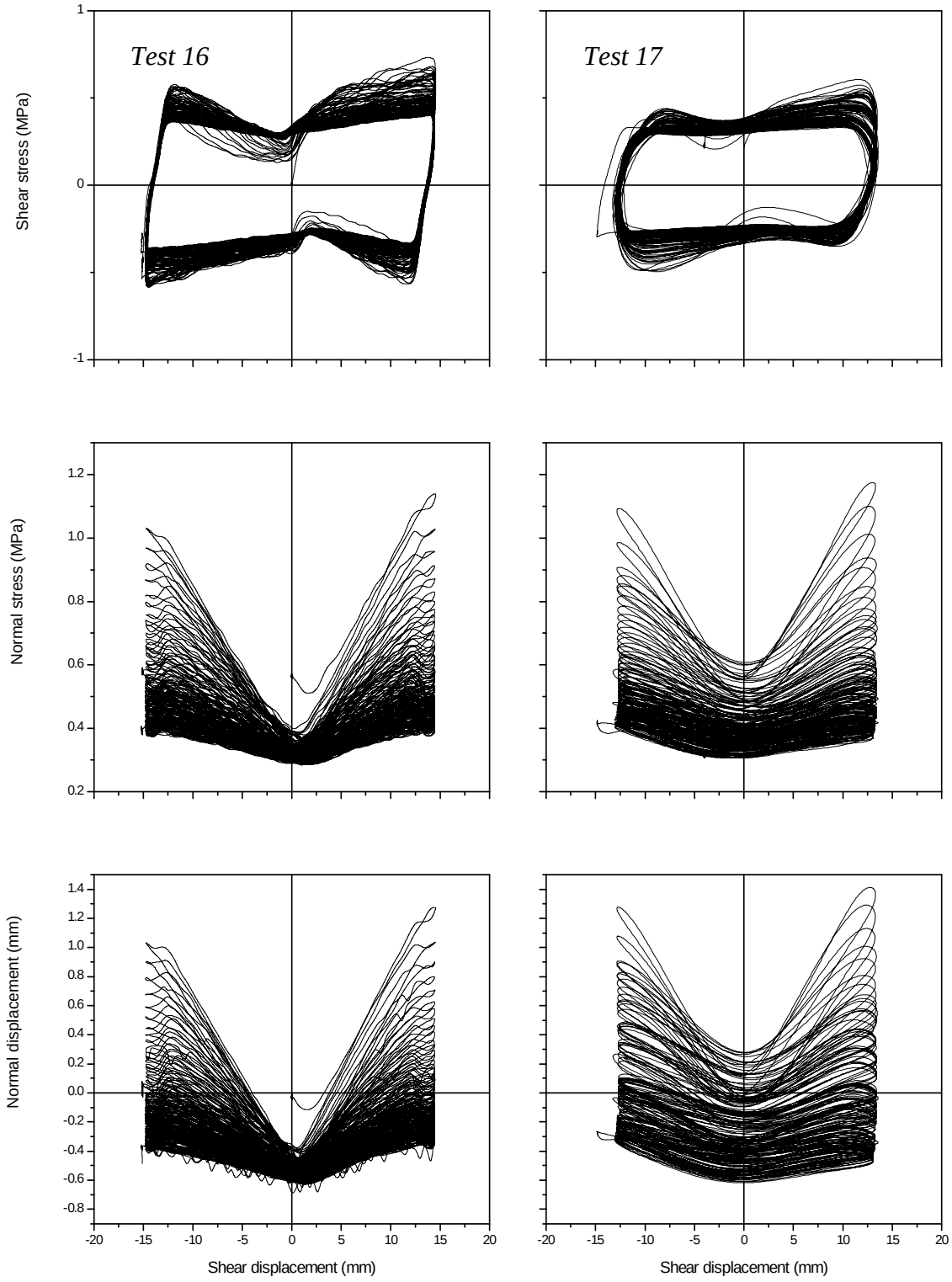

Figure 4-15 Cyclic loading shear behaviour of rock joints with Type I asperity surface and σ_{n0} = 0.56 MPa: [left] 5 mm/s of shear rate, [right] 20 mm/s of shear rate

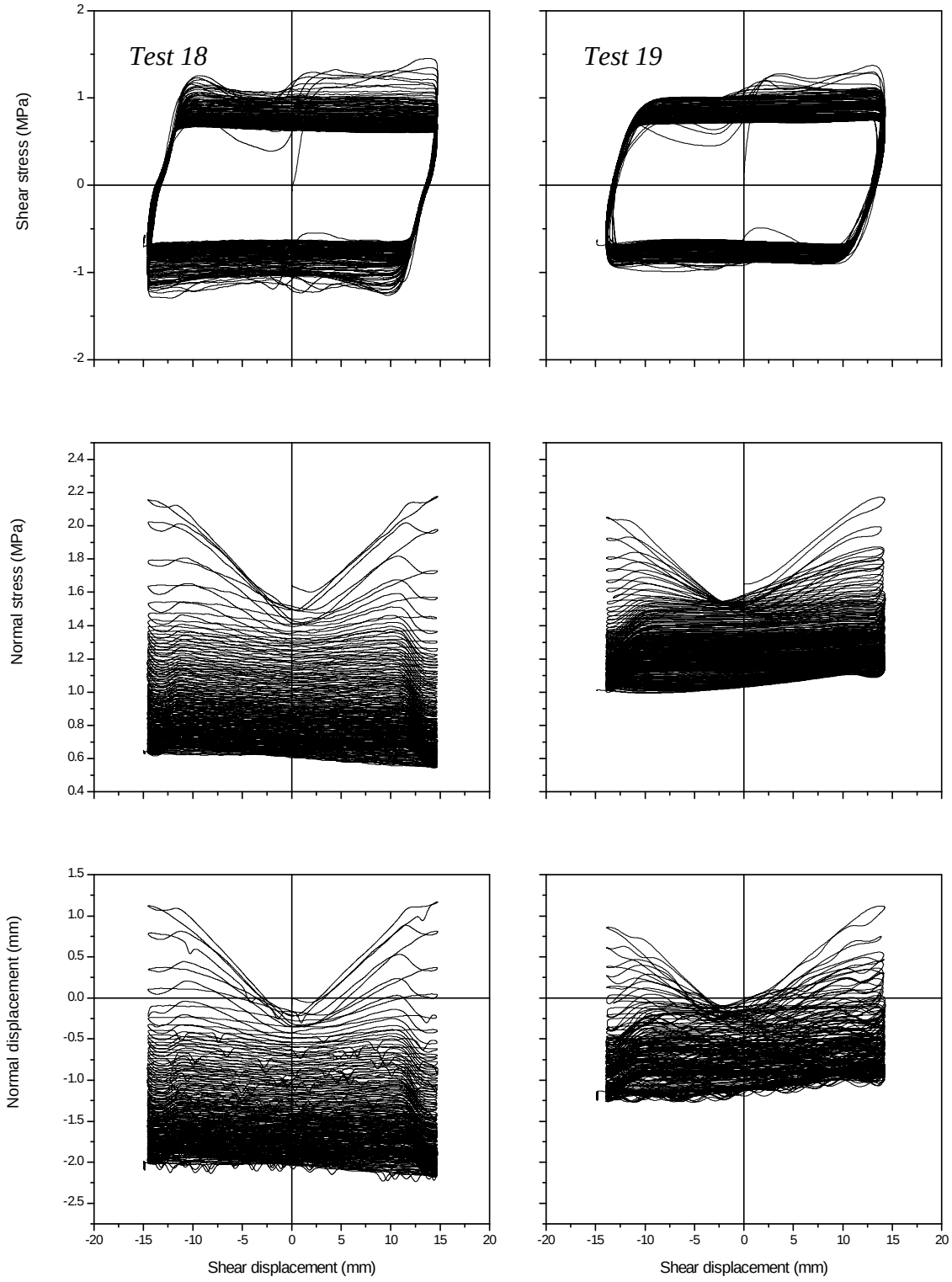

Figure 4-16 Cyclic loading shear behaviour of rock joints with Type I asperity surface and σ_{n0} = 1.64 MPa: [left] 5 mm/s of shear rate, [right] 20 mm/s of shear rate

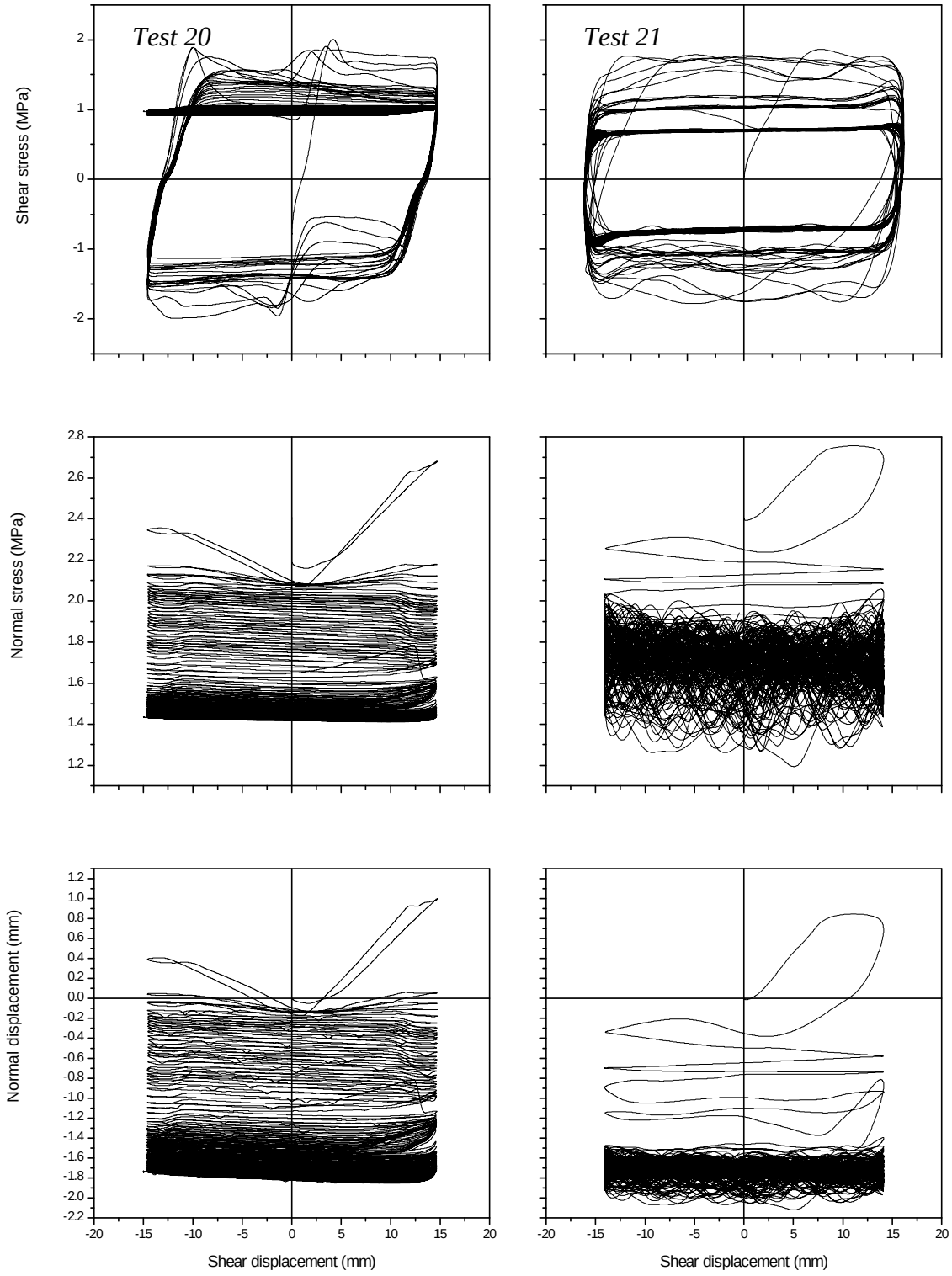

Figure 4-17 Cyclic loading shear behaviour of rock joints with Type I asperity surface and σ_{n0} = 2.4 MPa: [left] 5 mm/s of shear rate, [right] 20 mm/s of shear rate

The shear strength decreased at least 4% when the shear rate increased from 5 mm/s to 20 mm/s during the first four loading cycles for asperity shearing with 2.4 MPa of initial normal stress (Figure 4-17).

4.4.1. Shear strength and dilation angle

In Figure 4-18, the normalised shear strength (normalised to the initial normal stress) and normalised secant dilation angle (normalised to the initial asperity angle) were plotted against the shear rate for the first four loading cycles and different initial normal stresses. The experimental data indicates that the effect of shear rate on shear strength decreases with increase in the number of shear cycles as roughness degradation occurs. Because there are no asperities, it is expected that the variation of shear rate does not affect the cyclic loading shear behaviour of planar joints. In addition, as the initial normal stress increases, the effects of shear rate are less pronounced due to asperity breakage mechanism. The data reveals that the normalised secant dilation angle varies non-monotonically with the change in the shear rate. There might be different mechanisms involved such as sliding under low normal stress, asperity breakage and production and dilation of gauge under medium and large normal stresses. The variation of normalised shear strength (normalised to the initial normal stress) against number of loading cycles (100 loading cycles) under 5 mm/s and 20 mm/s of shear rates at different initial normal stresses is plotted in Figure 4-19. The effects of increase in the shear rate and loading cycles in reducing the shear strength are evident for asperity shearing under CNS conditions.

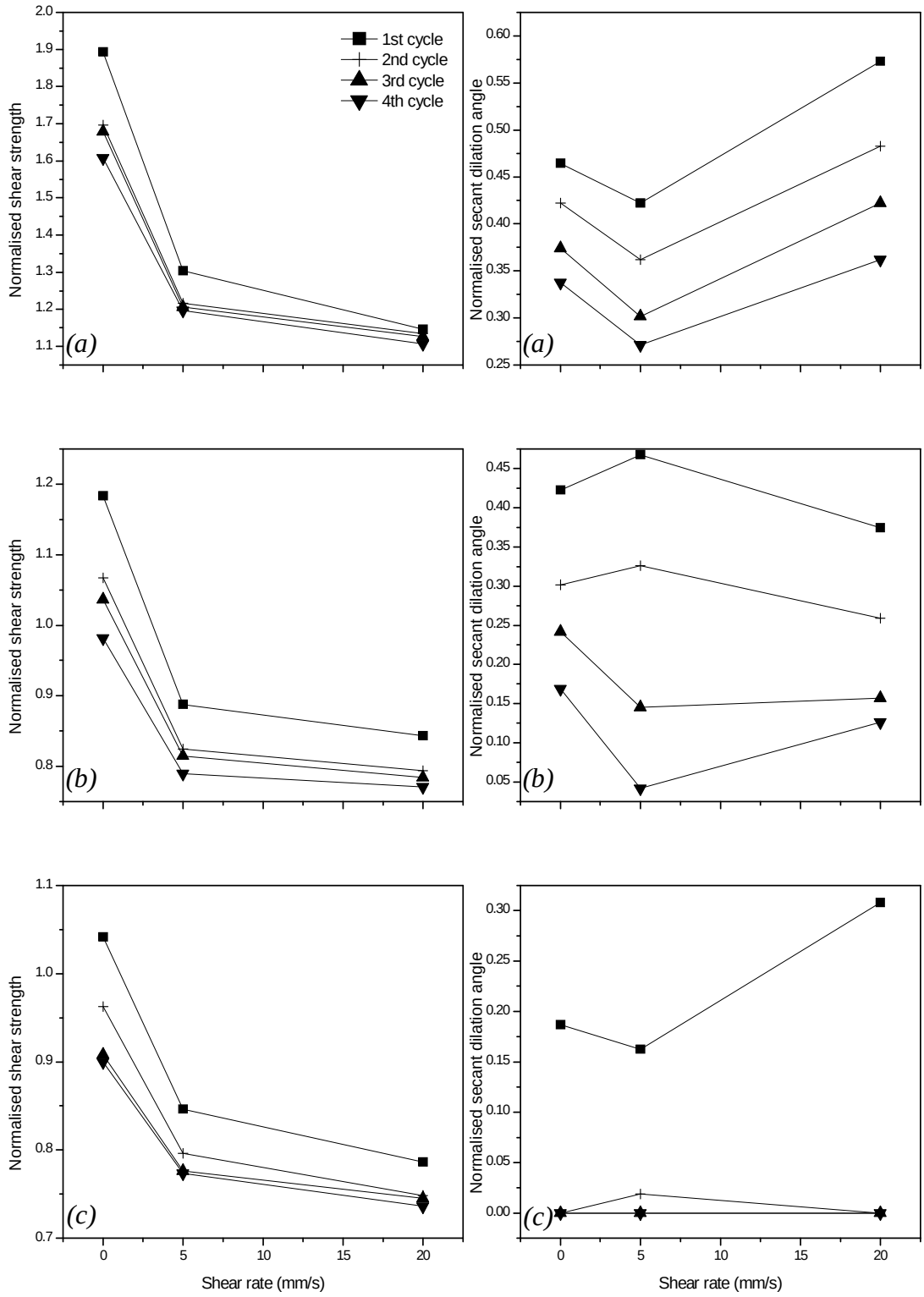

Figure 4-18 Variations of normalised shear strength and normalised secant dilation angle against shear rate: (*a*) σ_{n0} = 0.56 MPa, (*b*) σ_{n0} = 1.64 MPa, (*c*) σ_{n0} = 2.4 MPa

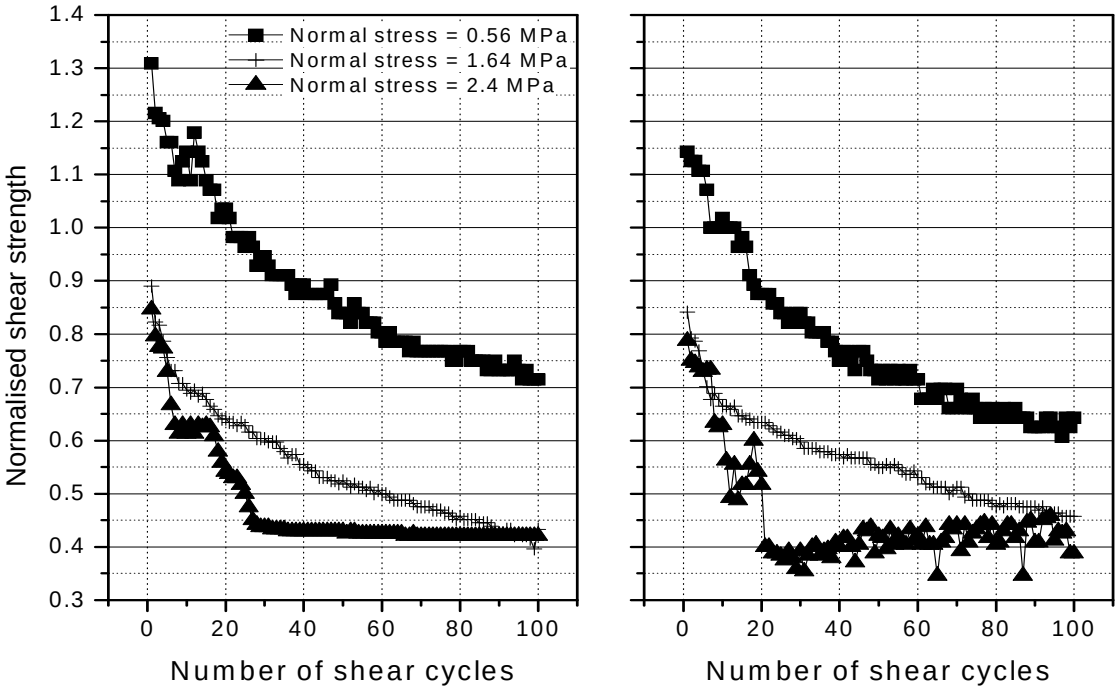

Figure 4-19 Variation of normalised shear strength against number of shear cycles: [left] Shear rate of 5 mm/s, [right] Shear rate of 20 mm/s

4.4.2. Profile of damaged joints

The surfaces of asperities sheared for 100 loading cycles with 5 mm/s of shear rate and under 0.56 MPa and 2.4 MPa of initial normal stresses are shown in Figure 4-20. The effects of a high number of loading cycles (100 loading cycles) on asperities surfaces can be noted by comparing Figures 4-13, 4-14 and 4-20. In Figure 4-13 [up], the damage is only limited to the tips, while asperities were more extensively degraded as shown in Figure 4-20 [up] after application of 100 loading cycles.

This can be due to the asperity fatigue in repeated loading conditions which decreases the joint strength. Furthermore, the asperities shapes are closer to the trapezoid rather than the sinusoidal profile of the four loading shear cycles. Although both of the asperities surfaces shown in Figures 4-14 and 4-20 [down] have been sheared off under the normal stress of 2.4 MPa, in the case of 4 loading cycles, residual friction angle was

still observed. Nevertheless, the asperities surface subjected to 100 loading shear cycles, has been completely damaged and is almost similar to the planar joints.

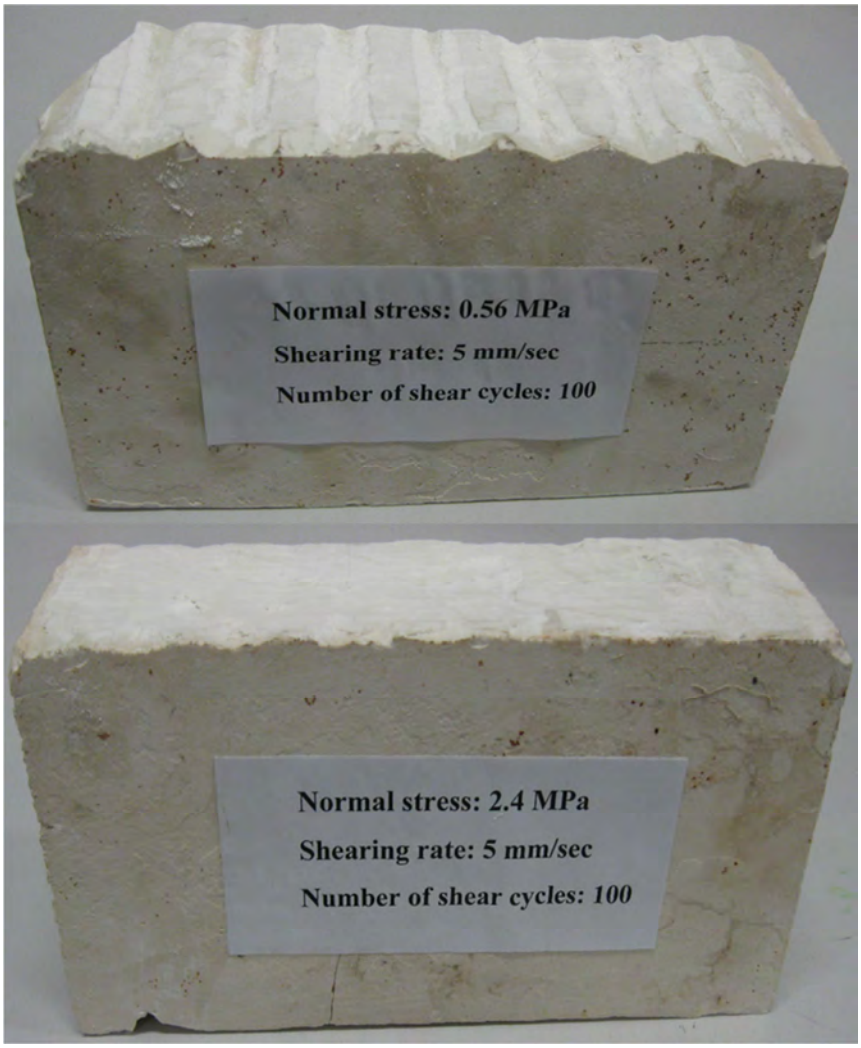

Figure 4-20 Asperities surfaces after 100 shear cycles with 5 mm/s of shear rate: [up] σ_{n0} = 0.56 MPa, [down] σ_{n0} = 2.4 MPa

4.5. Summary

Two series of cyclic loading direct shear tests were carried out using the CNS apparatus for rock joints at initial normal stress ranging from 0.5 MPa to 2.5 MPa. The first series of tests studied the effects of cyclic loading on shear behaviour of rock joints under CNS conditions. In the second series of tests, the effects of shear rate on cyclic loading

shear behaviour of rock joints were investigated. Both artificial saw tooth shaped asperities and a replicas of real rock surface were sheared under cyclic loading.

Generally, the shear strength decreased with increase in the number of loading cycles due to asperity damage. The laboratory tests indicate that for low levels of initial normal stress, the shear strength was higher in the forward shearing rather than the loading reversal. However, as the amount of initial normal stress increased the dependency of shear strength on the loading direction became less apparent. Asperity degradation was shown to be a function of the shear and normal energies subjected to them such that less asperity damage was observed in the backward shearing and subsequent cycles in comparison to the forward shearing and initial cycle. As shearing was conducted under CNS conditions, the normal stress and dilation showed similar trends that affected the cyclic loading shear strength and asperity damage. For replicas of a real rock surface sheared with initial normal stress of 0.5 MPa, the shear strength of the first cycle was affected by the presence of the second order asperities. Second order asperities were mostly damaged in the first cycle and the shear behaviour was dominated by first order asperities in further shearing.

Furthermore, the cyclic loading shear strength decreases with increase in the shear rate. As the normal stress increased, the effect of shear rate on shear strength became less pronounced. With increase in the number of loading cycles, the shear strength for higher shear rates become closer to those of lower shear rates. The normalised secant dilation angle varies non-monotonically with increase in the shear rate.

The cyclic loading shear tests described here showed the importance of cyclic loading on shear behaviour of rock joints under CNS conditions. The joint surfaces that sheared cyclically were fully mated and no infill material was introduced between them. In the

field, joints may be filled up with sand, clay and/or silt that considerably affects the overall cyclic loading shear behaviour of the joints. The following chapter discusses the shear behaviour of infilled rock joints under cyclic loading and CNS conditions.

Chapter V

5. SHEAR BEAHVIOUR OF INFILLED ROCK JOINTS UNDER CYCLIC LOADING

5.1. Introduction

The knowledge of properties as well as shear behaviour of rock joints is essential for the design of various underground engineering structures. To determine such properties of rock joints, the laboratory tests are usually carried out. Rock masses containing infilled joints may be subjected to repeated cycles of shearing. To investigate the cyclic loading shear behaviour of infilled rock joints, triangular asperities inclined at angles of 9.5º (Type I) and 18.5º (Type II) to the shear movement were cast using high strength Plaster of Paris and infilled with mixture of clay and sand. These joints were sheared cyclically in a CNS testing machine in a similar manner to the testing of clean joints.

5.2. Laboratory investigation

Selection of infill material, sample preparation and an experimental plan for the study of cyclic loading effects on shear behaviour of infilled rock joints under CNS conditions is described.

5.2.1. Selection of infill material

Mixture of clay and sand has been widely incorporated in the past for laboratory investigations since mixture of clay and sand infilled joints often contribute to the instability of jointed rock structures (Oliveira 2010). Mixture of clay and sand (75%

fine sand and 25% Kaolinite) at initial moisture content of 12.5% was selected as infill material. After preparation of the infill material, it was kept inside a sealed container to ensure retention of the percentage of moisture. Direct shear tests performed on the mixture of clay and sand for various normal stresses indicated a friction angle (φ_{fill}) of 28° and cohesion (C_{fill}) of 46 kPa (Figure 5-1). Consolidation tests were carried out on the infill material under loading and unloading conditions with different loads. The infill showed compression index (*Cc*) and swelling index (*Cs*) of 0.16 and 0.07, respectively.

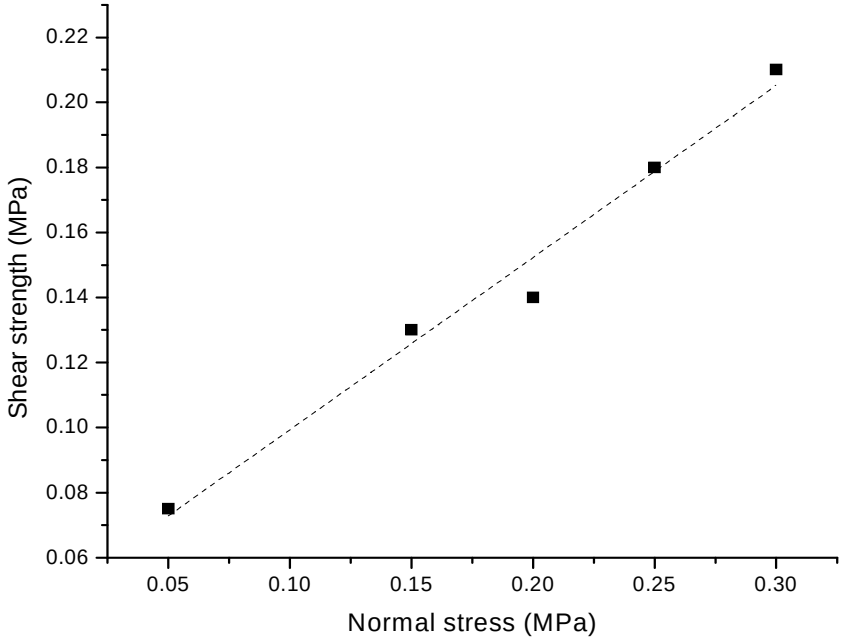

Figure 5-1 Shear strength envelope for mixture of clay and sand infill in direct shear

5.2.2. Sample preparation

The procedure for sample casting was the same as that for clean joints described in section 4.2.2. Type I and II asperity surfaces with initial asperity angles (i_0) of 9.5° and 18.5° to the shear movement were considered for cyclic loading shear testing of infilled joints. In order to prepare the infill surface, the cured bottom block was positioned inside the bottom shearing box in a way that allowed the surface profile to stay slightly

above the edge of the bottom box. A closure over the specimen from the joint plane was provided by attaching an adjustable collar with the same shape as the surface profile on the top of the specimen. The collar was set to create the required infill thickness by precisely measuring the closure at four corner points. The infill material was then placed inside the collar and extended over the surface area using a spatula. Once, the collar was filled, the infill material was trimmed and compacted with a steel plate having the same triangular shape as the asperities. The collar was then removed and the bottom part of the sample was placed in the shear apparatus. The top shear box containing the upper sample was then mounted on top of the lower sample, thus sandwiching the infill layer between the two matching plaster surfaces. The smooth lateral confinement, on both sides of the sample, made from stainless steel was assembled to prevent loss of the infill material during cyclic shearing. The sample preparation procedure is illustrated in Figure 5-2.

5.2.3. Experimental plan

More than 18 cyclic loading direct shear tests as listed in Table 5.1 were carried out on the samples. Some of the tests were repeated to ensure the accuracy and precision of the measured data. The applied initial normal stresses were 0.56 MPa, 1.64 MPa and 2.4 MPa. Three different ratios 0.3, 0.6 and 1 of infill thickness (t) to asperity height (a) were tested. Illustrations of the Type I joint with t/a ratio of 1 and Type II joint with t/a ratio of 0.6 are shown in Figure 5-3. Infill joints were subjected to predetermined initial normal stress (σ_{n0}) for an hour before shearing. All samples were sheared for four consecutive cycles with total accumulated displacement of 240 mm and a shear rate of 0.5 mm/min to ensure a uniform drained condition of infilled joints. As in clean joints

testing, a constant normal stiffness of 8 kN/mm was applied to restrict the dilation. The maximum shear displacement was set to 15 mm.

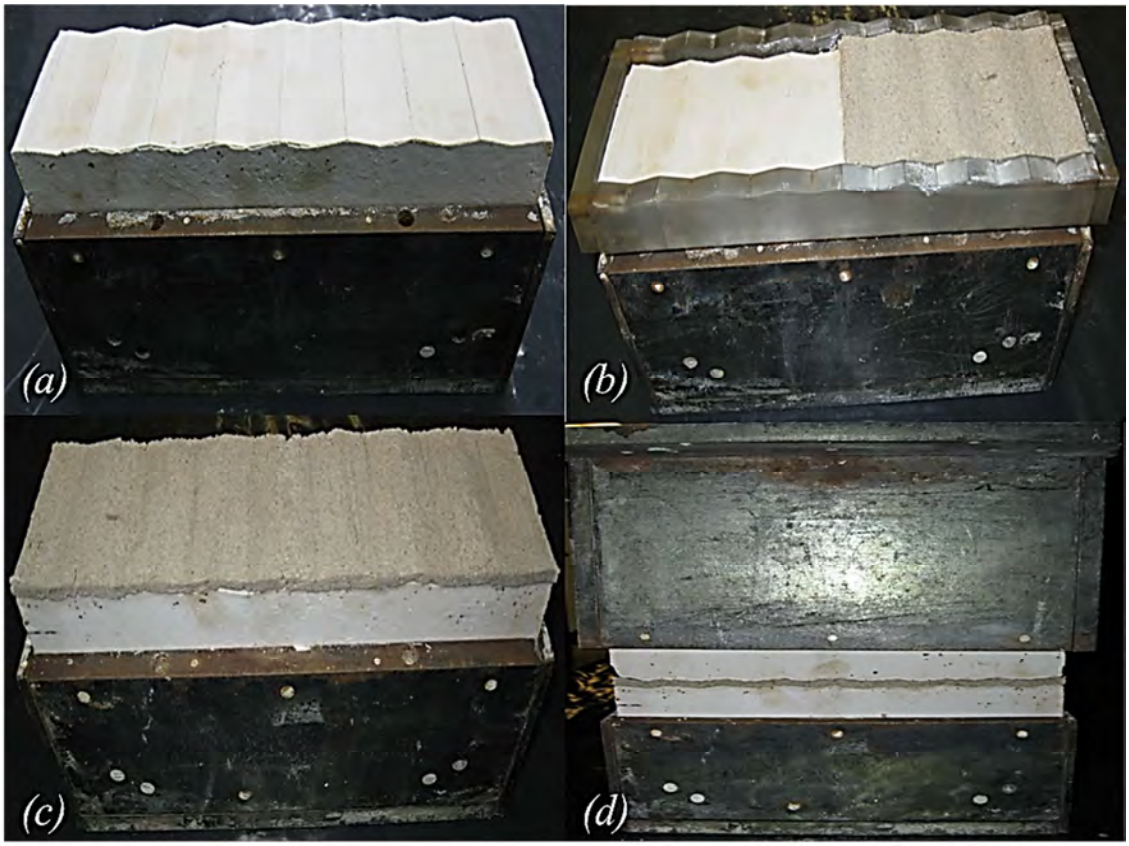

Figure 5-2 Sample preparation procedure: Type I and t/a = 1, (*a*) Lower sample, (*b*) Lower sample with collar, (*c*) Lower sample with infill material, (*d*) Whole sample with the upper and lower blocks and infill material

Shear and normal loads and shear and normal displacements were measured at the same time and almost continuously during the whole length of each test. The tests were carried out using the CNS testing apparatus described in section 4.2.3.

5.3. Experimental results

The results of the cyclic loading shear tests for infilled rock joints with various infill thicknesses to asperity height, initial normal stresses and asperity types are plotted in Figures 5-4 to 5-12.

Table 5-1 Experimental program for the study of cyclic loading effects on shear behaviour of infilled rock joints

Test number	*Asperity Type*	*Applied normal stress (MPa)*	*Infill thickness per asperity height*
1 to 9	Type I	0.56, 1.64,2.4	0.3, 0.6, 1
10 to 18	Type II	0.56, 1.64,2.4	0.3, 0.6, 1

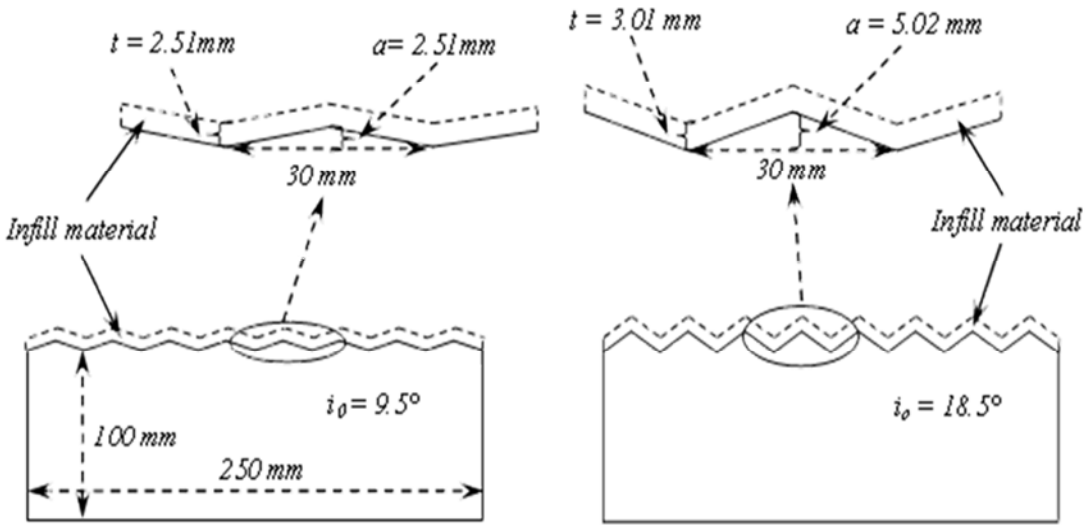

Figure 5-3 Illustrations of infilled rock joints: [left] Type I with t/a = 1, [right] Type II with t/a = 0.6

5.3.1. Shear strength

For t/a = 0.3 and σ_{n0} = 0.56 MPa, the shear strength in Figure 5-4 was higher in the forward shearing than the reverse shearing represented by the second quadrant as the negative component. The effect of asperity degradation on reduction of friction angle and, therefore, the shear strength with increase in the shear cycles is evident since t/a = 0.3 and the rock to rock contact occurs readily after squeezing the infill material.

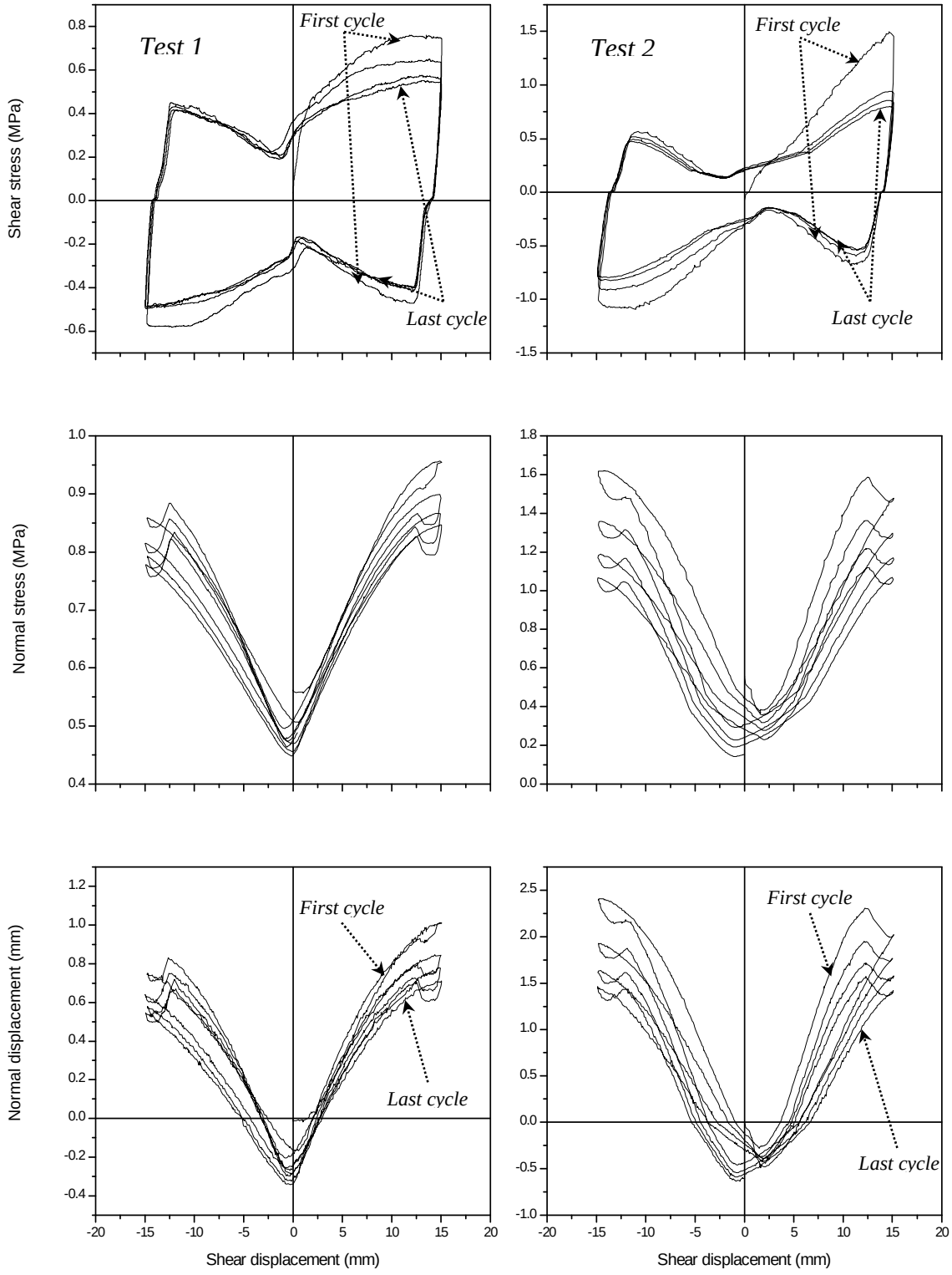

Figure 5-4 Cyclic loading shear behaviour with t/a = 0.3 and σ_{n0} = 0.56 MPa: [left] Type I, [right] Type II

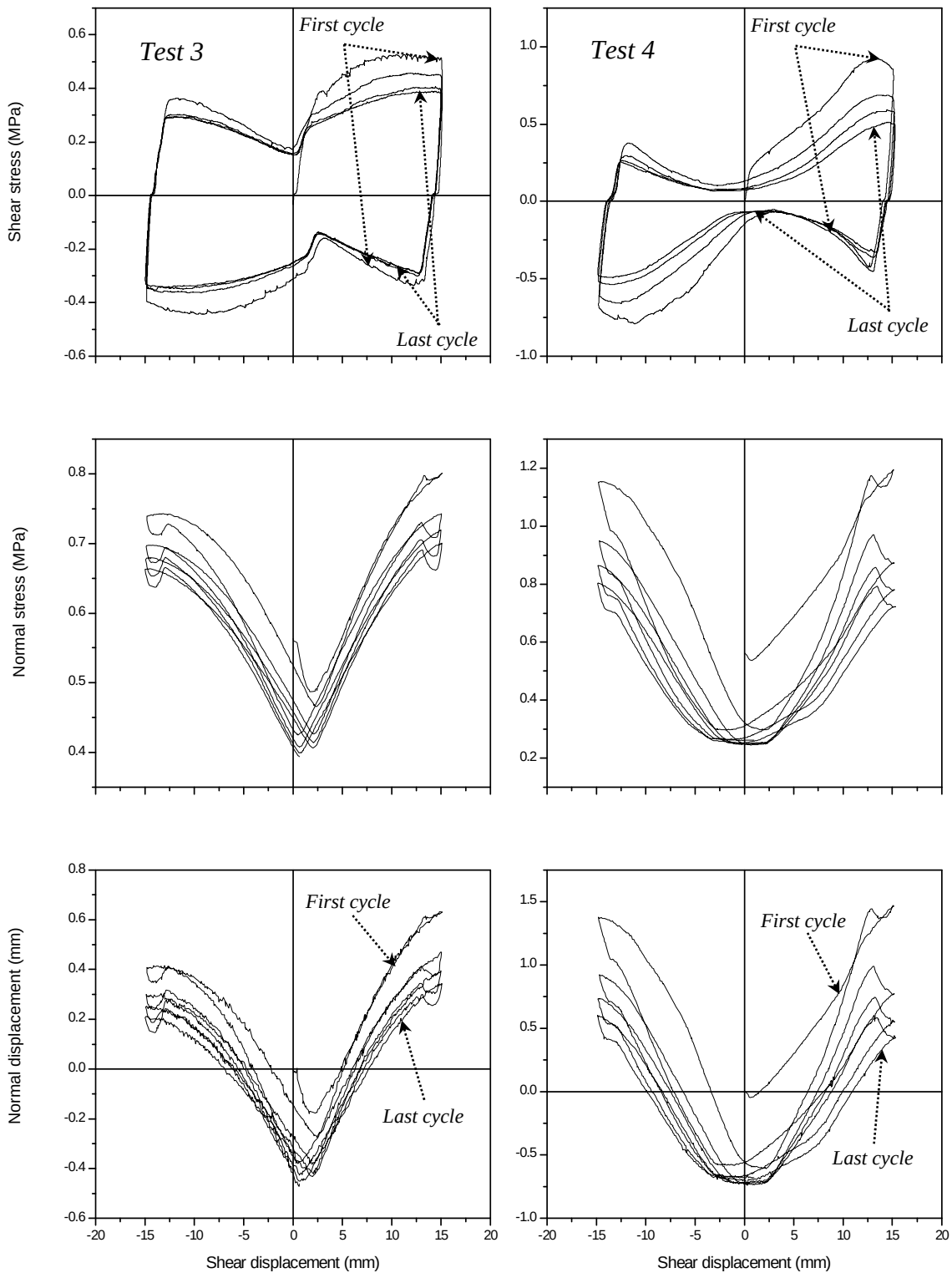

Figure 5-5 Cyclic loading shear behaviour with t/a = 0.6 and σ_{n0} = 0.56 MPa: [left] Type I, [right] Type II

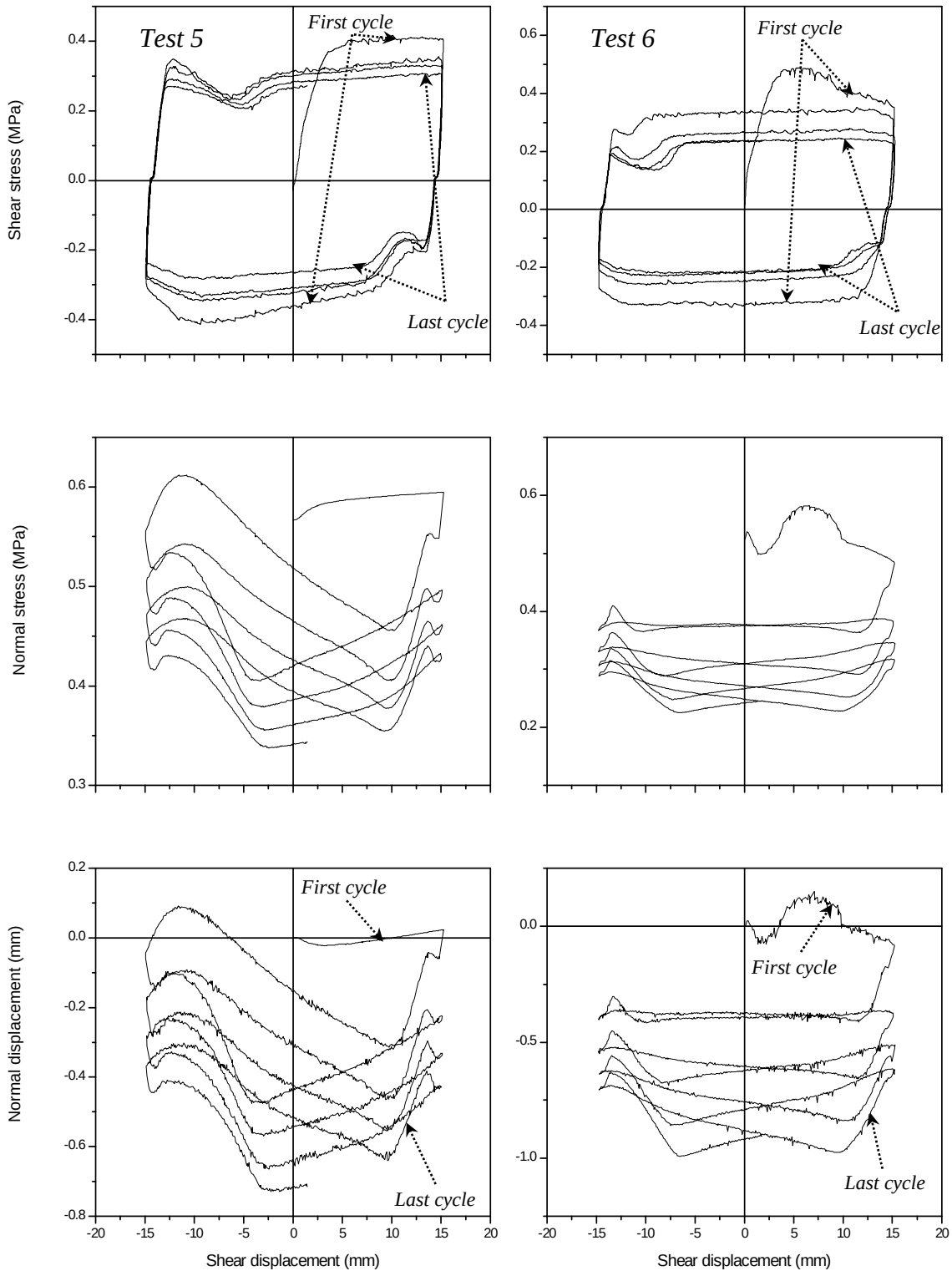

Figure 5-6 Cyclic loading shear behaviour with t/a = 1 and σ_{n0} = 0.56 MPa: [left] Type I, [right] Type II

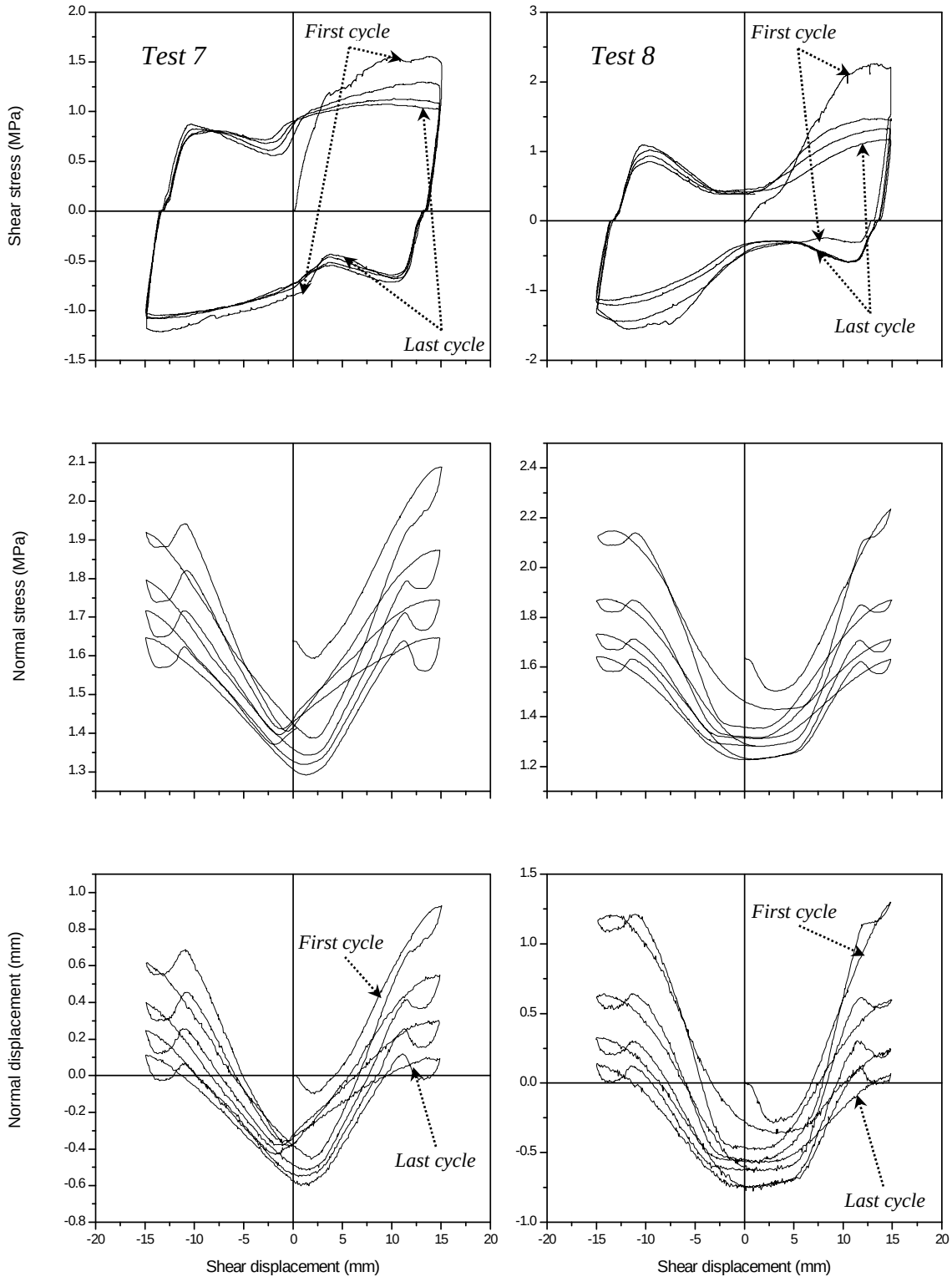

Figure 5-7 Cyclic loading shear behaviour with t/a = 0.3 and σ_{n0} = 1.64 MPa: [left] Type I, [right] Type II

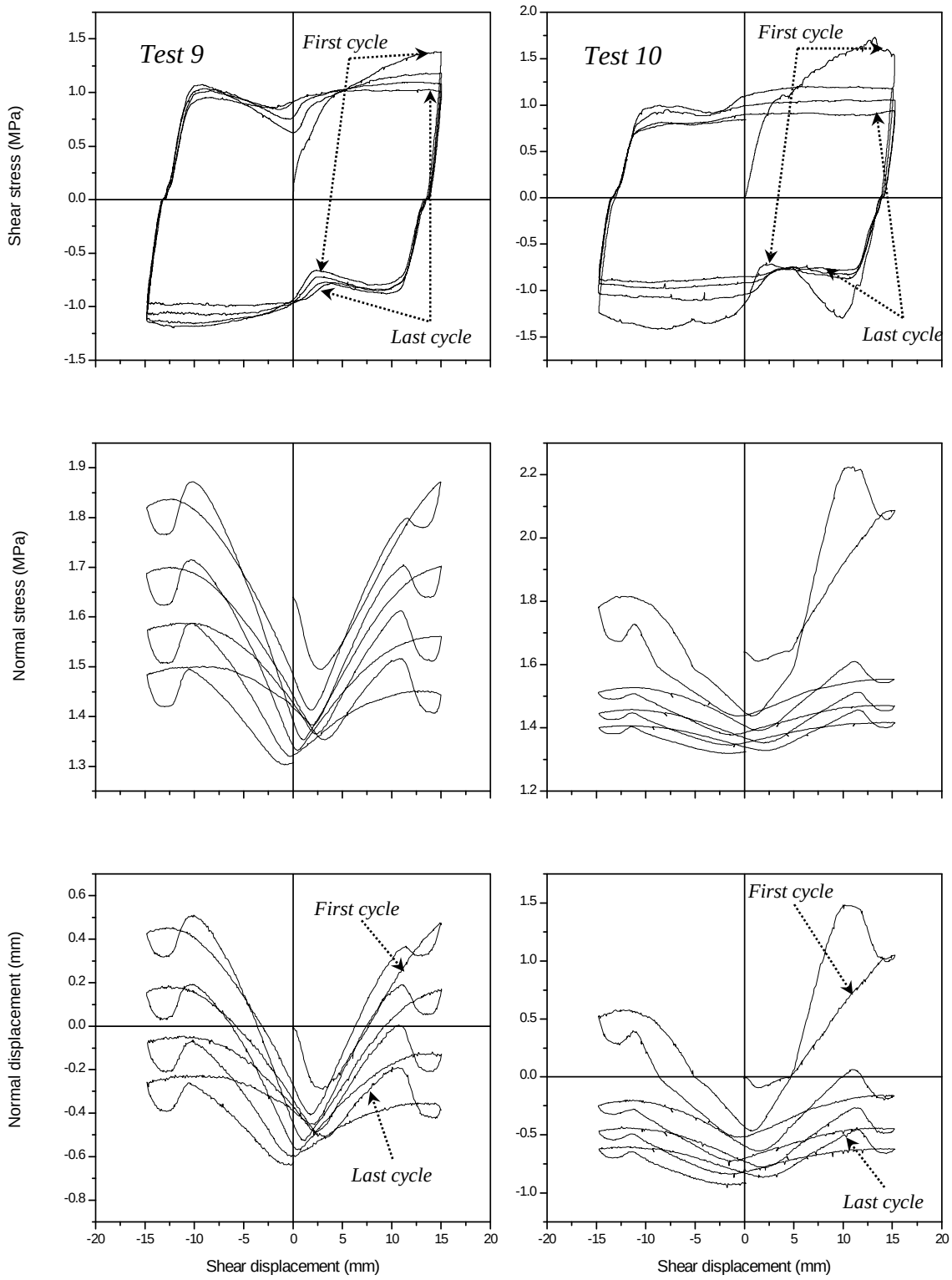

Figure 5-8 Cyclic loading Shear behaviour with t/a = 0.6 and σ_{n0} = 1.64 MPa: [left] Type I, [right] Type II

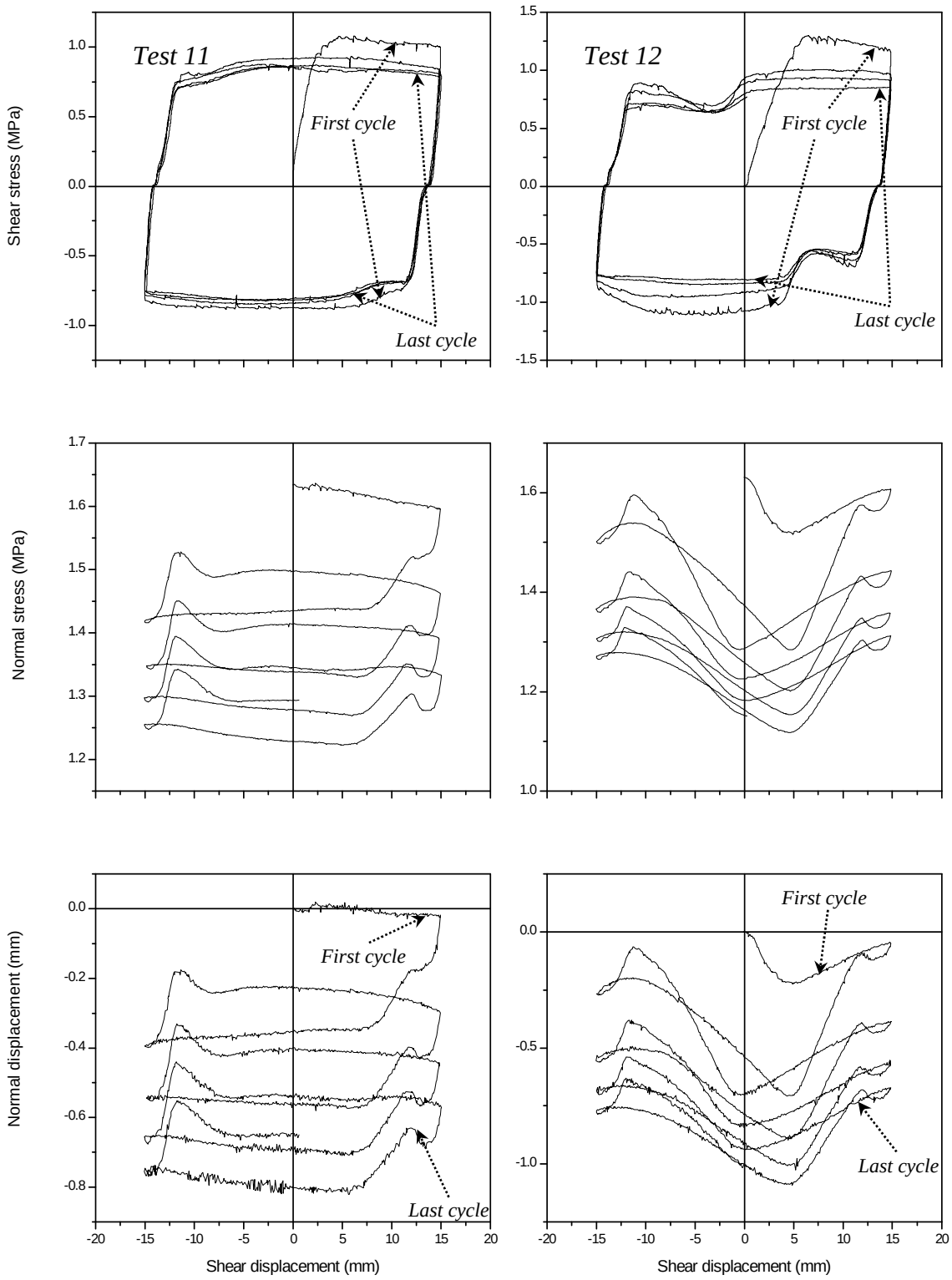

Figure 5-9 Cyclic loading shear behaviour with t/a = 1 and σ_{n0} = 1.64 MPa:
[left] Type I, [right] Type II

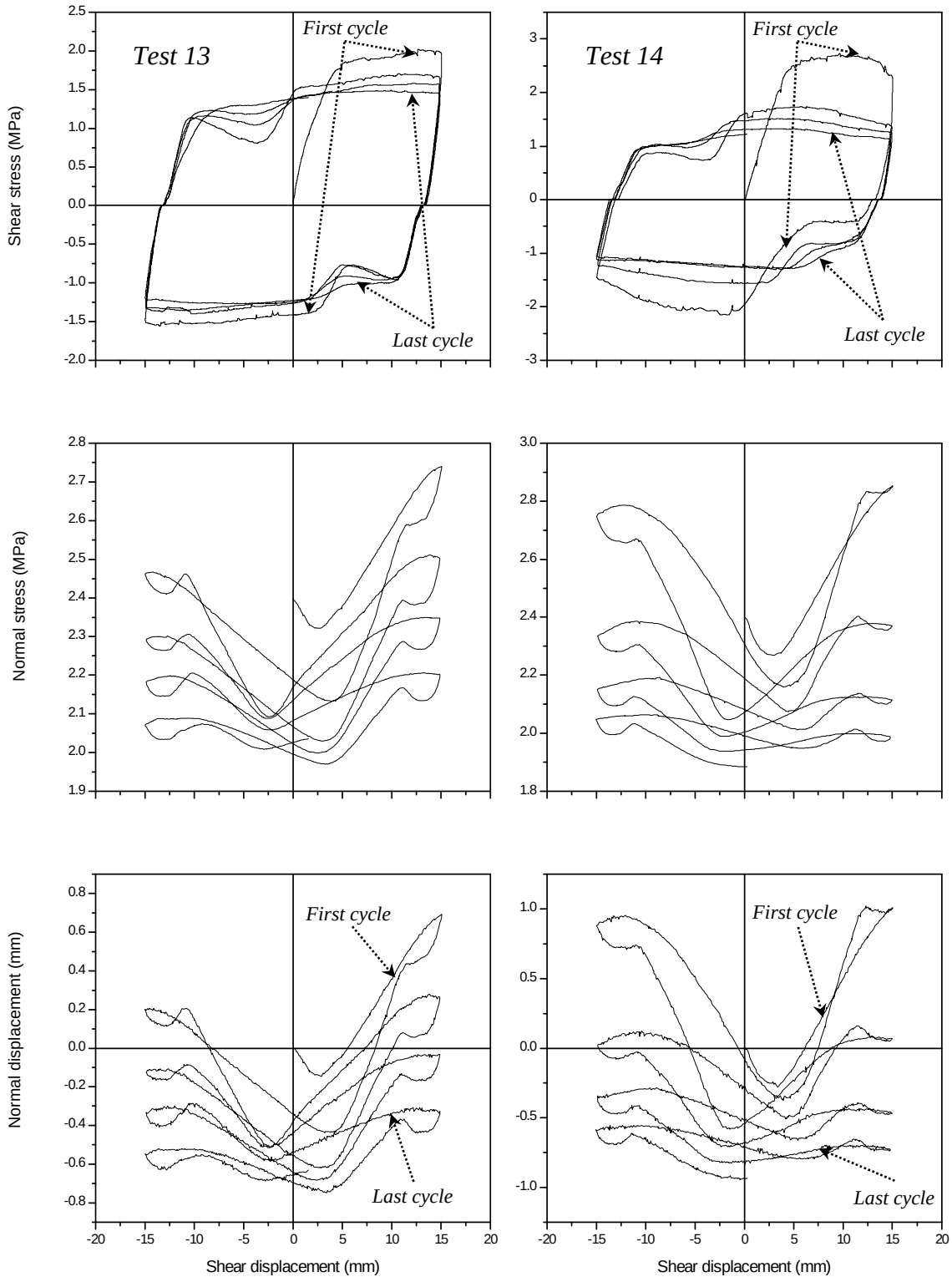

Figure 5-10 Cyclic loading shear behaviour with t/a = 0.3 and σ_{n0} = 2.4 MPa: [left] Type I, [right] Type II

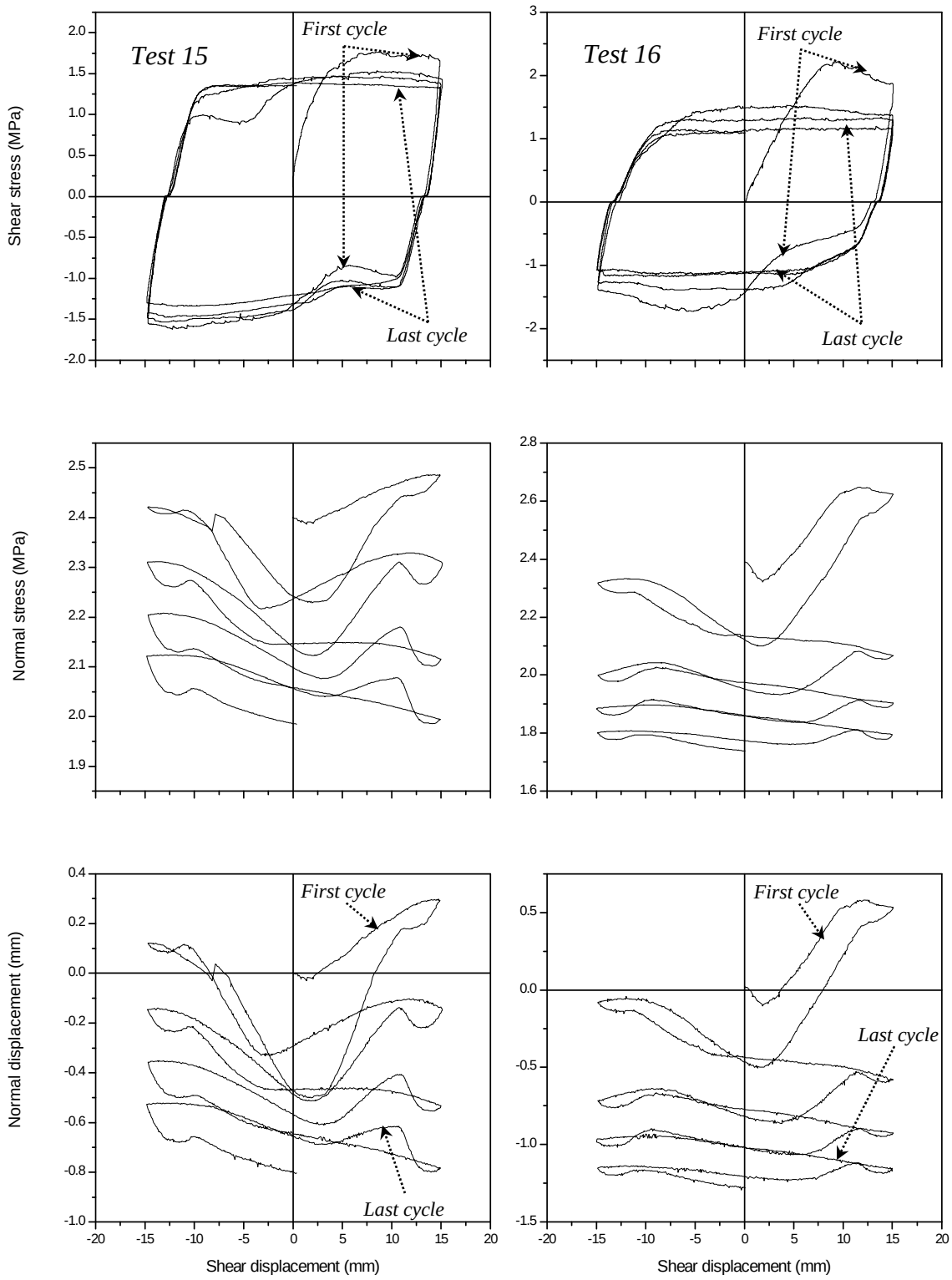

Figure 5-11 Cyclic loading Shear behaviour with t/a = 0.6 and σ_{n0} = 2.4 MPa: [left] Type I, [right] Type II

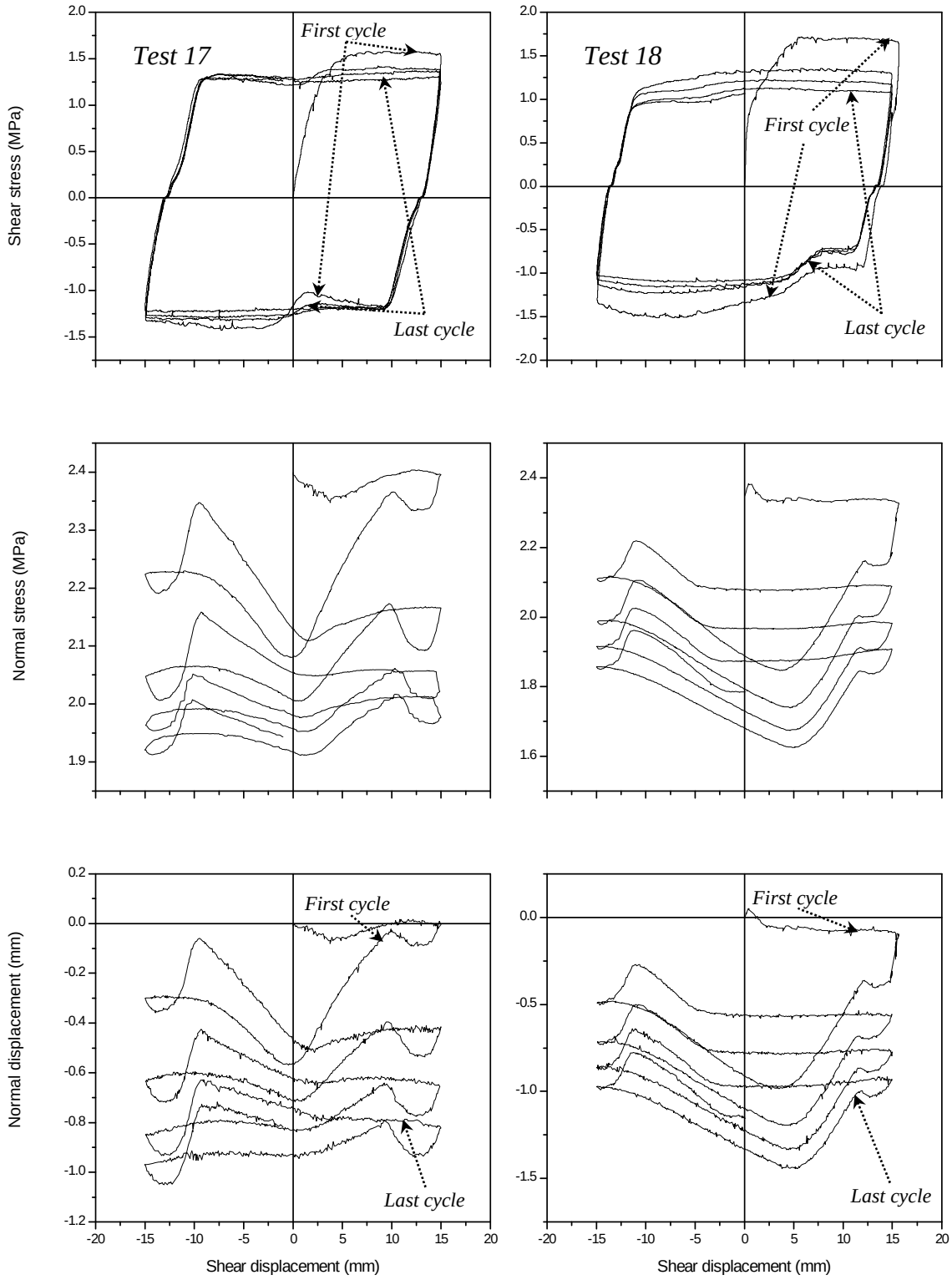

Figure 5-12 Cyclic loading **s**hear behaviour with t/a = 1 and σ_{n0} = 2.4 MPa: [left] Type I, [right] Type II

The peak shear strength for Type I asperity surface corresponding to t/a = 0.3 and σ_{n0} = 0.56 MPa decreased from 0.76 MPa to 0.55 MPa during four loading cycles (Figure 5-4 left). The gap between shear stress profiles gradually becomes marginal with increase in the number of shear cycles. In the tests shown in Figures 5-6, 5-9 and 5-12 where t/a = 1, the friction angle is mostly dominated by the infill material and reduction in the shear strength is related to the change in the effective normal stress (i.e. effect of asperities is reduced). The cyclic loading shear strength is affected by the value of initial normal stress such that the difference between the shear stress profiles increases with increase in the initial normal stress for the same ratio of infill thickness to asperity height and asperity type. When t/a = 0.3 and σ_{n0} = 2.4 MPa, the effect of asperity degradation in the first cycle decreases the asperities contact in further shearing due to a higher infill thickness (Figure 5-6). The recorded cyclic loading shear strength (peak value) for Type II asperity surface with t/a = 1 and σ_{n0} = 1.64 MPa during four loading cycles, were 1.3 MPa, 1.01 MPa, 0.94 MPa and 0.85 MPa. This shows less reduction in the shear strength with increase in the loading cycles rather than the test results of Type II asperity surface with the same initial normal stress but t/a = 0.3 (comparison between Figures 5-7 and 5-9). For the same ratio of infill thickness to asperity height and initial normal stress, the reduction in the shear strength under cyclic loading was higher for greater asperity angles where contraction of infill material and asperity damage were more pronounced (comparison between left and right parts of Figures 5-4 to 5-12).

5.3.2. Normal displacement

The normal displacement behaviour of infilled rock joints during cyclic loading is affected by the joint roughness and the deformability of the infill material. When t/a = 0.3, the governing mechanism is dilation with reduction in dilation angle upon asperity

damage after squeezing the infill material (Figures 5-4, 5-7 and 5-10). Nevertheless, as *t/a* increases from 0.3 to 1, the variation of normal displacement against shear displacement is dominated by contraction behaviour due to compaction of infill material (Figures 5-6, 5-9 and 5-12). Generally, the increase in the normal stress is associated with higher suppression of dilation factor for *t/a* = 0.3 and greater compaction of infill material when *t/a* = 1. The maximum dilation in the first shear cycle for Type I asperity surface ranged between 1.02 mm (corresponding to *t/a* = 0.3 and σ_{n0} = 0.56 MPa) and 0.03 mm (corresponding to *t/a* = 1 and σ_{n0} = 2.4 MPa), depending on the initial normal stress and infill thickness. These values for Type II asperity surface were 2.02 mm and 0.05 mm respectively. The gap between dilation curves decreased with increase in the loading cycles. For *t/a* = 0.3 and 0.6 and σ_{n0} = 0.56 MPa and 1.64 MPa, the reduction in dilation was higher in the forward shearing than reverse loading. The maximum values of compaction measured for Type I asperity surface with *t*/*a*=1 and various initial normal stresses were lower in comparison to Type II asperity surface.

5.3.3. Normal stress

As shearing is conducted under CNS conditions to simulate the effects of surrounding rock mass, the normal stress follows similar trends to the normal displacement. Thus, the variation of normal stress shows different behaviours depending on the infill thickness. For *t/a* = 0.3, the normal stress increases during dilation followed by a reducing trend toward its initial value in reverse loading (Figures 5-4, 5-7 and 5-10). However, as *t/a* increases from 0.3 to 1, the normal stress decreases upon compaction of infill material that affects the shear strength under cyclic loading (Figures 5-6, 5-9 and 5-12). The data reveals that the increase in normal stress is greater at lower infill thickness to asperity height ratios and initial normal stresses. The values of maximum

normal stress measured for Type II asperity surfaces during first and last loading cycles with σ_{n0} = 1.64 MPa and 2.4 MPa were 2.24 MPa, 1.64 MPa and 2.85 MPa and 2.19 MPa respectively when t/a = 0.3. Also, the gap between normal stress profiles decreased with increase in the number of loading cycles.

5.3.4. Strength envelope

Figure 5-13 shows variations of the strength envelopes for infilled rock joints subjected to cyclic loading for different conditions of infill thickness to asperity height and initial asperity angles. At low infill thickness (t/a = 0.3) and Type I asperity surface, there is a slight difference in strength envelopes between the first and second shear cycles (Figure 5-13/left *a*). As the infill thickness to asperity height was increased to 1, the difference between the strength envelopes of consecutive shear cycles became marginal, verifying the earlier finding that, at high infill thickness to asperity height ratios, the shear behaviour is dominated by the infill material (Figure 5-13/left *c*). For t/a = 0.3 and Type II asperity surface, the strength envelope of the first cycle lies significantly above the later cycles (Figure 5-13/right *a*). As the number of loading cycles was increased, the strength envelopes under cyclic loading tended to become close to each other and approached that of infill material. It is deduced from strength envelopes of Type I and II asperity surfaces that the gap between the cyclic loading strength envelopes increases with increase in the asperity angle for the same infill thickness to asperity height ratio.

5.3.5. Profile of shear plane

Figure 5-14 shows the profiles of shear planes for selected infilled joints at different initial normal stresses under cyclic loading. The cyclic loading shear planes were

estimated from the measured normal displacement against the shear displacement data, and they are shown by dashed lines in Figure 5-14.

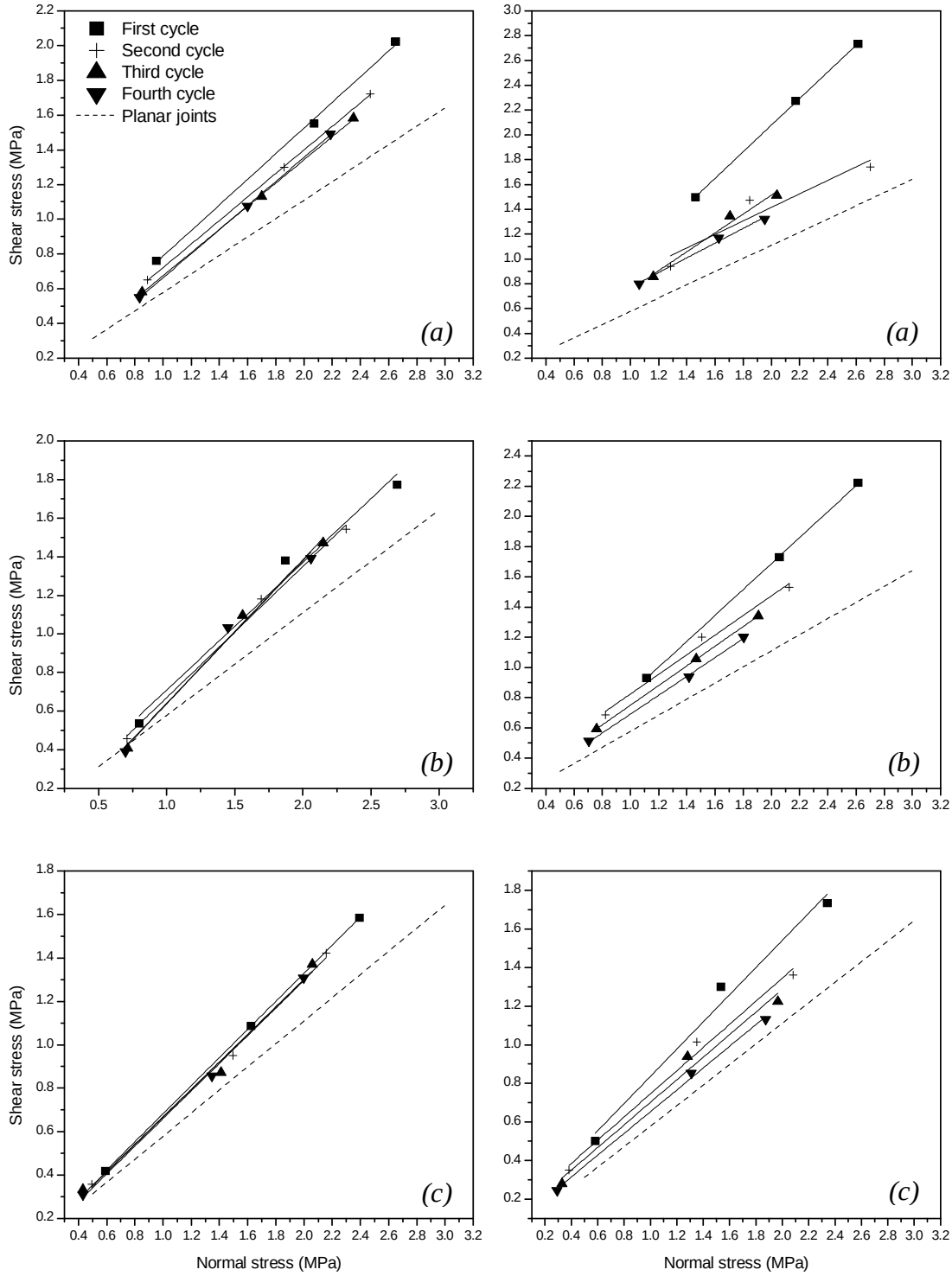

Figure 5-13 Strength envelope under Cyclic loading: [left] Type I asperity surface, [right] Type II asperity surface, (*a*) *t*/*a* =0.3, (*b*) *t*/*a*=0.6, (*c*) *t*/*a*=1

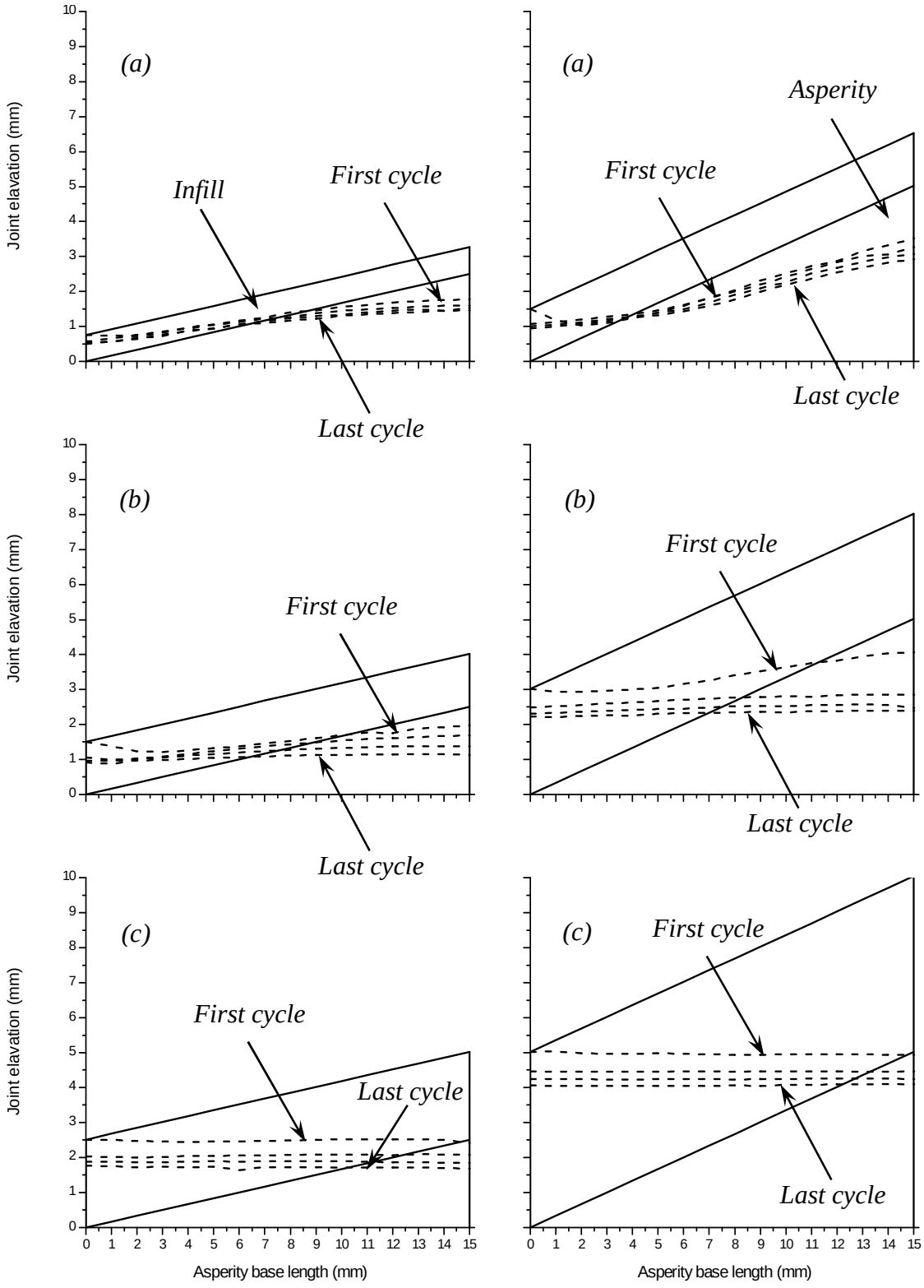

Figure 5-14 Relative location of shear plane through infilled joints under cyclic loading, (dashed lines = shear planes): [left] Type I asperity surface, [right] Type II asperity surface, (*a*) t/a = 0.3 and σ_{n0} = 0.56 MPa, (*b*) t/a = 0.6 and σ_{n0} = 1.64 MPa, (*c*) t/a = 1 and σ_{n0} = 2.4 MPa

For *t/a*=0.3 and 0.6, the shear planes pass through both infill and asperities (Figures 5-14 *a* and *b*). For *t/a* equals to unity, the shear planes for the first cycle pass slightly below the tips of asperities (Figure 5-14 *c*). As the number of loading cycles increases, for all the cases the shear planes pass always along a lower elevation as compared to the previous cycles, indicating either asperity damage or deformation of infill material. The portion of the asperity surface that contributes to the shear planes, increases with the number of shear cycles. The difference between the elevations of shear planes decreases during cyclic loading. The reduction in the elevations of shear planes for the same values of infill thickness to asperity height and initial normal stress is greater for Type II asperity surfaces in comparison to Type I asperity surfaces. The gap between the shear planes of the first and last cycles of the joints with the same asperity type is higher for greater infill thickness to asperity height ratios and initial normal stresses.

5.3.6. Comparison between the shear strength of clean and infilled joints

Figure 5-15 shows the comparison between the peak shear strength of clean and infilled joints under cyclic loading and CNS conditions for the various levels of infill thickness to asperity height, asperity type and initial normal stress. It is inferred from the Figure 5-15 that the cyclic loading shear strength of clean joints is always higher than infilled joints. For Type II asperity surface, the shear strength of clean joints becomes closer to that of infilled joints with increase in the loading cycles (Figure 5-15/right). The same behaviour is observed for the infilled joints of Type I asperity surface with *t*/*a*=0.3 that gets closer to the results of *t*/*a*=0.6 and *t*/*a*=1 as the number of loading cycles increases (Figure 5-15/left). However, the difference between the cyclic loading shear strength of clean and infilled joints of Type I asperity surface, rises as the number of loading cycles exerted on asperities increases.

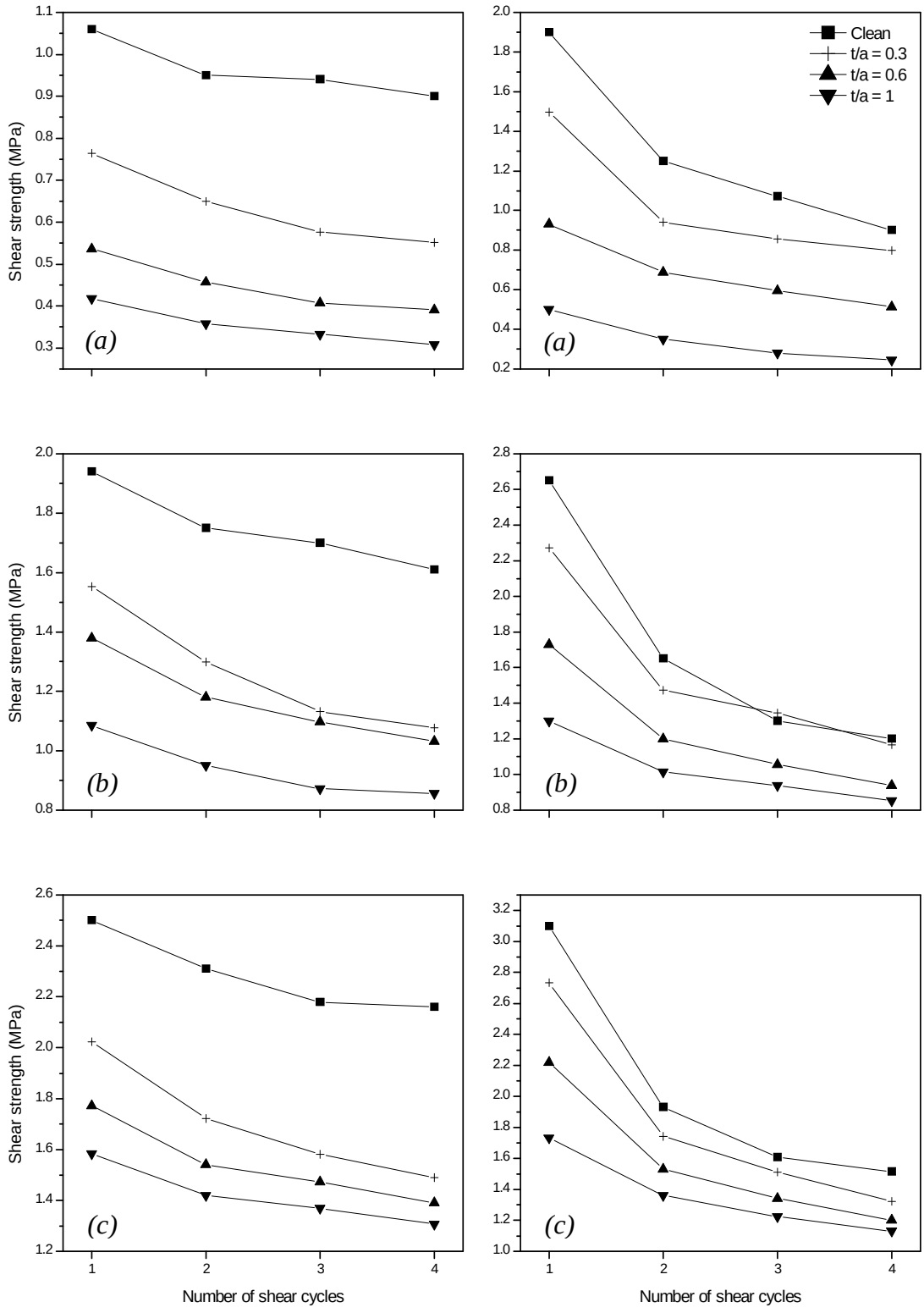

Figure 5-15 Comparison between the cyclic loading shear behaviour of clean and infilled rock joints: [left] Type I asperity surface, [right] Type II asperity surface, (*a*) σ_{n0} = 0.56 MPa, (*b*) σ_{n0} = 1.64 MPa, (*c*) σ_{n0} = 1.64 MPa

For instance, the drop in the shear strength of Type I asperity surface with 2.4 MPa of initial normal stress with the introduction of 0.75 mm of infill (t/a=0.3) in the first cycle is 19%. This value for the last cycle is 31% which shows a 12 % increase in the difference between the shear strength of clean and infilled joints due to the application of cyclic loading (Figure 5-15/left *c*).

5.4. Summary

The results of the systematic experimental study conducted on artificial triangular joints infilled with mixture of clay and sand with various initial normal stresses and infill thickness to asperity height ratios were presented and critically analysed. The tests were intended at investigating the effects of cyclic loading on shear behaviour of infilled joints under CNS conditions. The main findings can be summarised as:

- Due to asperity damage and deformation of infill material, the shear strength decreased with increase in the number of shear cycles.

- For t/a = 0.3 and σ_{n0} = 0.56 MPa, the shear strength was higher during forward shearing rather than during reverse loading.

- For t/a = 0.3 and σ_{n0} = 2.4 MPa, the effect of asperity breakage in the first loading cycle reduced the rock to rock contact in further shearing.

- The behaviour of normal displacement under cyclic loading was shown to be governed by dilation and contraction mechanisms. This was dependent on the infill thickness to asperity height and the applied initial normal stress.

- The normal stress showed similar trends to normal displacement. This affected the shear strength, asperity damage and compaction of infill material under cyclic loading.

- There is a slight difference in strength envelopes between the first and second shear cycles at low infill thickness (t/a = 0.3) and Type I asperity surface.

- For t/a = 0.3 and Type II asperity surface, the strength envelope of the first cycle lies considerably above the later cycles.

- The difference between the strength envelopes of consecutive shear cycles became less pronounced as the infill thickness to asperity height was increased to 1.

- The shear planes always pass along a lower elevation as compared to the previous cycles, implying either asperity damage or deformation of infill material.

- The shear strength of clean joints under cyclic loading is always higher than infilled joints. The shear strength of clean joints became closer to that of infilled joints with increase in the loading cycles for Type II asperity surface.

In the next chapter, models will be proposed to simulate the cyclic loading shear behaviour of rock joints under CNS conditions.

Chapter VI

6. MODELLING OF THE SHEAR BEAHVIOUR OF ROCK JOINTS UNDER CYCLIC LOADING

6.1. Introduction

One of the most crucial and challenging tasks when designing rock mass structures such as underground caverns, power plants and dam foundations is to describe correctly the mechanical behaviour. This difficulty is mainly related to the discontinuities that divide the intact rock into the discrete blocks. There are two main approaches to quantify the mechanical properties of rock joints, namely, theoretical and empirical. The theoretical approach mostly incorporates elasto-plastic and energy balance theories while the empirical approach relays on the analysis of experimental data.

6.2. Requirements of new mathematical models

Various models for predicting the shear strength of rock joints under monotonic and cyclic loading were reviewed in Chapters II and III.

Most of the models that were proposed for clean joints under cyclic loading are based on the sliding mechanism. These models may not necessarily estimate the shear strength accurately under CNS conditions when applied to non-planar joints as they do not take into account the additional shear resistance generated by the asperity damage. Accordingly, the formulation of an elasto-plastic constitutive model based on the energy balance theory is described to simulate the cyclic loading shear behaviour of clean rock

joints under CNS conditions. In addition, an empirical relationship is proposed to consider the effects of shear rate on the shear strength of rock joints under cyclic loading and CNS conditions.

From the literature review in chapter III, it was concluded that no studies have been conducted on the shear behaviour of infilled joints under cyclic loading and CNS conditions. As far as can be determined, all the available relationships for predicting the shear strength of rock joints were proposed only for clean joints or monotonic loading shear behaviour of infilled rock joints. In the light of this shortcoming, a cyclic loading failure criterion for infilled rock joints was introduced here to replicate the reduction in the shear strength with increase in the number of loading cycles.

6.3. Elasto-plastic constitutive model for shear behaviour of clean rock joints under cyclic loading

In this section, a brief description of the incremental elasto-plastic relationship is given followed by yield and plastic potential functions that were extended to model the shear behaviour of clean rock joints under cyclic loading and CNS conditions. The model was then calibrated for different initial normal stresses, asperity types, and replicas of a field joint.

6.3.1. Brief description of the incremental elasto-plastic relationship

The displacement increments at asperities contact can be divided into elastic and plastic parts as:

$$du = du_e + du_p \tag{6.1a}$$

$$dv = dv_e + dv_p \tag{6.1b}$$

where, *du* and *dv* are increments of shear and normal displacements and subscripts *e* and *p* denote elastic and plastic states respectively.

The elastic deformation at asperities contact generates stresses that are related via the asperities contact stiffness (E^e) as:

$$\begin{bmatrix} d\tau \\ d\sigma \end{bmatrix} = \begin{bmatrix} E_s^e & 0 \\ 0 & E_n^e \end{bmatrix} \begin{bmatrix} du_e \\ dv_e \end{bmatrix} \tag{6.2}$$

where, $d\tau$ and $d\sigma$ are increments of shear and normal stresses and subscripts *s* and *n* denote shear and normal directions.

The plastic component can be determined by defining a plastic potential function (Q) whereby the plastic displacement increment is related to stress as:

$$\begin{bmatrix} du_p \\ dv_p \end{bmatrix} = \begin{cases} 0 \quad if \rightarrow F < 0 or dF < 0 \\ d\lambda \begin{bmatrix} \dfrac{\partial Q}{\partial \tau} \\ \dfrac{\partial Q}{\partial \sigma} \end{bmatrix} \quad if \rightarrow F = dF = 0 \end{cases} \tag{6.3}$$

where, $d\lambda$ is a proportional scalar factor and F is a scalar function (yield function).

$F<0$ corresponds to the elastic state while plastic deformation occurs when the yield function is equal to zero and condition where $F>0$ is impossible. When F and Q are different, the shear behaviour is non-associated which is the usual case for the discontinuities media.

By applying the plastic flow rule and consistency relationship, the total stress - displacement relationship is obtained as:

$$\begin{bmatrix} d\tau \\ d\sigma \end{bmatrix} = E_{ij}^{ep} \begin{bmatrix} du \\ dv \end{bmatrix} \tag{6.4a}$$

$$E_{ij}^{ep} = \begin{bmatrix} E_s & 0 \\ 0 & E_n \end{bmatrix} - \frac{\begin{bmatrix} E_s & 0 \\ 0 & E_n \end{bmatrix} \begin{Bmatrix} \frac{\partial Q}{\partial \tau} & \frac{\partial Q}{\partial \sigma_n} \end{Bmatrix}^T \begin{Bmatrix} \frac{\partial F}{\partial \tau} & \frac{\partial F}{\partial \sigma_n} \end{Bmatrix} \begin{bmatrix} E_s & 0 \\ 0 & E_n \end{bmatrix}}{\begin{Bmatrix} \frac{\partial F}{\partial \tau} & \frac{\partial F}{\partial \sigma_n} \end{Bmatrix} \begin{bmatrix} E_s & 0 \\ 0 & E_n \end{bmatrix} \begin{Bmatrix} \frac{\partial Q}{\partial \tau} & \frac{\partial Q}{\partial \sigma_n} \end{Bmatrix}^T} \tag{6.4b}$$

The above set of equations is able to provide a relationship between stress and displacement either in elastic or plastic states once the specific forms of yield and potential functions are determined according to the shear behaviour of joints.

6.3.2. Yield and plastic potential functions

The constitutive model developed in this section, is an extension of the monotonic loading model introduced by Seidel and Haberfield (1995*a*) to cyclic loading, applying the sliding degradation concept proposed by Plesha (1987).

For determination of the specific form of yield function, the energy balance theory is applied for asperity shearing shown in Figure 6-1 under shear (*S*) and normal (*N*) forces where the dilation angle (*i*) is positive for forward shearing.

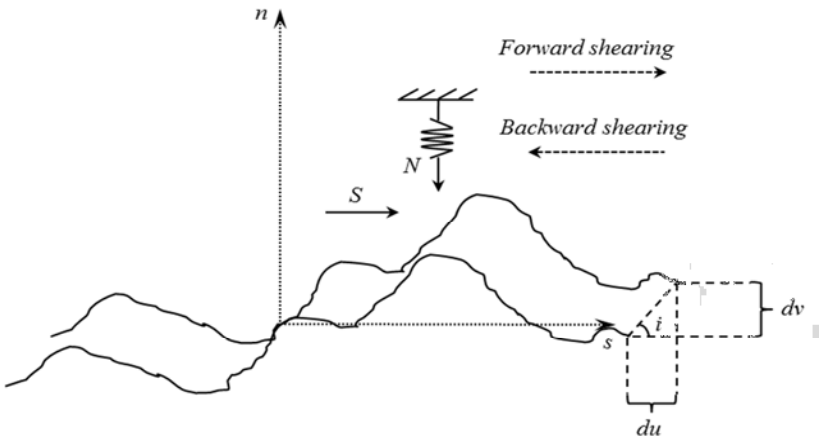

Figure 6-1 Asperity shearing under shear and normal forces

The energy balance theory incorporates the first law of thermodynamics in which the energy is neither created nor destroyed but only changing in its form. Applying the energy balance theory for the arrangement shown in Figure 6-1 by considering the energy dissipated due to asperity damage for the first forward shear cycle, then:

- $E_1 = Sdu$ *(work done by the shear force)*
- $E_2 = -Ndv$ *(work done against dilation due to normal force)*
- $E_3 = \mu[Ndu]$ *(work done against friction by the normal force)*
- $E_4 = \mu[S(\tan i)du]$ *(work done against friction by the shear force)*
- $E_5 = -E_d$ *(work done in the process of asperity damage)*

where, μ is the surface friction coefficient which is equal to the tangent of basic friction angle (φ_b).

The energy balance theory requires the sum of all the energy terms stated above to be zero, therefore:

$$F = \sum_{i=1}^{5} E_i = 0 \tag{6.5}$$

Introducing energy terms in Equation (6.5) and dividing by the increment of shear displacement and simplifying yields:

$$F = [S - N\tan i] - \mu[N + S\tan i] - E_d / du = 0 \tag{6.6}$$

Similarly to work done by Seidel and Haberfield (1995*a*), the energy dissipated due to asperity damage (E_d) is assumed to be equal to the inelastic work done due to dilation against the normal force, thus:

$$F = [S - N \tan i_0] - \mu[N + S \tan i] = 0 \tag{6.7}$$

where, i_0 is the initial asperity angle.

Dividing F to a unit of shearing area gives:

$$F = [\tau - \sigma_n \tan i_0] - \mu[\sigma_n + \tau \tan i] = 0 \tag{6.8a}$$

The value of initial asperity angle in the above equation can be estimated by scanning and quantifying the joint surface. Alternatively, i_0 can be related to the value of *JRC* using the method suggested by Xie and Pariseau (1992).

After the first forward shear cycle at the accumulated shear displacement equals to the half of the asperity length, it is assumed that the sliding mechanism (i.e. $E_d=0$) governs the shear behaviour at the asperities contact, thus:

$$F = [\tau - \sigma_n \tan i] - \mu[\sigma_n + \tau \tan i] = 0 \tag{6.8b}$$

To consider the dilatation behaviour of the joint, the plastic potential function is extended as:

$$Q = [\tau \cos i - \sigma_n \sin i] = 0 \tag{6.9}$$

As shown in the above equation and Figure 6-2, a different function is adopted for the plastic potential to allow for the different dilation behaviour. Therefore, the flow rule is non-associated and no dilation will be predicted at failure.

The dilation curve (Figure 6-3) typically describes the change of normal displacement during shearing. In order to obtain the dilation curve at the first forward shear cycle, asperities are considered to dilate on the secant dilation angle (i_{sec}) as:

$$i_{\sec} = \tan^{-1}(2v^* / T) \tag{6.10a}$$

where, v^* is the normal displacement at half of the asperity length and T is the asperity length.

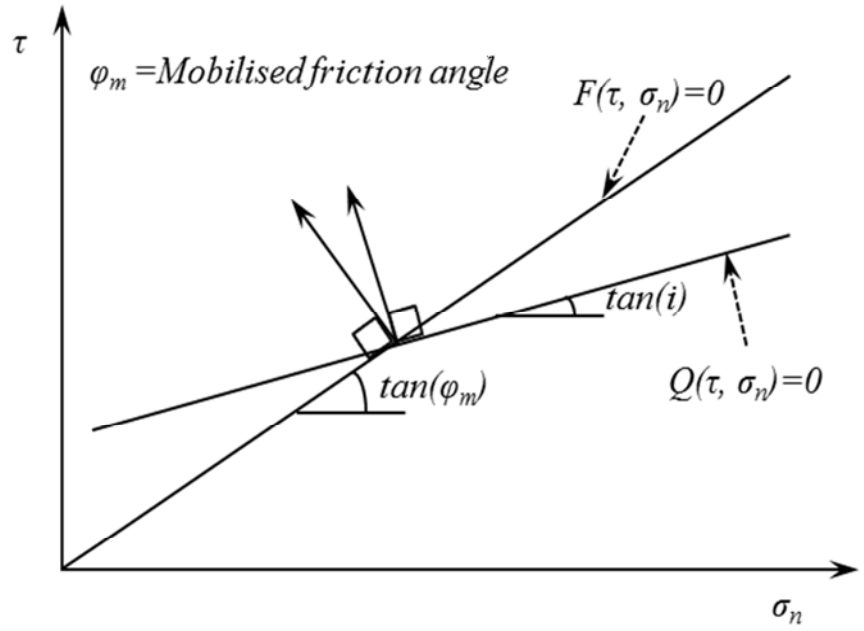

Figure 6-2 Plastic potential and yield functions

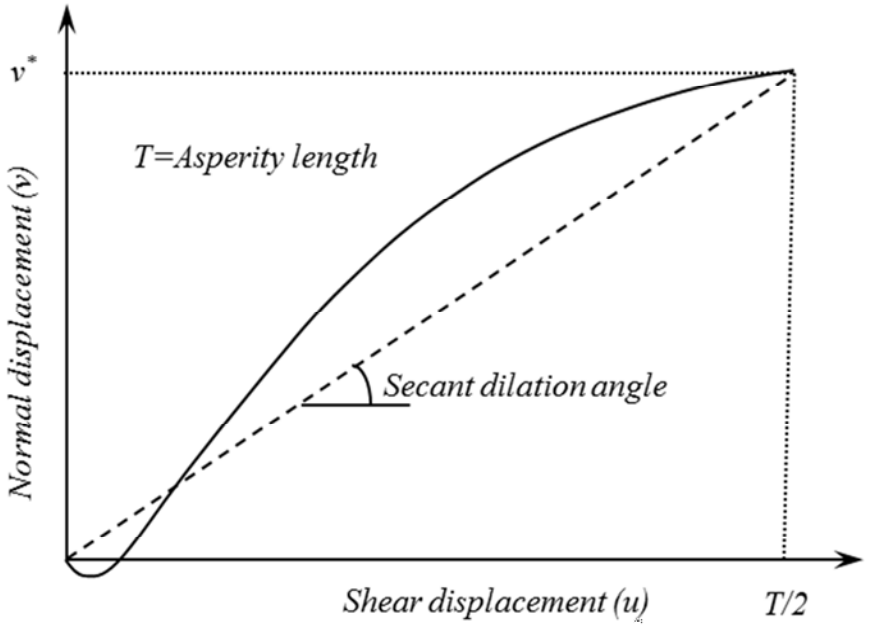

Figure 6-3 A typical dilation curve against shear displacement

During the sliding mechanism, the secant dilation angle is assumed to degrade exponentially due to a portion of the generated sliding shear energy as (see Plesha 1987):

$$i = i_{\text{sec}} \exp(-c_s \int_{T/2}^{u'} \tau du) \tag{6.10b}$$

where, c_s is the sliding damage coefficient that varies between 0 and 1 and u' is the accumulated shear displacement.

The value of coefficient c_s can be found by best-fitting the above equation to the plot of secant dilation angle versus sliding shear work. Low values of the coefficient c_s (close to zero) are usually associated with strong rock joint and low asperity degradation, while high values are associated with weak joints where asperity degradation is significant.

Once the dilation of the joints under cyclic loading is calculated for a particular shear displacement, the effective normal stress on the joint plane can be calculated using the following equation:

$$\sigma_n = \sigma_{n0} + kv \tag{6.11}$$

where, σ_{n0} and k are initial normal stress and boundary normal stiffness respectively.

For the current tests data, the secant dilation angle and sliding damage coefficient were calculated for Types I, II, III and replicas of the real rock surfaces under different initial normal stresses, as listed in Table 6.1 for T = 30 (mm).

Table 6-1 Model parameters for various asperity types and initial normal stresses

Asperity type	*Initial normal stress (MPa)*	i_{sec}°	$c_s(MPa^{-1}.mm^{-1})$
Type I	0.16	5.8	0.004
	0.56	5.24	0.005
	1.64	4.52	0.004
	2.4	4.55	0.013
Type II	0.16	12.66	0.008
	0.56	11.68	0.009
	1.64	8.69	0.015
	2.4	6.36	0.027
Type III	0.16	12.28	0.008
	0.56	11.76	0.011
	1.64	6.94	0.018
	2.4	2.83	0.08
Replicas	0.5	6.21	0.007
	1.5	3.97	0.007
	2.4	3.26	0.038

6.3.3. Computer program for simulating the shear behaviour of rock joints under cyclic loading

For faster and accurate processing, a computer program was extended in *MATLAB*, to calculate the shear stress, normal stress and normal displacement against shear

displacement using the proposed constitutive model. The computer code for this program is given in Appendix I. The input data for the program includes model parameters, initial normal stress, initial asperity angle, basic friction angle, boundary normal stiffnesses and the number of loading cycles. Using the program, the complete shear stress, normal stress and normal displacement profiles can be plotted and compared with the laboratory results.

6.3.4. Model verification

Using the above mentioned computer program, the shear behaviour of rock joints under cyclic loading and CNS conditions at different initial normal stresses and asperity types were simulated and plotted in Figures 6-4 to 6-11. The experimental results of the cyclic loading shear behaviour of rock joints were discussed and shown in section 4.3 which are used here for model verification. As can be seen in Figures 6-4, 6-6 and 6-8, for low values of initial normal stress (σ_{n0}=0.16 MPa and 0.56 MPa), lower shear strength in backward shearing and later cycles rather than forward shearing and earlier cycles is well replicated by the proposed model. The effect of higher external energy on asperities resulting in greater damage in initial cycles and forward shearing is evident in comparison to later cycles and backward shearing. This is represented by the proposed model in predicted dilation and normal stress curves. It can be noted from Figures 6-5, 6-7, 6-9 and 6-11 that the proposed model is able to predict the additional shear strength generated by the asperity breakage, subject to the high level of initial normal stress (σ_{n0}=1.64 MPa, 2.4 MPa, 2.5 MPa) in the first forward shear cycle. For subsequent cycles, both the proposed model and the experimental data approach the residual friction angle when asperities were almost degraded.

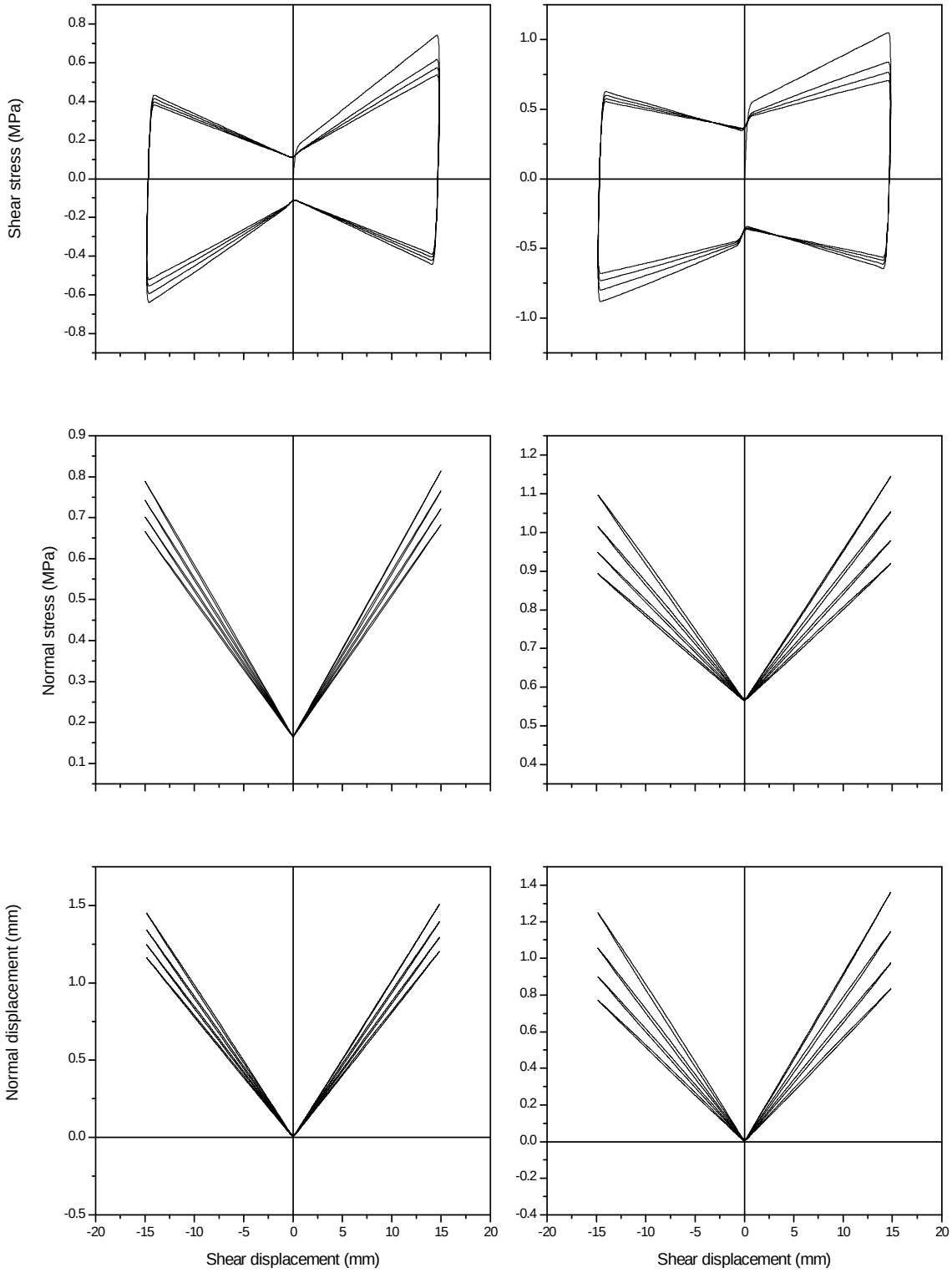

Figure 6-4 Model simulations of Type I asperity surface: [left] 0.16 MPa of initial normal stress, [right] 0.56 MPa of initial normal stress

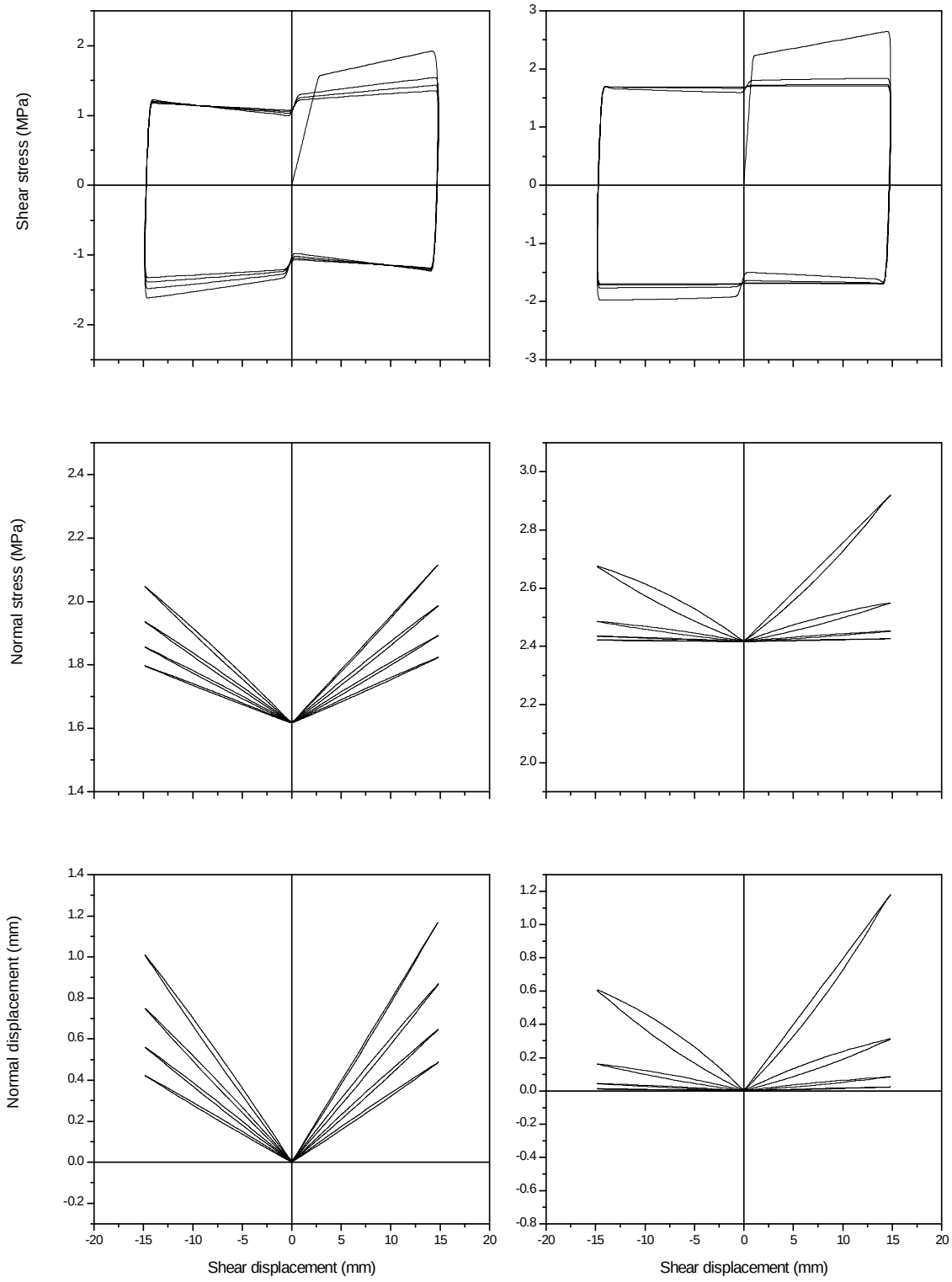

Figure 6-5 Model simulations of Type I asperity surface: [left] 1.64 MPa of initial normal stress, [right] 2.4 MPa of initial normal stress

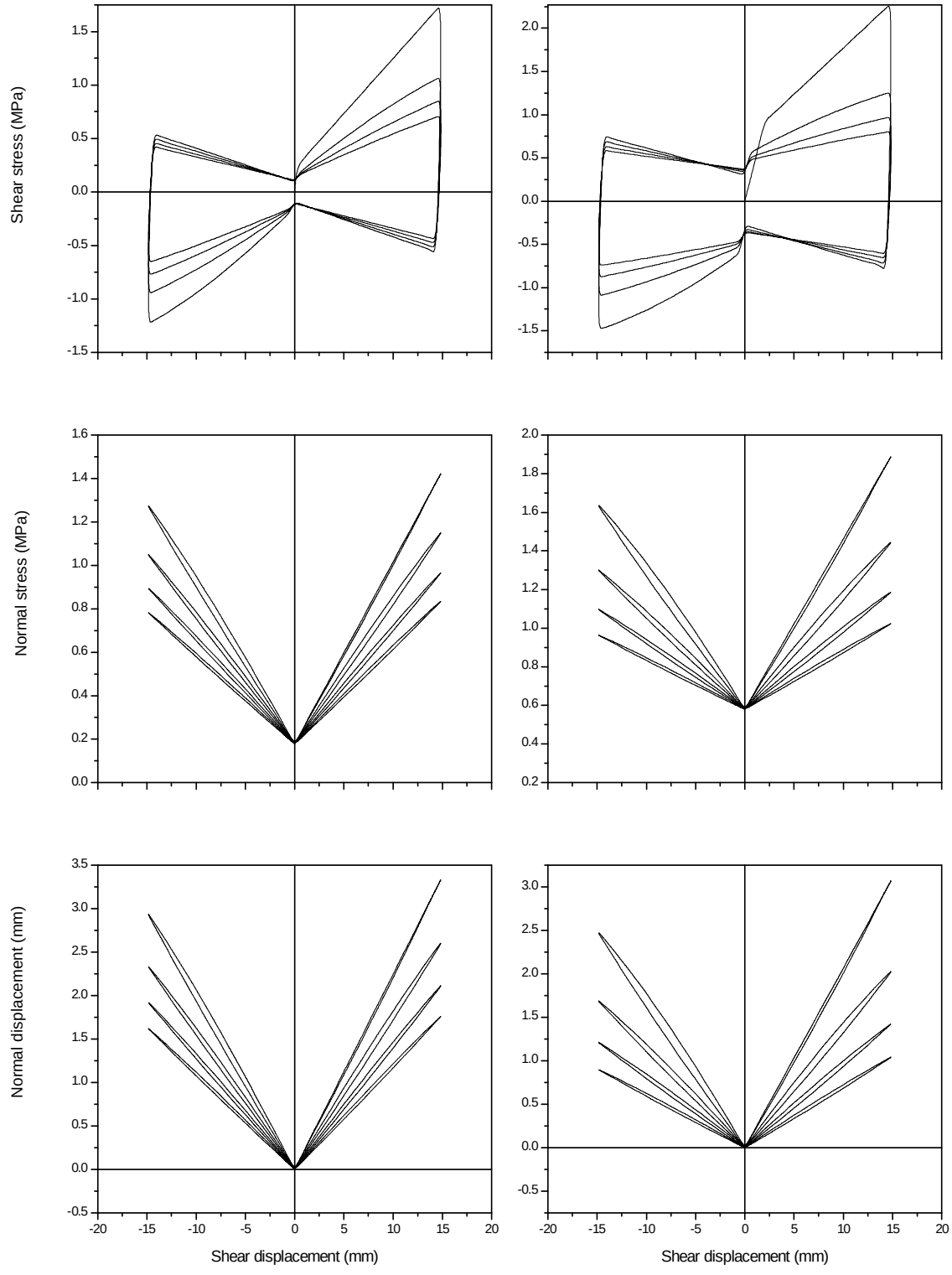

Figure 6-6 Model simulations of Type II asperity surface: [left] 0.16 MPa of initial normal stress, [right] 0.56 MPa of initial normal stress

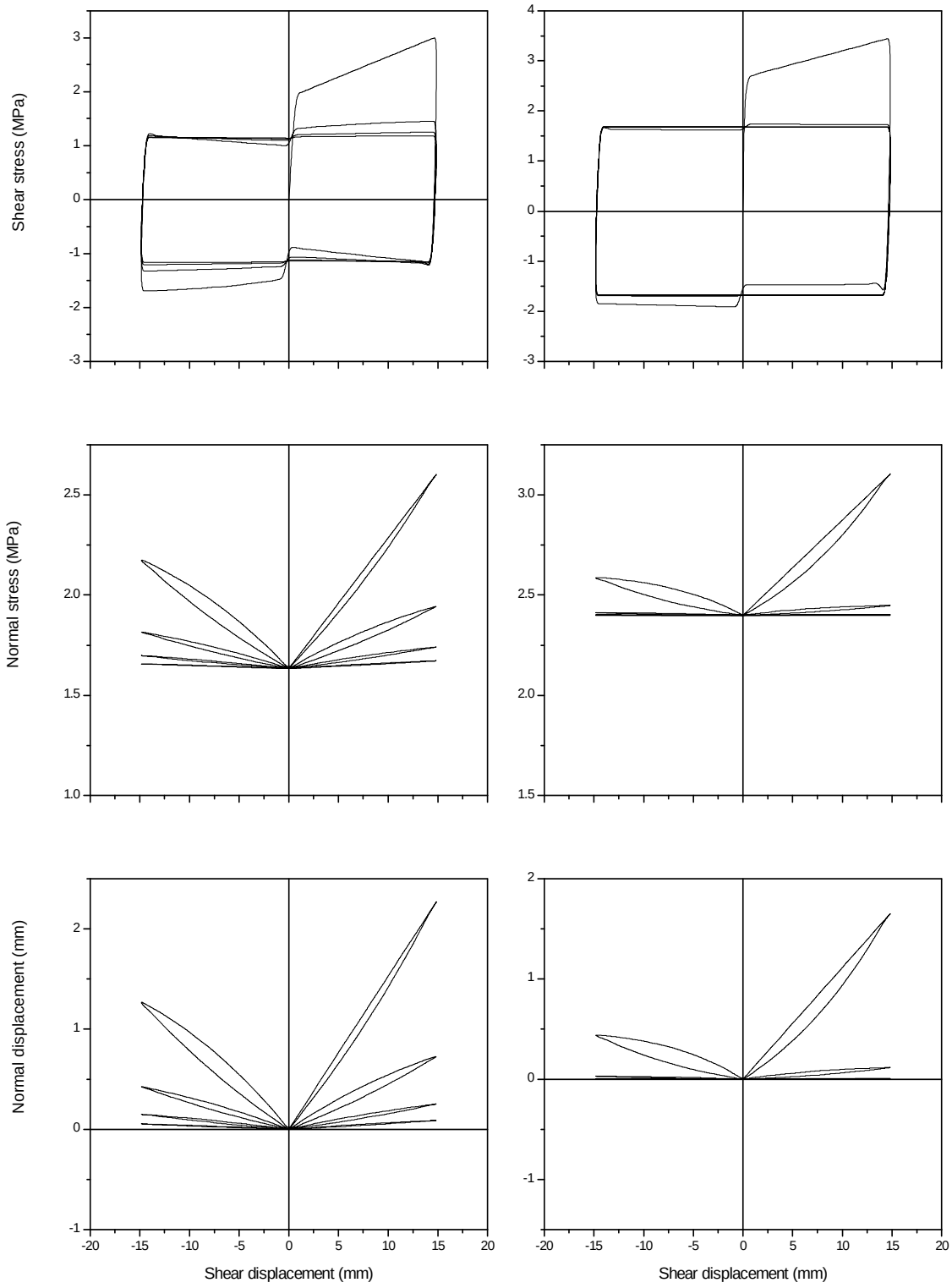

Figure 6-7 Model simulations of Type II asperity surface: [left] 1.64 MPa of initial normal stress, [right] 2.4 MPa of initial normal stress

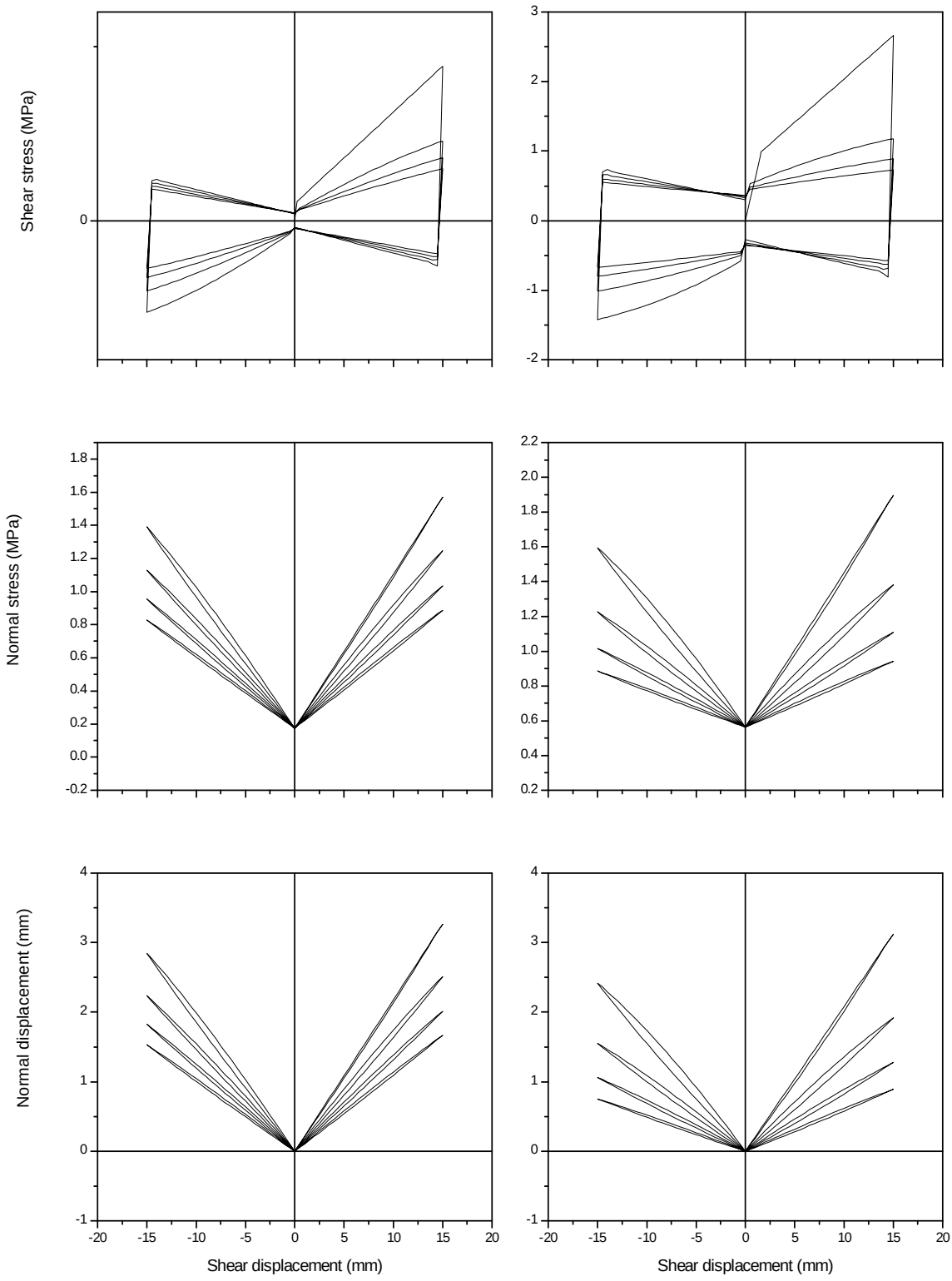

Figure 6-8 Model simulations for Type III asperity surface: [left] 0.16 MPa of initial normal stress, [right] 0.56 MPa of initial normal stress

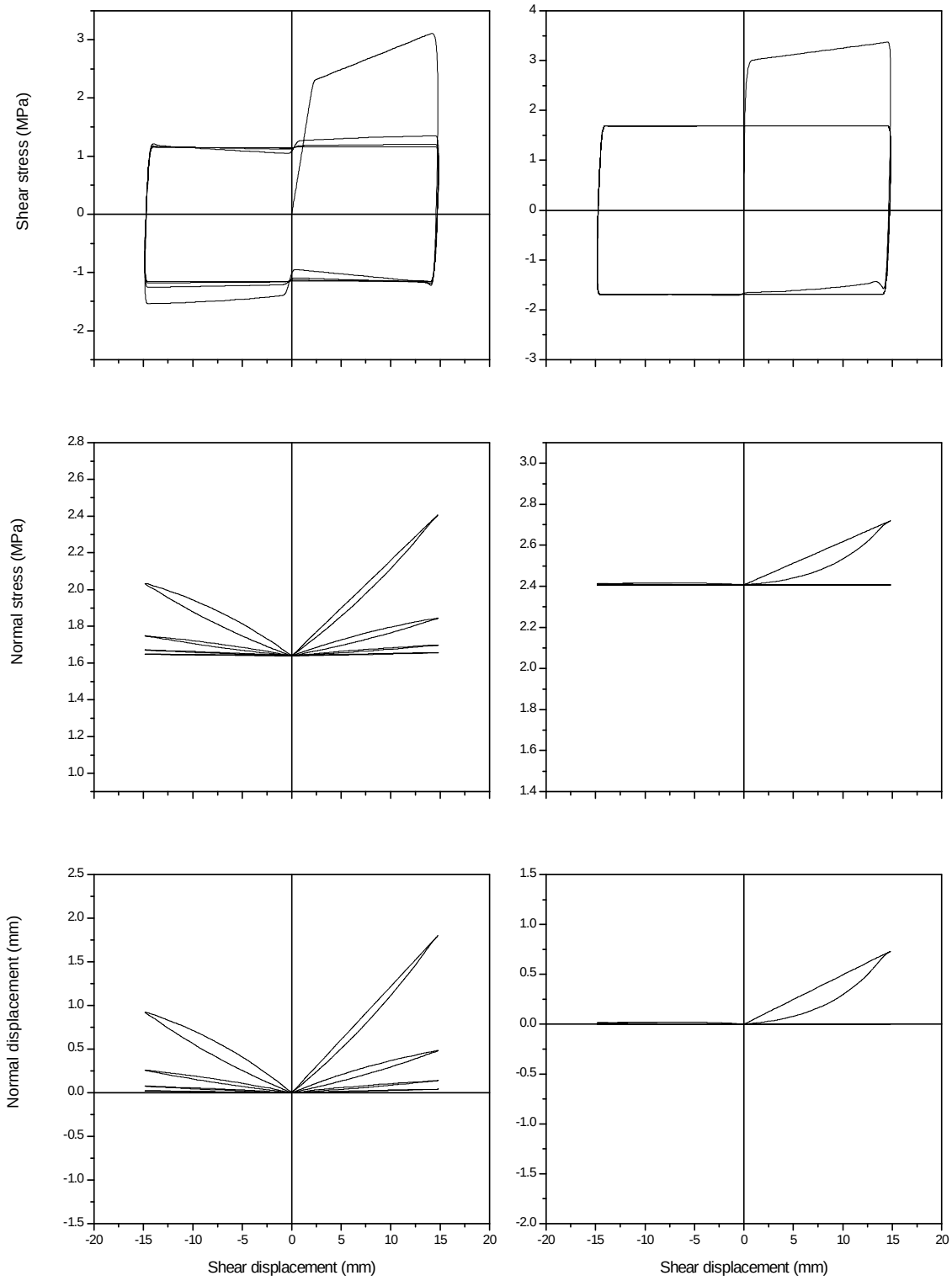

Figure 6-9 Model simulations of Type III asperity surface: [left] 1.64 MPa of initial normal stress, [right] 2.4 MPa of initial normal stress

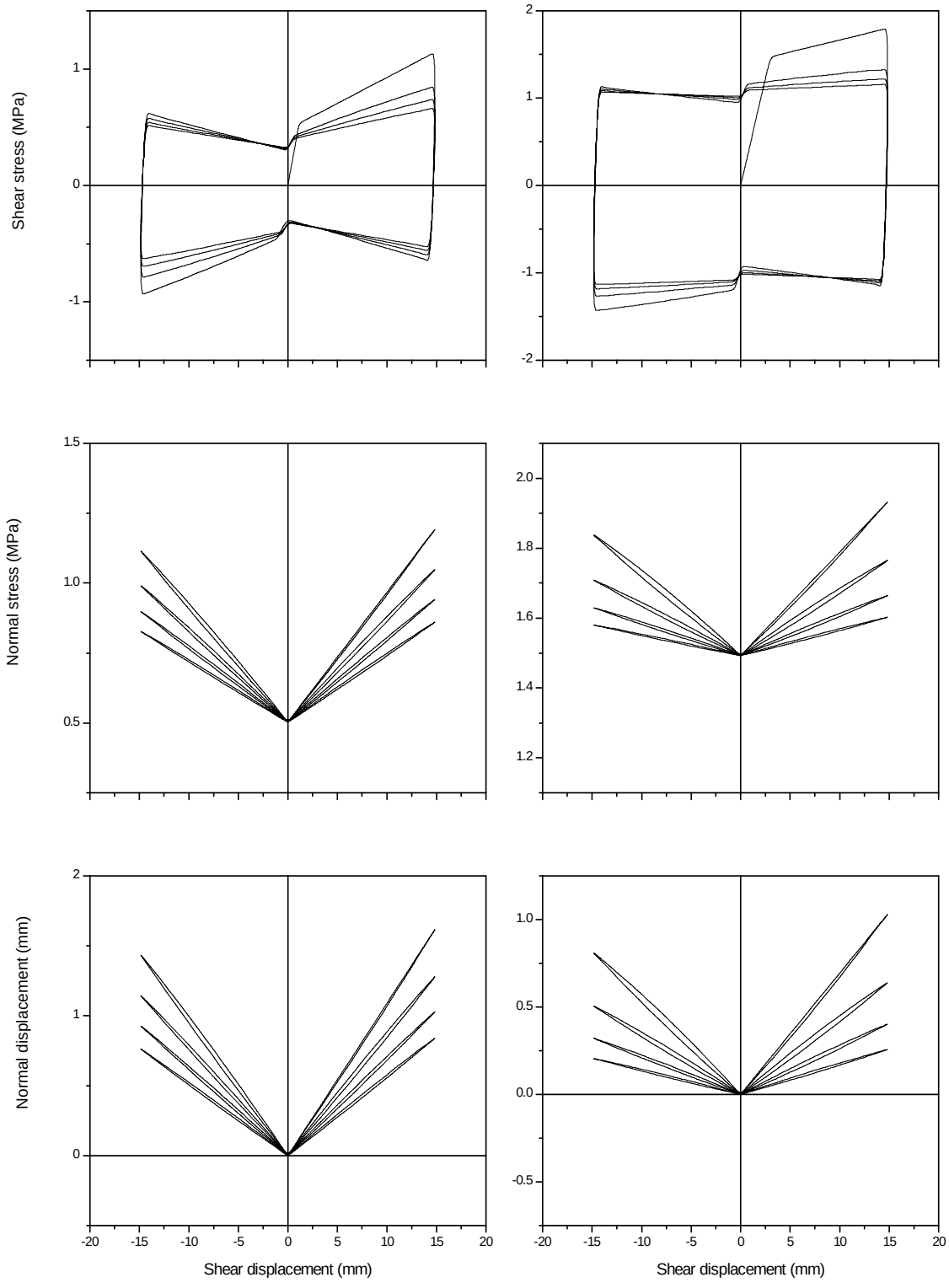

Figure 6-10 Model simulations of replicas of real asperity surface: [left] 0.5 MPa of initial normal stress, [right] 1.5 MPa of initial normal stress

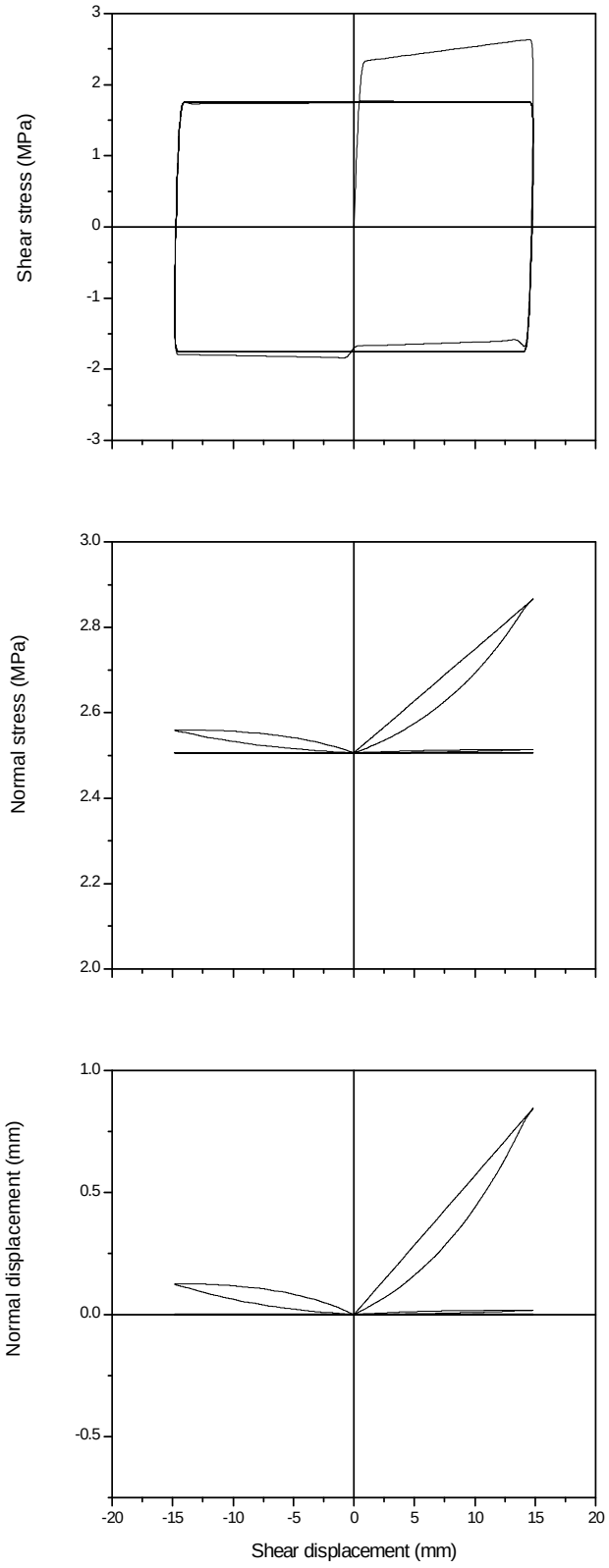

Figure 6-11 Model simulations of replicas of real asperity surface with 2.5 MPa of initial normal stress

Nevertheless, some discrepancies were observed between the predicted results of normal displacement, normal stress with shear displacement and the measured data after the first forward shear cycle. The differences (i.e. contraction after the rapid degradation in the first forward shear cycle) related to the loss of the damaged material at the sample edge of the shear box during cyclic shearing, when debris from the broken asperities fell out from the test apparatus. This behaviour would not occur along the field joints where the surrounding media prevent the damaged material from escaping. Figure 6-10 [left] shows that the computed results for replicas of the real rock surface with spatial roughness are in agreement with the measured data, particularly for the first shear cycle that second order asperities were damaged (σ_{n0}=0.5 MPa).

6.3.5. Correction for the shear rate

The constitutive model presented in the previous section was calibrated with the shear rate of 0.5 mm/min. In order to estimate the cyclic loading shear strength of rock joints at desired shear rate, the following equation that fits well with the experimental data of four consecutive loading cycles (Figure 6-12) is proposed as:

$$\frac{\tau_h^c}{\tau_l^c} = 1 - c_1^s \exp\left[-c_2^s \left(N_c - 1\right)\right] \tag{6.12}$$

where, τ^c_h is the cyclic loading shear strength of high shear rate, τ^c_l is the cyclic loading shear strength of low shear rate (0.5 mm/min), c^s_1 and c^s_2 are model coefficients calibrated for different conditions as listed in Table 6.2 and N_c is the number of shear cycles.

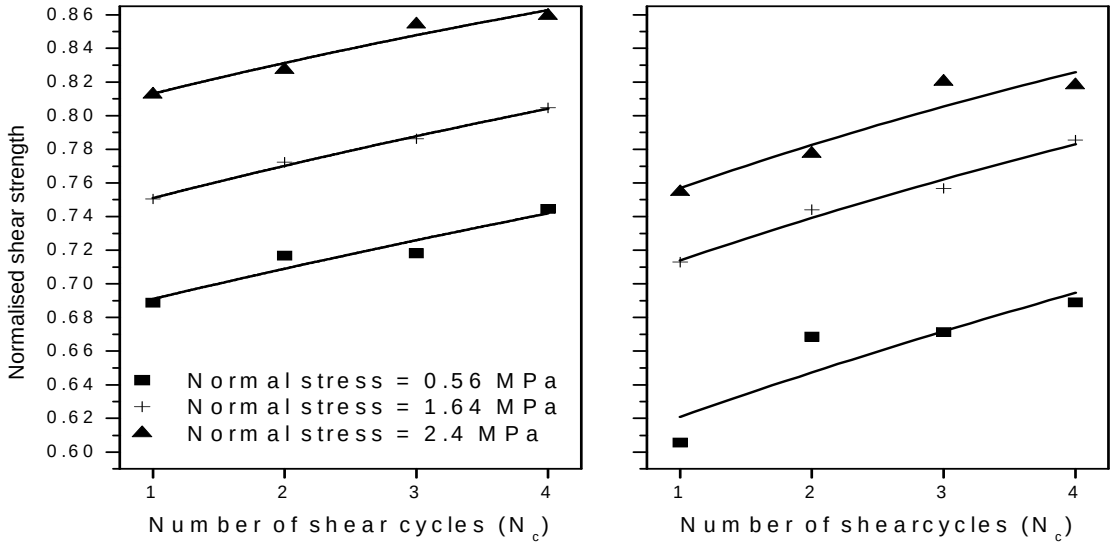

Figure 6-12 Comparison between measured data and model predicted results: [left] Shear rate of 5 mm/s, [right] Shear rate of 20 mm/s (symbols = measured data and lines = model results)

Table 6-2 Model coefficients for different shear rates and initial normal stresses

Shear rate (mm/s)	*Initial normal stress (MPa)*	c^s_1	c^s_2
5	0.56	0.309	0.06
	1.64	0.249	0.08
	2.4	0.187	0.103
20	0.56	0.379	0.072
	1.64	0.286	0.092
	2.4	0.243	0.111

Model coefficients given in Table 6.2 are zero for shear rate of 0.5 mm/min. In Figure 6-12, the shear strength is normalised to the values of shear strength obtained based on 0.5 mm/min of shear rate.

It is noted that according to Equation (6.12), the shear strength of higher shear rates becomes closer to those of lower shear rates with increase in the asperity damage. These values will be the same as the number of loading cycles approaches infinity when joints are theoretically planar.

6.4. Modelling of shear strength of infilled rock joints under cyclic loading

The shear strength model for infilled rock joints under cyclic loading is developed by considering the monotonic loading shear strength and reduction in strength due to cyclic loading. Accordingly, in the first step, the shear strength of infilled rock joints under monotonic loading is obtained by applying Equation (3.14) and then the reduction in the shear strength due to cyclic loading is calculated based on a hyperbolic model. Finally, the shear strength of infilled joints under cyclic loading is determined by deducting the reduction in the shear strength due to cyclic loading from the monotonic loading shear strength. Thus, the failure criterion for infilled rock joints under cyclic loading is proposed as:

$$\tau_p^{ci} = \tau_p^{mi} - \Delta\tau^i \tag{6.13}$$

where, $\tau^{ci}{}_p$ is the peak shear strength of infilled rock joints under cyclic loading, $\tau^{mi}{}_p$ is the peak shear strength of infilled rock joints under monotonic loading and $\Delta\tau^i$ is the reduction in shear strength with increase in the number of loading cycles.

In the above equation, the peak shear strength refers to the maximum shear strength in a complete loading cycle.

A Normalised Cyclic Strength Reduction of infilled rock joints ($NCSR^i$) is proposed here. This is defined as the ratio of reduction in peak shear strength with increase in the number of shear cycles, divided by the initial normal stress (Figure 6-13). Based on the experimental observation of this study, the impact of cyclic loading on $NCSR^i$ can be fitted using a hyperbolic function:

$$NCSR^i = \frac{N_c - 1}{\alpha(N_c - 1) + \beta} \tag{6.14}$$

where, α and β are model coefficients taking into account the effect of asperity damage and compaction of infill material.

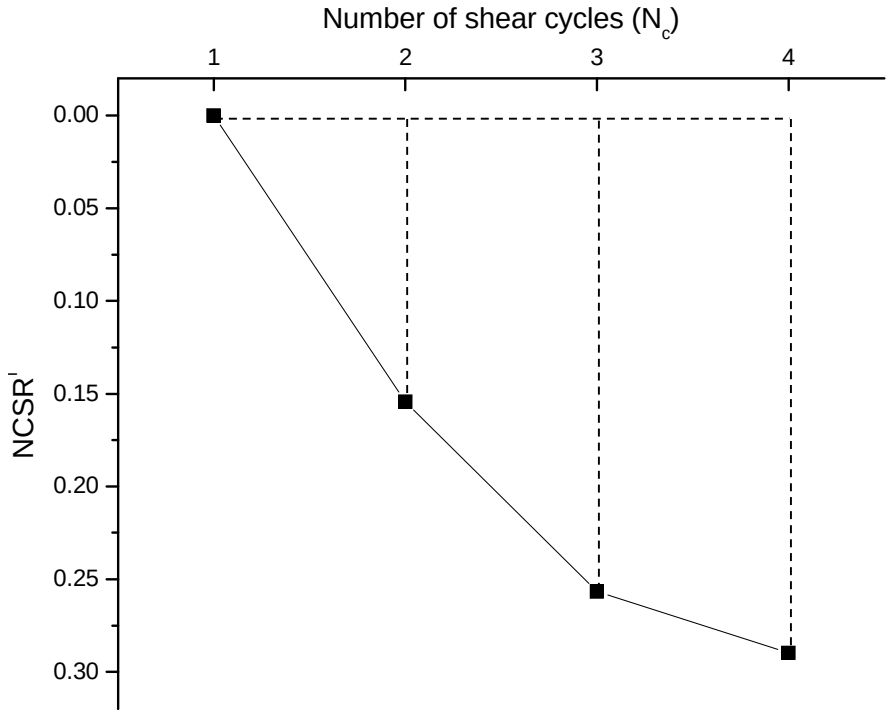

Figure 6-13 Variation of $NCSR^i$ with number of shear cycles

In order to easily determine the hyperbolic coefficients, Equation (6.14) is rearranged to give the following linear relationship for N_c >1:

$$\frac{N_c - 1}{NCSR^i} = \alpha(N_c - 1) + \beta \tag{6.15}$$

The values of α and β can now be readily determined by plotting the relationship between $(N_c\text{-}1)$ and $NCSR^i$ as illustrated in Figure 6-14.

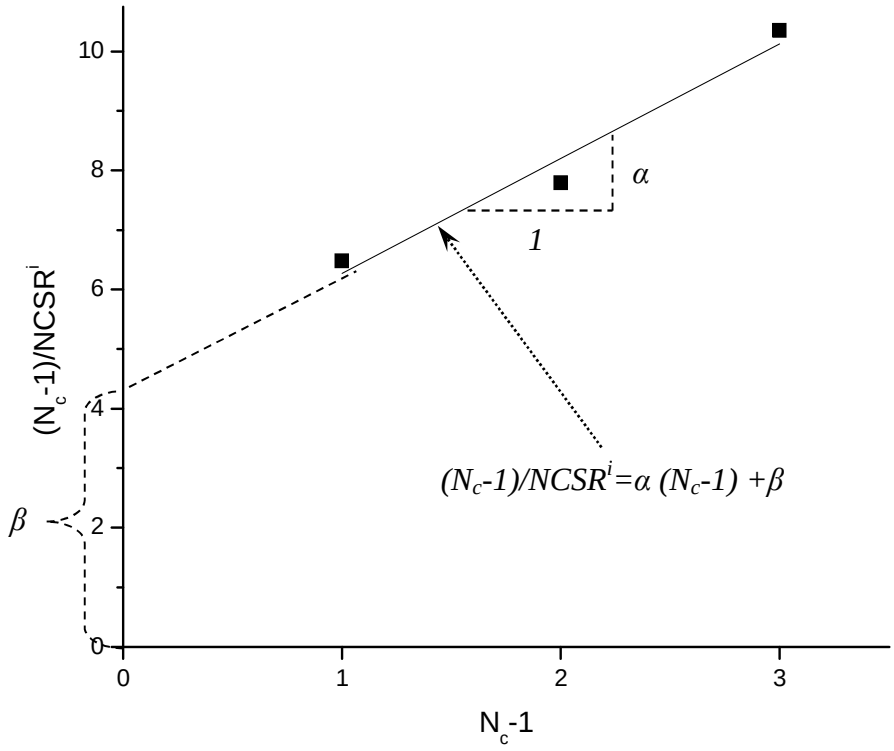

Figure 6-14 Determination of hyperbolic relationship coefficients

Once the $NCSR^i$ is calculated, the peak shear strength of infilled rock joints under cyclic loading can be obtained by extending the peak shear strength of infilled rock joints under monotonic loading as per Equation 3.4:

$$\tau_p^{ci} = \sigma_n \left[\tan(\varphi_b + i_0)(1-\kappa)^{c_1} + \tan(\varphi_{fill})\left(\frac{2}{1+1/\kappa}\right)^{c_2} \right] + C_{fill} - \sigma_{n0} NCSR^i \tag{6.16a}$$

$$\kappa = \frac{(t/a)}{(t/a)_{cr}} \tag{6.16b}$$

$$\sigma_n = \sigma_{n0}\left[\frac{1.8}{1+\kappa}\right]^{c_3} \tag{6.16c}$$

where, φ_{fill} is the infill material friction angle, C_{fill} is the cohesion of the infill material, t is the infill thickness, a is the asperity height, $(t/a)_{cr}$ is the critical value of infill thickness to asperity height and c_1, c_2, c_3, α and β are model coefficients.

In Equation (6.16), φ_b is determined by the tilt test on the planar interface of the joint surface, i_0 is related to the value of joint roughness coefficient using the method suggested by Xie and Pariseau (1992), c_1 and c_2 are constants defining the contribution of joint friction and infill material to the monotonic loading shear strength and are determined by multi-regression, φ_{fill} and C_{fill} are determined by direct shear tests on infill material, α and β are determined as illustrated in Figure 6-14, a is equal to the average asperity height, $(t/a)_{cr}$ is determined by direct shear tests on infilled rock joints under monotonic loading and c_3 is a constant determined by curve fitting.

6.4.1. Determination of model coefficients

The relevant model coefficients including c_1, c_2, c_3, $(t/a)_{cr}$, α and β are determined according to the experimental data for different asperity types, initial normal stresses, and infill thickness to asperity height ratios as listed in Table 6.3. Additional monotonic loading tests with various infill thicknesses to asperity height were conducted to determine $(t/a)_{cr}$.

Table 6-3 Model coefficients for various infill thicknesses to asperity height, initial normal stresses and asperity types

Asperity type	$(t/a)_{cr}$	c_1	c_2	*Initial normal stress (MPa)*	c_3	*Infill thickness to asperity height*	α	β
Type I	1.5	1.05	2.7	0.56	1.3	0.3	1.51	3.26
						0.6	2.21	4.69
						1	3.01	6.58
				1.64	0.5	0.3	1.93	4.34
						0.6	2.98	5.37
						1	4.66	7.01
				2.4	0.22	0.3	2.77	5.23
						0.6	4.23	6.58
						1	5.68	9.65
Type II	1.6	1	4.1	0.56	2.2	0.3	0.7	0.32
						0.6	0.86	1.51
						1	1.42	2.31
				1.64	1	0.3	1.2	0.95
						0.6	1.56	1.61
						1	2.64	3.33
				2.4	0.17	0.3	1.34	1.14
						0.6	1.79	1.76
						1	2.76	3.79

Equation (6.15) represents a straight line with the horizontal axis as $(N_c\text{-}1)$ and the vertical axis as $(N_c\text{-}1)/ NCSR^i$ respectively. The model predicted results of $NCSR^i$ along

with the laboratory experiments against the number of shear cycles is shown in Figure 6-15. Correlation coefficients with the minimum and maximum of 0.96 and 0.99 were found for these straight lines, thus indicating that the variation of $NCSR^i$ against the number of shear cycles can be predicted with reasonable accuracy using Equation (6.14). It is noted that the hyperbolic coefficients are higher for greater initial normal stresses and infill thickness to asperity height ratios and smaller asperity angles.

The piecewise linear method can be applied to estimate the model coefficients at the desired values of asperity angle, initial normal stress and infill thickness to asperity height ratio. Figure 6-16 shows the shear strength predicted using the model (as per Equation 6.16) and those obtained from the laboratory tests. As can be seen from Figure 6-16, the effects of cyclic loading on shear strength reduction due to asperity damage and deformation of infill material is reasonably represented by the proposed model under different conditions of initial asperity angle, initial normal stress and infill thickness to asperity height ratio.

Figure 6-15 shows that as the number of loading cycles increases, decrease in $NCSR^i$ becomes less pronounced. However, the hyperbolic relationship gives $1/\alpha$ as the asymptote when the number of loading cycles approaches infinity. Therefore, it is anticipated that the maximum reduction in shear strength under cyclic loading is reached before it becomes asymptote to $1/\alpha$. As the model coefficients are evaluated based on the four shear cycles, the shear strength of the fourth cycle is considered to be the residual shear strength. By careful investigation of the measured data for different conditions, 75% and 55% of the monotonic loading shear strength ($\tau^{mi}{}_p$) are assigned to the residual shear strength of Types I and II asperity surfaces.

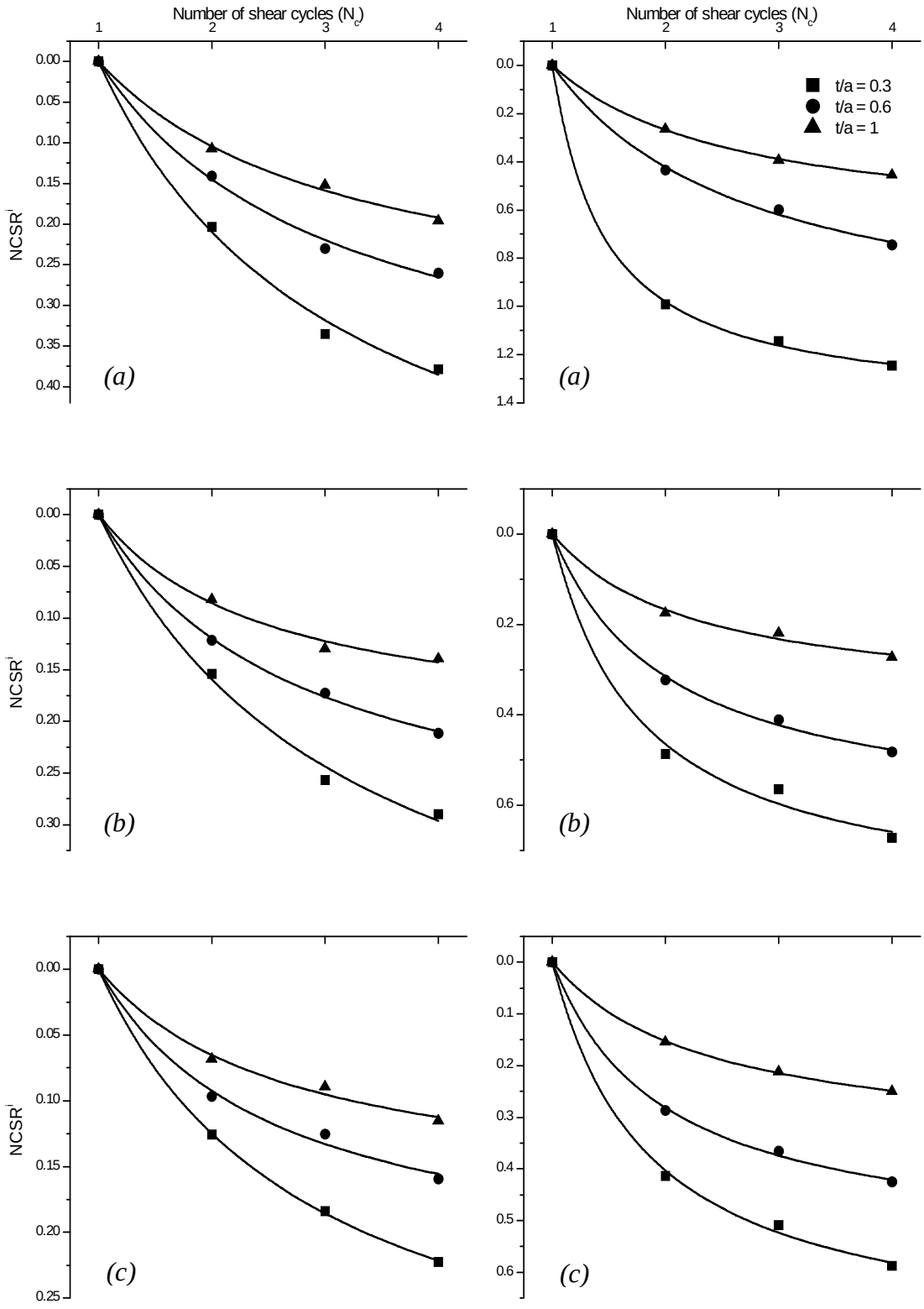

Figure 6-15 Comparison between measured and model predicted results of $NCSR^i$ against number of shear cycles, (line = model predictions and symbols = measured data): [left] Type I asperity surface, [right] Type II asperity surface, (*a*) σ_{n0} =0.56 MPa, (*b*) σ_{n0} =1.64 MPa, (*c*) σ_{n0} =2.4 MPa

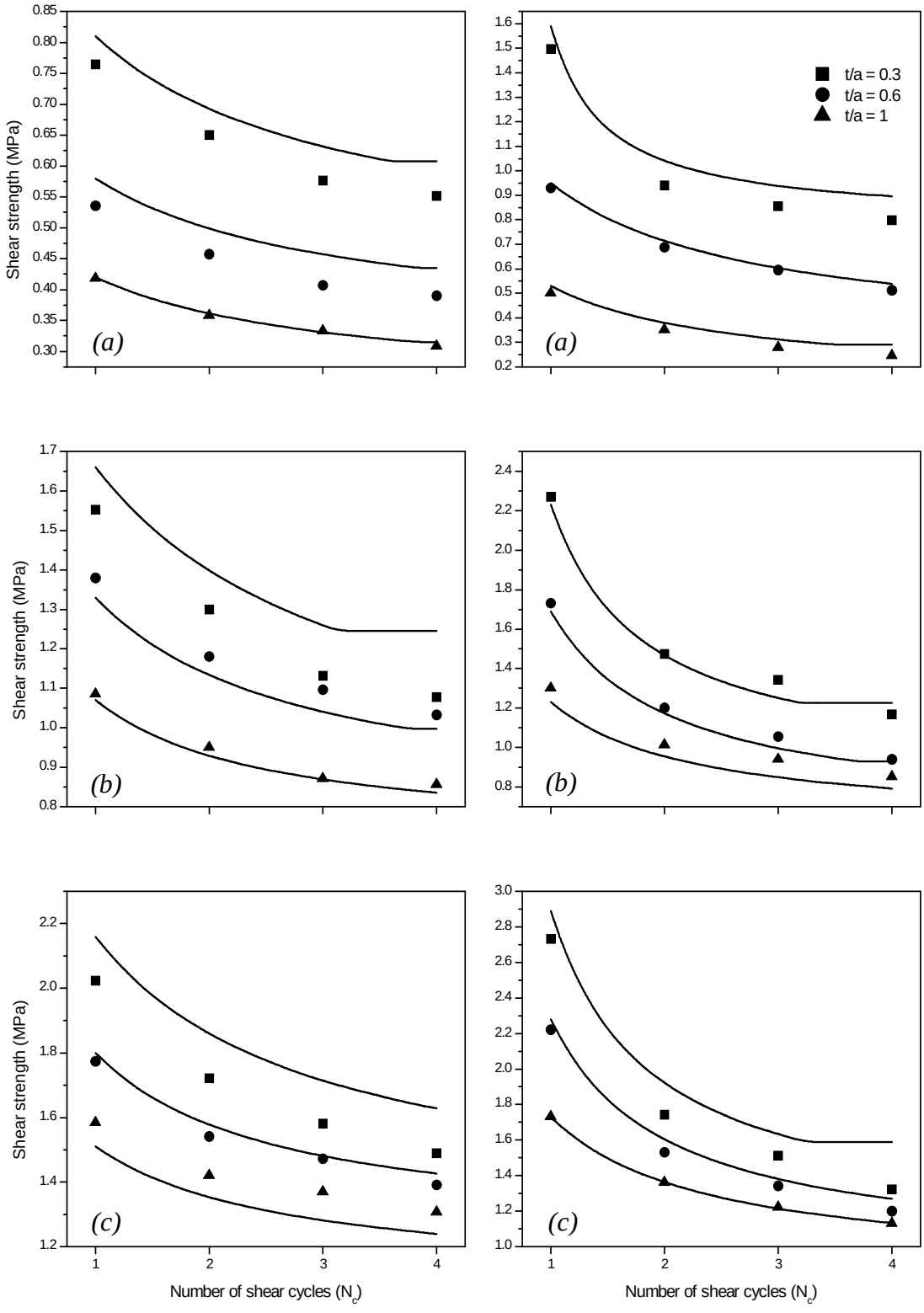

Figure 6-16 Comparison between measured and model predicted results of shear strength against number of shear cycles, (line = model predictions and symbols = measured data): [left] Type I asperity surface, [right] Type II asperity surface, (*a*) σ_{n0} =0.56 MPa, (*b*) σ_{n0} =1.64 MPa, (*c*) σ_{n0} =2.4 MPa

6.5. Summary

An elasto-plastic constitutive model in an incremental framework was introduced for asperity shearing under cyclic loading and CNS conditions. The model can predict specific characteristics of rock joints shearing subject to cyclic loading such as dependency of shear strength on friction angle and loading direction, dependency of friction and dilation angles on asperity damage and dependency of asperity damage on external energy. The model was calibrated using the measured data for three different initial asperity angles as well as replicas of a real rock surface at various initial normal stresses. Generally, the results of simulations using the constitutive model are in good agreement with the measured laboratory data observed for the shear and normal stresses versus shear displacement responses and the associated dilation behaviour. Furthermore, an empirical relationship was presented and calibrated for different initial normal stresses to consider the effects of shear rate on cyclic loading shear strength of rock joints.

A mathematical model was introduced and applied to simulate the reduction in the shear strength of infilled rock joints with increase in the number of loading cycles incorporating the concept of $NCSR^i$. The model includes important features of infilled rock joints such as infill thickness to asperity height ratio, infill friction angle, initial asperity angle, initial normal stress, basic friction angle of the joint surface and number of loading cycles. The model coefficients were determined according to the experimental data for different asperity angles, initial normal stresses and infill thicknesses to asperity height. The coefficients of $NCSR^i$ relationship were found to be always higher for greater initial normal stresses and infill thickness to asperity height ratios and smaller asperity angles.

Chapter VII

7. SIMULATION OF AN UNDERGROUND EXCAVATION SUBJECTED TO SEISMIC EVENTS USING UDEC

7.1. Introduction

Shear behaviour of rock joints under monotonic loading has been studied in the past using numerical tools. The main advantage of numerical methods is that the model can be built and further modified to perform sensitivity studies based on laboratory tests and theoretical assumptions. In numerical simulation, the discontinuities are modelled as assemblage of discrete blocks. One of the most powerful numerical software which is able to represent discontinuities in the rock mass is the Universal Distinct Element Code (UDEC). This software is equipped with an embedded programming language (FISH) that offers a wide range of applications to the users.

7.2. UDEC overview

The shear behaviour of jointed rocks, flow through discontinuities, and slope stability problems have been simulated successfully using UDEC. The UDEC calculations are based on Newton's second law of motion, conservation of mass, and momentum and energy principles. There are four built-in constitutive models available in UDEC program to represent the material behaviour of discontinuities as:

- Point contact – Coulomb slip (joint model point)
- Joint area contact – Coulomb slip (joint model area)

- Joint area contact – Coulomb slip with residual strength (joint model residual)
- Continuously yielding

The joint constitutive models are defined to be representative of the physical response of rock joints. The point contact model represents the discontinuity between two blocks in which the contact area is very small relative to the dimension of the block. The joint area contact model is developed for closely packed blocks with area contact. This model is based on the elastic stiffness, frictional, cohesive, tensile strength properties and dilation characteristics common to rock joints. The residual strength version of this model is intended to simulate displacement weakening of the joint by loss of friction, cohesion and/or tensile strength at the onset of shear or tensile failure. The continuously yielding joint model is a more complex model that replicates continuous weakening behaviour as a function of the accumulated plastic shear displacement.

This chapter investigates the capabilities of Coulomb slip criterion (joint model area) and continuously yielding model in simulating the shear behaviour of rock joints under cyclic loading and CNS conditions. Furthermore, an underground excavation is modelled in UDEC and its stability against seismic events is investigated in different conditions.

7.3. Constitutive model

The Coulomb slip and continuously yielding models are presented here in details for completeness in discussion of analysis.

7.3.1. Coulomb slip model

This criterion provides a linear deformation model that relates shear strength (τ_0) to normal stress (σ_n) by:

$$\tau_0 = \sigma_n \tan(\varphi) + c \tag{7.1}$$

where, φ and c are friction angle and cohesion of the joint.

Once τ_0 is reached, the joint deformation is assumed to be perfectly plastic. During elastic deformation, the shear response is governed by constant shear stiffness (k_s) as:

$$\Delta\tau = k_s \Delta u_s^e \tag{7.2}$$

where, $\Delta\tau$ is the incremental shear stress and Δu^e_s is the elastic compound of incremental shear displacement.

The Coulomb slip model in its basic form does not simulate joint wear and dilation behaviour, however, the dilation may be considered after onset of plastic deformation. The joint dilation remains constant during shearing as there is no wear of the joint. The dilation angle is assigned to zero after reaching a critical shear displacement. A form of the model is described by Itasca Consulting Group, Inc. (1996) as:

$$\begin{cases} \quad If \quad |\tau < \tau_0| \quad then \quad \psi = 0 \\ If \quad |\tau = \tau_0| \quad and \quad |u_s| \geq u_{cs} \; then \quad \psi = 0 \end{cases} \tag{7.3}$$

where, ψ is the dilation angle, u_s is the joint shear displacement and u_{cs} is the critical shear displacement.

7.3.2. Continuously yielding model

In order to simulate the internal mechanism of progressive damage of joints under shearing, Cundall and Hart (1984) proposed the continuously yielding model. This model is more realistic than the Coulomb failure criterion as it replicates the non-linear behaviour observed in physical tests such as joint degradation, normal stiffness, dependence on normal stress and the decrease in dilation angle with plastic shear displacement. The continuously yielding model can be described by the following features:

- The shear stress against shear displacement curve approaches a 'target' shear strength curve.
- The target shear strength decreases continuously with the accumulated plastic shear displacement indicating the damage of joints under shearing.
- The dilation angle is calculated as the difference between the apparent friction angle and the residual friction angle.

In this model, the response to normal loading is expressed incrementally by:

$$\Delta\sigma_n = k_n \Delta u_n \tag{7.4}$$

where, $\Delta\sigma_n$ is the increment of normal stress, k_n is the normal stiffness which may be written as a function of the normal stress and Δu_n is the increment of normal displacement.

During shear loading, the model behaves non-linearly from the onset of shearing as shown in Figure 7-1. The shear stress increment is calculated as:

$$\Delta\tau = F k_s \Delta u_s \tag{7.5}$$

where, F is a factor controls the shear stiffness (k_s) and Δu_s is the increment of shear displacement.

In Equation (7.5), the shear stiffness (k_s) may also be written as a function of the normal stress.

Factor F depends on the distance from the current stress curve to the target strength curve or bounding strength curve (τ_m, see Figure 7-1) and is obtained by:

$$F = \frac{1-\tau/\tau_m}{1-r} \tag{7.6}$$

where, τ is the current shear stress, τ_m is the failure stress at a given plastic displacement and r is factor initially set to zero. The factor r is aimed to restore the elastic stiffness immediately after load reversal. At the onset of a load reversal r is assigned to a value of τ/τ_m, thus F would become 1. The bounding stress is given by:

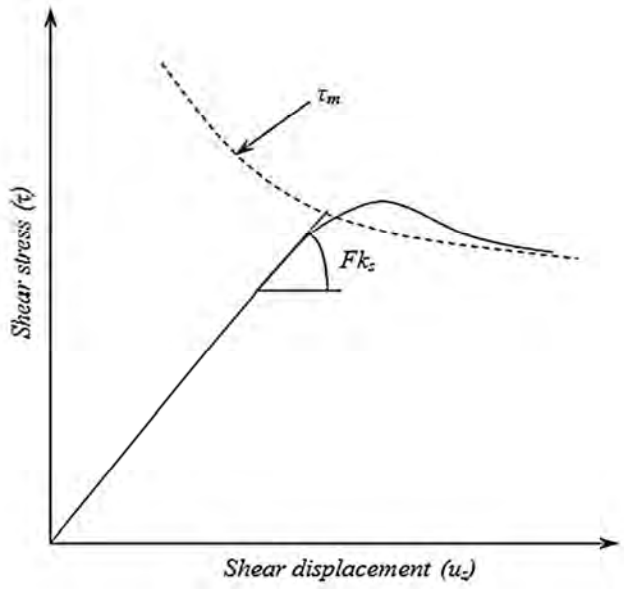

Figure 7-1 Continuously yielding joint model (after Itasca Consulting Group, Inc. 1996)

$$\tau_m = \sigma_n \tan(\varphi_m) \tag{7.7}$$

where, φ_m is the mobilised friction angle which includes asperity sliding and shearing. Due to asperity damage, the mobilised friction angle continuously reduces according to the following relationship:

$$\Delta\varphi_m = -\frac{(\varphi_m - \varphi_b)}{R}\Delta u_s^p \tag{7.8}$$

where, R is the amplitude of joint roughness with a dimension of length and $\Delta u^p{}_s$ is the plastic displacement increment as a function of the shear displacement increment Δu_s, defined as:

$$\Delta u_s^p = (1-F)\left|\Delta u_s\right| \tag{7.9}$$

The asperity degradation is governed by the following empirical law:

$$\varphi_m = \left(\varphi_m^i - \varphi_b\right)\exp(-u_s^p / R) + \varphi_b \tag{7.10}$$

where, $\varphi^i{}_m$ is the initial friction angle usually taken as the basic friction angle plus the initial asperity angle (φ_b+i_0). The current dilation angle (i) is calculated by:

$$i = \tan^{-1}\left|\tau / \sigma_n\right| - \varphi_b \tag{7.11}$$

7.4. Simulation of shear behaviour of rock joints under cyclic loading and CNS conditions using UDEC

Figure 7-2 shows the conceptual model incorporated in the UDEC analysis for simulating the shear behaviour of rock joints under cyclic loading and CNS conditions as tested in the laboratory. The block size was proportional to the actual model dimensions used in the laboratory. The boundary conditions assigned to the model ensured the following laboratory conditions:

- The bottom shear box moves only in the *X* direction (i.e. displacement in the *Y* direction is zero, whereas displacement in the *X* direction is free).
- The top shear box moves only in the *Y* direction (i.e. displacement in the *X* direction is zero, whereas displacement in the *Y* direction is free).
- The spring block moves only in the *Y* direction. All the movements of the block were restricted to the lower part of the spring, which was governed by the upward movement of the top specimen. The upper part of the spring block was fixed with the rigid load cell assembly, which in turn was attached to the body of the CNS equipment.
- A periodic horizontal velocity was applied to the bottom shear box to produce the required cyclic shear displacement with amplitude of 15 mm.

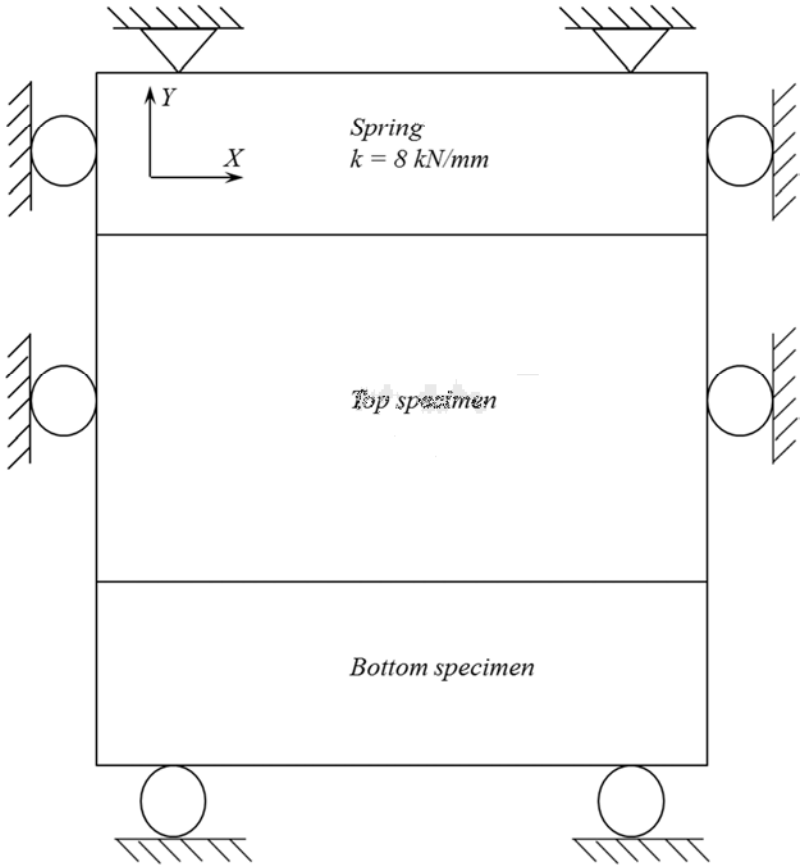

Figure 7-2 Conceptual CNS model for simulating shear behaviour of rock joints under cyclic loading

As with every other UDEC model, initially, the first block was created. It was then split into three blocks representing bottom specimen, top specimen and the spring. Once the blocks were created, they were discretised into appropriate sizes using FISH functions in UDEC. The material properties were then assigned to blocks via appropriate FISH functions. Finally, the boundary conditions and normal stress were applied. The following material properties were used in this model:

Spring block (material properties):

Bulk modulus: 21.3 MPa

Shear modulus: 31.95 MPa

Density: 2600 kg/m^3

Material properties:

Bulk modulus: 1.4 GPa

Shear modulus: 0.792 GPa

Density: 2600 kg/m^3

Joint material properties:

Joint normal stiffness: 14 GPa/m

Joint shear stiffness: 14 GPa/m

Joint frictional properties: Assigned according to the asperity type and constitutive model

The material properties of the spring block were prescribed in a way to precisely simulate the stiffness of the springs set (8 kN/mm). Figure 7-3 shows the output from UDEC for discretised joint block. Subsequently, the desired normal stress was applied to the joint and the model was allowed to reach equilibrium. A periodic horizontal velocity was applied to the bottom block to produce the required cyclic shear displacement. The average normal and shear stresses along the joint were calculated using a FISH function. The associated dilation and shear displacement were also determined via FISH functions. The Coulomb slip and continuously yielding models were applied separately to replicate the observed experimental behaviour using the simulated CNS direct shear test in UDEC. Appendix II shows the UDEC code used to model the shear behaviour of rock joints under cyclic loading and CNS conditions.

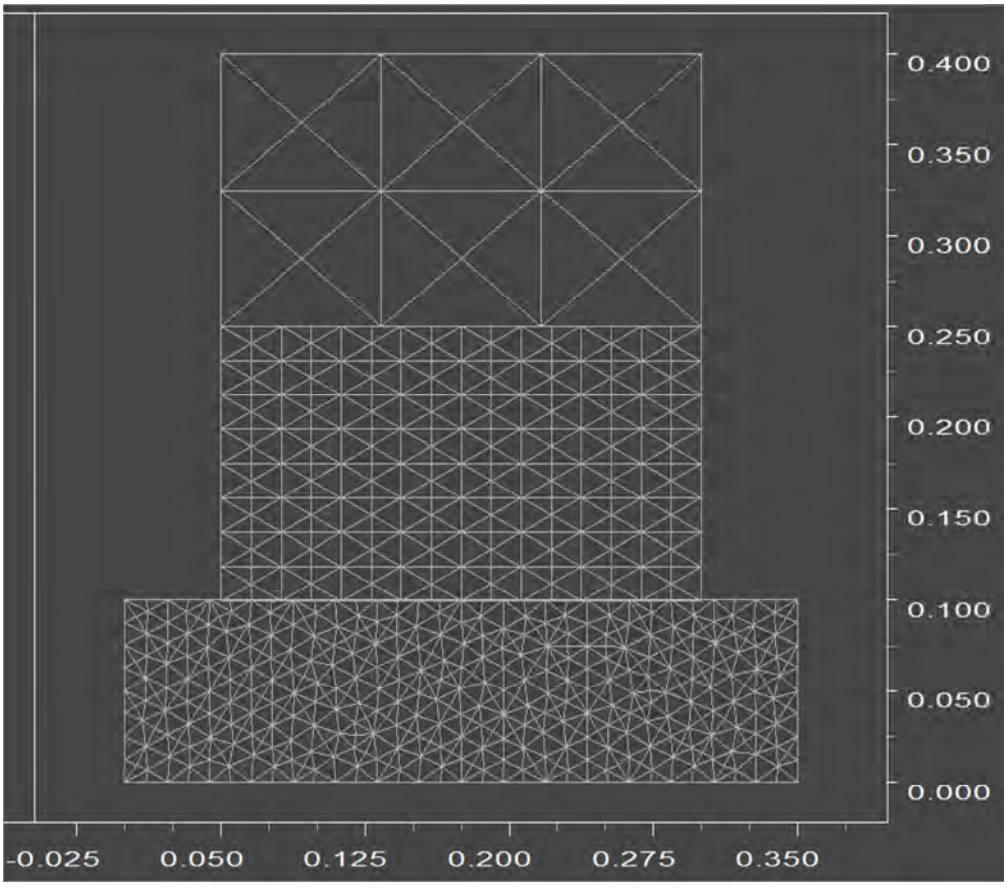

Figure 7-3 Simulated direct shear test under CNS conditions (dimensions in m)

Figures 7-4 to 7-5 show the simulated shear behaviour of rock joints under CNS conditions for Types I and III asperity types and selected initial normal stresses (σ_{n0} = 0.56 MPa and 2.4 MPa). The relevant model parameters used in the analysis for different conditions are listed in Table 7.1.

Table 7-1 Model parameters for Coulomb slip and continuously yielding models

Model	σ_{n0} = *0.56 MPa*	σ_{n0} = *2.4 MPa*
Coulomb slip	Ψ = 5.2°	Ψ = 4.1°
Continuously yielding	φ^i_m = 44.5° and R =0.012 (mm)	φ^i_m = 40.7° and R = 0.005 (mm)

It is observed that for σ_{n0} = 0.56 MPa and Type I asperity surface when asperity damage is not significant, the Coulomb slip model simulated different frictional resistance for the forward and backward shearing and recovery of dilation during load reversal (Figure 7-4/left). However, for the asperity breakage mechanism (σ_{n0} = 2.4 MPa) when asperities are highly degraded in the first forward shear cycle, the Coulomb slip model cannot represent approaching the residual shear strength (i.e. no contribution of roughness in shear strength) and the effect of asperity damage on dilation. In contrast to the Coulomb slip model, the continuously yielding model cannot replicate different shear behaviour in the forward and backward shearing for σ_{n0} = 0.56 MPa and Type I as shown in Figure 7.5 [left]. As can be seen from Figure 7-5 [right], for σ_{n0} = 2.4 MPa and Type III asperity surface, the appearance of residual shear strength was reasonably captured by the continuously yielding model.

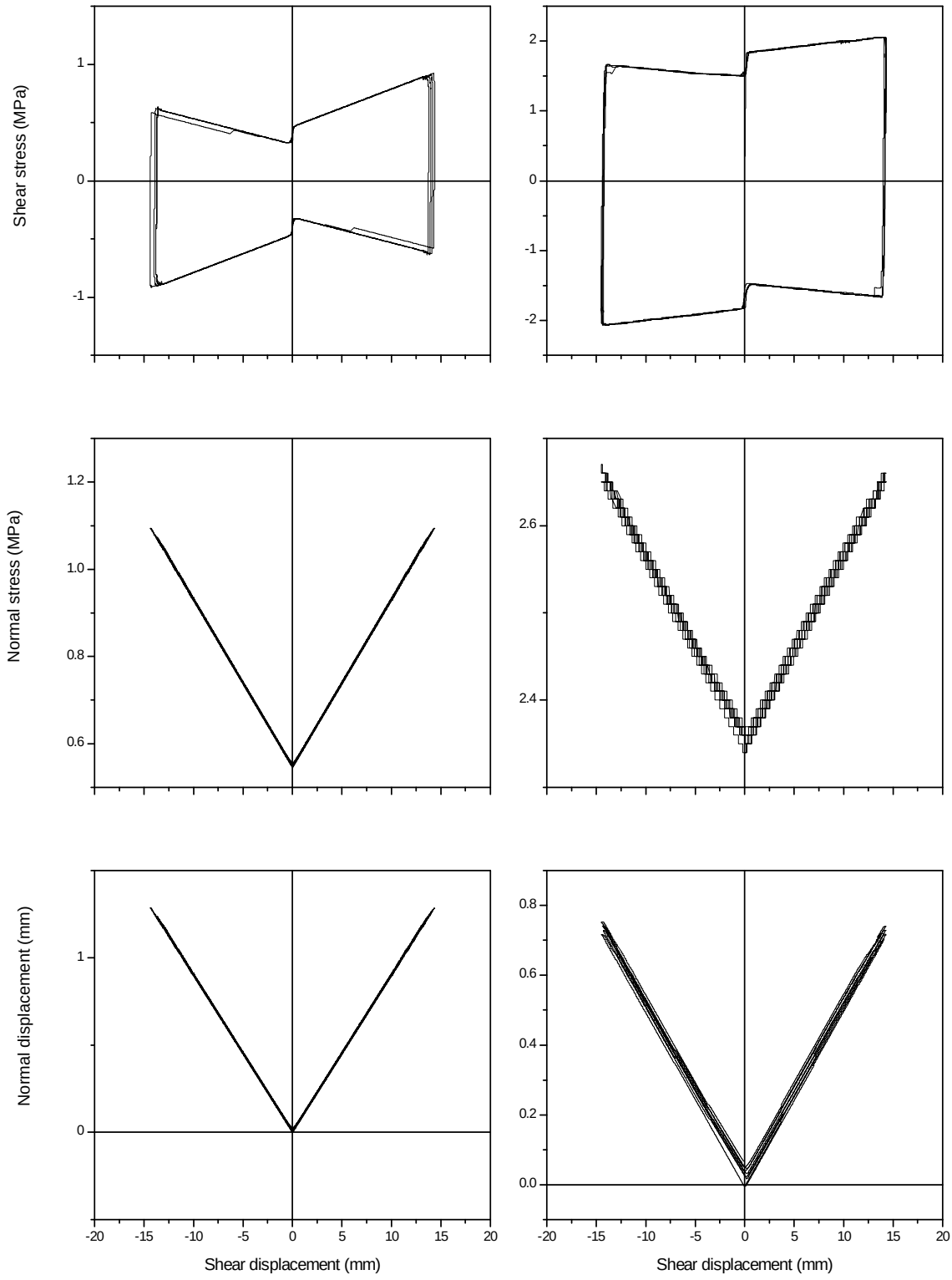

Figure 7-4 Coulomb slip model simulated results: [left] Type I asperity surface with 0.56 MPa of initial normal stress, [right] Type III asperity surface with 2.4 MPa of initial normal stress

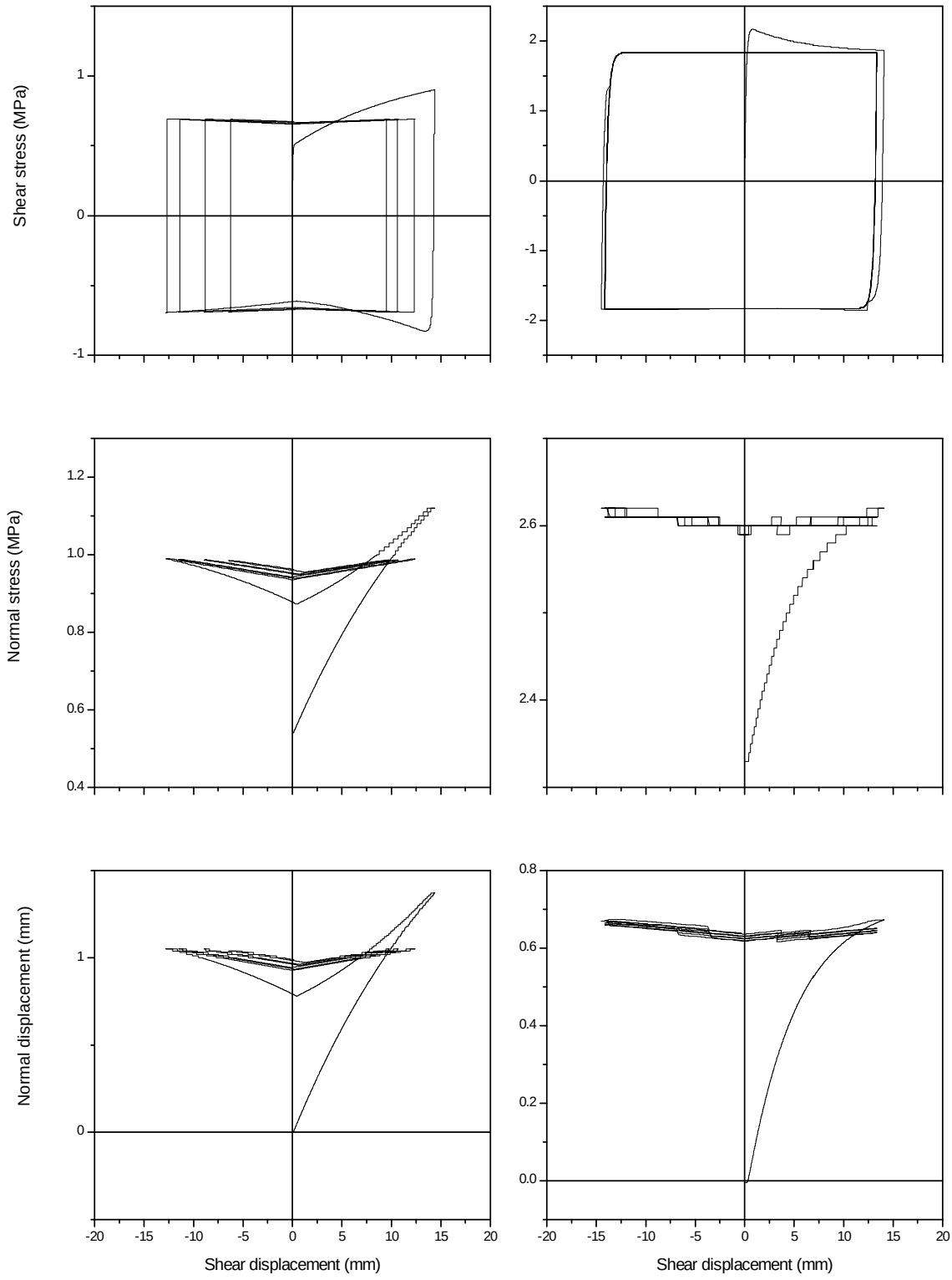

Figure 7-5 Continuously yielding model simulated results: [left] Type I asperity surface with 0.56 MPa of initial normal stress, [right] Type III asperity surface with 2.4 MPa of initial normal stress

Nevertheless, the predicted shear strength was underestimated in the first forward shear cycle by both models since the additional shear strength generated by the asperity damage is neglected.

7.5. Stability analysis of an underground structure subjected to seismic events

Stability analysis of an underground structure subjected to seismic events was carried out in UDEC by extending FISH subroutine program as given in Appendix III.

The modelled underground structure is a rectangular tunnel constructed 60 m below the surface with dimensions of 6×9 m. Two joint sets dipping at 60° and 120° with constant spacing of 4 and 3 m as well as a vertical joint, were created and extended only within a limited region around the tunnel. The model configuration is shown in Figure 7-6. The vertical and horizontal *in situ* stresses were assigned as 2.6 MPa and 0.7 MPa respectively. Initially, static analysis was performed and the model reached the equilibrium state. Then, sinusoidal shear waves with different amplitudes, frequencies, and durations representing seismic events were applied to the model base and allowed to propagate upward. Free field and viscous boundaries were used for the sides and base of the model to simulate the wave propagation through the modelled strata.

The Coulomb slip constitutive model due to its simplicity was prescribed to the joints. The relevant model parameters and loading characteristics are listed in Tables 7.2. The model parameters were evaluated based on Type I asperity surface. Joints that do not cross the tunnel were assigned a friction angle of 40.35° (based on laboratory data) with zero dilation angle. The rock mass was considered to behave elastically with bulk and shear modules of 1400 MPa and 792 MPa respectively. The vertical and horizontal

displacements and stresses at the tunnel roof (model location: 0.2m, 26m) and side (model location: -3.2m, 21m) were monitored during analysis.

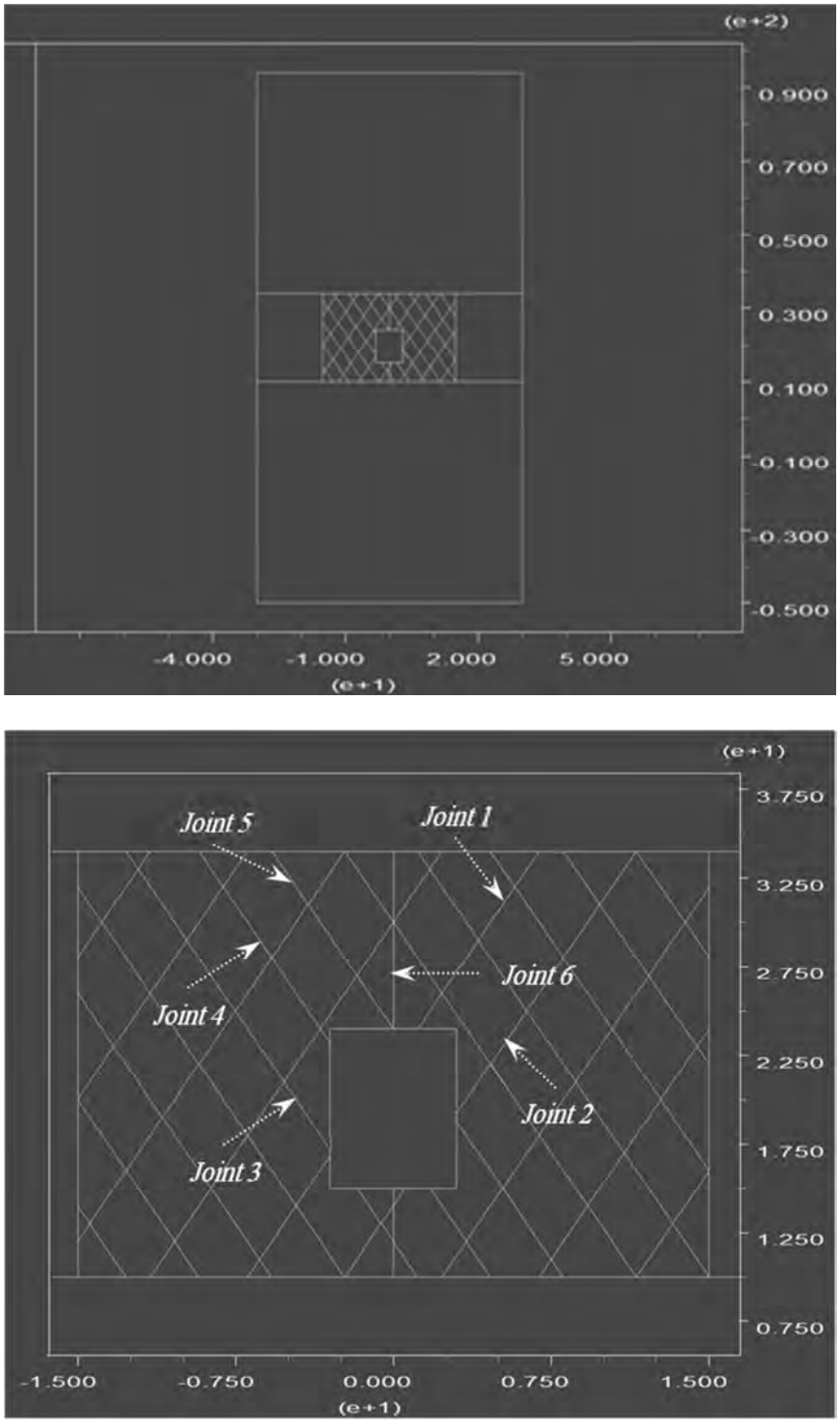

Figure 7-6 UDEC model configuration (dimensions in m): [up] Full UDEC model of rectangular tunnel region, [down] Close-up view of tunnel region

Table 7-2 Relevant model parameters and loading characteristics for analysis

Joint	*Ψ°*	*Seismic events*	*Amplitude (MPa)*	*Frequency (Hz)*	*Duration(s)*
Joint 1	4.54	1	2.4	11	2
Joint 2	4.53	2	0.8	8	4
Joint 3	4.61	3	0.45	10	6
Joint 4	4.89				
Joint 5	4.52				
Joint 6	5.18				

The roof and side displacements of the tunnel subjected to seismic loading are shown in Figure 7-7. The side closure has increased during the first five seconds of loading. Subsequently, it converged to 1.46 m. The magnitude of roof closure reached 157 mm after application of three seismic events. In Figure 7-8, vertical and horizontal stresses at roof and side of the tunnel against time of loading are plotted. It is noted that the vertical and horizontal stresses at the roof and side levels approached 1.03 MPa and 130 kPa at the end of the analysis. The simulated tunnel subjected to 12 seconds of seismic loading is shown in Figure 7-9. Two blocks from the roof and side of the tunnel have fallen down showing unstable behaviour.

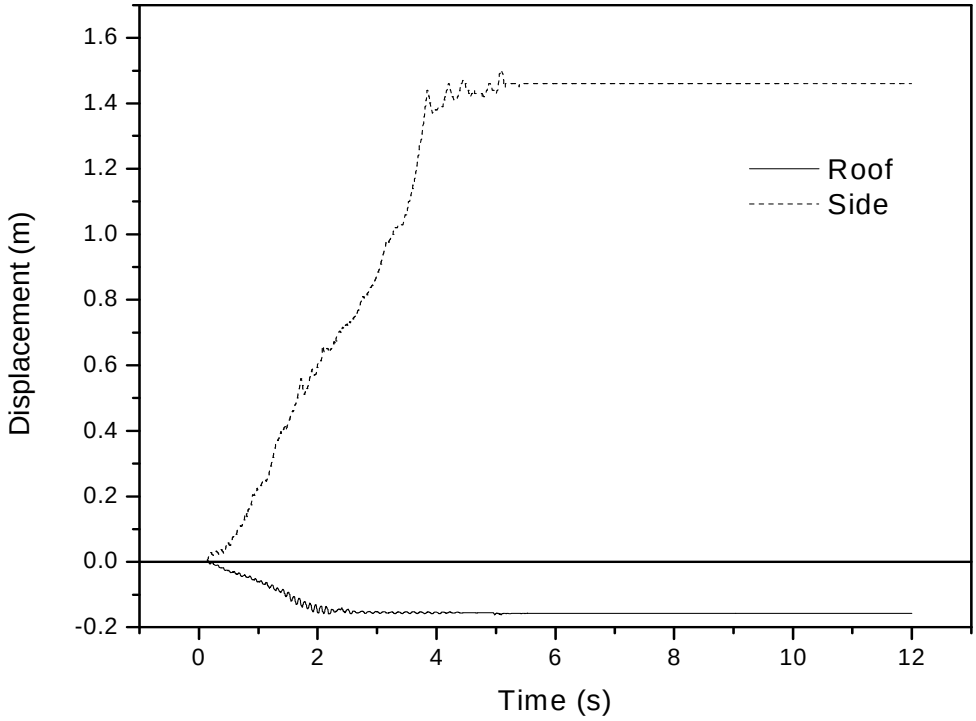

Figure 7-7 Closures around the rectangular tunnel against time of loading

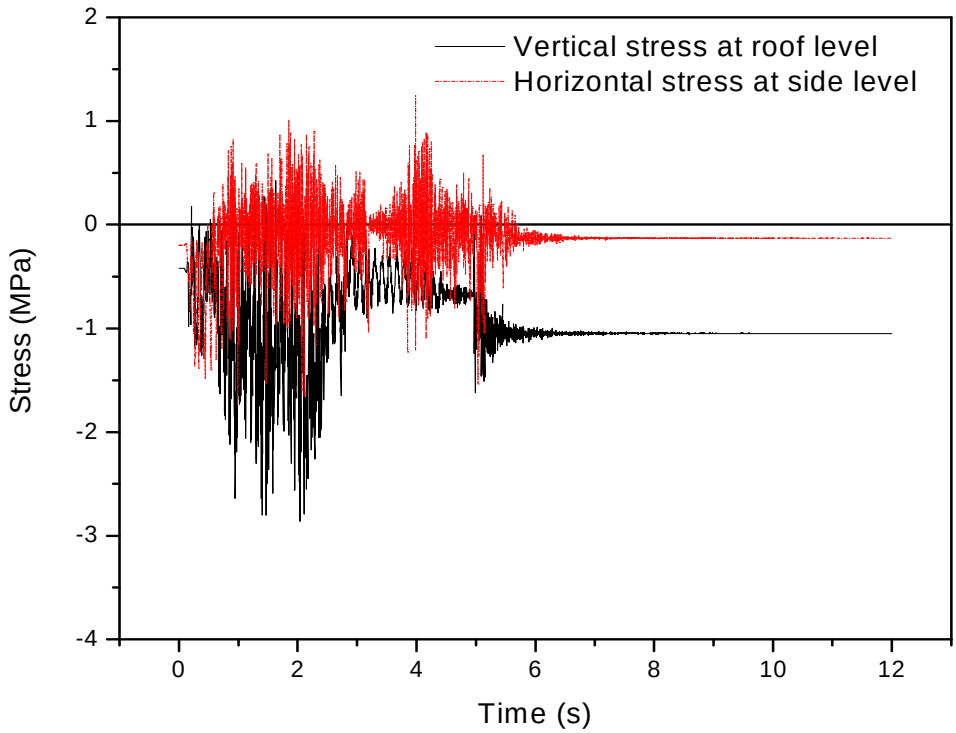

Figure 7-8 Vertical and horizontal stresses around the rectangular tunnel against time of loading

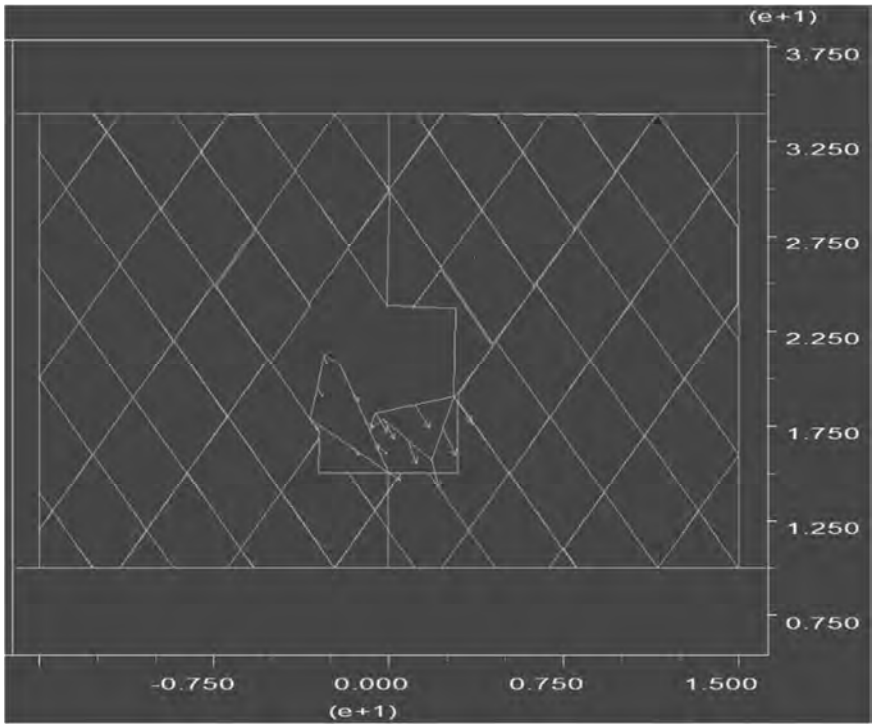

Figure 7-9 Simulated tunnel after 12 seconds of loading for clean joints (dimensions in m)

7.5.1. Stability analysis of an underground structure with infilled joints subjected to seismic events

To investigate the influence of infill material on the stability of an underground structure in seismic loading conditions, the rectangular tunnel described in the previous section was again analysed with the same loading characteristics and by considering infilled joints. Model parameters were estimated based on Type I asperity surface with 0.3 ratio of infill thickness to asperity height. Joints were prescribed the Coulomb slip constitutive mode with friction angle of 38.66° and cohesion of 0.29 MPa. Similar characteristics of rock as used in the clean joints analysis were applied to the rock mass. The magnitudes of closures at the roof level (model location: 0.2m, 26m) and the side level (model location: -3.2m, 21m) of the tunnel were recorded during analysis.

Figure 7-10 illustrates the comparison between tunnel closures with clean and infilled joints. The presence of infill within the joints with thickness to asperity height ratio of 0.3 has increased the roof displacement 3.85 times with respect to the tunnel with clean joints. This can be described by the reduction in the rock to rock contact and as a result the joint friction angle due to the infill material. The side closure of the tunnel with infilled joints (left side of the tunnel) shows similar unstable behaviour to the tunnel with clean joints.

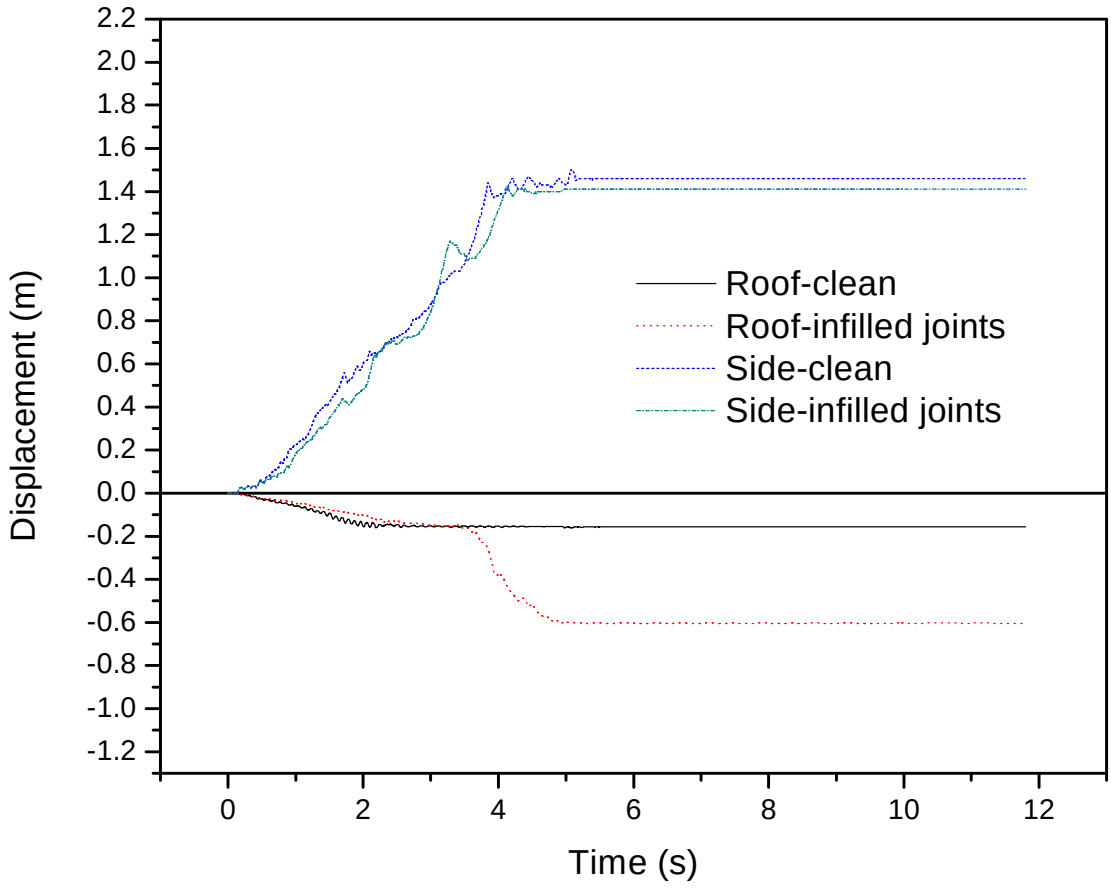

Figure 7-10 Closures around the rectangular tunnel with clean and infilled joints

The tunnel configuration after three seismic events with infilled joints is plotted in Figure 7-11. As expected, the tunnel stability has decreased due to the lower friction

angle of infilled joints when compared with the tunnel stability with the clean joints (see also Figure 7-9). Blocks from both sides of the tunnel as well as the roof have detached.

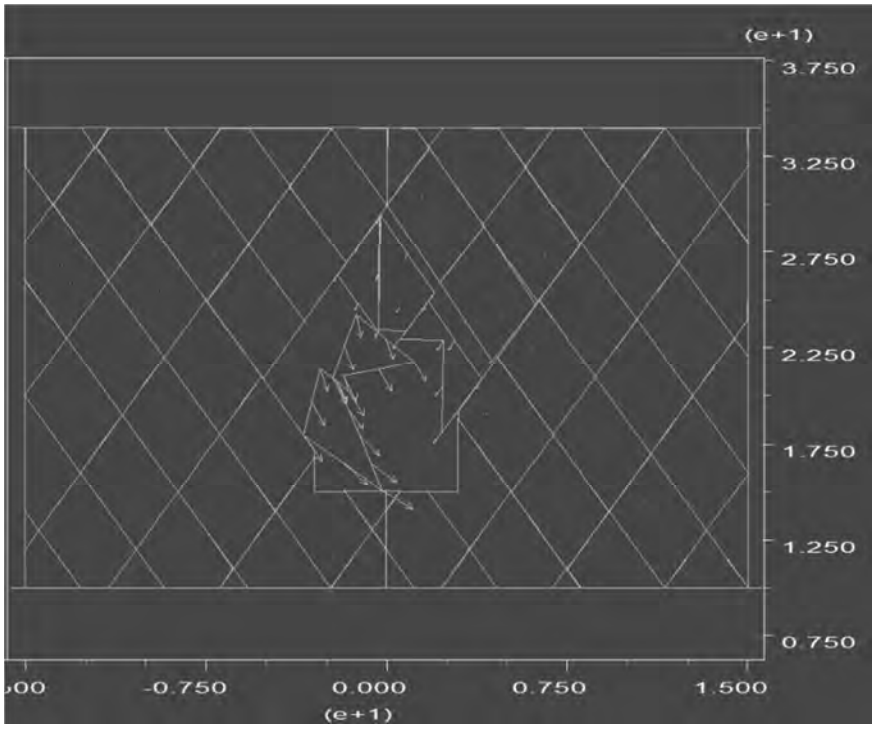

Figure 7-11 Simulated tunnel after 12 seconds of loading for infilled joints (dimensions in m)

7.5.2. Stability analysis of a deep underground structure subjected to seismic events

The previous model of rectangular tunnel (section 7.5) was further analysed with high magnitudes of vertical and horizontal stresses to investigate the stability of a deep underground structure subjected to seismic loading. The vertical and horizontal *in situ* stresses were considered as 13 MPa and 9.5 MPa representing a deep underground excavation. Loading and rock mass characteristics were assigned in the same manner as described in section 7.5. Joints crossing the tunnel were postulated to be extremely damaged under high values of normal stress, thus, the dilation angle was taken as zero. The tunnel displacements at the same locations as described in section 7.5 were investigated.

The comparison between the magnitudes of roof and side closures for shallow and deep underground tunnel subjected to seismic events is depicted in Figure 7-12.

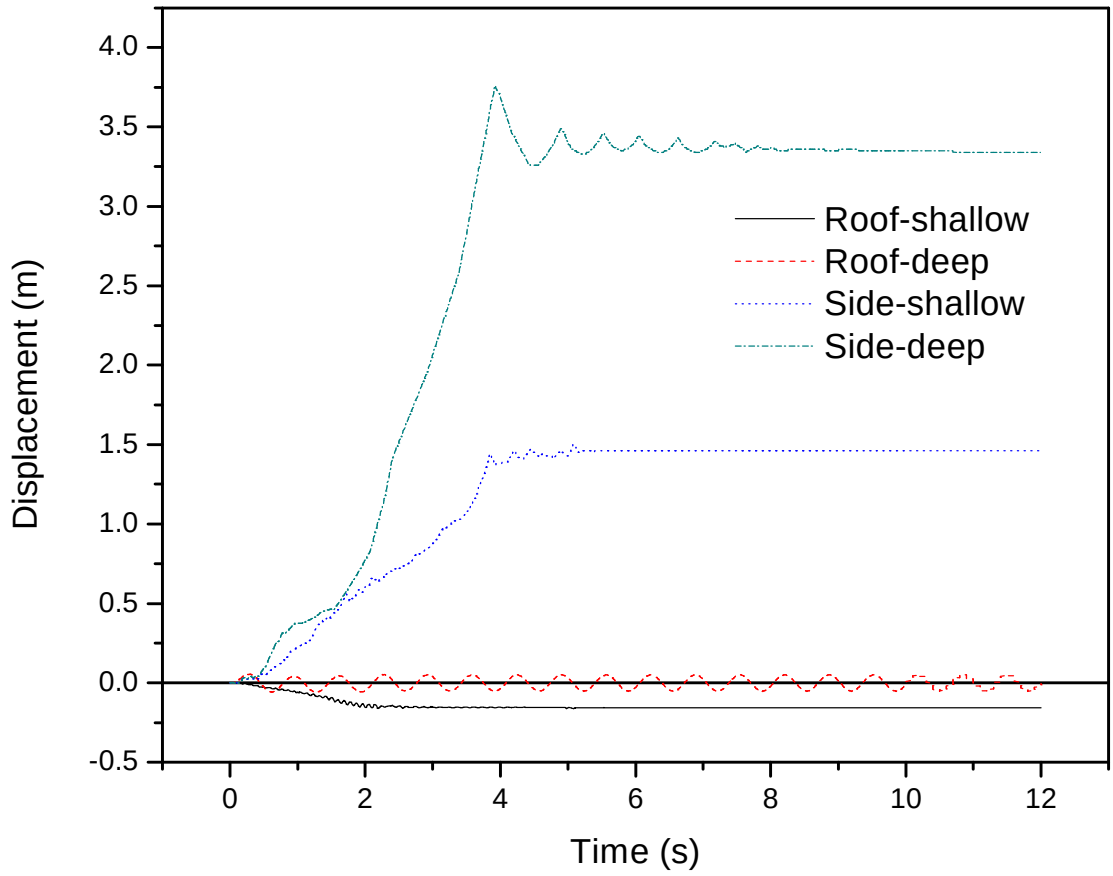

Figure 7-12 Closures around the rectangular tunnel at low and high depths

It is observed that when subjected to cyclic loading, the roof of deep rectangular tunnel shows stable behaviour in comparison to the shallow tunnel due to higher normal joint stress. Nevertheless, an increase of normal stress on the joint surface at the greater depth has not improved tunnel side stability. This may be described by lower friction angle caused by the breakage mechanism, deteriorating joint stability. The same conclusions can be drawn from Figure 7-13 that shows the state of deep rectangular tunnel after 12 seconds of cyclic loading.

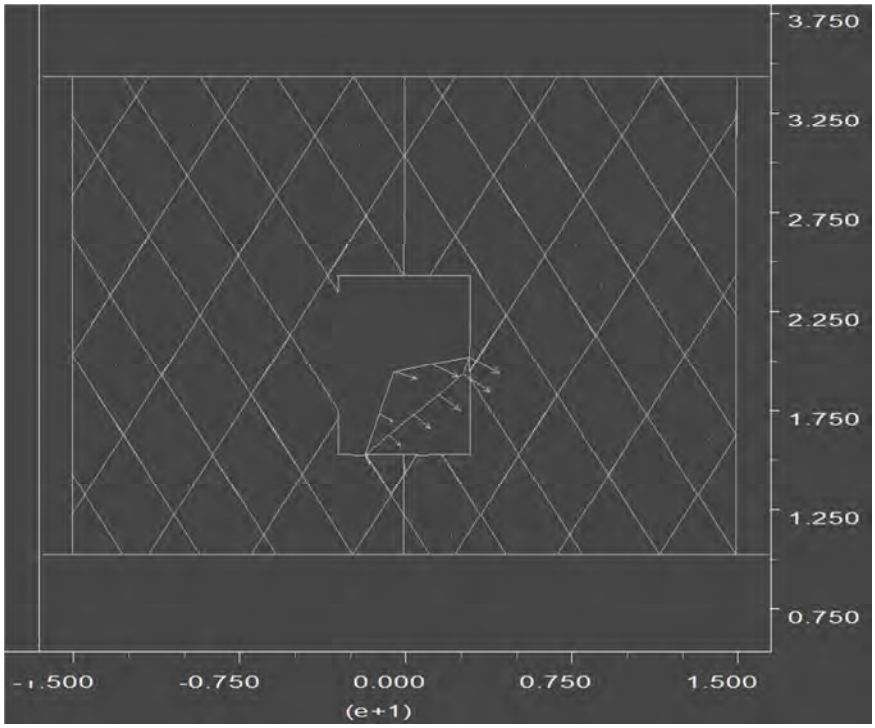

Figure 7-13 Simulation of deep tunnel after 12 seconds of loading (dimensions in m)

These analyses were extended to infilled joints with the same characteristics as those described in section 7.5.1. Figure 7-14 shows the comparison between the closures around rectangular tunnel with infilled joints for low and high depths.

It is inferred from Figure 7-14 that the tunnel in the roof level has been stabilised with increase in depth while the sides show unstable behaviour.

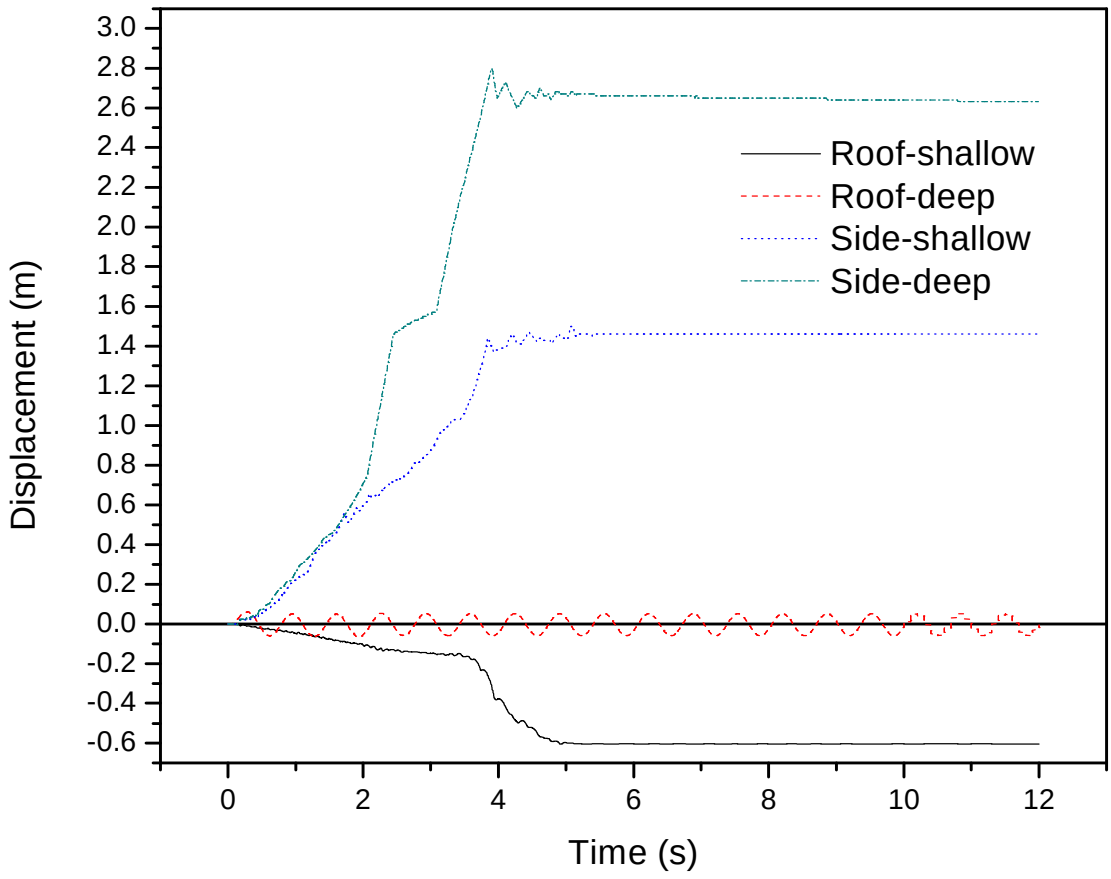

Figure 7-14 Closures around the rectangular tunnel with infilled joints for low and high depths of cover

7.6. Summary

The shear behaviour of rock joints was simulated in a simplified manner using two available constitutive models in UDEC under cyclic loading and CNS conditions. For a given set of data, the variations of cyclic average shear stress, average normal stress, and normal displacement with shear displacement were studied and simulated using Coulomb slip and continuously yielding models. The results indicate that the capabilities of Coulomb slip and continuously yielding models in simulating shear behaviour of rock joints under cyclic loading and CNS conditions depends on the governing shearing mechanism. For low levels of applied normal stress and asperity

angle when considerable asperity damage does not take place, the Coulomb slip model simulated different frictional behaviour in forward and backward shearing and recovery of dilation during load reversal. However, for the asperity breakage mechanism, this model excluded the effect of asperity damage on dilation behaviour. On the other hand, the continuously yielding model represented the progressive damage of asperities under cyclic loading conditions.

Stability analysis of an underground structure subjected to seismic events was carried out in UDEC for both clean and infilled joints. The rectangular tunnel stability decreased due to presence of infill material within the joints compared to the tunnel with clean joints. Furthermore, it was concluded that the excavation becomes more stabilised when subjected to cyclic loading with increase in the depth.

Chapter VIII

8. CONCLUSIONS AND RECOMMENDATIONS

Several aspects of the shear behaviour of rock joints under cyclic loading and CNS conditions were studied. The laboratory testing programme included:

- Assessing the shear behaviour of artificial tooth shaped asperities and replicas of real joints under cyclic loading and CNS conditions. The samples were cast using high strength Plaster of Paris. Experiments were conducted on clean joints with different initial asperity angles 9.5° (Type I), 18.5° (Type II) and 26.5° (Type III) under constant normal stiffness of 8 kN/mm. The initial applied normal stresses were in the range of 0.16 MPa to 2.5 MPa. Samples were sheared for four consecutive cycles with 0.5 mm/min of shear rate.
- Assessing the shear rate effects on shear behaviour of rock joints under cyclic loading and CNS conditions. Triangular asperities (Type I) were sheared cyclically with shear rates of 5 mm/s and 20 mm/s for 100 loading cycles.
- Assessing the shear behaviour of infilled rock joints under cyclic loading and CNS conditions. Triangular joints (Types I and II) were infilled with mixture of clay and sand at initial moisture content of 12.5% and sheared for four consecutive cycles.

An incremental elasto plastic constitutive model was proposed to predict the shear behaviour of clean rock joints under cyclic loading and CNS conditions. This model was accompanied by an empirical relationship to consider the effect of shear rate on cyclic loading shear strength. Furthermore, a mathematical model was proposed and

calibrated to simulate the reduction in the shear strength of infilled joints under cyclic loading. The following paragraphs describe the main conclusions extracted from this study.

Joint Research

To date, most of the research is concerned with the estimation of shear strength under monotonic loading and CNL or CNS conditions. While some of the published research is intended to study the shear behaviour of rock joints under cyclic loading and CNL conditions, only a limited research work is reported on the influence of normal stiffness on the shear behaviour of rock joints under cyclic loading. The past research work on the effects of shear rate on shear strength of rock joints was only conducted under the monotonic loading. No study has been published to investigate the effects of cyclic loading on the shear behaviour of infilled rock joints.

Shear Behaviour of Clean Rock Joints under Cyclic loading

- As the number of loading cycles increased, the shear strength of rock joints decreased.
- Reduction in shear strength with increase in the loading cycles was higher for joints with greater values of initial normal stress and asperity angle.
- Due to asperity damage, the dilation component was decreased with increase in the number of shear cycles.
- The asperity damage is in direct relationship with the initial normal stress, initial asperity angle and number of loading cycles for a particular normal stiffness.

- The cyclic loading shear strength decreased with increase in the shear rate. As the number of loading cycles increased, the effects of shear rate became less significant.

Shear Behaviour of Infilled Rock Joints under Cyclic loading

- The cyclic loading shear strength of infilled rock joints decreased with increase in the loading cycles.
- The reduction in the cyclic loading shear strength was higher for greater values of infill thickness to asperity height ratio and initial normal stress.
- The increase in the number of loading cycles was associated with a lower reduction trend in shear strength.
- Dilation and contraction were the two mechanisms involved in the variation of normal displacement with shear displacement of infilled rock joints subjected to cyclic loading.
- At t/a = 0.3, dilation is the governing mechanism in the variation of normal displacement with shear displacement. As t/a approaching unity, the normal displacement shows compaction due to deformation of infill material.

Modelling of the Shear Behaviour of Rock Joints under Cyclic Loading

- The values of shear stress, normal stress and normal displacement versus shear displacement of clean rock joints predicted by the constitutive model, were in good agreement with the laboratory results for the initial normal stress range of 0.16 MPa to 0.56 MPa.

- The additional shear resistance generated by the asperity damage in the first forward shear cycle was captured by the model for clean rock joints particularly for σ_{n0}=1.64 MPa and 2.4 MPa.
- Reduction in the shear strength of infilled rock joints with increase in the number of loading cycles, as predicted by the hyperbolic equation, was in a good agreement with the laboratory results from several tests (regression coefficients greater than 0.96).
- The Coulomb slip model available in UDEC simulated different frictional resistance in forward and backward shearing of rock joints subjected to cyclic loading. The continuously yielding model replicated the asperity damage in cyclic loading conditions.
- The UDEC models underestimated the shear strength of rock joints in the first loading cycle when compared with the laboratory test results

8.1. Recommendations for future research

The study of the shear behaviour of rock joints under cyclic loading and CNS conditions can be extended to address the following recommendations, which have not been fully investigated within the scope of this research.

- Scale effects

The variations of properties with the size of the specimens are defined as the scale effects. As discussed in Chapter II, the increase in the specimen size decreases the strength of the joint. The effects of scale factor were not studied as all the prepared samples had the same joint area and asperity frequency. It is suggested that the scale effects on shear behaviour of clean rock joints under cyclic loading and CNS conditions

be studied in future research. As the model used in this research for the clean joints does not include the effects of specimen size, it can be revised based on the observed governing mechanisms. However, according to Infanti and Kanji (1978), the shear behaviour of infilled joints is not influenced significantly by the change in the specimen size.

- Normal stiffness

Cyclic loading shear tests were conducted under a constant normal stiffness of 0.43 MPa/mm provided by the 8 kN/mm springs set. Although this amount is reasonable for sedimentary rock joints, different stiffness values may be required for softer or stiffer joints, therefore, cyclic loading shear tests on clean and infilled rock joints should be carried out for different values of normal stiffness. The models proposed in this study, can still be used in future studies to predict the shear strength of clean and infilled joints under cyclic loading and different conditions of normal stiffness. However, the models coefficients need to be calibrated.

- Pore water pressure

Joints obey the effective stress principle as discussed in Chapter II. Thus, the strengthening effect of normal stress acting on the joint plane may either decrease or increase depending on the development of positive or negative pore water pressure. This might influence the shear behaviour of rock joints under cyclic loading and eventually the stability of underground structures constructed in proximity of active seismic zones. In order to investigate the effects of pore water pressure development on shear behaviour of rock joints during cyclic shearing, the CNS apparatus used in this study requires further modifications.

- Extension in numerical modelling

An example of stability analysis of a rectangular tunnel subjected to seismic events was given in Chapter VII. The analysis was carried out in UDEC using Coulomb slip constitutive model for joints. The built in constitutive models in UDEC cannot represent the actual shear behaviour of rock joints under cyclic loading (see Chapters IV and VII). The authors' recommendation is to extend a series of computer FISH subroutines to replicate the true shear behaviour of rock joints under cyclic loading. The models proposed in this study for simulation of shear behaviour of rock joints under cyclic loading can be considered for subroutines developments.

- Infill material

Mixture of clay and sand (75% fine sand and 25% Kaolinite) at initial moisture content of 12.5% was selected as infill material. In the field, joints are often infilled with sand, clay and/or silt, therefore, different types of infill material collected from the field should be tested at varying thicknesses under cyclic loading and CNS conditions. The applicability of the proposed model should be reassessed and model coefficients need to be evaluated based on the experimental results.

- Real rock joints

The experimental study for infilled joints was only conducted on artificial triangular asperities cast using high strength Plaster of Paris (σ_c = 60 MPa). Real rock joints have spatial and arbitrarily distributed roughness with various values of uniaxial compressive strength. The shear strength model used for this thesis can be extended to predict the field shear strength of infilled joints subjected to cyclic loading once the surface geometry is mapped and model coefficients are determined. Surface geometry can be

mapped using either the Fractal method or Fourier transform. Alternatively, the concept of *JRC* can be incorporated to describe the roughness of field joints.

REFERENCES

ARCHAMBAULT, G., POIRIER, S., ROULEAU, A., GENTIER, S. and RISS, J. (1998). The behaviour of induced pore fluid pressure in undrained triaxial shear test on fracture porous analog rock material specimens. *In: Mechanics of Jointed and Faulted Rock.*, H. R. ROSSMANITH (ed), Balkema, Rotterdam.

ARCHAMBAULT, G., POIRIER, S., ROULEAU, A., GENTIER, S. and RISS, J. (1999). Pore pressure behaviour in undrained triaxial shear tests on joints. *In: 9th ISRM International Congress on Rock Mechanics.*, Paris, France, Balkema, pp. 741-746.

ASADOLLAHI, P. and TONON, F. (2010). Constitutive model for rock fractures: Revisiting Barton's empirical model. *Engineering Geology.*, Vol. 113**,** pp. 11-32.

AUBRY, D., MODARESSI, A. and MODARESSI, H. (1990). A constitutive model for cyclic behaviour of interfaces with variable dilatancy. *Computers and Geotechnics.,* Vol. 9**,** pp. 47-58.

BABANOURI, N., KARIMI NASAB, S., BAGHBANAN, A. and MOHAMADI, H. R. (2011). Over-consolidation effect on shear behavior of rock joints. *International Journal of Rock Mechanics and Mining Sciences.*, Vol. 48**,** pp. 1283-1291.

BANDIS, S., LUMSDEN, A. C. and BARTON, N. R. (1981). Experimental studies of scale effects on the shear behaviour of rock joints. *International Journal of Rock Mechanics and Mining Sciences & Geomechanics Abstracts.,* Vol. 18**,** pp. 1-21.

BARLA, G., FORLATI, F. and ZANIENETTI, A. (1985). Shear behaviour of filled discontinuities. *In: Int. Symp. on Fundamentals of Rock Joints.*, Bjorkliden, pp. 163-172.

BARTON, N. (1973). Review of a new shear-strength criterion for rock joints. *Engineering Geology.*, Vol. 7**,** pp. 287-332.

BARTON, N. (1974). Review of shear strength of filled discontinuities in rock. *No. 105. Oslo: Norwegian Geotechnical Institute.***,** pp. 38.

BARTON, N. (1976). The shear strength of rock and rock joints. *International Journal of Rock Mechanics and Mining Sciences.,* Vol. 13**,** pp. 255-279.

BARTON, N., BANDIS, S. and BAKHTAR, K. (1985). Strength, deformation and conductivity coupling of rock joints. *International Journal of Rock Mechanics and Mining Sciences & Geomechanics Abstracts.,* Vol. 22**,** pp. 121-140.

BARTON, N. and CHOUBEY, V. (1977). The shear strength of rock joints in theory and practice. *Rock Mechanics Felsmechanik Mécanique des Roches.,* Vol. 10**,** pp. 1-54.

BARTON, N. R. and BANDIS, S. C. (1982). Effects of block size on the the shear behaviour of jointed rock. *In: 23rd U.S. Symp. on Rock Mechanics.,* Berkeley.

BELEM, T., HOMAND-ETIENNE, F. and SOULEY, M. (1997). Fractal analysis of shear joint roughness. *International Journal of Rock Mechanics and Mining Sciences & Geomechanics Abstracts.,* Vol. 34**,** pp. 395.

BELEM, T., SOULEY, M. and HOMAND, F. (2007). Modeling surface roughness degradation of rock joint wall during monotonic and cyclic shearing. *Acta Geotechnica.,* Vol. 2**,** pp. 227-248.

BELEM, T., SOULEY, M. and HOMAND, F. (2009). Method for quantification of wear of sheared joint walls based on surface morphology. *Rock Mechanics and Rock Engineering.,* Vol. 42**,** pp. 883-910.

BENJELLOUN, Z. H., BOULON, M. and BILAUX, D. (1990). Experimental and numerical investigation on rock joints. *In: International Symposium on Rock Joints*., N. BARTON (ed), Loen, Norway. Balkema, Rotterdam, pp. 171-178.

BENMOKRANE, B. and BALLIVY, G. (1989). Laboratory study of shear behavior of rock joints under constant normal stiffness conditions. *In: Rock Mechanics as a Guide for Effieient Utilization of Natural Resources*., West Virginia University, Balkema, Rotterdam, pp. 899-906.

BERTACCHI, P., ZANIENETTI, A., BARLA, G. and FORLATI, F. (1986). Laboratory tests on the shear behaviour of filled discontinuities. *In: Int. Symp. on Engineering in Complex Rock Formation*., Beijing, China, pp. 262-270.

BREKKE, T. L. and HOWARD, T. R. (1972). Stability problem caused by seems and faults. *Rapid Tunnenilg and Excavation Conference.,* pp. 25-41.

CHENG, F., HABERFIELD, C. M. and SEIDEL, J. P. (1996). Laboratory study of bonding and wall smear in rock soketed piles. *In: 7th ANZ Conf. on Geomechanics*., Adelaide, Australia, pp. 69-74.

CRAWFORD, A. M. and CURRAN, J. H. (1981). The influence of shear velocity on the frictional resistance of rock discontinuities. *International Journal of Rock Mechanics and Mining Sciences & Geomechanics Abstracts.,* Vol. 18**,** pp. 505-515.

DE TOLEDO, P. E. C. and DE FREITAS, M. H. (1993). Laboratory testing and parameters controlling the shear strength of filled rock joints. *Geotechnique.,* Vol. 43**,** pp. 1-19.

DONG, J. J. and PAN, Y. W. (1996). A hierarchical model of rough rock joints based on micromechanics. *International Journal of Rock Mechanics and Mining Sciences & Geomechanics Abstract.,* Vol. 33**,** pp. 111-123.

DURHAM, W. B. and BONNER, B. P. (1995). Closure and fluid flow in discrete fractures. *In: Fractured Andjointed Rock Masses.,* L. R. MYER, N. G.W. COOK, R. E. GOODMAN and C. F. TSANG (eds), Lake Tahoe, Califomia, Balkema, Rotterdam, pp. 441-446.

FOX, D. J., KAÑA, D. D. and HSIUNG, S. M. (1998). Influence of interface roughness on dynamic shear behavior in jointed rock. *International Journal of Rock Mechanics and Mining Sciences.,* Vol. 35**,** pp. 923-940.

GENS, A., CAROL, I. and ALONSO, E. E. (1990). A constitutive model for rock joints formulation and numerical implementation. *Computers and Geotechnics.,* Vol. 9**,** pp. 3-20.

GOODMAN, R. (1970). The deformability of joints. Determination of the insitu modulus of deformation of rocks. *Special Technical Publication (ASTM), No. 477, Philadelphia: Americal Society for Testing and Materials.***,** pp. 174-196.

GOODMAN, R. (1976). *Methods of geological engineering*, West Publishing Company, St. Paul.

GOODMAN, R. and OHNISHI, Y. (1973). Undrained shear testing of jointed rock. *Rock Mechanics.,* Vol. 5**,** pp. 129-149.

GRASSELLI, G. and EGGER, P. (2003). Constitutive law for the shear strength of rock joints based on three-dimensional surface parameters. *International Journal of Rock Mechanics and Mining Sciences.,* Vol. 40**,** pp. 25-40.

HABERFIELD, C. M. and JOHNSTON, I. W. 1994. A mechanistically-based model for rough rock joints. *International Journal of Rock Mechanics and Mining Sciences.,* Vol. 31**,** pp. 279-292.

HEUZE, F. E. and BARBOUR, T. G. 1982. New models for rock joints and interfaces. *Journal of the Geotechnical Engineering Division (ASCE).,* Vol. 108**,** pp. 757-776.

HOMAND-ETIENNE, F., LEFEVRE, F., BELEM, T. and SOULEY, M. (1999). *In: Rock Joints Behavior under Cyclic Direct Shear Tests.,* Leiden, Balkema Publishers.

HOMAND, F., BELEM, T. and SOULEY, M. (2001). Friction and degradation of rock joint surfaces under shear loads. *International Journal for Numerical and Analytical Methods in Geomechanics.,* Vol. 25**,** pp. 973-999.

HUANG, X., HAIMSON, B. C., PLESHA, M. E. and QIU, X. (1993). An investigation of the mechanics of rock joints-Part I. Laboratory investigation. *International Journal of Rock Mechanics and Mining Sciences.,* Vol. 30**,** pp. 257-269.

HUTSON, R. W. and DOWDING, C. H. (1990). Joint asperity degradation during cyclic shear. *International Journal of Rock Mechanics and Mining Sciences.,* Vol. 27**,** pp. 109-119.

INDRARATNA, B. and HAQUE, A. (2000). *Shear behaviour of rock joints*, Balkema, Rotterdam, Netherlands.

INDRARATNA, B., HAQUE, A. and AZIZ, N. (1998). Laboratory modelling of shear behaviour of soft joints under constant normal stiffness conditions. *Geotechnical and Geological Engineering.,* Vol. 16**,** pp. 17-44.

INDRARATNA, B., HAQUE, A. and AZIZ, N. (1999). Shear behaviour of idealized infilled joints under constant normal stiffness. *Geotechnique.,* Vol. 49**,** pp. 331-355.

INDRARATNA, B., JAYANATHAN, M. and BROWN, E. T. (2008). Shear strength model for overconsolidated clay-infilled idealised rock joints. *Geotechnique.,* Vol. 58**,** pp. 55-65.

INDRARATNA, B., OLIVEIRA, D. A. F. and BROWN, E. T. (2010). A shear-displacement criterion for soil-infilled rock discontinuities. *Geotechnique.,* Vol. 60**,** pp. 623-633.

INDRARATNA, B., WELIDENIYA, H. S. and BROWN, E. T. (2005). A shear strength model for idealised infilled joints under constant normal stiffness. *Geotechnique.,* Vol. 55**,** pp. 215-226.

INFANTI, N. and KANJI, M. A. (1978). In-situ shear strength, normal and shear stiffness determinations at Agua Vermelha Project. *In: Int. Congress of IAEG.*, Buenos Aires, pp. 371-373.

ISLAM, M. N. (1990). An analysis of maching accuracies in CNC maching operation. M.E (Hons) thesis, University of Wollongong.

JAEGER, J. C. (1971). Friction of rocks and stability of rock slopes. *Geotechnique.*, Vol. 21**,** pp. 97-134.

JAFARI, M. K., AMINI HOSSEINI, K., PELLET, F., BOULON, M. and BUZZI, O. (2003). Evaluation of shear strength of rock joints subjected to cyclic loading. *Soil Dynamics and Earthquake Engineering.,* Vol. 23**,** pp. 619-630.

JAFARI, M. K., PELLET, F., BOULON, M. and HOSSEINI, K. A. (2004). Experimental Study of Mechanical Behaviour of Rock Joints Under Cyclic Loading. *Rock Mechanics and Rock Engineering.,* Vol. 37**,** pp. 3-23.

JAYANATHAN, M. (2007). Shear behaviour of normally consolidated and overconsolidated infilled rock joints under undrained triaxial conditions. PhD thesis, University of Wollongong.

JING, L., NORDLUND, E. and STEPHANSSON, O. (1994). A 3-D constitutive model for rock joints with anisotropic friction and stress dependency in shear stiffness. *International Journal of Rock Mechanics and Mining Sciences.,* Vol. 31**,** pp. 173-178.

JING, L., STEPHANSSON, O. and NORDLUND, E. (1993). Study of rock joints under cyclic loading conditions. *Rock Mechanics and Rock Engineering.,* Vol. 26**,** pp. 215-232.

JOHNSTON, I. W. and LAM, T. S. K. (1989). Shear behavior of regular triangular concrete/rock joints. Analysis. *Journal of Geotechnical Engineering.,* Vol. 115**,** pp. 711-727.

KANJI, M. A. (1974). Unconventional laboratory for the determination of the shear strength of soil-rock contacts. *In: 3rd Congr. Int. Soc. Rock Mech.,* Denver, USA, pp. 241-247.

KUTTER, H. K. and RAUTENBERG, A. (1979). The residual shear strength of filled joints in rock. *In: 4th Int. Congr. Rock Mech.,* Montreux, pp. 221-227.

LADANYI, B. and ARCHAMBAULT, G. (1969). Simulation of shear behavior of a jointed rock mass. *In: Eleventh Symposium on Rock Mechanics.,* University of California, Berkeley, California, pp. 105-125.

LADANYI, B. and ARCHAMBAULT, G. (1977). Shear strength and deformability of filled indented joints. *In: 1st International Symposium on Geotechnics of Structurally Complex Formations.*, Capri, pp. 317-326.

LADD, C. C. and FOOTT, R. (1974). New design procedure for stability of soft clays. *International Journal of Rock Mechanics and Mining Sciences & Geomechanics Abstracts.,* Vol. 11**,** A220.

LAMA, R. D. (1978). Influence of clay fillings on shear behaviour of joints. *In: 3rd Congr. Int. Assoc. Eng. Geol.,* Madrid, Spain, pp. 27-34.

LEE, H. S., PARK, Y. J., CHO, T. F. and YOU, K. H. (2001). Influence of asperity degradation on the mechanical behavior of rough rock joints under cyclic shear loading. *International Journal of Rock Mechanics and Mining Sciences.,* Vol. 38**,** pp. 967-980.

LEICHNITZ, W. (1985). Mechanical properties of rock joints. *International Journal of Rock Mechanics and Mining Sciences & Geomechanics Abstracts.,* Vol. 22**,** pp. 313-321.

LOTFI, H. R. and SHING, P. B. (1994). Interface model applied to fracture of masonry structures. *Journal of Structural Engineering.,* Vol. 120**,** pp. 63-80.

MA, M. and BRADY, B. H. (1999). Analysis of the dynamic performance of an underground excavation in jointed rock under repeated seismic loading. *Geotechnical and Geological Engineering.,* Vol. 17**,** pp. 1-20.

MAKSIMOVIC, M. (1996). The shear strength components of a rough rock joint. *International Journal of Rock Mechanics and Mining Sciences.,* Vol. 33**,** pp. 769-783.

MILOVIC, D. M., TRIZOT, G. and TRURNIER, J. P. (1970). Stresses and displacements in an elastic layer due to inclined and ecentric load over a rigid strip. *Geotechnique.,* Vol. 20**,** pp. 231-252.

NEWLAND, P. L. and ALLEY, B. H. (1957). Volume changes in drained triaxial tests on granular materials. *Geotechnique.,* Vol. 7**,** pp. 17–34.

OBERT, L., BRADY, B. T. and SCHMECHEL, F. W. (1977). The effect of normal stiffness on the shear resistance of rocks. *Rock Mechanics and Rock Engineering.*, Vol. 8**,** pp. 57-52.

OHNISHI, Y. and DHARMARATNE, P. G. R. (1990). Shear behavior of physical models of rock joints under constant normal stiffness conditions. *In: International Symposium on Rock Joints*., N. BARTON (ed), Loen, Norway, Balkema, Rotterdam, pp. 267-274.

OHNISHI, Y. and YOSHINAKA, R. (1992). Laboratory investigation of scale effect in mechanical behavior fo rock joint. *In: Second International Conference on Mechanics of Jointed and Faulted Rock*., H. P. ROSSMANITH (ed),Vienna, Austria, Balkema, Rotterdam, pp. 465-470.

OLIVEIRA, D. (2009). An advancement in analytical modelling of soil-infilled rock joints and their practical applications. PhD thesis, University of Wollongong.

OLIVEIRA, D. A. F., INDARARATNA, B. and NEMCIK, J. (2009). Critical review on shear strength models for soil-infilled joints. *Geomechanics and Geoengineering: an International Journal.*, Vol. 4**,** pp. 237-244.

OLIVEIRA, D. A. F. and INDRARATNA, B. (2010). Comparison between models of rock discontinuity strength and deformation. *Journal of Geotechnical and Geoenvironmental Engineering.*, Vol. 136**,** pp. 864-874.

PAPALIANGAS, T., HENCHER, S. R., LUMSDEN, A. C. and MANOLOPOULOU, S. (1993). The effect of frictional fill thickness on the shear strength of rock discontinuities. *International Journal of Rock Mechanics and Mining Sciences.*, Vol. 30**,** pp. 81-91.

PAPALIANGAS, T., LUMSDEN, A. C., HENCHER, S. R. and MANOLOPOULOU, S. (1990). Shear strength of modelled filled rock joints. *In: Int. Conf. on Rock Joints.*, N. BARTON and O. STEPHANSSON (eds), Balkema, Rotterdam, pp. 275–282.

PATTON, F. D. (1966). Multiple modes of shear failure in rocks. *In: 1st Cong. ISRM.*, Lisbon, pp. 509-513.

PEREIRA, J. P. (1990). Shear strength of filled discontinuities. *In: International Conference on Rock Joints.*, O. STEPHANSSON (ed), Balkema, Rotterdam, pp. 283-287.

PHIEN-WEJ, N., SHRESTHA, U. B. and RANTUCCI, G. (1991). Effect of infill thickness on shear behaviour of rock joints. *International Journal of Rock Mechanics and Mining Sciences & Geomechanics Abstracts.,* Vol. 28**,** A70.

PLESHA, M. E. (1987). Constitutive models for rock discontinuities with dilatancy and surface degradation. *International Journal for Numerical and Analytical Methods in Geomechanics.,* Vol. 11**,** pp. 345-362.

PUNTEL, E., BOLZON, G. and SAOUMA, V. E. (2006). Fracture mechanics based model for joints under cyclic loading. *Journal of Engineering Mechanics.,* Vol. 132**,** pp. 1151-1159.

QIU, X. and PLESHA, M. E. (1991). Theory for dry wear based on energy. *Journal of Tribology.,* Vol. 113**,** pp. 442-451.

ROOSTA, R. M., SADAGHIANI, M. H., PAK, A. and SALEH, Y. (2006). Rock joint modeling using a visco-plastic multilaminate model at constant normal load condition. *Geotechnical and Geological Engineering.,* Vol. 24**,** pp. 1449-1468.

SAEB, S. and AMADEI, B. (1990). Modelling joint response under constant or variable normal stiffness boundary conditions. *International Journal of Rock Mechanics and Mining Sciences*., Vol. 27**,** pp. 213-217.

SAEB, S. and AMADEI, B. (1992). Modelling rock joints under shear and normal loading. *International Journal of Rock Mechanics and Mining Sciences.,* Vol. 29**,** pp. 267-278.

SEIDEL, J. P. and HABERFIELD, C. M. (1995*a*). The application of energy principles to the determination of the sliding resistance of rock joints. *Rock Mechanics and Rock Engineering.,* Vol. 28**,** pp. 211-226.

SEIDEL, J. P. and HABERFIELD, C. M. (1995*b*). Toward an understanding of joint roughness *Rock Mechanics and Rock Engineering*., Vol. 28**,** pp. 69-92.

SKINAS, C. A., BANDIS, S. C. and DEMIRIS, C. A. (1990). Experimental investigations and modelling of rock joint behaviour under constant stiffness, *In: Conf. on Fractured and Jointed rock masses - Rock Joints.*, pp. 301-308.

SON, B. K., LEE, Y. K. and LEE, C. I. (2004). Elasto-plastic simulation of a direct shear test on rough rock joints. *International Journal of Rock Mechanics and Mining Sciences.,* Vol. 41.

SOULEY, M., HOMAND, F. and AMADEI, B. (1995). An extension to the Saeb and Amadei constitutive model for rock joints to include cyclic loading paths.

International Journal of Rock Mechanics and Mining Sciences., Vol. 32**,** pp. 101-109.

STUPKIEWICZ, S. and MRÓZ, Z. (2001). Modelling of friction and dilatancy effects at brittle interfaces for monotonic and cyclic loading. *Journal of Theoretical and Applied Mechanics.,* Vol. 3**,** pp. 707-739.

SWAN, G. and ZONGQI, S. (1985). Prediction of shear behavior ofjoints using profiles. *Rock Mechanics and Rock Engineering.,* Vol. 18**,** pp. 183-212.

TSE, R. and CRUDEN, D. M. (1979). Estimating joint roughness coefficients. *International Journal of Rock Mechanics and Mining Sciences & Geomechanics Abstracts.,* Vol. 16**,** pp. 303-307.

TULINOV, R. and MOLOKOV, L. (1971). Role of joint filling material in shear strength of rocks. *In: ISRM Symp.,* Nancy.

VAN SINT JAN, M. L. (1990). Shear tests of model rock joints under stiff normal loading. *In: International Symposium on Rock Joints.,* N. BARTON (ed), Loen, Norway. Balkema, Rotterdam, pp. 323-328.

WANHE, S., TIEMIN, Z. and MINGYING, L. (1981). The mechanical effect of the thickness of the weak intercalary layers. *In: Int. Symp. on Weak Rock.,* Tokyo, pp. 49-54.

WIBOWO, J. T., AMADEI, B., STURE, S., ROBERTSON, A. B. and PRIEE, R. (1992). Shear response of a rock under different boundary conditions: A experimental study. *In: Second International Conference on Mechanics of*

Jointed and Faulted Rock., H. P. ROSSMANITH (ed), Vienna, Austria. Balkema, Rotterdam, pp. 425-430.

XIE, H. and PARISEAU, W. G. (1992). Fractal estimation of joint roughness coefficient. *In: Int. Conf. on Fractured and Jointed Rock Masses*., L. R. MYER, C. F. TSANG, N. G. W. COOK, and R. E. GOODMAN (eds), Lake Tahoe, California, USA, Rotterdam, Balkema, pp. 125-131.

YANG, Z. Y. and CHIANG, D. Y. (2000). An experimental study on the progressive shear behavior of rock joints with tooth-shaped asperities. *International Journal of Rock Mechanics and Mining Sciences.,* Vol. 37**,** pp. 1247-1259.

YOSHINAKA, R., YOSHIDA, J., SHIMIZU, T., ARAI, H. and ARISAKA, S. (1991). Scale effect in shear strength and deformability of rock joints. *In: 7th Congress of International Soeiety for Rock Mechanics.,* Aachen, Germany, pp. 371-374.

APPENDIX I

MATLAB CODE PROGRAM FOR THE SIMULATION OF THE CYCLIC LOADING SHEAR BEHAVIOUR OF ROCK JOINTS UNDER CNS CONDITIONS

```
clear
clc

N = input('Enter number of loading cycles =');
NS0 = input('Enter initial normal stress (MPa) =');
BF = input('Enter basic friction angle (Degree) =');
Cd = input('Enter damage coefficient (1/MPa.mm) =');
KCNS = input('Enter value of normal stiffness (MPa/mm) =');
L = input('Enter asperity length (mm) =');
Ke = input('Enter elastic stiffness (MPa/mm) =');
Ue = input('Enter shear displacement at onset plastic
displacement (mm) =');
I0 = input ('Enter initial asperity angle (Degree) =');
isec = input ('Enter secant dilation angle (Degree) =');

NC=1;
SS(1,6000)=0;
NS(1,6000)=0;
NS(1,1)=NS0;
V(1,6000)=0;
U(1,6000)=0;
dils=0;
ds=0;
s1=0;
s2=0;
AN=1;
Uac=0;
Wp=0;

while (Uac<=L/2)
    V(1,AN)=U(1,AN)*cos(isec*pi/180);
    NS(1,AN)=NS0+V(1,AN)*KCNS;
    di=isec;
    if (U(1,AN)<Ue)
        SS(1,AN)=U(1,AN)*Ke;
    else
```

```
SS(1,AN)=NS(1,AN)*(tan(I0*pi/180)+tan(BF*pi/180))/(1-
(tan(BF*pi/180))*tan(di*pi/180));
    end
    Uac=Uac+0.5;
    U(1,AN+1)=U(1,AN)+0.5;
    AN=AN+1;
end

AN=AN-1;
V(1,1)=0;
NS(1,1)=NS0;
Iave= isec*pi/180;
di=Iave;
Q=2;
Uac=0;
dia=0;

while(NC<=N)
    while (Q<=4)
         if (Q ==1)
             dils=1;
             ds=1;
         end
         if (Q ==2)
             dils=-1;
             ds=-1;
         end
         if (Q==3)
             dils=1;
             ds=-1;
         end
         if (Q==4)
             dils=-1;
             ds=1;
         end
         U(1,AN+1)=U(1,AN)+ds*0.5;
         V(1,AN+1)=abs(U(1,AN+1)*tan(di*pi/180));
         dia=abs(atan(V(1,AN+1)-V(1,AN))/(U(1,AN+1)-
U(1,AN)));
         SS(1,AN+1)=ds*NS(1,AN)*tan(BF*pi/180+dia*dils);
         NS(1,AN+1)=NS0+V(1,AN+1)*KCNS;
         s2=abs(SS(1,AN));
         Uac=Uac+0.5;
         AN=AN+1;
         if (Uac<=L/2)
             Wp=(s1+s2)*0.5*0.5+Wp;
             di=Iave*exp(-Cd*Wp);
             s1=s2;
         else
             Uac=0;
```

```
            Q=Q+1;
            AN=AN-1;
        end
    end
    NC=NC+1;
    Q=1;
end

plot (U,SS)
plot (U,NS)
plot (U,V)
```

APPENDIX II

FISH SUBROUTINE PROGRAM FOR THE NUMERICAL SIMULATION OF THE CYCLIC LOADING SHEAR BEHAVIOUR OF ROCK JOINTS UNDER CNS CONDITIOS

Coulomb slip model: Type I asperity surface with initial normal stress of 2.4 MPa

```
new
round 0.001
; This creates block
bl (0,0)  (0,0.4)  (0.35,0.4)  (0.35,0)
; This creates cracks
crack  0.05 0.1 0.05 0.4
crack  0.3 0.1 0.3 0.4
crack  0 0.1  0.35 0.1
crack -1,0.25 1,0.25
del  range 0 0.05  0.1 0.4
del  range 0.3 0.35   0.1 0.4
; This generates mesh
gen edge 0.02  range 0 0.35  0 0.1
gen edge 0.02  range 0.05 0.3 0.1 0.25
gen quad 0.1   range 0.05 0.3 0.25 0.4
plot hold zone block
; Array to peak up joint
```

```
def arrayjoint
ic = contact_head
array a1(2,5000)
ncount1=1
ncount2=1
  loop while ic # 0
      if c_y(ic) = 0.25
        a1(1,ncount1)=ic
      ncount1=ncount1+1
      else
        a1(2,ncount2)=ic
      ncount2=ncount2+1
      endif
      ic = c_next(ic)
   endloop
end
arrayjoint
; This determines material properties
prop  mat=1   d=2.6e3  bu=1400e6  s=792e6
prop  mat=2   d=2.6e3  bu=21.3e6  s=31.95e6
; Changing material properties
change mat=2 range 0.048,0.32 0.245,0.41
plot hold mat
; Coulomb joint model
change jcons=2
set jcondf=2
set add_dil on
```

```
prop jmat=1  jkn=1.4e10   jks=1.4e10   &
          jfric=35  jdil=4.55  zdil=15e-3
prop jmat=2  jkn=1.4e10   jks=1.4e10   &
          jfric=0   jdil=0   zdil=15e-3
; Changing joint material propoerties
change jmat=2 range 0.048,0.31 0.24,0.26
plot hold mat joint
; This provides the boundary condition
bound  xvel=0  range   0.0499,0.051 0.099,0.401
bound  xvel=0  range   0.299,0.301  0.099,0.401
bound  yvel=0  range   -0.0018,0.351 -0.00156,0.00119
bound  yvel=0  range   0.049,0.35 0.33,0.41
; Apply normal stress
ini syy = -2.4e6 range 0.05,0.3 0.25,0.4
ini syy = -2.4e6 range 0.05,0.3 0.1,0.25
ini syy = -2.4e6 range 0,0.35 0,0.1
hist unbal
cycle 1000
; Functions to calculate average joint stresses and average joint displacements
def ini_jdisp
  njdisp0 = 0.0
  sjdisp0 = 0.0
  ncount3=1
  loop while ncount3 <= ncount2
     njdisp0 = njdisp0 + c_ndis(a1(2,ncount3))
     sjdisp0 = sjdisp0 + c_sdis(a1(2,ncount3))
     ncount3 = ncount3 + 1
```

```
  endloop
end
ini_jdisp
def av_str
  whilestepping
  sstav = 0.0
  nstav = 0.0
  njdisp = 0.0
  sjdisp = 0.0
  jl   = 0.237012              ; joint length
  ncount4=1
  loop while ncount4 <= ncount2
     sstav = sstav + c_sforce(a1(2,ncount4))
     nstav = nstav + c_nforce(a1(2,ncount4))
     njdisp = njdisp + c_ndis(a1(2,ncount4))
     sjdisp = sjdisp + c_sdis(a1(2,ncount4))
     ncount4 = ncount4 + 1
  endloop
  if ncount2 # 0
    sstav = sstav / jl
    nstav = nstav / jl
    njdisp = (njdisp-njdisp0) / ncount2
    sjdisp = (sjdisp-sjdisp0) / ncount2
  endif
end
reset hist jdisp
hist ncycle=200 unbal  nc 1
```

```
hist ncycle=200 sstav  nstav njdisp sjdisp
plot hold syy fill bl
; Boundary velocity
bou  xvel=-8.33e-3 range -5,5 -0.001,0.001
step 280000
bou  xvel=8.33e-3 range -5,5 -0.001,0.001
step 280000
step 280000
bou  xvel=-8.33e-3 range -5,5 -0.001,0.001
step 280000
; Boundary velocity
bou  xvel=-8.33e-3 range -5,5 -0.001,0.001
step 280000
bou  xvel=8.33e-3 range -5,5 -0.001,0.001
step 280000
step 280000
bou  xvel=-8.33e-3 range -5,5 -0.001,0.001
step 280000
; Boundary velocity
bou  xvel=-8.33e-3 range -5,5 -0.001,0.001
step 280000
bou  xvel=8.33e-3 range -5,5 -0.001,0.001
step 280000
step 280000
bou  xvel=-8.33e-3 range -5,5 -0.001,0.001
step 280000
; Boundary velocity
```

```
bou  xvel=-8.33e-3 range -5,5 -0.001,0.001
step 280000
bou  xvel=8.33e-3 range -5,5 -0.001,0.001
step 280000
step 280000
bou  xvel=-8.33e-3 range -5,5 -0.001,0.001
step 280000
pl syy fil blo blu hold
pl sxx fil blo blu hold
plot hold hist 2 vs 5 yr
plot hold hist 4 vs 5
plot hold hist 3 vs 5
return
```

APPENDIX III

STABILITY ANALYSIS OF AN UNDERGROUND STRUCTURE SUBJECTED TO SEISMIC EVENTS IN UDEC

```
new
round = 0.008
block -30,-50 -30,94 30,94 30,-50
; Boundary cracks for jointed region
crack -30,10  30,10
crack -30,34  30,34
crack -15,10 -15,34
crack  15,10  15,34
; Excavation boundary crack
crack  0,10  0,34
crack -3,15 -3,24
crack -3,24  3,24
crack  3,15  3,24
crack -3,15  3,15
; Jointed region
jreg id=1 -15,10 -15,34 15,34 15,10
jset 60,0 35,0 0,0 4,0 0,30 range jreg 1
jset 120,0 35,0 0,0 3,0 0,30 range jreg 1
del range area 0.1
; Zoning
```

```
gen edge 3 range -15 15 10 34
gen quad 4
; Boundary and initial condition
insitu stress (-7e5, 0, -2.6e6) ygrad (10000,0,20000)
grav 0, -9.81
bound xvel 0 range -33 -27 -55  100
bound xvel 0 range  27  33 -55  100
bound yvel 0 range -33  33 -55  -45
; Rock mass
prop  mat=1   d=2.6e3  bu=1400e6  s=792e6
; Joint constitutive model
change jcons=2
set jcondf=2
set add_dil on
; Joint set 1
prop jmat=1  jkn=1.4e10   jks=1.4e10   &
          jfric=40.35  jdil=0  zdil=15e-3
; Joint set 2
change jmat 2 range ang 110 130
prop jmat=2  jkn=1.4e10   jks=1.4e10   &
          jfric=40.35  jdil=0  zdil=15e-3
; Joint set 3 (1)
change jmat 3 range 2.8 7.238 27.223 40.814 ang  55 65
change jmat 3 range 0.251 4.93 23.63 28 ang  55 65
change jmat 3 range -6.189 -1.693 12.018 17.45 ang  55 65
change jmat 3 range -9.288 -4.913 9.546 12.842 ang  55 65
prop jmat=3  jkn=1.4e10   jks=1.4e10   &
```

```
        jfric=35  jdil=4.54 zdil=15e-3
; Joint set 4 (2)
change jmat 4 range 7.171 11.77 26.99 40.992 ang  55 65
change jmat 4 range 3.248 7.8 20.51 27.445 ang  55 65
change jmat 4 range 2.099 4.357 17.67 20.95 ang  55 65
change jmat 4 range -3.331 0.87 9.91 15.72 ang  55 65
prop jmat=4  jkn=1.4e10   jks=1.4e10   &
        jfric=35  jdil=4.53 zdil=15e-3
; Joint set 5 (3)
change jmat 5 range -12.96 -9.354 28.67 40.94 ang  110 130
change jmat 5 range -10.107 -6.659 24.221 29.106 ang  110 130
change jmat 5 range -7.214 -4.202 19.92 24.905 ang  110 130
change jmat 5 range -4.799 -2.142 16.551 19.99 ang  110 130
change jmat 5 range -1.9 1.425 9.95 15.525 ang  110 130
prop jmat=5  jkn=1.4e10   jks=1.4e10   &
        jfric=35  jdil=4.61  zdil=15e-3
; Joint set 6 (4)
change jmat 6 range -9.433 -5.906 28.569 34.041 ang  110 130
change jmat 6 range -6.382 -2.934 23.146 28.667 ang  110 130
change jmat 6 range 1.346 4.833 9.95 15.378 ang  110 130
prop jmat=6  jkn=1.4e10   jks=1.4e10   &
        jfric=35  jdil=4.89  zdil=15e-3
; Joint set 7 (5)
change jmat 7 range -6.4 -4.4 32 34  ang  110 130
change jmat 7 range -5.128 -2.459 27.885 34.041 ang  110 130
change jmat 7 range -2.46 -0.16 22.8 28 ang  110 130
change jmat 7 range  -1.64 0.5 23 26 ang  110 130
```

```
change jmat 7 range  2.5 5.9 13.64 18.97 ang  110 130
change jmat 7 range  5.28 8.45 9.9 14.19 ang  110 130
prop jmat=7  jkn=1.4e10   jks=1.4e10   &
          jfric=35  jdil=4.52 zdil=15e-3
; Joint set 8 (6)
change jmat 8 range -0.6 0.6 9.4 35 ang  89 91
prop jmat=8  jkn=1.4e10   jks=1.4e10   &
          jfric=35  jdil=5.18 zdil=15e-3
; Array to peak up joints
def arrayjoint
ic = contact_head
array a1(2,5000)
array a2(3,5000)
array a3(1,5000)
ncount1=1
ncount2=1
ncount3=1
ncount4=1
ncount5=1
ncount6=1
  loop while ic # 0
        if c_y(ic)<1.71*c_x(ic)+23.05
          if C_y(ic)>1.72*c_x(ic)+21.429
            a1(1,ncount1)=ic
            ncount1=ncount1+1
          endif
        endif
```

```
if c_y(ic)<1.7*c_x(ic)+15.4
  if C_y(ic)>1.69*c_x(ic)+13.501
    a1(2,ncount2)=ic
    ncount2=ncount2+1
  endif
endif
if c_y(ic)<-1.7045*c_x(ic)+13.29
  if C_y(ic)>-1.68*c_x(ic)+11.72
    a2(1,ncount3)=ic
    ncount3=ncount3+1
  endif
endif
if c_y(ic)<-1.69*c_x(ic)+19.22
  if C_y(ic)>-1.69*c_x(ic)+17.23
    a2(2,ncount4)=ic
    ncount4=ncount4+1
  endif
endif
if c_y(ic)<-1.7*c_x(ic)+25.574
  if C_y(ic)>-1.69*c_x(ic)+22.983
    a2(3,ncount5)=ic
    ncount5=ncount5+1
  endif
endif
if c_x(ic)=0
    a3(1,ncount6)=ic
    ncount6=ncount6+1
```

```
        endif
        ic = c_next(ic)
    endloop
end
arrayjoint
; Average displacements and stresses
def ini_jdisp
  njdisp01 = 0.0
  sjdisp01 = 0.0
  njdisp02 = 0.0
  sjdisp02 = 0.0
  njdisp03 = 0.0
  sjdisp03 = 0.0
  njdisp04 = 0.0
  sjdisp04 = 0.0
  njdisp05 = 0.0
  sjdisp05 = 0.0
  njdisp06 = 0.0
  sjdisp06 = 0.0
  ncount7=1
  ncount8=1
  ncount9=1
  ncount10=1
  ncount11=1
  ncount12=1
  loop while ncount7 <= ncount1
     njdisp01 = njdisp01 + c_ndis(a1(1,ncount7))
```

```
    sjdisp01 = sjdisp01 + c_sdis(a1(1,ncount7))
    ncount7 = ncount7 + 1
endloop
loop while ncount8 <= ncount2
    njdisp02 = njdisp02 + c_ndis(a1(2,ncount8))
    sjdisp02 = sjdisp02 + c_sdis(a1(2,ncount8))
    ncount8 = ncount8 + 1
endloop
loop while ncount9 <= ncount3
    njdisp03 = njdisp03 + c_ndis(a2(1,ncount9))
    sjdisp03 = sjdisp03 + c_sdis(a2(1,ncount9))
    ncount9 = ncount9 + 1
endloop
loop while ncount10 <= ncount4
    njdisp04 = njdisp04 + c_ndis(a2(2,ncount10))
    sjdisp04 = sjdisp04 + c_sdis(a2(2,ncount10))
    ncount10 = ncount10 + 1
endloop
loop while ncount11 <= ncount5
    njdisp05 = njdisp05 + c_ndis(a2(3,ncount11))
    sjdisp05 = sjdisp05 + c_sdis(a2(3,ncount11))
    ncount11 = ncount11 + 1
endloop
loop while ncount12 <= ncount6
    njdisp06 = njdisp06 + c_ndis(a3(1,ncount12))
    sjdisp06 = sjdisp06 + c_sdis(a3(1,ncount12))
    ncount12 = ncount12 + 1
```

```
  endloop
end
ini_jdisp
def av_str
  whilestepping
  sstav1 = 0.0
  nstav1 = 0.0
  njdisp1 = 0.0
  sjdisp1 = 0.0
  jl1   = 19.23          ; joint length
  sstav2 = 0.0
  nstav2 = 0.0
  njdisp2 = 0.0
  sjdisp2 = 0.0
  jl2   = 22.58          ; joint length
  sstav3 = 0.0
  nstav3 = 0.0
  njdisp3 = 0.0
  sjdisp3 = 0.0
  jl3   = 24.77          ; joint length
  sstav4 = 0.0
  nstav4 = 0.0
  njdisp4 = 0.0
  sjdisp4 = 0.0
  jl4   = 37.23          ; joint length
  sstav5 = 0.0
  nstav5 = 0.0
```

```
njdisp5 = 0.0
sjdisp5 = 0.0
jl5   = 21.32          ; joint length
sstav6 = 0.0
nstav6 = 0.0
njdisp6 = 0.0
sjdisp6 = 0.0
jl6   = 14.76          ; joint length
ncount13=1
ncount14=1
ncount15=1
ncount16=1
ncount17=1
ncount18=1
loop while ncount13 <= ncount1
   sstav1 = sstav1 + c_sforce(a1(1,ncount13))
   nstav1 = nstav1 + c_nforce(a1(1,ncount13))
   njdisp1 = njdisp1 + c_ndis(a1(1,ncount13))
   sjdisp1 = sjdisp1 + c_sdis(a1(1,ncount13))
   ncount13 = ncount13 + 1
endloop
if ncount13 # 0
  sstav1 = sstav1 / jl1
  nstav1 = nstav1 / jl1
  njdisp1 = (njdisp1-njdisp01) / ncount13
  sjdisp1= (sjdisp1-sjdisp01) / ncount13
endif
```

```
loop while ncount14 <= ncount2
    sstav2 = sstav2 + c_sforce(a1(2,ncount14))
    nstav2 = nstav2 + c_nforce(a1(2,ncount14))
    njdisp2 = njdisp2 + c_ndis(a1(2,ncount14))
    sjdisp2 = sjdisp2 + c_sdis(a1(2,ncount14))
    ncount14 = ncount14 + 1
endloop
if ncount14 # 0
  sstav2 = sstav2 / jl2
  nstav2 = nstav2 / jl2
  njdisp2 = (njdisp2-njdisp02) / ncount14
  sjdisp2= (sjdisp2-sjdisp02) / ncount14
endif
loop while ncount15 <= ncount3
    sstav3 = sstav3 + c_sforce(a2(1,ncount15))
    nstav3 = nstav3 + c_nforce(a2(1,ncount15))
    njdisp3 = njdisp3 + c_ndis(a2(1,ncount15))
    sjdisp3 = sjdisp3 + c_sdis(a2(1,ncount15))
    ncount15 = ncount15 + 1
endloop
if ncount15 # 0
  sstav3 = sstav3 / jl3
  nstav3 = nstav3 / jl3
  njdisp3 = (njdisp3-njdisp03) / ncount15
  sjdisp3= (sjdisp3-sjdisp03) / ncount15
endif
loop while ncount16 <= ncount4
```

```
    sstav4 = sstav4 + c_sforce(a2(2,ncount16))
    nstav4 = nstav4 + c_nforce(a2(2,ncount16))
    njdisp4 = njdisp4 + c_ndis(a2(2,ncount16))
    sjdisp4 = sjdisp4 + c_sdis(a2(2,ncount16))
    ncount16 = ncount16 + 1
endloop
if ncount16 # 0
  sstav4 = sstav4 / jl4
  nstav4 = nstav4 / jl4
  njdisp4 = (njdisp4-njdisp04) / ncount16
  sjdisp4= (sjdisp4-sjdisp04) / ncount16
endif
loop while ncount17 <= ncount5
    sstav5 = sstav5 + c_sforce(a2(3,ncount17))
    nstav5 = nstav5 + c_nforce(a2(3,ncount17))
    njdisp5 = njdisp5 + c_ndis(a2(3,ncount17))
    sjdisp5 = sjdisp5 + c_sdis(a2(3,ncount17))
    ncount17 = ncount17 + 1
endloop
if ncount17 # 0
  sstav5 = sstav5 / jl5
  nstav5 = nstav5 / jl5
  njdisp5 = (njdisp5-njdisp05) / ncount17
  sjdisp5= (sjdisp5-sjdisp05) / ncount17
endif
loop while ncount18 <= ncount6
    sstav6 = sstav6 + c_sforce(a3(1,ncount18))
```

```
      nstav6 = nstav6 + c_nforce(a3(1,ncount18))
      njdisp6 = njdisp6 + c_ndis(a3(1,ncount18))
      sjdisp6 = sjdisp6 + c_sdis(a3(1,ncount18))
      ncount18 = ncount18 + 1
  endloop
   if ncount18 # 0
    sstav6 = sstav6 / jl6
    nstav6 = nstav6 / jl6
    njdisp6 = (njdisp6-njdisp06) / ncount18
    sjdisp6= (sjdisp6-sjdisp06) / ncount18
  endif
end
av_str
pl bl zone yel hold
pl syy fil blo blu hold
pl sxx fil blo blu hold
hist unb ydis 0 26
damp auto
step 3000
pl hold hist 1
; Excavate tunnel
del -2.98 2.98 15.2 23.8
pl hold bl
; Static analysis
reset disp jdisp hist
reset hist time disp
hist ncycle=50 ydis  0.2,26
```

```
hist ncycle=50 xdis -3.2,21
hist ncycle=50 sstav1  nstav1 njdisp1 sjdisp1
hist ncycle=50 sstav2  nstav2 njdisp2 sjdisp2
hist ncycle=50 sstav3  nstav3 njdisp3 sjdisp3
hist ncycle=50 sstav4  nstav4 njdisp4 sjdisp4
hist ncycle=50 sstav5  nstav5 njdisp5 sjdisp5
hist ncycle=50 sstav6  nstav6 njdisp6 sjdisp6
hist type 1
cycle 5500
pl bl zone yel hold
pl syy fil blo blu hold
pl sxx fil blo blu hold
pl hold hist 1
pl hold hist 2
pl hold hist 3
pl hold hist 7
pl hold hist 11
pl hold hist 15
pl hold hist 19
pl hold hist 23
; Generate free-field (55 nodes) ; both lateral bound ; fixed bottom
ffield gen yrange (-60,100) np 55
ffield change mat=1 cons=1
; Initialize FF stresses (same as insitu stresses)
ffield ini sxx -7e5 10000
ffield ini syy -2.6e6 20000
; Cycle with FF not attached to the model
```

```
; Joint properties for dynamic analysis
; To bring FF stresses to equilibrium
ffield base xvel 0
ffield base yvel 0
hist ffyd 0 1
hist ffsxx 0 1
step 1100
; Histories
reset hist time disp
hist ncycle=400 ydis  0.2,26
hist ncycle=400 Syy   0.2,26
hist ncycle=400 xdis -3.2,21
hist ncycle=400 Sxx  -3.2,21
hist ncycle=400 sstav1
hist ncycle=400 sstav2
hist ncycle=400 sstav3
hist ncycle=400 sstav4
hist ncycle=400 sstav5
hist ncycle=400 sstav6
hist ncycle=400 nstav1
hist ncycle=400 nstav2
hist ncycle=400 nstav3
hist ncycle=400 nstav4
hist ncycle=400 nstav5
hist ncycle=400 nstav6
hist ncycle=400 njdisp1
hist ncycle=400 njdisp2
```

```
hist ncycle=400 njdisp3
hist ncycle=400 njdisp4
hist ncycle=400 njdisp5
hist ncycle=400 njdisp6
hist ncycle=400 sjdisp1
hist ncycle=400 sjdisp2
hist ncycle=400 sjdisp3
hist ncycle=400 sjdisp4
hist ncycle=400 sjdisp5
hist ncycle=400 sjdisp6
; Apply dynamic boundary condition
bound mat 1
bound ff range -33,-27 -55,100
bound ff range  27,33  -55,100
bound xvisc range -33,33 -55,-45
damp 0.0001 10
mscale part 1e-5
set ovtol 0.5
; First seismic event
; Amplitude of shear wave: 2.4 MPa; freq = 11 Hz, duration 2 sec.
bound stress 0 -2.4e6 0 hist sine (11 2) range -33 33 -55 -45
; Fix y-vel at bottom
bound yvel=0 range -33 33 -55 -45
; Free-field boundary condition at base
ffield base sxy=-2.4e6 hist sine (11 2)
ffield base yvel=0
ffield base xvisc
```

```
cycle time 2
; Second seismic event
; Amplitude of shear wave: 0.8 MPa; freq = 8 Hz, duration 4 sec. (total=6sec)
bound stress 0 -8e5 0 hist sine (8 4) range -33 33 -55 -45
; Fix y-vel at bottom
bound yvel=0 range -33 33 -55 -45
; Free-field boundary condition at base
ffield base sxy=-8e5 hist sine (8 4)
ffield base yvel=0
ffield base xvisc
cycle time 4
; Third seismic event
; Amplitude of shear wave: 0.45 MPa; freq = 10 Hz, duration 6 sec. (total=12 sec)
bound stress 0 -4.5e5 0 hist sine (10 6) range -33 33 -55 -45
; Fix y-vel at bottom
bound yvel=0 range -33 33 -55 -45
; Free-field boundary condition at base
ffield base sxy=-4.5e5 hist sine (10 6)
ffield base yvel=0
ffield base xvisc
cycle time 6
plot hold hist 1
plot hold hist 2
plot hold hist 3
plot hold hist 4
plot hold hist 5
plot hold hist 6
```

plot hold hist 7

plot hold hist 8

plot hold hist 9

plot hold hist 10

plot hold hist 11

plot hold hist 12

plot hold hist 13

plot hold hist 14

plot hold hist 15

plot hold hist 16

plot hold hist 17

plot hold hist 18

plot hold hist 19

plot hold hist 20

plot hold hist 21

plot hold hist 22

plot hold hist 23

plot hold hist 24

plot hold hist 25

plot hold hist 26

plot hold hist 27

plot hold hist 28

plot hold bl dis yel